TU/e EINDHOVEN UNIVERSITY OF TECHNOLOGY

Kinetic and selectivity modelling of the iron-based low-temperature Fischer-Tropsch synthesis

Citation for published version (APA):
Botes, F. G. (2008). *Kinetic and selectivity modelling of the iron-based low-temperature Fischer-Tropsch synthesis*. [Phd Thesis 2 (Research NOT TU/e / Graduation TU/e), Chemical Engineering and Chemistry]. Technische Universiteit Eindhoven. https://doi.org/10.6100/IR638544

DOI:
10.6100/IR638544

Document status and date:
Published: 01/01/2008

Document Version:
Publisher's PDF, also known as Version of Record (includes final page, issue and volume numbers)

Please check the document version of this publication:

• A submitted manuscript is the version of the article upon submission and before peer-review. There can be important differences between the submitted version and the official published version of record. People interested in the research are advised to contact the author for the final version of the publication, or visit the DOI to the publisher's website.
• The final author version and the galley proof are versions of the publication after peer review.
• The final published version features the final layout of the paper including the volume, issue and page numbers.

Link to publication

General rights
Copyright and moral rights for the publications made accessible in the public portal are retained by the authors and/or other copyright owners and it is a condition of accessing publications that users recognise and abide by the legal requirements associated with these rights.

• Users may download and print one copy of any publication from the public portal for the purpose of private study or research.
• You may not further distribute the material or use it for any profit-making activity or commercial gain
• You may freely distribute the URL identifying the publication in the public portal.

If the publication is distributed under the terms of Article 25fa of the Dutch Copyright Act, indicated by the "Taverne" license above, please follow below link for the End User Agreement:

www.tue.nl/taverne

Take down policy
If you believe that this document breaches copyright please contact us at:

openaccess@tue.nl

providing details and we will investigate your claim.

Download date: 19. May. 2025

Kinetic and Selectivity Modelling of the Iron-Based Low-Temperature Fischer-Tropsch Synthesis

PROEFSCHRIFT

ter verkrijging van de graad van doctor aan de
Technische Universiteit Eindhoven, op gezag van de
Rector Magnificus, prof.dr.ir. C.J. van Duijn, voor
een commissie aangewezen door het College voor
Promoties in het openbaar te verdedigen op
dinsdag 2 december 2008 om 16.00 uur

door

Frederick Gideon Botes

geboren te Stellenbosch, Zuid-Afrika

Dit proefschrift is goedgekeurd door de promotor:

prof.dr.ir. J.C. Schouten

Copromotor:
dr. M.H.J.M. de Croon

A catalogue record is available from the Library Eindhoven University of Technology

ISBN: 978-90-386-1440-3

Cover design and photography: Gideon Botes; Marieta Lamprecht; Gert Lamprecht

Aan my ma, Anna Maria, wie ek nog elke dag mis.

Contents

Samenvatting (Dutch)

De Fischer-Tropsch (FT) synthese is een methode voor de omzetting van synthesegas, verkregen vanuit de vergassing van alternatieve energiebronnen voor ruwe olie zoals kolen, aardgas of biomassa, naar vloeibare brandstoffen te gebruiken in conventionele automotoren. De economische haalbaarheid van een commerciële FT fabriek is sterk afhankelijk van de ruwe olieprijs, welke aanzienlijk heeft gefluctueerd gedurende de laatste decennia. Waarschijnlijk vanwege het risico van een plotselinge, onvoorziene daling in de ruwe olieprijs is de wereldwijde toepassing van de FT technologie nog beperkt. Er is echter een hernieuwde interesse in kolen en aardgas als alternatieve energiebronnen vanwege de huidige hoge ruwe olieprijzen, waardoor het FT proces ruime aandacht krijgt. De FT synthese wordt commercieël toegepast op verschillende manieren, maar de specifieke focus van deze studie is de ijzer-gebaseerde Lage Temperatuur Fischer-Tropsch (Fe-LTFT) synthese. Dit proces wordt gekarakteriseerd door het gebruik van een alkali-gepromote ijzer katalysator, synthesetemperaturen rond de 240°C en een productverdeling strekkend tot ver in het gebied van de synthetische wassen. Een nauwkeurige voorspelling van de proces karakteristieken is erg belangrijk voor het ontwerp van een commerciële FT fabriek. Er zijn drie hoofdaspecten te bestuderen in termen van de modellering van de Fe-LTFT synthese, namelijk de snelheid van CO omzetting naar koolwaterstoffen (FT kinetiek), de snelheid van CO omzetting naar CO_2 ("Water-Gas-Schuif" of WGS kinetiek) en de productverdeling van de koolwaterstoffen (product selectiviteiten)

FT kinetiek

Alhoewel water (of kooldioxide) traditioneel een rol speelt in FT snelheidsvergelijkingen voor de ijzer-gebaseerde FT synthese, toonde een kritisch beschouwing van de literatuur aan dat er geen sluitende bewijsvoering is voor het uitgangspunt dat een van deze twee componenten de FT reactiesnelheid negatief zou beïnvloeden. In plaats daarvan werd aangetoond dat de schijnbare invloed van

water op de FT reactiesnelheid ook verklaard kan worden vanuit het effect van water op de WGS reactiesnelheid, welke vervolgens de gas fase partiaalspanningen van de reactanten koolmonoxide (CO) en waterstof (H_2) beïnvloedt en daardoor indirect de vormingssnelheden van de koolwaterstoffen. De FT reactiesnelheidsvergelijkingen, zoals voorgesteld in deze studie, bevatten in eerste instantie een water-afhankelijke term. Na verder testen van de vergelijking op basis van een variëteit van bestaande data reeksen, viel te concluderen dat er geen statistische basis is voor deze water-afhankelijke term. Een experimentele ontwerpprocedure volgende werden nieuwe kinetische data gemeten, op basis waarvan op conclusieve wijze onderscheid te maken viel tussen de traditionele snelheidsvergelijkingen en de volgende, nieuwe FT snelheidsvergelijking welke geen invloed van water op de FT kinetiek veronderstelt:

$$r_{FT} = A\frac{P_{H_2}{}^{0.5} P_{CO}}{\left(1 + k_{CO} P_{CO}\right)^2}$$

WGS kinetiek

Historisch gezien werd er in de literatuur voorgesteld de WGS kinetiek te beschrijven met een eenvoudige eerste orde snelheidsvergelijking in CO. Meer recent schijnt de voorkeur te worden gegeven aan modelvergelijkingen afgeleid vanuit mechanismen gebaseerd op de vorming van een formaat-intermediair. In deze studie werd aangetoond dat alhoewel een eerste orde vergelijking in CO een redelijke beschrijving van de WGS snelheid geeft, deze ook systematische afwijkingen te zien geeft, die indicatief zijn voor haar empirische aard. Er werd verder gevonden dat modellen, gebaseerd op het formaat-mechanisme, de historische data beter beschreven. Na evalueren van de rivaliserende snelheidsvergelijkingen met nieuw gemeten data kwam de volgende snelheidsvergelijking naar voren als de preferentiële WGS snelheidsvergelijking:

$$r_{WGS} = A \frac{P_{CO}P_{H_2O} - \frac{1}{K_{WGS}} P_{H_2}P_{CO2}}{\left(1 + k_{H_2O}P_{H_2O} + k_{OH}\frac{P_{H_2O}}{P_{H_2}^{0.5}}\right)^2}$$

Deze nieuwe snelheidsvergelijkingen voor de FT synthesereactie en de WGS reactie impliceren dat deze reacties verlopen over verschillende typen actieve katalysatorplaatsen. Terwijl de actieve plaatsen voor de FT synthese hoofdzakelijk bezet zijn met geabsorbeerd CO of gerelateerde C_1 oppervlakteverbindingen zijn de actieve plaatsen voor de WGS reactie vooral bezet met geadsorbeerd water of de gerelateerde hydroxygroep.

Selectiviteitsmodellering

Twee typen productverdelingsmodellen zijn bekend in de literatuur voor de FT synthese, namelijk dubbel-α modellen en olefine herinsertie modellen. In deze studie werd aangetoond dat er sprake is van een hoge mate van ongewenste kruis-correlatie tussen de onafhankelijke parameters van de dubbel-α modellen. Vanwege de lage waarschijnlijkheid van secundaire olefine reacties over ijzer-LTFT katalysatoren werd er ook geconcludeerd dat olefine herinsertie modellen niet van toepassing zijn voor de Fe-LTFT synthese. Een nieuw productverdeling model werd daarop voorgesteld. Volgens dit ketenlengte-afhankelijke desorptiemodel worden olefine- en parafinevorming bepaald door drie generieke reacties: ketengroei met een koolstofatoom tegelijkertijd, ketendesorptie resulterend in de vorming van een olefine, en ketenhydrogenering resulterend in de vorming van een parafine. De sleutelaanname in het model is dat de snelheden van ketengroei en ketenhydrogenering onafhankelijk van de ketenlengte zijn, maar dat de desorptiesnelheid een functie van het koolstofgetal is via de fysisorptie van de keten op het katalysatoroppervlak. Des te langer de keten, des te sterker deze fysisorptie en, dientengevolge, des te langzamer de desorptiesnelheid wordt ten opzichte van de snelheden van ketengroei en ketenhydrogenering. Als gevolg

hiervan is er een toename in de groeiwaarschijnlijkheid en de mate van productverzadiging met toenemende ketenlengte. Het nieuwe model kon de olefine en parafine productverdeling in het C_3-C_{10} interval nauwkeurig beschrijven. Na het maken van enkele aanpassingen in de modelvergelijking van het C_2-intermediair, gerationaliseerd vanuit reactiemechanistische overwegingen, kon het model ook geëxtrapoleerd worden naar C_1 en C_2 producten. Dit is een daadwerkelijke extrapolatie aangezien de experimentele data voor C_1 en C_2 producten niet werden gebruikt voor regressie van corresponderende parameters. Het aangepaste model is daarom vermoedelijk dan ook het eerste productverdelingsmodel dat ook succesvol geëxtrapoleerd kan worden naar C_1 en C_2 producten zonder het introduceren van additionele (unieke) parameters voor deze producten.

Het ketenlengte afhankelijke desorptiemodel bleek de etheen / ethaan verhouding te overschatten en een hogere olefine / parafine verhouding te voorspellen voor de C_2 fractie dan voor de C_3 fractie. In overeenstemming met de resultaten uit literatuur studies met nevenvoeding van etheen werd dit toegeschreven aan secundaire hydrogenering van etheen. Data verkregen in een laboratorium slurry reactor bedreven onder circulatie condities werden gebruikt als verdere ondersteuning voor enkele van de aannames en implicaties van het nieuwe productverdelingsmodel. Deze resultaten lieten verwaarloosbare herinsertie snelheden zien voor zowel etheen en propeen, hoge snelheden voor secundaire hydrogenering van etheen en zeer lage (bijna te verwaarlozen) snelheden voor secundaire hydrogenering van propeen. Na afschatting van de snelheidsconstantes voor secundaire hydrogenering kon worden aangetoond dat de voorspelde primaire etheen / ethaan verhouding groter is dan de voorspelde primaire propeen / propaan verhouding, hetgeen in overeenstemming met het ketenlengte-afhankelijke desorptiemodel is.

Opsomming (Afrikaans)

Die Fischer-Tropsch (FT) sintese behels die omsetting van CO en waterstof na 'n wye bereik van koolwaterstowwe met 'n koolstofverspreiding kenmerkend aan dié van 'n polimerisasiemeganisme. Dit verskaf 'n metode om sintesegas, verkry vanaf die vergassing van ru-olie alternatiewe bronne soos steenkool, aardgas of biomassa, om te skakel na vloeibare brandstowwe geskik vir gebruik in standaard voertuie. Die ekonomiese lewensvatbaarheid van 'n kommersiële FT aanleg is hoogs afhanklik van die ru-olie prys, wat aansienlik gevarieer het in die afgelope paar dekades. Tot dusver is die tegnologie slegs tot 'n beperkte mate op wêreldskaal aangewend, oënskynlik weens die bedreiging wat 'n ontydige skerp daling in die olieprys sou inhou. Daar is egter tans 'n hernude belangstelling in steenkool en aardgas as alternatiewe energiebronne weens huidige hoë oliepryse, wat die FT proses weer deeglik in die kollig geplaas het.

Kommersiëel is die FT sintese reeds in verkeie vorme aangewend, maar die fokus van hierdie studie is spesifiek op die "ystergebasseerde Lae-Temperatuur Fischer-Tropsch" (Fe-LTFT) sintese. Die gebuik van 'n alkali-gepromoveerde ysterkatalisator, asook 'n bedyrfstemperatuur rondom 240°C en 'n produkspektrum wat tot ver in die wasbereik strek, is kenmerkend aan die proses. Die akkurate modellering van die proses is van die uiterste belang tydens die ontwerp van 'n kommersiële aanleg. Daar is drie aspekte wat in dié verband aangespreek moet word, naamlik die tempo waarteen CO omgesit word na koolwaterstowwe (*FT kinetika*), die tempo waarteen CO omgesit word na CO_2 (*WGS kinetika*), en die produkverspreiding (*produkselektiwiteite*).

FT Kinetika

Water (of CO_2) is tradisioneel ingesluit in FT reaksiesnelheidsvergelykings vir die Fe-LTFT sintese. Desnieteenstaande het 'n kritiese oorsig van die literatuur aangetoon dat daar geen geloofwaardige ondersteuning is dat enige van hierdie twee komponente die reaksiesnelheid negatief beïnvloed nie. Inteendeel, dit kon

aangetoon word dat die invloed van water ook toegeskryf kan word aan die rol van die water-gas-skuif (WGS) reaksie, wat die parsiële drukke van CO en waterstof in die gasfase affekteer, en sodoende ook die vormingstempo van koolwaterstowwe. Die FT kinetiese model wat in hierdie studie ontwikkel is, het aanvanklik 'n waterterm bevat, maar na evaluasie met 'n aantal bestaande stelle data is bevind dat daar geen statistiese ondersteuning is om water in te sluit nie. Nuwe kinetiese data, wat gemeet is volgens 'n eksperimentele ontwerpsprosedure, kon oortuigend onderskeid tref tussen die tradisionele FT snelheidsvergelykings (wat voorsiening maak vir 'n invloed van water) en die volgende vergelyking (wat geen waterterm bevat nie):

$$r_{FT} = A\frac{P_{H_2}{}^{0.5} P_{CO}}{\left(1 + k_{CO} P_{CO}\right)^2}$$

WGS kinetika

Aanvanklik is daar in die literatuur voorgestel dat die WGS kinetika beskryf kan word deur 'n eenvoudige eerste-orde vergelyking in CO. Van meer onlangse publikasies blyk dit egter dat die mees akkurate modelle gebasseer is op 'n meganisme wat voorstaan dat die reaksie via a formaatintermediêr verloop. Daar is in hierdie studie aangetoon dat eerste-orde kinetika in CO bestaande kinetiese data redelik kan beskryf, maar dat die model sistematiese afwykings bevat weens sy empiriese karakter. Verder is daar ook bevind dat drie snelheidsvergelykings gebasseer op die formaatmeganisme die historiese data die beste beskryf, maar geen onderskyd kon getref word tussen hierdie modelle nie. Na verdere evaluasie met nuwe data het die volgende vergelyking na vore getree as die beste WGS kinetiese model:

$$r_{WGS} = A \frac{P_{CO}P_{H_2O} - \frac{1}{K_{WGS}} P_{H_2}P_{CO_2}}{\left(1 + k_{H_2O}P_{H_2O} + k_{OH}\frac{P_{H_2O}}{P_{H_2}^{0.5}}\right)^2}$$

Die implikasie van die nuwe kinetiese modelle vir die Fe-LTFT sintese is dat die FT en WGS reaksies op verskillende tipes aktiewe punte plaasvind. Waar die FT punte hoofsaaklik bedek is met geadsorbeerde CO of verwante C_1 intermediêre, is die WGS punte hoofsaaklik bedek met geadsorbeerde water en OH-spesies.

Selektiwiteitsmodellering

Daar is twee tipes produkkarakteriseringsmodelle bekend in die literatuur, naamlik dubbel-α modelle en olefienherinkorporasiemodelle. Dubbel-α modelle kan nóg die daling in olefien / paraffien verhouding, nóg die afwykings in die C_1 and C_2 seleketiwiteite, beskryf. Daar is ook in hierdie studie aangetoon dat daar ’n groot mate van kovariansie tussen die onafhanklike parameters van dubbel-α modelle is. Weens die lae geneigtheid van sekondêre olefienreaksies op ysterkatalisatore is daar tot die gevolgtrekking gekom dat olefienherinkorporasiemodelle ook nie van toepassing is op die Fe-LTFT sintese nie. Gevolglik is die nuwe "kettinglengte-afhanklike desorpsiemodel" voorgestel. Hiervolgens word die vorming van olefiene en paraffiene bepaal deur drie generiese reaksies: kettinggroei deur die toevoeging van een koolstofatoom op 'n keer; desorpsie, wat lei tot die vorming van 'n olefien as eindproduk; hidrogenasie, wat die vorming van 'n paraffien tot gevolg het. Die sleutelaanname is dat die onderskeie tempo's van kettinggroei en hidrogenasie onafhanklik is van kettinglengte, maar dat die desorpsietempo afhanklik is van koolstofgetal weens die fisiesorpsie van die intermediêr op die katalisatoroppervlak. Hoe langer die ketting, hoe groter die fisiesorpsie en hoe laer die tempo van desorpsie relatief tot die tempo's van groei en hidrogenasie; gevolglik is daar 'n toename in groeiwaarskynlikheid en in versadigtheid met kettinglengte. Die model kon die olefien- en paraffienverspreidings in die C_3 tot C_{10}

bereik baie akkuraat voorspel. Op grond van meganistiese oorwegings is daar sekere aanpassings in die modelvergelykings van die C_2 intermediêr aangebring, waarna die model suksesvol geëkstrapoleer kon word na die C_1 and C_2 produkte. Hierdie is 'n werklike ekstrapolasie, aangesien die C_1 and C_2 data nie gebruik is vir die afskatting van die parameterwaardes nie. Hierdie is vermoedelik die eerste produkkarakteriseringsmodel wat suksesvol toegepas kan word op die C_1 and C_2 komponente sonder dat addisionele (unieke) modelparameters aangewend hoef te word vir genoemde produkte.

Daar is bevind dat die nuwe produkkarakteriseringsmodel die etileen / etaan verhouding oorskat en boon-op 'n hoër olefien / paraffien verhouding vir die C_2 fraksie voorspel as vir die C_3 fraksie. Hierdie verskil tussen modelvoorspellings en gemete waardes is toegeskryf aan die sekondêre hidrogenasie van etileen, in lyn met eksperimentele bevindings in die literatuur. Ter bevestiging van sommige aannames en implikasies van die model is data wat onder hersirkulasie in 'n laboratorium-flodder reaktor gemeet is, geanaliseer. Die resultate het die volgende aangetoon: (a) geen merkbare herinkorporasie van etileen of propileen nie; (b) hoë tempo's van skondêre etileenhidrogenasie; (c) lae (byna weglaatbare) tempo's van skondêre propileenhidrogenasie. Nadat snelheidskonstantes vir sekondêre hidrogenasie afgeskat is, kon aangetoon word dat die voorspelde primêre etileen / etaan verhouding inderdaad hoër is as die voorspelde propileen / propaan verhouding, in presiese ooreenstemming met die kettinglengte-afhanklike desorpsiemodel.

Summary

Kinetic and Selectivity Modelling of the Iron-Based Low-Temperature Fischer-Tropsch Synthesis

The Fischer-Tropsch (FT) synthesis provides a method of converting syngas, obtained from the gasification of crude oil alternative sources such as coal, natural gas or biomass, to liquid fuels suitable for use in standard motor vehicles. The economic viability of a commercial FT plant is highly dependent on the crude oil price, which has fluctuated considerably during the past few decades. Probably due to the risk of an ill-timed slump in crude oil prices, world-wide application of the technology has been somewhat restricted. However, due to the current high oil prices, there is at present a renewed interest in coal and natural gas as alternative energy sources, and consequently the FT process is receiving wide-spread attention. The FT synthesis has been applied commercially in different forms, but the focus of this study has been specifically on the "iron-based Low-Temperature Fischer-Tropsch" (Fe-LTFT) synthesis. This process is characterised by the use of an alkali-promoted iron catalyst, synthesis temperatures around 240°C, and a product slate that extends well into the wax range. An accurate prediction of the process performance is very important for the design of a commercial FT plant. There are three main aspects that should be addressed in terms of the modelling of the Fe-LTFT synthesis, namely the rate of CO conversion to hydrocarbons (*FT kinetics*), the rate of CO conversion to CO_2 (*WGS kinetics*) and the distribution of hydrocarbon products (*product selectivities*).

FT kinetics

Even though water (or carbon dioxide) has traditionally been included in FT rate expressions for the iron-FT synthesis, a critical literature review revealed that there is no conclusive evidence for the premise that either of these two components adversely affects the FT kinetics per se. Instead is was shown that the observed influence of water can also be explained by its effect on the water-gas-shift (WGS) reaction rate, which in turn affects the gas phase partial pressures of the reactants (CO and hydrogen) and therefore indirectly also the hydrocarbon formation rate. The FT rate equation proposed in this study did originally contain a water term, but after testing the expression against a variety of existing data sets, it was concluded that there was no statistical basis for including water in the kinetic model. Following an experimental design procedure, new kinetic data were measured which could conclusively discriminate between the traditional rate equations (accounting for an influence of water) and the following new kinetic expression (which assumes no influence of water on the FT kinetics):

$$r_{FT} = A\frac{P_{H_2}{}^{0.5}P_{CO}}{\left(1+k_{CO}P_{CO}\right)^2}$$

WGS kinetics

Originally it was proposed in literature that the WGS kinetics can be described by a simple first order expression in CO, but more recently models derived from mechanisms based on the formation of a formate intermediate seem to be favoured. In this study it was shown that a first order rate equation in CO is a reasonable description of the WGS rate, but contains systematic deviations indicative of its empirical nature. It was further found that models based on the formate mechanism described the historic data the best. After evaluating the rival equations with newly measured data, the following expression emerged as the preferred WGS kinetic model:

$$r_{WGS} = A \frac{P_{CO}P_{H_2O} - \frac{1}{K_{WGS}}P_{H_2}P_{CO2}}{\left(1 + k_{H_2O}P_{H_2O} + k_{OH}\frac{P_{H_2O}}{P_{H_2}^{0.5}}\right)^2}$$

The new kinetic models for the Fe-LTFT synthesis imply that the FT and WGS reactions occur on different types of sites. Whereas the FT sites are predominantly covered with adsorbed CO or C_1 intermediates, the WGS sites are mostly covered with adsorbed water and OH species.

Selectivity modelling

Two types of product characterisation models for the FT synthesis are known in literature, namely double-α models and olefin reinsertion models. In this study it was shown that there is a high degree of cross-correlation between the independent parameters of double-α models. Due to the low propensity of iron-FT catalysts for secondary olefin reactions, it was also concluded that olefin reinsertion models are not appropriate for the Fe-LTFT synthesis. Consequently, a new product characterisation model was proposed. According to the chain length dependent desorption model, olefin and paraffin formation is governed by three generic reactions: chain growth by one carbon atom at a time; chain desorption, resulting in the formation of an olefin; chain hydrogenation, resulting in the formation of a paraffin. The cornerstone assumption is that the rates of chain growth and hydrogenation are independent of chain length, but that the rate of desorption is a function of carbon number due to the physisorption of the chain on the catalyst surface. The longer the chain, the greater the physisorption and the slower the rate of desorption relative to growth and hydrogenation; consequently, there is an increase in growth probability and saturation with chain length. The model could accurately describe the olefin and paraffin distributions in the C_3 to C_{10} range. After making some mechanistically-rationalised adjustments to the model equations for the case of the C_2 intermediate, the model could be extrapolated to the C_1 and C_2

products as well. This is a true extrapolation, as the C_1 and C_2 data were not used for the estimation of the parameter values. This may be the first product characterisation model that can successfully be extrapolated to the C_1 and C_2 components without introducing additional (unique) parameter values for these products.

It was found that the chain length dependent desorption model overestimates the ethylene / ethane ratio and predicts a higher olefin / paraffin ratio for the C_2 fraction than for the C_3 fraction. Consistent with the results of ethylene co-feeding studies reported in literature, this was ascribed to the secondary hydrogenation of ethylene. Data measured in a laboratory slurry reactor operated under recycle were used as further support for some of the assumptions and implications of the product characterisation model. These results indicated negligible reinsertion rates of both ethylene and propylene, high rates of secondary ethylene hydrogenation and very low (almost negligible) rates of secondary propylene hydrogenation. After estimating rate constants for secondary hydrogenation, it was shown that the predicted primary ethylene / ethane ratio was higher than the predicted primary propylene / propane ratio, consistent with the chain length dependent desorption model.

Chapter 1

Introduction

1. Brief history and relevance of the Fischer-Tropsch synthesis

Due to a drive for petroleum independence, the Fischer-Tropsch (FT) synthesis was initially applied industrially in Germany from the late 1930's in the form of the "cobalt medium pressure synthesis", but operation of these plants ceased after the second world war[1]. Motivated by a world-wide anticipation of rising crude oil prices, the next large scale commercial operation was built in Sasolburg, South Africa, during the 1950's by Sasol[2]. This factory employed two different types of iron-based FT processes, namely the tubular fixed bed Arge process and the circulating fluidised bed process from Kellogg[1]. Prompted by the oil crises in the 1970's, Sasol decided on an enormous expansion of its FT production capacity by building two much larger plants in Secunda. Both were based on improved circulating fluidised bed technology and came on stream in 1980 and 1982, respectively[2]. Originally all of Sasol's operations in South Africa used synthesis gas derived from coal, although in recent years this has been supplemented by syngas obtained from natural gas reforming. In fact, the commercial plant in Sasolburg currently exclusively uses reformed natural gas as feedstock. Some significant advances in reactor technology at Sasol saw the circulating fluidised bed reactors being replaced by fixed fluidised bed reactors (known as Sasol Advanced Synthol or "SAS" reactors) in Secunda, while a slurry phase reactor was built in Sasolburg as an alternative to the Arge fixed bed process[3,4,5]. Two more commercial FT plants were commissioned during the early 1990's, both based on natural gas as feedstock. These were the Shell Middle Distillate Synthesis performed in multi-tubular trickle-bed reactors (Bintulu, Malaysia – 1992)[6] and the Mossgas plant based on Sasol's improved iron-FT circulating fluidised bed technology (Mosselbay, South Africa – 1993)[2,7]. With the recent commissioning of Sasol's cobalt-based slurry phase FT process in Qatar (also utilising natural gas as

feedstock), the Oryx plant became the latest commercial FT production facility in the world. A brief summary of the most important commercial FT plants is provided in Table 1. More information on the historical development of the FT process and some general aspects of the synthesis can be found elsewhere[2,8,9].

Despite the commercial ventures presented in Table 1, the large scale application of FT in the wider world has never really materialised. The reason for this is probably related to the fact that the economic viability of a synthetic fuels plant is highly dependent on the crude oil price, which has varied considerably over the past few decades[2]. Due to the high investment costs of these production facilities, there is obviously a substantial risk associated with the construction of an FT complex. As pointed out by Dry[2], this has led to mixed success, since the FT factory in Secunda came on stream at a time when oil prices were very high, while other plants (the original plant in Sasolburg, as well as those in Bintulu and Mosselbay) only started producing when the oil price had already dropped down to much lower levels than when the respective projects were initiated. Sasol's latest plant in Qatar may prove to be another success story, as it is also coming on stream at a time of record high oil prices. Despite this apparent mixture of commercial fortunes, it is clear from Table 1 that (apart from the factories in Word War II Germany), all FT plants are still in production and currently probably highly profitable. It thus seems as if history has taught us that FT plants are economically viable when judged over extended periods of time (say two to three decades). Presumably then the problem with investing in a large scale FT complex is that a company may not be able to maintain acceptable cash flow during an ill-timed period of unfavourable oil prices, compounded by the fact that share holders typically expect much quicker returns on their investments.

The world is currently in an era where a rising crude oil price makes coal and natural gas increasingly attractive as feedstocks. For example, there has in recent years been a renewed interest in the conversion of coal to liquid fuels, which is especially relevant for countries with abundant coal reserves and a shortage of other energy sources, such as the USA, China, India, Australia and South Africa[1]. Additionally, the gasification of biomass is expected to become increasingly more

Table 1: Most important commercial FT plants

Company	Location	Carbon feedstock	Catalyst type	Reactor type	Period of operation	Total plant capacity (approx.) (bbl / day)
Ruhrchemie[1,2,12,13]	Germany	Coke	Co/kieselguhr	Packed bed (vertical metal sheets)	1936 – after second world war	2 000 – 2 500
Sasol [1,2,3,13]	Sasolburg, South Africa	Initially coal, currently natural gas	Fused Fe/K	Circulating fluidised bed (decommissioned)	1955 – ca. 1985	5 000 (currently)
			Precipitated Fe/K	Multi-tubular fixed bed	1955 – present	
			Precipitated Fe/K (spray dried)	Slurry phase reactor	1993 – present	
Sasol [1,2,3,4,13]	Secunda, South Africa	Mostly coal, now supplemented by natural gas	Fused Fe/K	Circulating fluidised bed	1980 – 1999	> 124 000 (currently)
				SAS reactor	1995 – present	
Shell [2,6,7,10,11]	Bintulu, Malaysia	Natural gas	Co/SiO_2	Multi-tubular fixed bed	1992 – present	12 000
Mossgas (PetroSA) [1,2,3]	Mosselbay, South Africa	Natural gas	Fused Fe/K	Circulating fluidised bed	1993 – present	20 000
Sasol [3,10]	Ras Laffan, Qatar	Natural gas	Co/Al_2O_3	Slurry phase	1997 – present	34 000

important in future as there is a strong world-wide drive to exploit renewable energy sources. In principle, any carbon source that can be gasified to produce synthesis gas (a mixture of CO and hydrogen) can be converted to high quality transportation fuels by utilising the FT synthesis[10].

2. FT as a heterogeneously catalysed synthesis

In short, the FT reaction involves the hydrogenation of CO over a heterogeneous catalyst to an array of hydrocarbons. Even though a variety of metals are known to catalyse CO hydrogenation reactions in general and the FT reaction in particular, only catalysts based on iron or cobalt are of industrial significance for the FT synthesis[11,12]. The FT synthesis is distinguished from other CO hydrogenation reactions in that the product spectrum consists mainly of linear alkanes and alkenes (from methane to long chain waxes) with a carbon number distribution characteristic of a polymerisation mechanism. Additional products that are formed include branched aliphatic compounds, alcohols, aldehydes, ketones, acids and (at sufficiently high operating temperatures) even aromatics[13]. It is not always clear which of these compounds are primary products of the FT synthesis and which are formed subsequently by secondary reactions. However, it is known that certain compounds (e.g. olefins and alcohols) can undergo a variety of secondary reactions, such as hydrogenation, double bond shift, chain branching, conversion to heavier compounds, etc[7,14].

Normally the bulk of the oxygen from CO dissociation is discarded as water, but over certain catalysts a significant portion of the oxygen is also discarded as carbon dioxide. The latter occurs especially over iron-FT catalysts and is often visualised as a separate consecutive reaction, namely the water-gas-shift (WGS)[7]. Stoichiometrically, the overall process can be represented as follows[8]:

$$\text{FT:} \quad CO + 2H_2 \rightarrow -CH_2- + H_2O \qquad ...1$$

$$\text{WGS:} \quad CO + H_2O \rightleftharpoons H_2 + CO_2 \qquad ...2$$

Three FT catalyst platforms have been applied commercially, namely alkali-promoted fused iron catalysts, alkali-promoted precipitated iron catalysts, and supported cobalt catalysts. Iron-based catalysts need alkali promotion to attain the desired activity and selectivity, since there is a strong shift in the product spectrum towards heavier products as the alkali level in the catalyst increases[12,13]. Structural promoters, such as silica or alumina, and a reduction promoter, such as copper, are often also added[12,13]. Due to the cost of the metal, cobalt-FT catalysts are normally supported on stable oxides[11]. From the patent literature, it appears as if Shell has concentrated on silica and Exxon on titania as supports, while other companies (e.g. Sasol, Statoil and Syntroleum) seem to prefer alumina[11]. These supports are often modified to enhance stability and performance.

Typically, FT catalysts are reduced (e.g. in hydrogen) to the metallic form prior to synthesis. It is important to understand the solid phase reactions and changes that the catalysts undergo during the FT synthesis. The most vivid of these comes from the fact that metallic iron is not stable under synthesis conditions and is transformed to a mixture of iron carbides and iron oxides[13]. Furthermore, both iron- and cobalt-based catalysts can deactivate via a variety of mechanisms, e.g. poisoning by sulphur compounds or other components, reoxidation, formation of carbonaceous deposits, etc.[11,13]. These issues of phase changes and deactivation can complicate kinetic and selectivity measurements and have to be taken into account during such studies. It also means that laboratory investigations using freshly reduced catalyst for fairly short periods are not always of industrial relevance, as the possible deterioration of activity and selectivity is of major importance.

3. Classification of FT processes

There are obviously various ways to classify the different types of FT processes. Such a classification can, for example, be based on the type of metal that catalyses the reaction, the temperature range in which the synthesis is performed, the phases present inside the reactor (i.e. gas-solid or gas-liquid-solid) or the type of reactor used. Sasol commercially operates three distinctly different types of FT processes

and has developed terminology to refer to each of these. The *iron-based Low-Temperature Fischer-Tropsch* (Fe-LTFT) synthesis is typically performed in the temperature range of 220°C to 250°C and the product spectrum includes substantial amounts of long chain molecules, giving rise to a three-phase system inside the reactor (gas, liquid and solid)[5]. The *cobalt-based Low-Temperature Fischer-Tropsch* (Co-LTFT) synthesis is operated towards the lower end of this temperature range and produces a similar product distribution. These two LTFT syntheses can commercially be operated either in multi-tubular packed bed reactors or in slurry phase reactors where the fine catalyst particles are suspended in the liquid product of the process[2]. The *iron-based High-Temperature Fischer-Tropsch* (Fe-HTFT) synthesis is characterised by operating temperatures well above 300°C, as well as a lighter product slate that is essentially completely in the gas phase under the conditions inside the reactor. This two-phase system is well suited to fluidised bed technology and the Fe-HTFT synthesis has therefore commercially been operated in circulating fluidised bed reactors (where the catalyst is transported out of the reactor before being circulated back) and more recently in fixed fluidised bed reactors [2,3].

Typical product distributions for the three commercial FT processes have been reported by Dry[8] and are presented here in Table 2. The olefin / paraffin ratios of selected product fractions are also included in this table. These data indicate the following: the HTFT product spectrum is much lighter than that of the two LTFT processes; iron-FT catalysts produce much more oxygenates than cobalt-FT catalysts; iron-FT catalysts, especially in the HTFT synthesis, produce a much more olefinic product spectrum than cobalt catalysts. This means that the Fe-HTFT synthesis is ideally suited to the production of gasoline and light olefins, whereas the two LTFT processes are best suited to the production of middle distillates (after wax hydrocracking) and speciality waxes (as well as heavier olefins in the case of Fe-LTFT).

Typical flow schemes for various types of FT plants have been presented in the literature[10,15,16]. Essentially these all consist of three basic steps. In the first step, the carbon source (e.g. coal or natural gas) is reacted in the presence of oxygen and

steam. After gas cleanup, the synthesis gas goes to the FT section where a variety of hydrocarbons are produced. The third step is separation and upgrading to final products. Low value light products can also be recycled to the first step and converted back to syngas.

Table 2: Typical product distributions reported by Dry[8] for Sasol's three commercial FT processes

Process	**Co-LTFT**	**Fe-LTFT**	**Fe-HTFT**
Reactor type	Slurry	Slurry	Fluidised bed
Synthesis Temperature (°C)	220	240	340
Selectivities (C atom %)			
CH_4	5	4	8
C_2H_4	0.05	0.5	4
C_2H_6	1	1	3
C_3H_6	2	2.5	11
C_3H_8	1	0.5	2
C_4H_8	2	3	9
C_4H_{10}	1	1	1
$C_5 - C_6$	8	7	16
C_7 – 160°C	11	9	20
160°C – 350°C	22	17.5	16
> 350°C	46	50	5
Oxygenates (water soluble)	1	4	5
Olefin / paraffin ratios			
$C_5 - C_{12}$ fraction	0.65	2.2	5.4
$C_{13} - C_{18}$ fraction	0.05	1.1	4.0

4. Scope and outline of the thesis

FT plants are generally large scale processes that are highly integrated to ensure maximum efficiency for energy and syngas utilisation. For example, an acceptable gas loop design of a plant may not allow for the laboratory-optimised process conditions. Furthermore, the scale-up of the catalyst manufacturing and of the reactors from laboratory, through pilot and demonstration scales to commercial

application always brings about unexpected problems that must be resolved. On both these accounts, an accurate description of the kinetic and selectivity behaviour of the catalyst is of the utmost importance. Kinetic and selectivity models are not only necessary to optimise the design of the process, but also to identify and quantify deviations from the expected behaviour during scale-up to ensure that acceptable performance is ultimately achieved on commercial scale. This thesis will focus exclusively on the kinetic and selectivity modelling of the Fe-LTFT synthesis.

In the Fe-LTFT synthesis, both the FT and WGS reactions (Equations 1 and 2, respectively) occur to a significant extent. Clearly the balance of CO and hydrogen in a commercial gas loop will be influenced by the relative rates of these two reactions; hence the necessity to model both the FT and the WGS kinetics. It is also important to predict the distribution of hydrocarbons produced by the process, as not all the product fractions are of equal value. Furthermore, light components (especially methane) are difficult to separate from the unconverted reagents and their build-up in recycle streams is one of the integral aspects that must be considered during plant design. This means that there are three main aspects that should be addressed in terms of the modelling of the Fe-LTFT synthesis, namely the rate of CO conversion to hydrocarbons, the rate of CO conversion to CO_2, and the distribution of hydrocarbon products. These will, respectively, be referred to as *FT kinetics*, *WGS kinetics* and *product selectivities* in the terminology of this dissertation.

After studying the literature on the Fe-LTFT synthesis, it became evident that there are certain beliefs regarding the FT kinetics and the hydrocarbon product distribution that are not necessarily supported by the published experimental results. The critical literature reviews of Chapters 2 and 3 on the kinetic and selectivity models, respectively, highlight these possible inconsistencies and attempt to define opportunities for improvement. The FT kinetic investigation reported in Chapter 4 was intentionally not constrained by some of the existing beliefs (e.g. FT rate inhibition by product water or CO_2) and yielded findings at variance with foregoing conclusions in the literature. Chapter 5 addresses the issue

of WGS kinetics and the outcome was essentially in line with the findings of other published studies on the subject. Since it was not believed that either of the two existing classes of selectivity models is appropriate for the Fe-LTFT synthesis, a new product characterisation model is proposed in Chapter 6. Some of the implications of this model were counterintuitive and are therefore addressed in Chapter 7. Finally, the overall conclusions of the Fe-LTFT modelling study and the scope for future work are discussed in Chapter 8.

References

1. Steynberg, A.P. Introduction to Fischer-Tropsch Technology. In Steynberg, A.P.; Dry, M.E., Eds. Fischer-Tropsch Technology, *Stud. Surf. Sci. Catal. Vol 152*, Elsevier: Amsterdam, 2004, Chapter 1.
2. Dry, M.E. The Fischer-Tropsch Process: 1950 – 2000. *Catal. Today* 2002, 71, 227.
3. Steynberg, A.P.; Dry, M.E.; Davis, B.H.; Breman, B.B. Fischer-Tropsch Reactors. In Steynberg, A.P.; Dry, M.E., Eds. Fischer-Tropsch Technology, *Stud. Surf. Sci. Catal. Vol 152*, Elsevier: Amsterdam, 2004, Chapter 2.
4. Steynberg, A.P.; Espinoza, R.L.; Jager, B.; Vosloo, A.C. High Temperature Fischer-Tropsch in Commercial Practice. *Appl. Cat. A* 1999, 186, 41.
5. Espinoza, R.L.; Steynberg, A.P.; Jager, B.; Vosloo, A.C. Low Temperature Fischer-Tropsch Synthesis from a Sasol Perspective. *Appl. Cat. A* 1999, 186, 13.
6. Senden, M.M.G.; Punt, A.D.; Hoek, A. Gas-to-Liquids Processes: Current Status & Future Prospects. *Stud. Surf. Sci. Catal.* 1998, 119, 961.
7. Van der Laan, G.P.; Beenackers, A.A.C.M. Kinetics and Selectivity of the Fischer-Tropsch Synthesis: A Literature Review. *Catal. Rev. – Sci. Eng.* 1999, 41 (3&4) 255.
8. Dry, M.E. Chemical Concepts Used for Engineering Purposes. In Steynberg, A.P.; Dry, M.E. , Eds. Fischer-Tropsch Technology, *Stud. Surf. Sci. Catal. Vol 152*, Elsevier: Amsterdam, 2004, Chapter 3.

9. Stranges, A.N. A History of the Fischer-Tropsch Process in Germany 1926-1945. In Davis, B.H.; Ocelli, M.L., Eds. Fischer-Tropsch Synthesis, Catalysts and Catalysis, *Stud. Surf. Sci. Catal. Vol 163*, Elsevier: Amsterdam, 2007, Chapter 1.
10. Dry, M.E.; Steynberg, A.P. Commercial FT Process Application. In Steynberg, A.P., Dry, M.E., Eds., *Stud. Surf. Sci. Catal. Vol. 152*, Elsevier, Amsterdam, 2004, Chapter 5.
11. Dry, M.E. FT Catalysts. In Steynberg, A.P.; Dry, M.E. , Eds. Fischer-Tropsch Technology, *Stud. Surf. Sci. Catal. Vol 152*, Elsevier: Amsterdam, 2004, Chapter 7.
12. Schulz, H. Short History and Present Trends of Fischer-Tropsch Synthesis. *Appl. Cat. A* 1999, 186, 3.
13. Dry, M.E. The Fischer-Tropsch Synthesis. In Anderson, J.R.; Boudart, M. Eds. *Catalysis Science and Technology Vol. 1*; Springer: Berlin, 1981, Chapter 4.
14. Tau, L.; Dabbagh, H.A.; Davis, B.H. Fischer-Tropsch Synthesis: Comparison of ^{14}C Distributions when Labelled Alcohol is Added to the Synthesis Gas. *Energy & Fuels* 1991, 5, 174.
15. Van der Laan, G.P. Kinetics, Selectivity and Scale Up of the Fischer-Tropsch Synthesis. Ph.D. Thesis, Rijksuniversiteit Groningen, 1999.
16. Van Dijk, H.A.J. The Fischer-Tropsch Synthesis: A Mechanistic Study using Transient Isotopic Tracing. Ph.D. Thesis, Technische Universiteit Eindhoven, 2001.

Chapter 2

Literature Review of FT Kinetic Models for the Fe-LTFT Synthesis

Publications from this chapter

Botes, F.G. The Effects of Water and CO_2 on the Reaction Kinetics in the Iron-Based Low-Temperature Fischer-Tropsch Synthesis: a Literature Review. *Catal. Rev. Sci. Eng.* 2008, accepted for publication.

Abstract

A review of kinetic models for the iron-based Fischer-Tropsch synthesis revealed some important areas of progress, namely (a) a transition from rate equations with a first order denominator (consistent with an Eley-Rideal type mechanism) to Langmuir-Hinshelwood expressions with a second order inhibition term; (b) whereas kinetic models originally specified full coverage of the catalytic surface, later models found the influence of vacant sites to be important; (c) whereas water or CO_2 was traditionally always included in the FT rate equations, the most recent kinetic expressions do not account for any influence of water. It was further concluded that the perceived inhibiting influence of water on the FT rate may have been an indirect effect via the water-gas-shift reaction that changed the hydrogen and CO partial pressures.

1. Introduction

The Fischer-Tropsch (FT) synthesis is a commercially proven method for converting synthesis gas (a mixture of hydrogen and carbon monoxide) to a broad range of hydrocarbons. Synthesis gas can be derived from a variety of feedstocks, e.g. coal, biomass or natural gas. In recent years there has been a renewed interest in the FT process, amongst others for the conversion of coal to liquid fuels. This is especially relevant for countries with abundant coal reserves and a shortage of other energy sources, such as the USA, China, India, Australia and South Africa[1]. The iron-based Low-Temperature Fischer-Tropsch (Fe-LTFT) synthesis is ideally suited for the conversion of coal-derived synthesis gas to an array of hydrocarbon products, including waxes and transportation fuels[2]. As highlighted in literature, the kinetic and selectivity modelling of the FT synthesis are important aspects for the commercial application of the technology[3].

Apart from some empirical power law rate equations, the models proposed in literature for describing the kinetics of the Fe-LTFT synthesis can broadly be organised into two classes. The first has been to derive rate expressions based on Eley-Rideal or Langmuir-Hinshelwood type mechanisms to predict the overall rate of CO (or syngas) conversion to hydrocarbons[3]. Since these rate expressions generally do not take any cognisance of the distribution of hydrocarbon products, an additional selectivity model would be required to fully describe the process. Another approach has been to develop comprehensive kinetic models describing the conversion of syngas to a distribution of final products[4-6].

2. Explicit rate expressions for the iron-FT synthesis

2.1 General background

From the review by Van der Laan and Beenackers[3], it is clear that there is little consensus in the literature on the form of the macro kinetic model for the rate of hydrocarbon formation in the iron-FT synthesis. Various research groups have proposed a new kinetic equation to describe their own data. Despite these discrepancies, there seems to be a few common features to the various kinetic

models. The most obvious is the usual assumption that water has a strong inhibiting influence on the reaction rate, a notion that has been explicitly stated or concluded in numerous publications on the iron-FT synthesis over the past 40 years[3,7-16]. In terms of the Langmuir-Hinshelwood-Hougen-Watson type of kinetic expressions, this has been rationalised as a competitive adsorption effect between water (a product of the FT reaction) and carbon monoxide (one of the reactants) on the catalyst surface[12,17]. For some kinetic studies where the water-gas-shift (WGS) reaction was so fast that almost all of the water was converted to carbon dioxide, it was necessary to include CO_2 in the inhibition term of the rate equation to be able to describe the data[18]. These researchers acknowledged that water has a much more substantial inhibition effect on the FT reaction rate than CO_2; consequently, the interpretation of the finding was that the weaker influence of carbon dioxide only became apparent in the absence of a significant water concentration. This has sparked some debate in the literature over whether or not carbon dioxide has an inhibiting effect on iron-FT kinetics. It thus appears as if the discrepancies between the popular iron-FT rate expressions have historically centred on the inhibition terms of the rate equations. There was disagreement on which product compounds (water and / or carbon dioxide) must be accounted for and how to include them in the denominator of the kinetic equations. Subsequently, it will be shown from the historic development of rate equations (presented in Table 1) that there has always been a question mark over the premise of product inhibition of the FT reaction rate over iron catalysts and that the latest findings are that the kinetics can be described well without accounting for an effect of water or CO_2.

2.2 Development of kinetic models based on the premise of rate inhibition by water or CO_2

From experimental studies performed at the US Bureau of Mines, it was concluded that the FT reaction rate was proportional to the hydrogen partial pressure up to conversions of about 60%[19]. Deviations at higher conversions were ascribed to a catalyst oxidation effect due the high partial pressures of product water. It was thus

Table 1: Eley-Rideal and Langmuir-Hinshelwood type FT rate expressions that have been proposed for the iron-based FT synthesis

Eq. nr.	Model	Reactors and catalysts
1	$r_{FT} = A\frac{P_{H_2}P_{CO}}{P_{CO} + k_{H_20}P_{H_20}}$	Fixed bed reactor; K-promoted fused iron catalyst (unnitrided and nitrided)[19]. Fixed bed and fluidised bed reactors; Precipitated, sintered and fused alkali promoted iron catalysts[20]. Well-mixed slurry reactor; K-promoted precipitated iron catalyst[22]. Gradientless recycle reactor; K-promoted precipitated iron catalyst[8].
2	$r_{FT} = A\frac{P_{CO}P_{H_2}}{P_{CO} + k_{H_20}\left(P_{H_20}/P_{H_2}\right)}$	Well-mixed slurry reactor; K-promoted fused iron catalyst[17]. Gradientless recycle reactor; K-promoted precipitated iron catalyst[8].
3	$r_{FT} = A\frac{P_{H_2}P_{CO}}{P_{CO} + k_{CO_2}P_{CO_2}}$	Well-mixed slurry reactor; K-promoted precipitated iron catalyst[18].
4	$r_{FT} = A\frac{P_{H_2}P_{CO}}{P_{CO} + k_{H_20}P_{H_20} + k_{CO_2}P_{CO_2}}$	Well-mixed slurry reactor; K-promoted precipitated iron catalyst[18,25].
5	$r_{FT} = A\frac{P_{H_2}^{0.5}P_{CO}}{P_{CO} + k_{H_20}P_{H_20}}$	Well-mixed slurry reactor; K-promoted precipitated iron catalyst[29].
6	$r_{FT} = A\frac{P_{H_2}^{3/2}P_{CO}/P_{H_2O}}{(1 + kP_{H_2}P_{CO}/P_{H_2O})^2}$	Well-mixed slurry reactor; Unpromoted iron catalyst, K-promoted precipitated iron catalyst, K-promoted precipitated Fe/Mn catalyst[7].
7	$r_{FT} = A\frac{P_{H_2}P_{CO}}{1 + k_{CO}P_{CO} + k_{H_2O}P_{H_20}}$	Gas-solid spinning basket reactor; K-promoted precipitated iron catalyst[34,35].
8	$r_{FT} = A\frac{P_{H_2}^{0.5}P_{CO}}{\left(1 + k_{CO}P_{CO} + k_{H_2O}P_{H_20}\right)^2}$	Gas-solid spinning basket reactor; K-promoted precipitated iron catalyst[34,35].
9	$r_{FT} = A\frac{P_{H_2}P_{CO}}{\left(1 + k_{CO}P_{CO} + k_{H_2O}P_{H_20}\right)^2}$	Gas-solid spinning basket reactor; K-promoted precipitated iron catalyst[34,35].
10	$r_{FT} = A\frac{P_{H_2}^{0.5}P_{CO}^{0.5}}{\left(1 + k_{CO}P_{CO}^{0.5} + k_{CO_2}P_{CO_2}\right)^2}$	Well-mixed slurry reactor; K-promoted precipitated iron catalyst[34].
11	$r_{FT} = A\frac{P_{H_2}^{0.5}P_{CO}}{\left(1 + k_{CO}P_{CO} + k_{CO_2}P_{CO_2}\right)^2}$	Well-mixed slurry reactor; K-promoted precipitated iron catalyst[34].
12	$r_{FT} = A\frac{P_{H_2}{}^{0.5}P_{CO}}{\left(1 + k_{CO}P_{CO}\right)^2}$	Well-mixed slurry reactor; K-promoted precipitated iron catalyst[33].
13	$r_{FT} = A\frac{P_{H_2}^{5/6}P_{CO}^{2/3}}{\left(1 + kP_{CO}^{2/3}P_{H_2}^{1/3}\right)^2}$	Berty CSTR reactor; Alumina-supported iron catalyst (no alkali promotion)[36].

postulated that the reaction rate would also be proportional to the fraction of reduced iron in the catalyst, which was assumed to be determined by the competition between the reduction by CO and the oxidation by water. By combining the first order kinetics in hydrogen with the ratio of CO to the weighted sum of CO and water, Anderson[19] proposed Equation 1 to describe the FT reaction rate over iron catalysts. It can therefore be argued that Anderson never intended the equation to purely be a model of chemical reaction kinetics, but that a reversible response of the catalyst to changes in its environment was incorporated in the expression. It was reported that Equation 1 fitted data from individual experiments reasonably well, but that the parameter values varied with feed gas composition, even at constant synthesis temperature.

Years later, Dry[20] independently proposed the same kinetic equation and presented a Langmuir-Hinshelwood-Hougen-Watson type derivation. In order to obtain a first order denominator, it had to be assumed that hydrogen reacts directly from the gas phase according to an Eley-Rideal type mechanism[12,20]. Eley-Rideal mechanisms are extremely rare[21], and most transition metals can adsorb hydrogen dissociatively[3]; it therefore seems unlikely that hydrogen reacts directly from the gas phase. The perceived negative influence of water on the reaction rate was ascribed to the competitive adsorption between water and CO on the catalyst surface. Since it was assumed that the catalyst surface is fully covered by these two species, no constant term was included in the denominator. It can thus be argued that the extent of coverage by water and CO could not be tested for statistical significance, but that the inhibiting influence of water was self-specified by a prematurely-simplified model. Nevertheless, Equation 1 became the basis of many subsequent kinetic studies and was (amongst others) used by Zimmerman and Bukur[22] and Shen et al.[8] to describe their own kinetic data. It is, however, significant to note that a wide range of values has been obtained at Sasol over the years for the water adsorption coefficient (k_{H_2O}) in the Anderson-Dry model, even for data measured with the same catalyst at the same temperature. This is consistent

with the reports by Anderson and implies that the extent of the apparent water inhibition is dependent on the feed gas composition.

When Huff and Satterfield[17] tested Equation 1 against their own data, it was found (like at the US Bureau of Mines and at Sasol) that the water adsorption coefficient varied with reactant partial pressures. It was proposed that k_{H_2O} is inversely proportional to the hydrogen partial pressure, which yielded the Satterfield-Huff expression (Equation 2).

A research group at the University of Oldenburg performed a number of Fe-LTFT kinetic studies, mostly on an alkali-promoted iron catalyst with a high WGS activity and syngas feeds with low H_2/CO ratios[18,23-26]. In some cases, the extent of WGS was so high that virtually all the water produced by the hydrocarbon synthesis was shifted to carbon dioxide. Nevertheless, a direct proportionality between the FT reaction rate and the hydrogen partial pressure (as would be expected from Equations 1 and 2 at very low water concentrations) was not found. Consequently, rate inhibition by CO_2 was assumed and Equation 3 was formulated[18]. After subsequent studies where a much wider range of process conditions was covered, the general conclusion was that rate inhibition by product water was only evident when the H_2/CO ratio of the syngas feed was above 0.8. At lower H_2/CO feed ratios, inhibition of the reaction rate by carbon dioxide had to be assumed to adequately describe the data. A generalised rate expression was proposed (Equation 4), which should in principle be able to account for a strong inhibiting effect of water and a slight inhibiting effect of carbon dioxide. However, it was reported that this kinetic model was not very successful when tested over a wide range of conditions[25]. In addition, there is strong evidence in literature that carbon dioxide, even up to very high partial pressures, has no significant influence on iron-FT kinetics[27,28]. At first glance the findings of the Oldenburg group regarding CO_2 rate inhibition seem to be at variance with other iron-FT kinetic studies, but in actual fact there is a remarkable agreement with the foregoing studies. In all cases the perceived inhibiting role of water was found to be highly dependent on the feed gas composition.

Van Berge[29] viewed Equations 1 to 4 as members of the same family and followed a statistical design procedure to discriminate between them. The statistical design method eventually selected operating conditions where each of the equations failed comprehensively. The conclusion was that a generalised expression was required to describe the reaction rate. After further parameter optimisation, it was concluded with a high degree of statistical confidence that the generalised model could be simplified to Equation 5. Evidently the difference between the rate equation proposed by Van Berge[29] and Equations 1 to 4 is that the hydrogen reaction order of the former has a value of 0.5 (as opposed to a value of unity or higher for the original models). The systematic statistical approach was very valuable to highlight shortcomings in the existing rate equations at the time. Unfortunately though, the first order denominator was retained, while the premise that the surface is fully covered with CO and water was still specified by the approach (and not tested for validity).

Keyser et al.[30] reported an FT kinetic study on a cobalt-manganese oxide catalyst, which (unusually for cobalt-based FT catalysts) exhibited substantial WGS activity. It was found that the Anderson-Dry rate expression (Equation 1) developed for iron catalysts could describe the FT kinetics with similar accuracy to one of the traditional cobalt-FT expressions. It was concluded that the cobalt-manganese oxide catalyst had an FT behaviour very similar to that of iron-based catalysts. Espinoza[31] used the data measured with the cobalt-manganese oxide catalyst, as well as data from other catalysts, to formulate a unified approach to the study of FT kinetics. By fitting the Anderson-Dry equation to the data from a variety of catalysts, it was shown that the water coefficient in the rate expression was determined by the WGS activity of the catalyst.

Van Steen and Schulz[7] proposed a kinetic scheme for the FT reaction where it was not necessary to apply the assumption of a slow, rate determining step. Instead, it was assumed that the FT reaction proceeds via a series of consecutive, irreversible hydrogenation steps. From the proposed scheme, Equation 6 was derived. Water still played a significant role in the kinetics, not by competing with CO for adsorption onto catalytic sites, but via a mechanism where water influences the

concentration of a surface carbon intermediate. In principle this novel approach could have explained the apparent ambiguities in the role of water (alluded to earlier). However, there are a few concerns about Equation 6. The model predicts a zero reaction rate in the absence of water, which is not consistent with observation[32]. Furthermore, there still seems to be a lack of proof that this rate expression can adequately describe iron-FT kinetic data[33].

Van der Laan initially studied the FT kinetics of a Ruhrchemie precipitated iron catalyst in a gas-solid environment (well-mixed spinning basket reactor)[34,35]. Various Langmuir-Hinshelwood-Hougen-Watson type kinetic expressions were derived for the FT reaction. Each model was optimised with two forms of the site balance equation: the first site balance accounted for vacant sites, adsorbed CO and adsorbed H_2O, while the second only accounting for adsorbed CO and H_2O (i.e. assuming complete coverage of the catalyst surface). By means of a statistical procedure, some of the rival kinetic models were eliminated, until three models (Equations 7-9) were left which were considered to be statistically indistinguishable. It is noteworthy that all three of these "best-fit" models accounted for the effect of vacant sites on the surface, suggesting that it is important to include this aspect in the site balance equation. The initial investigation was followed by a kinetic study in a well-mixed three phase (gas-liquid-solid) slurry reactor, utilising the same Ruhrchemie catalyst as before[34]. The same seven models developed earlier were tested with the new data set, but (without clearly explaining why) the water term in each equation was now replaced with CO_2. This was rationalised by the low concentration of H_2O compared to that of CO_2 and by the fact that some other researchers have considered CO_2 inhibition to be significant under certain conditions. As previously, two forms of the site balance equation were tested for each kinetic model, namely one that included and one that excluded the effect of vacant sites. The statistical procedure eliminated the models that could not describe the data well until two rate expressions (Equations 10 and 11) were left. As before, both "best-fit" equations included the effect of vacant sites in the inhibition term. However, considering the 95 % confidence intervals reported for the parameter values, it is not convincing that the CO_2

adsorption coefficients were significantly different from zero. It is thus doubtful whether CO_2 should have been included in the final rate equations developed from the slurry reactor experiments. The two kinetic studies performed by Van der Laan on the same catalyst are therefore in disagreement with each other regarding the effects of water and CO_2.

From Table 1, it is important to note the progression in iron-FT rate equations brought about Van Steen and Schulz[7] and Van der Laan and Beenackers[35]. Firstly, there was a transition from Eley-Rideal type mechanisms (where hydrogen was assumed to react directly from the gas phase) to arguably more plausible Langmuir-Hinshelwood mechanisms (where chemical reactions are assumed to occur between adsorbed species on the catalyst surface). The second was the inclusion of a constant term in the denominator which accounted for the effect of vacant sites.

2.3 Kinetic models that do not account for rate inhibition by water or CO_2

Based on a reinterpretation of the systematic study by Van Berge[29], an iron-FT kinetic model was recently proposed at Sasol[33]. Originally the expression had the form of Equation 8, but after testing the model against various historic sets of data from literature, it was concluded that there was no statistical basis for including the water term. Consequently, the model was simplified to Equation 12, which described the published kinetic data from a variety of studies better than the rate expressions incorporating effects of water or CO_2 (see Table 2, compiled from results reported by Botes and Breman[33]). After an experimental design exercise, new kinetic measurements were performed which conclusively discriminated between Equation 12 and those that accounted for an influence of water on the reaction rate (Equations 1-6). The consistency in the findings of the kinetic study was quite encouraging: the new expression described a variety of data sets better than any of the previously proposed models; in all cases it was found that water should not be included in the model; for most data sets, the value obtained for the

CO adsorption coefficient was around 0.1. This kinetic study will be discussed in full detail in Chapter 4 of this thesis.

In another recent kinetic study on a supported iron-FT catalyst[36], Equation 13 was derived from a proposed FT reaction mechanism. A rigorous statistical design approach was followed in an attempt to obtain accurate parameter values for the rate expression. The study can be criticised from certain perspectives. For example, the methane formation rate was not included in the FT reaction rate, apparently under the assumption that all methane was formed via a non-FT mechanism. This arbitrary and questionable assumption could have influenced the findings significantly, since the methane selectivity was generally quite high (sometimes above 40% on a carbon atom basis). Furthermore, no rate expressions other than Equation 13 were considered. Nevertheless, the study did show that FT kinetic data can be described with a model that does not account for any effect of water or carbon dioxide.

Table 2:The ability of Equation 12 (a kinetic model that does not include water or CO_2) to describe various historic Fe-LTFT kinetic data sets. Table compiled from results presented by Botes and Breman[33].

Kinetic study	Originally preferred kinetic model	R^2 of originally preferred model	R^2 of Equation 12
Van Berge[29]	Equation 5	0.76	0.82
Ledakowicz et al.[18]	Equation 3	0.99	0.99
Zimmerman and Bukur[22]	Equation 1	0.90	0.96
Huff and Satterfield[17]	Equation 2	0.85 (232°C) 0.71 (248°C) 0.65 (263°C)	0.83 (232°C) 0.82 (248°C) 0.81 (263°C)

3. Water and carbon dioxide co-feeding to the iron-FT synthesis

3.1 Co-feeding studies reported in literature

It has been reported that the rate of the iron-FT reaction increases roughly linearly with operating pressure, all other things being more or less equal[19]. This means that

the reaction rate is very sensitive to the syngas partial pressure. Therefore, if the effect of water or carbon dioxide on the reaction kinetics is to be studied by means of co-feeding, one requirement would be that the partial pressure of the reactants in the reactor feed should not be affected. This can for example be achieved by increasing the reactor pressure to an appropriate extent when water or carbon dioxide is co-fed. If such a precaution is not taken, an observed lowering in the FT reaction rate upon co-feeding may (at least in part) be ascribed to the dilution of the reactants. A further complicating factor, especially for the case of water co-feeding, is the WGS reaction. For catalysts with a high WGS activity, a higher water partial pressure could lead to an increase in the rate of the WGS reaction, thereby decreasing the partial pressure of carbon monoxide and increasing that of hydrogen. Since CO is often the reactant in short supply in the iron-FT process, this alone could cause a lowering of the FT reaction rate. Table 3 provides a brief summary of the water and CO_2 co-feeding studies to the iron-FT synthesis.

Based on the results of their co-feeding studies, Karn et al.[37] concluded that water was a strong inhibitor of the FT reaction rate while CO_2 was only a slight inhibitor (Studies 1a and 1b in Table 3). However, no adjustments were made to the reactor system when either of these components was co-fed, which meant that the co-fed component significantly diluted the reaction medium. A fairly crude attempt was made to correct the data for the differences in feed syngas partial pressure, but this involved lumping hydrogen and CO together. Especially for the case of water addition, a large increase in the extent of WGS was reported, which would have changed the H_2/CO ratio inside the reactor considerably. The study also shows the disadvantages of using an integral reactor for such an investigation, since the authors back extrapolated the synthesis results to conditions of zero conversion to obtain the initial reaction rates at the entrance to the catalyst bed. These estimated initial rates, which were used for comparative purposes, introduced unnecessary uncertainty to the results. Furthermore, from the information presented, it could be inferred that the CO partial pressure inside the reactor was lower during periods of water co-feeding. Again, the integral character of the reactor used in the experiments proved undesirable for comparisons between periods of co-feeding and

Table 3: Water and carbon dioxide co-feeding studies to the iron-FT synthesis

Study nr.	Co-fed component	Reactor and catalyst	Feed H_2/CO	Amount of co-fed component in feed	Reported results and observations			
					Influence on syngas partial pressure in feed	Hydrocarbon formation rate (FT rate)	CO_2 selectivity (Extent of WGS)	CO partial pressure inside reactor
1a [37]	H_2O	Fixed bed reactor; K-promoted nitrided fused iron catalyst.	1.0	Up to 30 mol%	Decreased	Decreased	Increased substantially	Decreased*
1b [37]	CO_2	Fixed bed reactor; K-promoted nitrided fused iron catalyst.	1.0	Significant (exact amount unknown)	Decreased	Decreased slightly	Unknown	Unknown
2a [10]	H_2O	Well-mixed slurry reactor; K-promoted fused iron catalyst.	0.96	Up to 27 mol%**	Decreased	Decreased	Increased	Decreased (from about 1 to 0.2 bar)
2b [10]	H_2O	Well-mixed slurry reactor; K-promoted fused iron catalyst.	0.52	20 mol%	Decreased	No influence	Increased*	Decreased
3 [27]	CO_2	Well-mixed slurry reactor; K-promoted fused iron catalyst.	0.67 – 0.72	20 and 50 mol%	No influence (adjusted reactor pressure)	No influence	No influence*	No influence*
4 [28]	CO_2	Well-mixed slurry reactor; K-promoted precipitated iron catalyst.	Unknown	Up to 40 mol% inside reactor	P_{H_2} and P_{CO} inside reactor stayed constant	No influence	Decreased	No influence

* Not explicitly reported, but inferred from information supplied
** Higher amounts were fed, but led to irreversible catalyst deactivation

no co-feeding, as the partial pressure profiles along the bed length are not known explicitly.

Satterfield et al.[10] performed water co-feeding to the iron-FT synthesis in a well-mixed slurry reactor with inlet H_2/CO ratios of 0.96 and 0.52 (Studies 2a and 2b of Table 3, respectively). Since the reactor pressure was not adjusted during periods of co-feeding, the water acted as a diluent of the reactants and (everything being the same) would have decreased the FT reaction rate roughly in proportion to the extent of dilution. From graphical results presented by Satterfield et al.[10] for the case of a feed H_2/CO ratio of 0.96 (Study 2a), Figure 1 could be constructed. Due to the decrease in the FT rate upon water co-feeding, it was concluded that water was an inhibitor of the hydrocarbon formation reaction. However, there was clearly a significant increase in the CO_2 selectivity due to the additional water. This increased extent of WGS, together with the water dilution effect, caused a substantial lowering in the CO partial pressure inside the well-mixed reactor (from about 1 to 0.2 bar). Considering Table 1, it is clear that many historic FT kinetic models only allow for positive CO reaction orders (Equations 1-5 and 7), while the rest suggest a strong positive order at low CO partial pressures. A lowering in the syngas conversion would therefore have been expected based purely on the substantial decrease in the CO partial pressure. The CSTR character of the reactor lends itself to an easy analysis of the experimental data, but Satterfield et al.[10] merely mentioned that their kinetic model (Equation 2) overestimated the negative effect of the additional water on the FT reaction rate. For the case of an inlet H_2/CO ratio of 0.52 (Study 2b), the addition of 20 mol % water to the feed had no influence on the FT reaction rate, despite the lowering of the syngas partial pressure in the feed. This means that water actually had a beneficial effect on the FT kinetics at low H_2/CO ratios.

Yates and Satterfield[27] added up to 50 mol % carbon dioxide to the syngas feed of a well-mixed iron-FT slurry reactor (Study 3 in Table 3). Proper adjustment of the reactor pressure ensured that the inlet syngas partial pressure was not affected during periods of co-feeding. Apparently the additional CO_2 did not notably affect the WGS rate either. It was reported that no significant effect of CO_2 on the FT

reaction rate was observed at either of the two temperatures investigated (232°C and 263°C), even for reactor CO_2 partial pressures in excess of 10 bar.

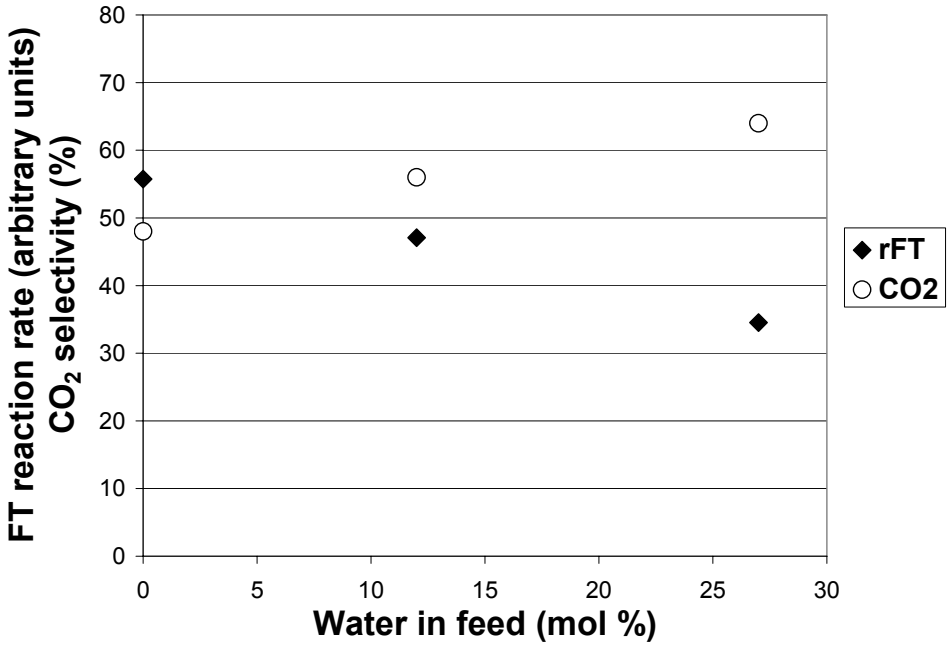

Figure 1: The experimentally observed influence of water co-feeding on the iron-FT synthesis. Data in figure are approximate values, as they were obtained from graphical information presented by Satterfield et al.[10]. Experimental conditions: inlet H_2/CO ratio of 0.96; temperature of 248°C; reactor pressure of 9.8 bar.

Riedel et al.[28] also added carbon dioxide to the iron-FT synthesis (Study 4 in Table 3). During periods of co-feeding, the argon flow rate to the reactor was decreased, while the hydrogen and CO feed rates were adapted appropriately. This ensured that the partial pressures of the other relevant components inside the well-mixed slurry reactor could be maintained at reasonably constant levels (as indicated in Table 4), even though the additional CO_2 suppressed the WGS reaction. This illustrates the advantage of using a CSTR for kinetic studies, because the direct measurements of the component partial pressures that the catalyst was exposed to showed that essentially only the CO_2 concentration was affected during co-feeding. A direct comparison of the results without any need for a kinetic analysis was therefore possible, which reduces uncertainties in the findings. It was concluded

that, within experimental accuracy, no evidence could be found that CO_2 affected the FT reaction rate.

From the foregoing discussion and the information contained in Table 3, it is clear that the co-feeding studies do not provide conclusive proof regarding the perceived inhibiting effect of water on the FT kinetics. In all cases, the addition of water to the FT synthesis significantly affected the CO and hydrogen partial pressures inside the reactor due to a dilution effect and an increased rate of WGS. Because of the changes in reagent partial pressure, the results should have been interpreted by means of a kinetic analysis, but this was not done properly. Furthermore, the role of water was apparently dependent on the feed H_2/CO ratio, as water addition to a low H_2/CO ratio feed actually proved to be beneficial to hydrocarbon product formation. To the contrary, at least two CO_2 co-feeding studies (Studies 3 and 4 in Table 3) were performed and interpreted properly. These studies conclusively showed a negligible influence of carbon dioxide on the FT reaction rate. The use of fully back-mixed slurry reactors was a notable advantage of these studies, as the reactant partial pressures that the catalyst was exposed to could be directly measured in the reactor tail gas. This enabled direct comparison between the baseline synthesis conditions and periods where carbon dioxide was co-fed.

Table 4: Variation in the reactor partial pressures of the kinetically relevant components when Riedel et al.[28] co-fed CO_2 to the iron-FT synthesis. Experimental details: well-mixed slurry reactor; temperature of 250°C; reactor pressure of 10 bar.

Component	Range of partial pressures inside CSTR (bar)
H_2	2.2 – 2.5
CO	1.2 – 1.4
H_2O	0.1 – 0.3
CO_2	0.8 – 3.9

3.2 Simulation results

It is not possible to perform a kinetic analysis on the results of the water co-feeding studies presented in Table 3, because insufficient data have been reported. Nevertheless, model simulations were performed to test whether a water dilution effect and an increased WGS rate could have caused the lowering of the FT reaction rate observed during some water co-feeding studies. To this end, it was assumed that the reactor was a perfect CSTR operated without any mass transfer limitations. The most recent rate equations published by Sasol for the FT reaction[33] (Equation 12 in Table 1) and the WGS reaction[38] in the Fe-LTFT synthesis were used. The process conditions chosen for the simulation were more or less in line with that of Study 2a in Table 3, i.e. a reactor pressure of 10 bar, a feed H_2/CO ratio of 1.0, and a temperature of 250°C. The kinetic constants for the catalyst used in the study by Satterfield et al.[10] are not known, but were chosen for simulation purposes so that a CO_2 selectivity of about 50% was obtained with a dry feed gas, similar to that reported by Satterfield et al.[10] (see also Figure 1).

The model was used to investigate the influence of water on the iron-FT synthesis when added in increasing amounts to the reactor feed without adjusting the reactor pressure. The model predictions presented in Figures 2 and 3 are remarkably in line with the experimental results reported by Satterfield et al.[10]. The syngas conversion (i.e. FT reaction rate) decreased with increasing amounts of water in the feed, while the CO_2 selectivity increased (compare Figures 1 and 2). Furthermore, the trends of increasing hydrogen partial pressure and decreasing CO partial pressure presented in Figure 3 were also found experimentally[10]. Even though these model simulations do not provide a proper kinetic analysis of the experimental data either, they do show that the trends observed during water co-feeding studies can be predicted by FT rate equations that do not contain any water term. This further indicates that the water co-feeding studies do not provide conclusive proof that water inhibits the hydrocarbon formation reaction.

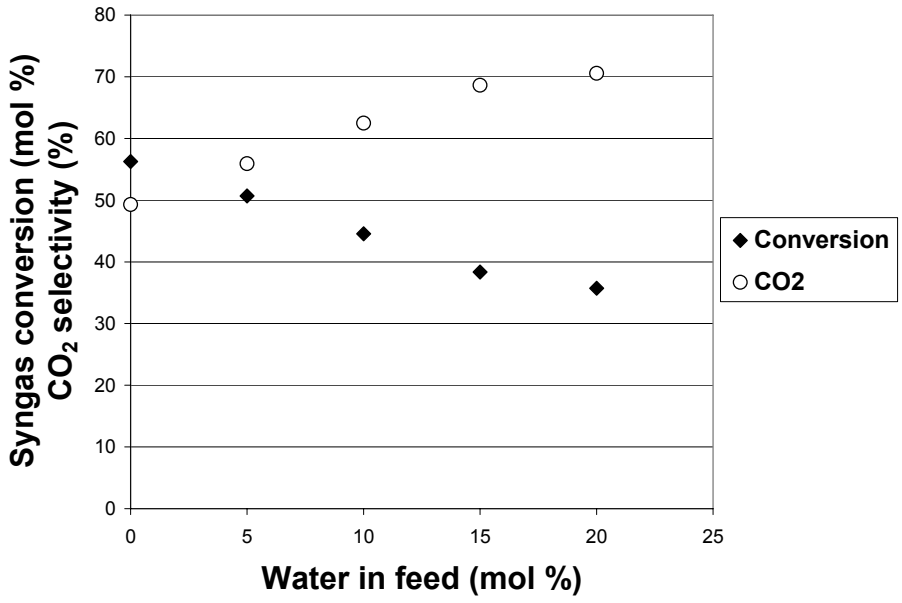

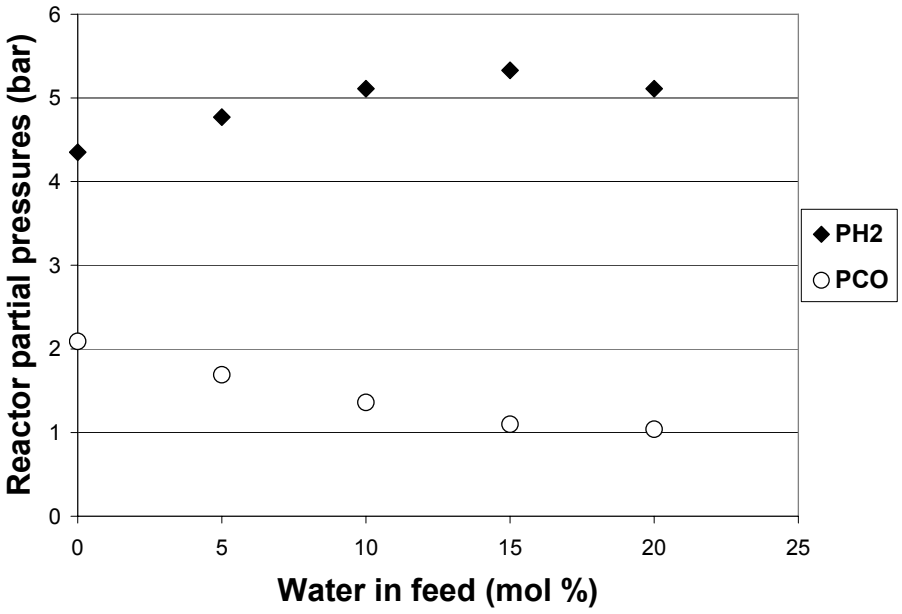

Figures 2 (Top: Syngas conversion and CO_2 selectivity) and 3 (Bottom: H_2 and CO reactor partial pressures) versus the water content in the reactor feed as obtained by model simulations for the following conditions: reactor pressure = 10 bar; temperature = 250°C; inlet H_2/CO ratio = 1.0. Equation 12 from Table 1, assuming no effect of water on the FT reaction rate, was used as the FT kinetic model, while an appropriate WGS kinetic model from literature[38] was used.

4. Detailed kinetic models

Attempts have been made to propose detailed kinetic models for the iron-FT synthesis (see brief summary in Table 5). These models describe the conversion of synthesis gas to final products, i.e. they incorporate both the rate of CO conversion and the hydrocarbon selectivities. An advantage of this approach is that the possible influence of the product distribution on the FT reaction rate can be accounted for. Bartholomew and Farrauto[39] observed that the results of these studies can be questioned, mentioning that they were probably greatly complicated by axial and radial temperature and concentration gradients typically associated with high-conversion operation in fixed bed, large-pellet reactors such as those used in these studies.

Table 5: Detailed kinetic models for the iron-FT synthesis

Model	Experimental set-up	Key features of model	Key findings and conclusions
Lox and Froment[4]	Fixed bed reactor. Catalyst mass = 5g. Particle diameter = 0.4 mm.	Assumed α-value and olefin / paraffin ratio were independent of carbon number. CO adsorbs from gas phase onto site already occupied by hydrogen or hydrocarbon intermediate. No olefin readsorption.	Slow steps are CO adsorption and product desorption. No influence of H_2O or CO_2 on reaction rate.
Wang et al.[5]	Fixed bed reactor. Catalyst amount = 3 ml. Particle diameter = 0.15 to 0.18 mm.	CO adsorbs from gas phase onto site already occupied by hydrogen or hydrocarbon intermediate. Included olefin readsorption. Predicted variable α-value.	Slow steps are CO adsorption and product desorption.
Yang et al.[6]	Fixed bed reactor. Catalyst amount =3.6 g. Particle diameter = 0.25 to 0.36 mm.	C_1 monomer is in equilibrium with reactant partial pressures in gas phase. Included olefin readsorption. Predicted variable α-value and olefin / paraffin ratio.	Slow steps are insertion of methylene into the metal-alkylidiene bond and product desorption.

Lox and Froment[4] considered various different reaction schemes for hydrocarbon product formation. Certain simplifying assumptions were made, e.g. that the chain growth probability and the olefin / paraffin ratio were independent of chain length (i.e. constant for a given product distribution). This assumption means that the surface concentrations of the various intermediates form a decaying, convergent series. Since the sum of all intermediates (C_1 to infinity) therefore had an analytical solution, the influence of the full product spectrum on the reaction kinetics could readily be accounted for. After applying various statistical criteria, the preferred model was selected. It was concluded that two types of reaction steps were intrinsically slower than the rest. The first type of slow step was CO adsorption onto a site already occupied by hydrogen or a hydrocarbon intermediate. We are not aware of any mechanistic evidence to support the notion that, in the FT synthesis, CO preferentially adsorbs onto sites that are already occupied. It is well known that pure CO adsorbs readily onto metals active for the FT synthesis (both molecularly and dissociatively) and the observation that CO displaces pre-adsorbed hydrogen from the metal surface[3] seems to be in opposition to the CO adsorption step assumed by the model. The second slow type of step was found to be the desorption of final products (although it should be said that the desorption of paraffins and olefins included the addition and abstraction, respectively, of a hydrogen atom).

Wang et al.[5] used essentially the same mechanistic scheme as Lox and Froment[4], so the same comments regarding CO adsorption onto occupied sites apply here. Their addition was that olefins were allowed to readsorb and form FT intermediates in order to account for the well-known chain length effects of the FT product spectrum (increase in α-value with carbon number). However, the implication is that the total site occupation by all intermediates cannot be calculated analytically, but have to be obtained numerically during model simulations for a finite product range. Since the FT product spectrum covers a very wide carbon number range (theoretically infinite), this numerical treatment presumably adds more complexity to the model and makes the kinetic description highly implicit. Conclusions

regarding the slow step in the reaction scheme were the same as that of Lox and Froment[4].

Yang et al.[6] followed a similar approach to the previous two studies, but in their preferred scheme the surface concentration of the CH_2 monomer is in thermodynamic equilibrium with hydrogen, CO and water in the gas phase. Olefin readsorption to form FT intermediates was also taken into account, which again presumably increased the numerical complexity of the model. The discrimination between the rival models was not convincing, but it was concluded that the rate determining steps in the synthesis were the insertion of methylene into the metal-alkylidiene bond and the desorption of hydrocarbon products. The model failed quite badly to describe the olefin / paraffin ratio as a function of carbon number, as a slight increase (as opposed to the actual strong decrease) in olefinicity with chain length was predicted.

Despite claims that detailed kinetic models should be preferred over the simpler explicit rate expressions[5,6], there are some serious practical drawbacks to the former approach. It has been pointed out in literature that there is a strong correlation between the rate constants obtained for a two-parameter kinetic model, and that the degree of covariance between the model parameters increases as the number of rate constants increases. Since the complicated nature of the detailed kinetic models requires an even greater number of independent model parameters, significant uncertainty remains over the validity of the models and the conclusions of the involved kinetic studies[39]. Ideally some of the rate constants of the elementary reactions steps should be obtained from micro kinetic data, as the confidence in values obtained from macro kinetic data only will be poor.

Further testimony to the complicated nature of the detailed models is the fact that some questionable simplifying assumptions were required to make the models of Table 5 more manageable. For instance, Lox and Froment[4] assumed an ideal Schulz-Flory product distribution with constant olefin / paraffin ratio, even though it is well established that both the α-value and olefinicity vary strongly with carbon number. This approximation makes it possible to derive an analytical expression for the total concentration of all intermediates on the surface, circumventing some

of the numerical solving required by the models of Wang et al.[5] and Yang et al.[6] However, the biggest concern over these models is their implicit assumption that there is no irreversible rate determining step involved when the monomer required for chain growth is formed from the reactants. In the preferred models of Lox and Froment[4] and Wang et al.[5], the monomer is CO, whereas Yang et al.[6] assumed thermodynamic equilibrium between the gas phase components (hydrogen, CO and water) and the CH_2 monomer on the surface. This simplification leads to a direct, explicit relationship between the gas phase reactant partial pressures and the surface concentration of the monomer. In a reaction scheme where an irreversible rate determining step is included in the formation of the monomer, the surface concentration of the monomer (as well as that of all the other intermediates) becomes a highly implicit function of the process conditions, with the result that a detailed kinetic model will become even more complex and cumbersome to apply.

From the above, it is thus clear that the classification of simple, explicit rate expressions as "lumped kinetic models" by Wang et al.[5] is not accurate. The difference between the so-called lumped and detailed models of Tables 1 and 5, respectively, centres on the assumptions regarding the rate determining steps. The inherent assumptions of the explicit rate equations are that there is a slow, irreversible step involved in the formation of the monomer and that any subsequent irreversible steps are relatively fast compared to the formation of the monomer. This implies (amongst others) that the chain growth of intermediates and the desorption to final products are sufficiently fast so that site occupation by heavier intermediates is negligible. In other words, the rate determining step in the formation of the monomer determines the overall rate of CO conversion, whereas subsequent rate determining steps determine the distribution of hydrocarbon products. There seems to be at least some microkinetic evidence to support this premise, e.g. the SSITKA study by Van Dijk[40], albeit on a cobalt-FT catalyst.

5. Conclusions

From the rate equations proposed for the iron-FT synthesis (presented more or less in chronological order in Table 1), some important progressions can be noted. Firstly, Eley-Rideal type expressions with their characteristic first order denominators (Equations 1-5 and 7) have been replaced by the arguably more plausible Langmuir-Hinshelwood kinetic models having second order inhibition terms (Equations 6 and 8-13). Secondly, whereas kinetic models originally specified full coverage of the catalytic surface (Equations 1-5), later models found the influence of vacant sites (represented by a constant term in the denominator) to be important (Equations 6-13). Lastly, whereas water (or carbon dioxide) was traditionally always included in the FT rate equations for the iron-FT synthesis, the most recent kinetic models do not account for any influence of either of these two components (Equations 12 and 13).

It has been found at Sasol, as well as reported in the open literature[19], that the adsorption parameters of the water-containing terms in rate equations accounting for water inhibition are in fact not constant, but dependent on the feed gas composition. Consistent with these reports, Deckwer et al.[25] only observed rate inhibition by water at inlet H_2/CO ratios above 0.8 and had to assume rate limitation by CO_2 at lower H_2/CO feed ratios (despite quite convincing evidence in literature that CO_2 has a negligible influence on FT kinetics[27,28]). Moreover, Satterfield et al.[10] only observed a negative influence of co-fed water on the FT reaction rate when the inlet H_2/CO ratio was around 1.0, while water co-feeding was actually beneficial at a feed H_2/CO ratio of 0.5. Espinoza[31] reported that the extent of rate inhibition of the FT reaction by water was dependent on the WGS activity of the involved catalyst. An explanation consistent with all of these observations is that water has essentially an indirect effect on the FT reaction rate by enhancing the WGS rate and thereby changing the CO and H_2 partial pressures in the gas phase. At high H_2/CO ratios, CO is the limiting reactant and an increase in the WGS rate therefore negatively impacts on the syngas conversion rate. On the

other hand, WGS becomes the supplier of hydrogen at low H_2/CO ratios and could therefore have a beneficial influence on the FT reaction rate.

Detailed kinetic models have the advantage that the product distribution is predicted simultaneously with the reaction rate, but there are some practical drawbacks to their application. The disadvantages centre on the statistical uncertainty of the values obtained for the fairly large number of kinetic constants, the highly implicit and complex nature of the models, and some questionable assumptions required to make the models more manageable. If the rate of monomer formation is indeed the rate limiting step of CO hydrogenation, then an explicit rate expression, supplemented with a separate selectivity model, is indeed the theoretically correct and practically desired approach for modelling the FT synthesis.

References

1. Steynberg, A.P. in Steynberg, A.P., Dry, M.E., Eds., *Stud. Surf. Sci. Catal. Vol. 152*, Elsevier, Amsterdam, 2004, Chapter 1.
2. Dry, M.E.; Steynberg, A.P. in Steynberg, A.P., Dry, M.E., Eds., *Stud. Surf. Sci. Catal. Vol. 152*, Elsevier, Amsterdam, 2004, Chapter 5.
3. Van der Laan, G.P.; Beenackers, A.A.C.M. Kinetics and Selectivity of the Fischer-Tropsch Synthesis: A Literature Review. *Catal. Rev. – Sci. Eng.* 1999, 41 (3&4) 255.
4. Lox, E.S.; Froment, G.F. Kinetics of the Fischer-Tropsch Reaction on a Precipitated Promoted Iron Catalyst. 2. Kinetic Modelling. *Ind. Eng. Chem. Res.* 1993, 32, 71.
5. Wang, Y.; Ma, W.; Lu, Y.; Yang, J.; Xu, Y.; Xiang, H.; Li, Y.; Zhao, Y.; Zhang, B. Kinetics Modelling of Fischer-Tropsch synthesis over an industrial Fe-Cu-K catalyst. Fuel 2003, 82, 195.
6. Yang, J.; Liu, Y.; Chang, J.; Wang, Y.; Bai, L.; Xu, L.; Xiang, H.; Li, Y.; Zhong, B. Detailed Kinetics of Fischer-Tropsch Synthesis on an Industrial Fe-Mn Catalyst. *Ind. Eng. Chem. Res.* 2003, 42, 5066.

7. Van Steen, E.; Schulz, H. Polymerisation Kinetics of the Fischer-Tropsch CO Hydrogenation using Iron and Cobalt Based Catalysts. *Appl. Catal. A* 1999, 186, 309.
8. Shen, W.; Zhou, J.; Zhang, B. Kinetics of Fischer-Tropsch Synthesis over Precipitated Iron Catalyst. *J. Nat. Gas Chem.* 1994, 4, 385.
9. Anderson, R.B.; Karn, F.S.; Shultz, J.F. Kinetics of the Fischer-Tropsch Synthesis on Iron Catalysts. US Bureau of Mines Bulletin 614, 1964.
10. Satterfield, C.N.; Hanlon, R.T.; Tung, S.E.; Zou, Z.; Papaefthymiou, G.C. Effect of Water on the Iron-catalysed Fischer-Tropsch Synthesis. *Ind. Eng. Chem. Prod. Res. Dev.* 1986, 25, 407.
11. Dry, M.E. Fischer-Tropsch Synthesis over Iron Catalysts. *Catalysis Letters* 1990, 7, 241.
12. Dry, M.E. Practical and Theoretical Aspects of the Catalytic Fischer-Tropsch Process. *Appl. Catal. A* 1996, 138, 319.
13. Raje, A.P.; O'Brien, R.J.; Davis, B.H. Effect of Potassium Promotion on Iron-based Catalysts for Fischer-Tropsch Synthesis. *J. Catal.* 1998, 180, 36.
14. Espinoza, R.L.; Steynberg, A.P.; Jager, B.; Vosloo, A.C. Low Temperature Fischer-Tropsch Synthesis from a Sasol Perspective. *Appl. Catal. A* 1999, 186, 13.
15. Dry, M.E. The Fischer-Tropsch Process: 1950-2000. *Catalysis Today* 2002, 71, 227.
16. Dry, M.E. in Steynberg, A.P., Dry, M.E., Eds., *Stud. Surf. Sci. Catal. Vol. 152*, Elsevier, Amsterdam, 2004, Chapter 7.
17. Huff, G.A.; Satterfield, C. N. Intrinsic Kinetics of the Fischer-Tropsch Synthesis on a Reduced Fused-magnetite Catalyst. *Ind. Eng. Chem. Process Des. Dev.* 1984, 23, 696.
18. Ledakowicz, S.; Nettelhoff, H.; KokuunR.; Deckwer, W.D. Kinetics of the Fischer-Tropsch Synthesis in the Slurry Phase on a Potassium-Promoted Iron Catalyst. *Ind. Eng. Chem. Process Des. Dev.* 1985, 24, 1043.
19. Anderson, R.B. in Emmett, P.H. (Ed.). *Catalysis Vol. IV*; Reinhold Publishing Corporation: New York, 1956, Chapter 3.

20. Dry, M.E. Advances in Fischer-Tropsch Chemistry. *Ind. Eng. Chem. Prod. Res. Dev.* 1976, 15, 282.
21. Chorkendorff, I.; Niemantsverdriet, J.W. Concepts of Modern Catalysis and Kinetics, Wiley-VCH, Weinheim, 2003, Chapter 2.
22. Zimmerman, W.H.; Bukur, D.B. Reaction Kinetics Over Iron Catalysts Used for the Fischer-Tropsch Synthesis. *Can. J. Chem. Eng.* 1990, 68, 292.
23. Nettelhoff, H. Produktinhibierung bei der Fischer-Tropsch-Synthese in suspensionsphase. D.Sc. Dissertation, University of Oldenburg, 1985.
24. Kokuun, R. Kinetische Untersuchungen zur Fischer-Tropsch-Synthese an suspendierten Katalysatoren. D.Sc. Dissertation, University of Oldenburg, 1985.
25. Deckwer, W.D.; Kokuun, R.; Sanders, E.; Ledakowicz, S. Kinetic Studies of Fischer-Tropsch Synthesis on Suspended Fe/K Catalyst – Rate Inhibition by CO_2 and H_2O. *Ind. Eng. Chem. Process Des. Dev.* 1986, 25, 643.
26. Sanders, E.; Deckwer, W.D.; Fischer-Tropsch Synthesis in Slurry Phase: Effect of CO_2 Inhibition on Performance of Bubble Column Slurry Reactors. *Can. J. Chem. Eng.* 1987, 65, 119.
27. Yates, I.C.; Satterfield, C.N. Effect of Carbon Dioxide on the Kinetics of the Fischer-Tropsch Synthesis on Iron Catalysts. *Ind. Eng. Chem. Res.* 1989, 28, 9.
28. Riedel, T.; Unruh, D.; Schaub, G. Fischer-Tropsch Synthesis in a Three Phase Slurry Reactor – Behaviour of CO_2. *DGMK Tagungsbericht* 2000, 2000-3, 231.
29. Van Berge, P.J. Fischer-Tropsch studies in the slurry phase favouring wax production. Ph.D. Dissertation, Potchefstroomse Universiteit vir Christelike Hoër Onderwys, 1994.
30. Keyser, M.J .; Everson, R.C.; Espinoza, R.L. Fischer-Tropsch Kinetic Studies with Cobalt-Manganese Oxide Catalysts. *Ind. Eng. Chem. Res.* 2000, 39, 48.
31. Espinoza, R.L. A Preliminary Unified Approach to the Study of Fischer-Tropsch Kinetics. *Prepr. Pap. – Am. Chem. Soc., Div. Fuel Chem.* 1995, 40, 172.

32. Claeys, M.; Van Steen, E. in Steynberg, A.P.; Dry, M.E. (Eds.), Fischer-Tropsch Technology. Stud. Surf. Sci. Catal. Vol. 125, Elsevier: Amsterdam, 2004, Chapter 8.
33. Botes, F.G.; Breman, B.B. Development and Testing of a New Macro Kinetic Expression for the Iron-Based Low-Temperature Fischer-Tropsch Reaction. *Ind. Eng. Chem. Res.* 2006, 45, 7415.
34. Van der Laan, G.P. Kinetics, Selectivity and Scale Up of the Fischer-Tropsch Synthesis. Ph.D. Thesis, Rijksuniversiteit Groningen, 1999.
35. Van der Laan, G.P.; Beenackers, A.A.C.M. Intrinsic Kinetics of the Gas-Solid Fischer-Tropsch and Water Gas Shift Reactions over a Precipitated Iron Catalyst. *Appl. Catal. A* 2000, 193, 39.
36. Critchfield, B.L. Statistical Methods for Kinetic Modelling of Fischer-Tropsch Synthesis on a Supported Iron Catalyst. Ph.D. Thesis, Brigham Young University, 2006.
37. Karn, F.S.; Shultz, J.F.; Anderson, R.B. Kinetics of the Fischer-Tropsch Synthesis on Iron Catalysts. III. Influence of water vapour. *Actes Congr. Int. Catal. 2nd* 1960, 2, 2439.
38. Botes, F.G. Water-Gas-Shift Kinetics in the Iron-Based Low-Temperature Fischer-Tropsch Synthesis. *Appl. Catal. A* 2007, 328, 237.
39. Bartholomew, C.H.; Farrauto, R.J. Fundamentals of Industrial Catalytic Processes, 2nd edition. John Wiley & Sons, Hoboken, New Jersey, 2006, Chapter 6.
40. Van Dijk, H.A.J. The Fischer-Tropsch Synthesis: A Mechanistic Study using Transient Isotopic Tracing. Ph.D. Thesis, Technische Universiteit Eindhoven, 2001.

Chapter 3

Literature Review of Selectivity Models for the Fe-LTFT Synthesis

Abstract

Two classes of models have been proposed to describe the chain length dependent deviations in the FT product spectrum, namely double-α models and olefin reinsertion models. Double-α models usually fit the carbon number distribution of the FT product spectrum very well, but it has been shown that there is a very high degree of covariance between the three model parameters. The reason for this is apparently that the system is over-specified, i.e. that too many independent parameters are used to describe the carbon number distribution. Olefin reinsertion models can describe both the increase in α-value and decrease in olefinicity with carbon number. However, at least for the iron-FT synthesis, the rate constants obtained from the models for secondary olefin reactions are vastly different from those obtained from experiments where olefins were co-fed to the process.

1. Introduction

In order to ensure an optimal design of a commercial FT process, trustworthy selectivity models are required. The FT product spectrum contains a vast number of components, making it impossible to consider the selectivity of each individual component separately. The only practical option is to characterise the product spectrum with a limited number of parameters. If these parameters can be successfully correlated with process conditions, the FT product slate can be reconstructed during model simulations. Since the FT reaction is believed to be a polymerisation-type synthesis where hydrocarbon chain growth occurs by the addition of one carbon atom at a time, the chain growth probability factor (α) is an example of one such parameter that can be used to characterise the product spectrum[1]. If the value of α is independent of carbon chain length, then the well-known ideal Schulz-Flory distribution would be obtained. It is, however, generally accepted that there are certain omnipresent deviations in the actual FT product spectrum from the ideal Schulz-Flory distribution[2,3]. These include a higher methane and a lower C_2 selectivity than predicted by the equation. In addition, there is an increase in the chain growth probability factor and concomitant decrease in the olefin / paraffin ratio with hydrocarbon chain length. The product characterisation models that have been proposed to describe these deviations can broadly be organised into two classes, namely multiple-α models and olefin reincorporation models.

2. The observed break in the Schulz-Flory product distribution

2.1 Historical realisation of an increase in the α-value with carbon number

Originally it was believed that the FT product spectrum followed the Schulz-Flory distribution and any deviation noted from this distribution was attributed to experimental errors or artefacts[4]. However, since 1967, and especially during the 1980's, the evidence for non-Schulz-Flory distributions has been mounting[4,5]. Many researchers reported that the α-value for longer chain products was higher

than for the lighter end of the spectrum and that the break in the Schulz-Flory line occurred in the region of C_{10} to C_{13} [6-9]. Initially it was thought that the break in the product distribution only occurred on potassium-promoted iron catalysts and not on cobalt or potassium-free iron catalysts[7,10]. This led to theories that such catalysts have two types of sites (potassium-promoted and promoter-free sites), each with a unique α-value, which reflected as a break in the product distribution[10]. Stenger[11] was of the opinion that this model of only two distinct sites could not be a realistic representation of the iron catalyst surface. Therefore, a distributed-site model was proposed which essentially assumed a distribution of α-values, but it merely described actual product spectra as accurately as the two-site model. Despite the inability of the new model to improve on the two-site model, Stenger[11] felt that the distributed-site model was a more convincing description of the catalyst surface, and therefore more plausible from a fundamental perspective. In very much a theoretical exercise, Inoue et al.[12] devised criteria to differentiate between a two-site and a distributed-site model.

The hypothesis that catalyst promoters was the cause of two or more types of sites on the iron catalyst seemed to come into disfavour after reports that a change in α was also observed on iron catalysts containing no potassium[6,7,13,14]. It is possible that the break was initially overlooked for the case of alkali-free catalysts due to the lighter product spectrum obtained with such catalysts where the bend would not be so prominent. Nowadays there is even wide belief that the break in the Schulz-Flory distribution is observed with cobalt-FT catalysts as well[5,15,16]. The increase in the chain growth probability has also been mechanistically related to the observed concomitant decrease in the olefin / paraffin ratio with carbon number[15,17]. Therefore, even though the bend may be the most significant and visible with alkali-promoted iron catalysts, it appears as if the increase in the chain growth probability with carbon number may be a general characteristic of all FT catalysts.

2.2 Recent proposals that the change in α-value may be due to reactor artefacts

Even though the observed increase in the α-value with chain length is not disputed, some researchers have recently started to question the notion that this is an inherent characteristic of the FT reaction. Artefacts related to reactor hydrodynamics have been offered as explanations for the observed phenomenon[18]. Along similar lines, Shi and Davis[19] pointed out that chain-length dependent deviations can be explained by the transient behaviour of laboratory slurry reactors. Their explanation centres on the fact that the residence time of long chain hydrocarbons in laboratory slurry reactors is normally very high; consequently the reactor takes a very long time to reach steady state with respect to all measured product selectivities. It can thus be argued that the observed (dynamic) product spectrum is the composite of different product spectra that have been formed in the past at a variety of conditions.

The bend in the product spectrum of Sasol's Fe-LTFT process is so prominent that it can hardly be solely due to reactor artefacts. Sasol has the benefit of a commercial slurry reactor where the liquid residence time is typically less than one day; consequently steady state can be reached with respect to all product compounds in a matter of days. Even though this reactor is not a perfect CSTR, a reconstruction of the complete product spectrum indicates a very significant increase in α-value with chain length. Furthermore, since the commercial process in Sasolburg is geared towards the production of speciality heavy waxes, the α-value measured in the wax fraction is well above 0.9. Very high α-values are indeed required to explain the high hard wax selectivity and the hard wax properties (congealing point) of this process. If the growth probability were independent of chain length, then it must at least sometimes be possible to measure an α-value well above 0.9 in the light end of the product spectrum (e.g. the C_3 to C_8 fraction). This fraction reaches steady state fairly quickly in laboratory slurry reactors and can therefore not be influenced significantly by transient effects. Notwithstanding, α-values measured in the light end have never come remotely close to the high values

typical of the wax fraction. In addition, Van der Laan and Beenackers[20] reported C_1 to C_{10} product selectivities obtained with an alkali-promoted iron catalyst in a gas-solid spinning basket reactor with CSTR properties. Even over this fairly small carbon number range, a bend in the Schulz-Flory plot of the paraffins was evident, while the olefin / paraffin ratio very clearly decreased with carbon number. Since all the components inside the reactor were in the gas phase (there was no bulk liquid phase), the residence time of all products was the same and quite short. This means that the deviations from the ideal product distribution cannot be ascribed to product hold-up in the spinning basket reactor. Consequently, although it is recognised that transient effects or non-ideal reactor behaviour can enhance the observed effects, there are strong indications that the increase in growth probability and decrease in olifinicity with carbon number is a real and inherent characteristic of the Fe-LTFT product spectrum.

3. Double-α models

3.1 Model formulation

According to the ideal Schulz-Flory product distribution, the total mol fraction (M_n) of products with n carbon numbers is given by[21]:

$$M_n = (1-\alpha)\alpha^{n-1} \qquad ...1$$

Double-α models are based on the presumed existence of two chain growth probabilities which separately contribute to the observed product spectrum. The two chain growth probabilities have been ascribed to two types of sites on the catalyst surface[6,7,10] or to two different types of growth mechanisms[16,22,23]. The product selectivities are calculated as the weighted sum of two ideal Schulz-Flory distributions (somewhat adapted from Donnelly et al.[21]):

$$M_n = W_1(1-\alpha_1)\alpha_1^{n-1} + W_2(1-\alpha_2)\alpha_2^{n-1} \qquad ...2$$

If the whole hydrocarbon product spectrum is described with Equation 2, then the sum of the weight factors (W_1 and W_2) must be unity to satisfy the mass balance requirement. However, because of the well-known deviations in the C_1 and C_2 selectivities from the Schulz-Flory distribution, the double-α model is only applied to the selectivities of the C_3 and higher carbon numbers. Then the experimentally-obtained C_1 and C_2 selectivities, together with the sum of the model-predicted C_{3+} selectivities, must count up to one[21]. The consequence of this is that the weight factors will sum up to a unique value for every product spectrum under consideration.

Even though the sum of the weight factors is determined by the mass balance requirement as explained above, an additional parameter is required in the double-α model to characterise the relative values of W_1 and W_2. Donnelly et al.[21] defined a "break point" – a hypothetical carbon number value (not necessarily an integer) where the contributions of α_1 and α_2 to the overall product spectrum are equal. Patzlaff et al.[16] pointed out that this break point does not have any physiochemical relevance and therefore rather used the parameter μ, defined as the total mol fraction of hydrocarbons formed with growth probability α_1:

$$\mu = \frac{W_1}{W_1 + W_2} \qquad ...3$$

It is therefore clear that the double-α model has three parameters, namely α_1 and α_2, as well as either the break point or μ. It should be noted that this model describes the shape of the carbon number distribution only in terms of primary reactions occurring on the catalyst surface. Since secondary reactions (i.e. those that involve readsorbed components) are not considered, the model is independent of the space velocity and can thus be formulated in explicit form. Furthermore, double-α models only describe the gradual increase in growth probability with carbon number from C_3 onwards, and not the concomitant decrease in the olefin / paraffin ratio, even though these two phenomena may be mechanistically related.

3.2 Mathematical considerations of two-α models

Donnelly et al.[21] proposed a mathematical method for obtaining the parameter values of a two-α model from a measured product distribution via non-linear regression of the available selectivity data. Because of mass balance requirements, the measured selectivities of the C_1 and C_2 components and the model predicted selectivities of the C_{3+} products had to add up to 100%. The model was tested with selectivity data obtained by analysing the overhead gaseous stream from a slurry reactor. Due to the higher solubility of heavier components in the wax phase, a long operating time would have been required for long chain hydrocarbons to attain a steady state concentration in the gas phase effluent; consequently, only the C_3 to C_{16} selectivities were normally used for estimating the model parameters. It was shown graphically that the double-α model was indeed able to describe the carbon number distributions well. However, in a subsequent publication, Donnelly and Satterfield[14] reported a repeatability of ±5% in the calculated alpha values when the catalyst was operated under some given baseline condition. This finding already hints at an inherent shortcoming in the double-α model, since a ±5% repeatability translates, for example, to a variation in the α_2-value from 0.84 to 0.92 at baseline conditions, which is an enormous range in terms of predicting the selectivities of the heavy products.

The selectivity data used by Donnelly et al.[21] were now obtained from a corresponding DOE Report[24]. Two data sets, namely Runs RC3.16 and RC3.19, were selected and used to perform some additional tests on the two-α model. The double-α model was applied exactly as proposed by Donnelly et al.[21] and contained three parameters, namely the two chain growth probabilities (α_1 and α_2) and the so-called breakpoint. The three independent parameter values were optimised for each of the two product spectra and the results are presented in the first columns of Tables 1 and 2, respectively. Taking the relative variance (S_{rel}) as a measure of the goodness of fit, it is clear that the double-α model can indeed describe the shape of the product distributions very well. Subsequently, the value of α_1 was specified to be significantly different from the optimised value, followed by re-optimisation of

Tables 1 (top) and 2 (bottom): Fitting the Donnelly model to the selectivity data (C_3 to C_{16}) of Runs RC3.16 and RC3.19, respectively, reported by Donnelly and Satterfield[24]

	Optimised Model	Decreased value of α_1 *	Increased value of α_1 *
α_1	0.52	0.47*	0.57*
α_2	0.86	0.85	0.87
Break point	4.4	4.0	5.1
S_{rel} (%)	4.5	5.0	5.1

	Optimised Model	Decreased value of α_1 *	Increased value of α_1 *
α_1	0.55	0.50*	0.60*
α_2	0.83	0.83	0.85
Break point	4.2	3.6	5.2
S_{rel} (%)	3.5	3.8	3.9

* Specified value of α_1, followed by re-optimisation of α_2 and the breakpoint.

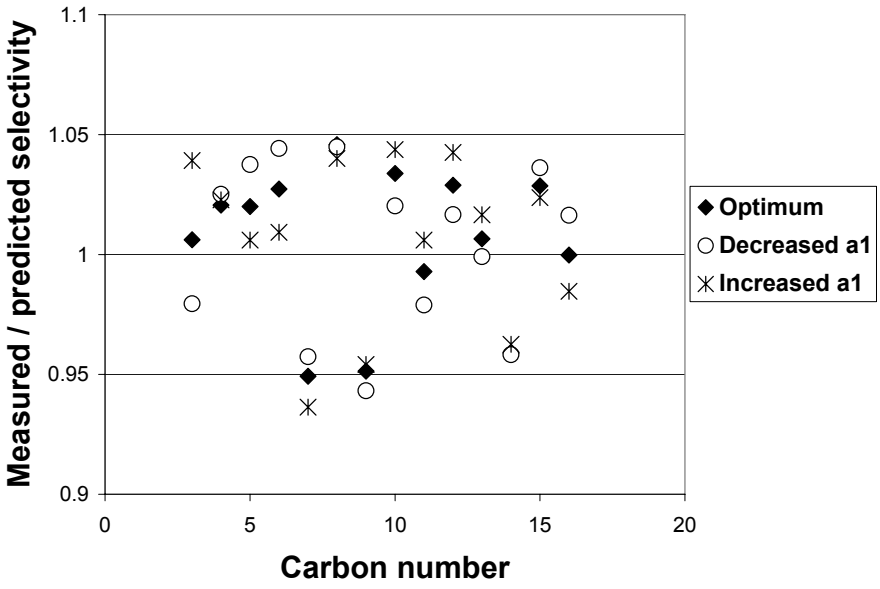

Figure 1: Accuracy of the double-α model for data from Run RC3.19 reported by Donnelly and Satterfield[24]. Three significantly different sets of parameter values were used, namely optimum values (α_1 = 0.55, α_2 = 0.83, break point = 4.2); decreased value of α_1 (α_1 = 0.50, α_2 = 0.83, break point = 3.6); increased value of α_1 (α_1 = 0.60, α_2 = 0.85, break point = 5.2). The three sets of parameter values yielded similar fits of the data.

the remaining two parameters (α_2 and the break point). The results of Tables 1 and 2 indicate that this had a relatively small influence on the value of α_2, but notably affected the value of the breakpoint. Despite these changes in the parameter values (α_1 varied from about 0.5 to 0.6), the goodness of fit was not affected much. This is also illustrated in Figure 1 for the case of the data from Run RC3.19, where the ratio of the measured to the predicted hydrocarbon selectivity is presented as a function of the carbon number for three different sets of parameter values. Even though the three different parameter sets covered a wide range of values (especially for α_1), all described the measured selectivities quite well (within about 5% for all carbon numbers). This confirms that there can be little confidence in the individual parameter values obtained for the double-α model due to the very high degree of covariance between the parameters.

A further investigation was performed to establish the influence of the mass balance accuracy on the values of the model parameters. To this end, the reported C_1 to C_{16} selectivities were all lowered by a certain percentage, followed by re-optimisation of all the model parameters. The results of this exercise as applied to the data of Runs RC3.16 and RC3.19 are presented in Tables 3 and 4, respectively. It is clear that a lowering of the reported selectivity values by 5% or more started to cause significant changes to the optimised parameter values. This indicates that the accuracy of the mass balance has a substantial influence on the values obtained for the model parameters and can, in particular, lead to variations in the value of α_2.

Trivial as the issue of a mass balance may seem, it is in fact quite a difficult requirement to satisfy in practice for the FT synthesis. Donnelly et al.[21] reported their selectivities on the basis of the molar percentage of each component in the product spectrum. This requires that the full product spectrum be known, since the molar selectivities of individual components cannot be calculated from the amount of CO converted to FT products. Considering the data reported by Donnelly and Satterfield[24], it appears as if they assumed that the sum of the measured amount of C_1 to C_{30} components represented the full product spectrum for the purpose of calculating individual (absolute) selectivities. However, by their own admission, the measured selectivities beyond C_{16} were not accurate, due to (amongst others)

the fact that insufficient time was allowed for these heavier components to attain a steady state concentration in the gas phase. Additionally, the contribution of the C_{31+} components to the overall product spectrum was neglected. It is therefore clear that an accurate mass balance for the purpose of fitting a double-α model could not have been guaranteed. It should further be noted that these effects will become increasingly more significant if the product spectrum is shifted towards the heavier end. For an Fe-LTFT process aimed at the production of heavy waxes, the molar selectivities of C_{31+} products will be much higher and more difficult to quantify.

Tables 3 (top) and 4 (bottom): Fitting the Donnelly model to the selectivity data (C_3 to C_{16}) of Runs RC3.16 and RC3.19, respectively, reported by Donnelly and Satterfield[24]: investigation of mass balance requirement

Lowering of reported selectivities	**0 %**	**3%**	**5%**	**7%**	**10%**
α_1	0.52	0.54	0.56	0.63	0.66
α_2	0.86	0.87	0.89	0.93	0.95
Break point	4.4	5.1	5.8	7.9	9.1

Lowering of reported selectivities	**0 %**	**3%**	**5%**	**7%**	**10%***
α_1	0.55	0.57	0.60	0.70	
α_2	0.83	0.84	0.86	0.95	> 1
Break point	4.2	5.0	6.3	11.6	

* No feasible solution: α_2 had to be higher than 1 to satisfy the mass balance requirement.

3.3 Implications of the characteristics of the double-α model

The implication of the foregoing is that there are various significantly different sets of parameter values that can each yield a good fit of a given product distribution. In other words, the three model parameters are in fact not independent from one another as implicitly assumed, but have a high degree of covariance. Therefore, if one of the parameters is considered in isolation from the rest, a significant scatter in the values may well be expected. This is probably the underlying reason for the poor repeatability reported by Donnelly and Satterfield[14] for α-values obtained with

the double-α model. The reason for the covariance is possibly that too many model parameters are used to describe the data, i.e. the system is over-specified.

4. Olefin reincorporation models

4.1 The background of olefin reincorporation models

The hydrogenation of ethylene and its incorporation into the product spectrum have been reported very early in the history of the FT synthesis. Since then, various studies have shown that longer chain olefins can also be converted to heavier components, especially over cobalt catalysts[15]. Due to these experimental observations, secondary reactions of olefins have been suggested as the reason for the variations in α-value and olefin / paraffin ratio with carbon number. This explanation could only be valid if the propensity for secondary reactions (hydrogenation and incorporation) increased with increasing olefin chain length, which is indeed claimed to be the case[15,25,26]. The reasons proposed for the dependency of secondary reactions on carbon number have sparked some debate in the literature and include the following: slower diffusion of longer molecules through catalyst pores[27]; higher concentrations of heavier olefins in the liquid phase due to an increase in solubility with chain length[28,29]; stronger physisorption of longer molecules on the catalyst surface[5,17,29]; variations in reactor residence times due to different solubilities in the liquid phase[28,30]. Nevertheless, various types of olefin reincorporation models have been successfully fitted to experimental selectivity data, even though the reasons assumed for the chain-length dependency of readsorption have varied extensively. The fact that fundamentally different models have been applied successfully seems to indicate that a good description of experimentally measured data is not sufficient proof of the validity of a reinsertion model.

It should be noted that reincorporation models have to account for the partial pressures of olefins inside the reactor, which are in turn influenced by the space velocity. Unlike double-α models, reinsertion models are therefore implicit (i.e.

they cannot be formulated explicitly in terms of reactant partial pressure and temperature, but have to be solved simultaneously with a reactor model).

4.2 Chain length dependency of secondary olefin reactions

4.2.1 Diffusion

Iglesia and co-workers[27] (and references therein) proposed a detailed model that not only accounted for the diffusion-enhanced readsorption of olefins, but also for the mass transfer restrictions of reactants. The model was validated with ruthenium- and cobalt-based FT catalysts and could describe various trends in the data, e.g. the effects of space velocity and catalyst particle diameter on the selectivity. A structural parameter (χ) was also defined for the catalyst that depends on the physical properties and site density of the catalyst pellets ($\chi = r_m^2\ \theta\Phi/r_p$, where r_m = mean particle radius, θ = Co atoms / m^2, Φ = catalyst porosity and r_p = mean pore radius). The larger the value of χ, the more significant the influence of internal diffusion becomes due to a larger particle diameter (longer diffusion pathways), higher catalyst activity (higher consumption rate of reactants and formation rate of products), etc. The model predicts that, with increasing values of χ, the C_{5+} selectivity will pass through a maximum value. This trend was corroborated by the experimental data measured in fixed bed reactors (solid symbols in Figure 2). The initial increase in C_{5+} selectivity was ascribed to the greater restriction on the transport of olefins through the catalyst pores that enhances olefin readsorption and promotes chain initiation. The decrease beyond the optimum value is caused by CO transport limitations, which will lead to an increase in the local H_2/CO ratio at the catalytic sites. This explanation of course implies that the onset of olefin diffusion limitations occurs well before the onset of CO diffusion limitations, despite the fact that the molar flux of CO in the catalyst pores is one to two orders of magnitude higher than the molar flux of olefins. (Note that a number of CO molecules are consumed in the formation of one olefin molecule.)

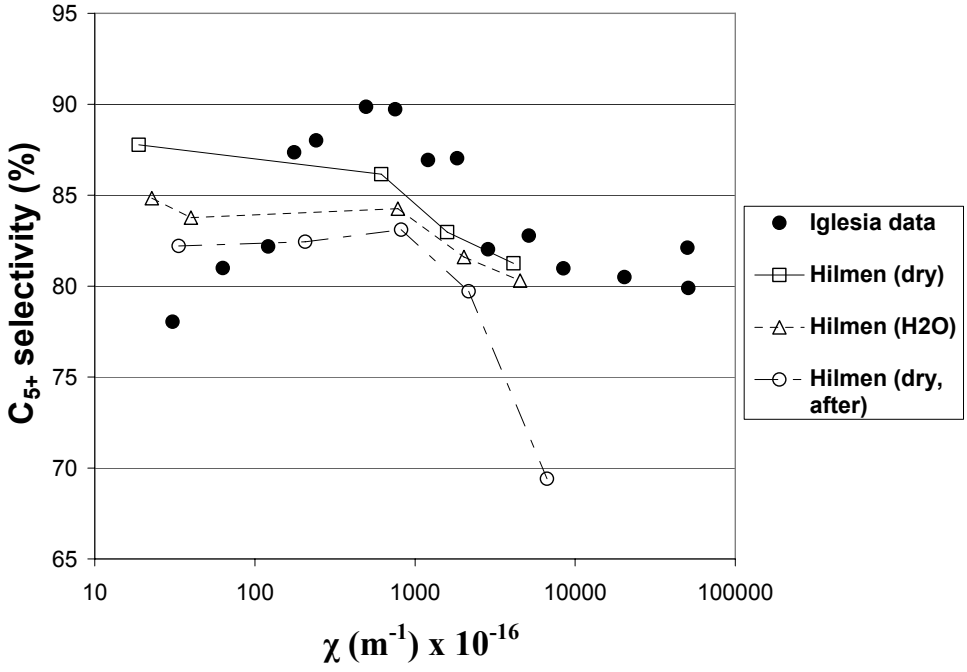

Figure 2: The influence of the structural parameter of cobalt-FT catalysts (χ) on the C_{5+} selectivity as measured in fixed bed reactors. Solid symbols: graphical results presented by Iglesia et al.[27] Open symbols: graphical results presented by Hilmen et al.[31]

In similar types of experiments, Hilmen et al.[31] varied the structural parameter of a Re-promoted Co/Al_2O_3 FT catalyst over more or less the same range of values of χ. The experiments were performed in a fixed bed reactor. Measurements were taken at dry feed conditions, during water addition and after removal of the water (results included as open symbols on Figure 2). In all three cases, a drop in the C_{5+} selectivity at higher values of the structural parameter was also noted, presumably due to the onset of CO diffusion limitations. Remarkably, the onset of this decrease was at almost exactly the same point as observed by Iglesia et al.[27], namely at a value of χ of just below 10^{19} m^{-1}. However, contrary to Iglesia et al.[27], no variation in the C_{5+} selectivity (Figure 2) or in the CH_4 selectivity (see original publications) was noted at lower values of χ. This suggests that Hilmen et al.[31] only observed the negative influence of CO transfer limitations, but not any significant effect of olefin reinsertion, on the product spectrum. Nevertheless, the results presented in Figure 2 still have significant implications for the design of cobalt-FT catalysts. Obviously a

commercial catalyst should have the highest possible intrinsic activity, while in general larger catalyst particles would be preferred for reactor design. Both these aspects will increase the value of χ and will ultimately result in CO diffusion limitations (causing a drop in the C_{5+} selectivity). The onset of CO diffusional constraints (which were found by two independent research groups to occur at about the same point) therefore represents the preferred value of χ for a commercial catalyst.

In their diffusion-enhanced olefin reinsertion model, Iglesia et al.[27] applied an empirical relationship to describe the influence of carbon number (n) on olefin and paraffin diffusivity:

$$D_n \propto e^{-0.3n} \qquad ...4$$

Van der Laan and Beenackers[20] pointed out that this relationship was not tested against measured diffusion rates. Moreover, the model-fitted dependency of the diffusivity on carbon number is a factor of three stronger than that observed by other researchers that specifically measured olefin diffusion rates.[32] Based on a similar line of reasoning, Shi and Davis[33] concluded that the model by Iglesia and co-workers would have underestimated the olefin / paraffin ratio if a more realistic correlation was used. Furthermore, a bend in the ideal Schulz-Flory distribution has also been reported for systems free from internal olefin diffusion limitations[34]. It thus seems that olefin mass transfer limitations alone cannot explain the chain length effects in the FT product spectrum.

4.2.2 Solubility

Longer chain olefins have higher concentrations in the liquid phase due to their lower vapour pressures. Some researchers have proposed that the higher liquid phase concentration of long chain olefins is a contributing reason for their higher rates of secondary reactions[20,28,29]. However, Iglesia et al.[27] argued that deviations from the Schulz-Flory distribution cannot be due to the higher solubility of larger

olefins, since the chemical potential (related to the gas phase partial pressure in an ideal system) is the driving force for a chemical reaction, and not the liquid phase concentration. Thermodynamic equilibrium between the gas and liquid phase requires that the chemical potential for each component be the same in the two phases. Therefore, in the absence of any mass transfer limitations, the liquid phase concentrations of olefins have no influence on the rates of secondary olefin reactions. The claim that the higher solubility of longer chain olefins increases their activity for secondary reaction thus seems to be in contradiction with the fundamentals of chemical reaction theory as explained by Eckert[35].

Due to their higher liquid phase concentrations, longer chain olefins have a higher hold-up in the liquid phase of a slurry reactor, and consequently a longer residence time inside the reactor. It has been mentioned in literature, e.g. by Shi and Davis[19], that the longer residence time of heavier products allows more extensive secondary conversion of longer chain olefins. However, if the fugacity of the olefin is indeed the driving force for secondary reactions, then this is not a fundamentally sound argument, as pointed out by Breman[36]. By taking a typical scheme of an olefin reincorporation model (e.g. that proposed by Van der Laan and Beenackers[20]) and assuming that the fugacity of the olefin determines the rate of secondary readsorption, the following equations can be derived for the growth probability and olefin / paraffin ratio as functions of carbon number (see Appendix A):

$$\alpha_n = \frac{k_g}{k_g + k_t^{PF} + k_t^{OF} - \dfrac{w k_t^{OF}}{\left(\dfrac{\phi_{VG}}{RTk_{ra}^{OF}} + \dfrac{\phi_{VL}}{V_{mL} H_n^{OF} k_{ra}^{OF}} + w \right)}} \qquad ...5$$

$$(O/P)_n^{obs} = \frac{k_t^{OF}}{k_t^{PF}} \left[1 - \frac{w}{\left(\dfrac{\phi_{VG}}{RTk_{ra}^{OF}} + \dfrac{\phi_{VL}}{V_{mL} H_n^{OF} k_{ra}^{OF}} + w \right)} \right] \qquad ...6$$

Since the Henry coefficient of olefins (H_n^{OF}) strongly decreases with increasing carbon number, Equations 5 and 6 predict a decrease in the α-value and increase in the olefin / paraffin ratio with carbon number, completely opposite to experimental observation. In other words, the higher volatility of light olefins means that they have a higher chemical potential and therefore a higher propensity for secondary reactions than heavier olefins. Therefore, it is concluded that the increasing solubility of olefins with carbon number cannot explain the chain lengths deviations in the FT synthesis. The only logical deduction then seems to be that one or more of the primary and / or secondary reaction rate constants (k_g, k_t^{PF}, k_t^{OF}, k_{ra}^{OF}) is a function of carbon number.

4.2.3 Physisorption

Chain length effects of the FT product spectrum have been ascribed to the stronger physisorption of longer olefins on the catalyst surface, resulting in an increase in secondary reaction rates with carbon number[5,17,20,29]. This is supported by the observation that the adsorption enthalpy of hydrocarbons on solids increases linearly with carbon number[20]. Recently, the chain length effects of the Fe-LTFT product spectrum have been modelled in terms of primary reactions only (i.e. not accounting for any effect of secondary reactions)[37]. The essence of this model was that the desorption of a growing intermediate from the catalyst surface (rather than the readsorption of gas phase olefins back onto the surface) is governed by its physisorption on the catalyst surface. In other words, in terms of Equations 5 and 6, the rate constant for the termination of an FT intermediate to an olefin (k_t^{OF}) is a function of carbon number, while the rate of readsorption was assumed to be negligible ($k_{ra}^{OF} = 0$). This will be fully discussed in Chapter 6 of this dissertation.

4.3 Secondary reactions of olefins over Fe-LTFT catalysts

The experience at Sasol when various commercial catalysts are operated in well-mixed slurry reactors is that the bend in the carbon number distribution is much

more significant with iron-based catalysts than with cobalt-based catalysts. This seems to be corroborated by reports in literature, since it was originally believed that the deviation from the ideal distribution only occurred with alkali-promoted iron catalysts (and not with cobalt catalysts)[7,10]. Yet, whereas secondary olefin reactions over cobalt catalysts have been clearly demonstrated, olefin co-feeding studies have indicated a negligible or low rate of secondary reactions of C_{3+} olefins in the iron-FT synthesis[22,38]. It is therefore ironic that iron-based catalysts, with a much lower propensity for secondary reactions (particularly reinsertion), seem to display a much more pronounced bend in the Schulz-Flory distribution than cobalt catalysts.

Studies where olefins have been added to the iron-FT synthesis are summarised in Table 5. Schulz et al.[25] found fairly high conversions of both ethylene and propylene, but the hydrogenation of the co-fed olefin far exceeded its conversion to higher hydrocarbons (especially for the case of propylene). Similarly, albeit with an unpromoted iron single crystal surface, Dwyer and Somorjai[39] also found that most of the added ethylene was hydrogenated and that propylene was even less likely than the C_2 olefin to insert. Hanlon and Satterfield[9] co-fed various olefins to the iron-FT synthesis operated in a well-mixed slurry reactor at both high CO conversion (low CO partial pressure) and low CO conversion (high CO partial pressure). Since unlabelled olefins were co-fed, the only secondary reactions that could be quantified unambiguously were hydrogenation to the corresponding paraffin and double bond isomerisation to the corresponding internal olefin. The portion of olefins that was unaccounted for was assumed to have been converted to higher hydrocarbons, but the authors expressed doubt over these estimates due to possible mass balance inaccuracies. Therefore, the ratios of growth to hydrogenation reported in Table 5 represent the highest possible values and in reality these values could have been lower. The results show low or negligible rates of secondary olefin reactions at high CO partial pressures. At low CO partial pressures (conditions where the olefin partial pressure was sometimes comparable to that of CO), higher conversions were observed, but the rate of hydrogenation always significantly exceeded the rate of reinsertion. Boelee et al.[40] also studied the

Table 5: Summary of olefin co-feeding studies to the iron-FT synthesis

Co-feeding study	Experimental details	H_2/CO ratio	Co-fed olefin	% of olefin converted	Ratio of growth to hydrogenation
Schulz et al.[25]	Plug flow reactor. K-promoted precipitated Fe catalyst. ^{14}C-labelled olefins.	2.0 (Feed)	Ethylene	77	0.13
			Propylene	44	0.02
Dwyer and Somorjai[39]	Isolation cell (batch reactor) – 90 minutes of reaction time. Iron (III) single crystal surface. Unlabelled olefins.	3.0 (Feed)	Ethylene	84	0.11
			Propylene	–	Less likely to reinsert than ethylene
Hanlon and Satterfield[9]	Well-mixed slurry reactor. K-promoted fused Fe catalyst. Unlabelled olefins	2.9	Ethylene (Low P_{CO})	59	0.25 – 0.34
		3.8	1-Butene (Low P_{CO})	38	< 0.33
		3.1	1-Hexene (Low P_{CO})	70	< 0.67
		5.2	1-Decene (Low P_{CO})	80	~ 0
		1.0	Ethylene (High P_{CO})	9	< 0.1
		1.0	1-Butene (High P_{CO})	< 1	~ 0
		1.0	1-Hexene (High P_{CO})	15	< 0.1
Boelee et al.[40]	Well-mixed slurry reactor. K-promoted fused Fe catalyst. Unlabelled olefins.	0.67 (Feed)	Ethylene	62	0.39
		0.67 (Feed)	Ethylene	3	0.24
		3.0 (Feed)	Ethylene	22	0.26
		0.67 (Feed)	Ethylene	14	0.03
Tau et al.[26]	Well-mixed slurry reactor. K-promoted fused Fe catalyst. ^{14}C-labelled olefins.	1.2 (Feed)	Ethylene	50 – 60	ca. 0.25
			1-Pentene	Negligible	–
			2-Pentene	Negligible	–
			1-Decene	–	–

iron-FT synthesis in a slurry reactor (CSTR) and co-fed ethylene under various process conditions. Again most of the converted ethylene was merely hydrogenated to ethane. It was reported that the rate of secondary reaction increased with an increasing ethylene / CO partial pressure ratio, in agreement with the findings of Hanlon and Satterfield[9]. Tau et al.[26] co-fed ^{14}C-labelled olefins to the iron-FT synthesis operated in a well-mixed slurry reactor. Labelling enabled the researchers to more accurately track the conversion pathways of the co-fed olefin. Around half of the added ethylene was converted, but again the rate of hydrogenation exceeded the rate of chain initiation (in this case by a factor of 4). Both 1- and 2-pentene were found to be essentially inert in the iron-FT synthesis. The conversion of 1-decene was somewhat more extensive than for the C_5 olefins, with both reinsertion and hydrogenation noted, but from the information supplied it was not readily possible to calculate exact values.

4.4 Apparent differences in behaviour between in-situ formed and co-fed olefins

A concern over olefin reinsertion models is the apparent discrepancies in behaviour between in-situ formed and co-fed olefins. These discrepancies have been alluded to by, for example, Van der Laan and Beenackers[2]. Furthermore, Kuipers et al.[5] found that the measured reinsertion rate of co-fed 1-olefins over a cobalt catalyst was much lower than expected on the basis of the changes in the net chain growth probability in the typical FT product spectrum. These authors also concluded that the apparent behaviour of an in-situ formed olefin is distinctly different from that of a co-fed olefin.

Due to the above, it seems imperative to compare the rate constants of secondary olefin reactions as indirectly obtained via model fitting of reincorporation models with the corresponding rate constants directly measured for co-fed olefins. To the extent of our knowledge, such a direct comparison has only been done by Patzlaff et al.[22] for the data and model presented by Schulz and Claeys[34]. The conclusion was that an unrealistically high selectivity of olefin reincorporation had to be

assumed for the cobalt-FT synthesis in order to explain the observed deviations from the ideal carbon number distribution.

A similar type of comparison will now be performed for the case of the iron-FT synthesis. Van der Laan and Beenackers[20] described the product selectivities of a precipitated iron catalyst with an olefin readsorption model. Using their notation, the ratio of growth (G) to hydrogenation (H) of gas phase ethylene undergoing secondary reactions can be expressed by Equation 7, while the G/H ratio for C_{3+} olefins is expressed by Equation 8.

$$\left(\frac{G}{H}\right)_{ethylene} = \frac{k_p \theta_M \theta_2}{k_{t,P}^2 \theta_H \theta_2} = \frac{k_p \theta_M}{k_{t,P}^2 \theta_H} = \frac{p}{t_P^2} = \frac{p}{1.59} \qquad ...7$$

$$\left(\frac{G}{H}\right)_{C3+\ Olefins} = \frac{k_p \theta_M \theta_n}{k_{t,P} \theta_H \theta_n} = \frac{k_p \theta_M}{k_{t,P} \theta_H} = p \qquad ...8$$

Similarly, the growth to hydrogenation ratio of all gas phase olefins (including ethylene) can be derived from the model proposed by Wang et al.[41] Using their notation and reported parameter values, the G/H ratio at a temperature of 250°C is expressed as a function of the CO and H_2 partial pressures as follows:

$$\left(\frac{G}{H}\right)_{All\ Olefins} = \frac{r_{n,1}}{r_{n,5}} = \frac{k_1 P_{CO}[C_n H_{2n+1} - \kappa]}{k_5 P_{H_2}[C_n H_{2n+1} - \kappa]} = \frac{k_1 P_{CO}}{k_5 P_{H_2}} = 39.9\left(\frac{P_{CO}}{P_{H_2}}\right) \qquad ...9$$

By using Equations 7 to 9 and the appropriate parameter values reported for the involved studies, the model predicted growth to hydrogenation ratios for ethylene and C_{3+} olefins are presented in Figures 3 and 4, respectively. Both the models of Van der Laan and Beenackers[20] and Wang et al.[41] predict a decreasing G/H ratio with increasing reactor H_2/CO ratio. The trends predicted by the two models are remarkably similar in shape. However, the predicted G/H ratios exceed the G/H

ratios measured during olefin co-feeding studies by at least one order of magnitude, even at the highest H_2/CO ratios (compare Table 5 with Figures 3 and 4). Here the co-feeding studies of Hanlon and Satterfield[9], Boelee et al.[40] and Tau et al.[26] are especially relevant. These investigations were all performed in well-mixed slurry reactors (CSTR's), which makes it possible to study the secondary olefin reactions

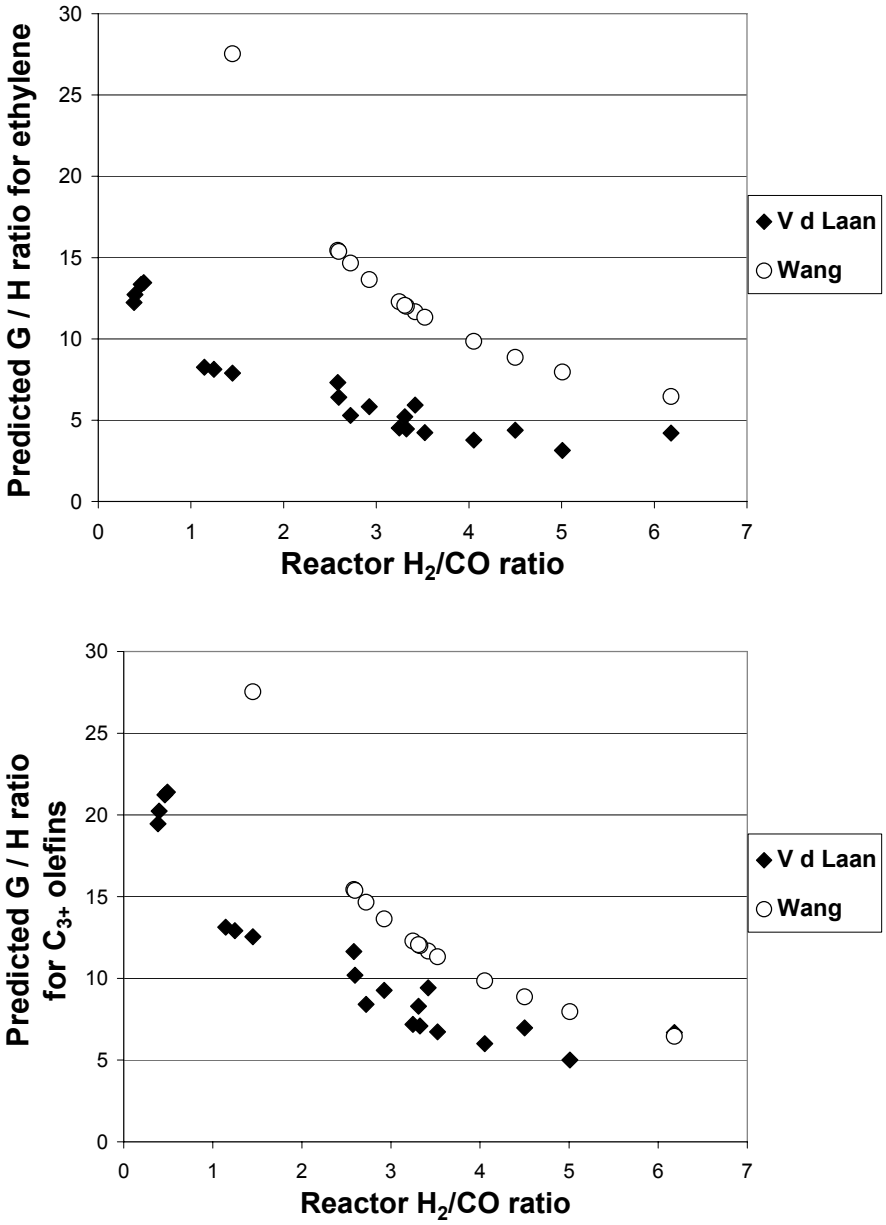

Figures 3 (top) and 4 (bottom): Ratio of growth to hydrogenation of gas phase ethylene and C_{3+} olefins, respectively, predicted by the models of Van der Laan and Beenackers[20] and Wang et al.[41] as a function of the reactor H_2/CO ratio.

at a single, well-defined operating point, i.e. the exact conditions under which the FT product spectrum is formed. The disagreement between the models and the actually measured behaviour of gas phase olefins becomes especially large at low H_2/CO ratios of around 1.0, with differences approaching two orders of magnitude. This vast discrepancy between the measured behaviour of co-fed olefins and the model-fitted behaviour necessary to describe chain length effects in the FT product spectrum places serious doubt over the applicability of olefin reinsertion models for the iron-FT synthesis.

5. Conclusions

The hydrocarbon product spectrum of the FT synthesis approximately follows a statistical distribution characterised by the Schulz-Flory equation. However, there are some deviations in the actual product spectrum from the ideal distribution, most notably that the chain growth probability increases and the olefin / paraffin ratio decreases with carbon number. Chain length effects have been described with two classes of models, namely double-α models and olefin reinsertion models.

Double-α models usually fit the carbon number distribution of the FT product spectrum very well, but it has not been shown that these models can also describe the variations in olefin / paraffin ratio. Furthermore, when fitting a double-α model to actual experimental data, it is found that there is a very high degree of covariance between the three model parameters. The reason for this could be that the system is over-specified, i.e. that too many parameters are used to describe the carbon number distribution.

Olefin reinsertion models are implicit and require that the reactor model be solved simultaneously with the selectivity model. The models can describe both the increase in α-value and decrease in olefinicity with carbon number. However, the parameter values obtained by fitting these models to FT product spectra seem to be in disagreement with directly measured quantities. For instance, the dependency of olefin diffusivity on carbon number as fitted by a reinsertion model is much stronger than that found by other researchers who explicitly measured the diffusion

rates of olefins. Furthermore, for the iron-FT synthesis, the ratios of olefin growth to hydrogenation as fitted by reinsertion models exceed the measured ratio for co-fed olefins by at least an order of magnitude. This places doubt over the validity of olefin reincorporation models for the iron-FT synthesis.

Appendix A: Derivation of alpha value and olefin / paraffin ratio as functions of carbon number for a well-mixed slurry reactor

Consider the following scheme that allows for growth, termination to paraffins (PF) and termination to olefins (OF). Provision is also made for olefins to readsorb and become an FT intermediate. It is assumed that olefin readsorption is governed by the fugacity of the olefin.

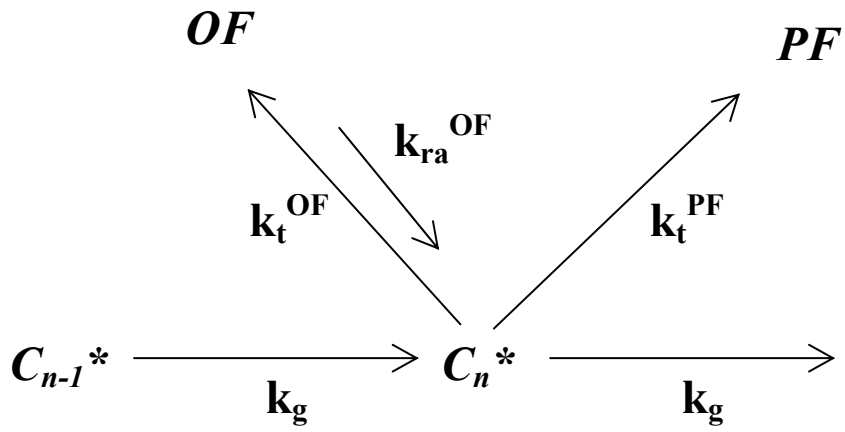

Olefin mass balance

From the definition of fugacity:

$$f_n^{OF} = y_n^{OF} P = x_n^{OF} H_n^{OF} \qquad \text{...A1}$$

Equation A2 represents the olefin mass balance for a well-mixed slurry reactor. Substitution of Equation A1 into the mass balance yields Equation A3.

$$\frac{\phi_{VG} P}{RT} y_n^{OF} + \frac{\phi_{VL}}{V_{mL}} x_n^{OF} = w\left(k_t^{OF} [C_n*] - k_{ra}^{OF} f_n^{OF}\right) \qquad \text{...A2}$$

$$\frac{\phi_{VG} P}{RT} y_n^{OF} + \frac{\phi_{VL} P}{V_{mL} H_n^{OF}} y_n^{OF} = w\left(k_t^{OF} [C_n^*] - k_{ra}^{OF} y_n^{OF} P\right) \quad \text{...A3}$$

After rearrangement:

$$y_n^{OF} P\left(\frac{\phi_{VG}}{RT} + \frac{\phi_{VL}}{V_{mL} H_n^{OF}} + w k_{ra}^{OF}\right) = w k_t^{OF} [C_n^*] \quad \text{...A4}$$

$$\frac{y_n^{OF} P}{[C_n^*]} = \frac{w k_t^{OF}}{\left(\frac{\phi_{VG}}{RT} + \frac{\phi_{VL}}{V_{mL} H_n^{OF}} + w k_{ra}^{OF}\right)} \quad \text{...A5}$$

Derivation of alpha value

Equation A6 represents the definition of the alpha value. By dividing above and below the line by $[C_n^*]$ and substituting Equation A1, Equation A7 is obtained.

$$\alpha_n = \frac{k_g [C_n^*]}{k_g [C_n^*] + k_t^{PF} [C_n^*] + k_t^{OF} [C_n^*] - k_{ra}^{OF} f_n^{OF}} \quad \text{...A6}$$

$$\alpha_n = \frac{k_g}{k_g + k_t^{PF} + k_t^{OF} - k_{ra}^{OF} \frac{y_n^{OF} P}{[C_n^*]}} \quad \text{...A7}$$

By substituting Equation A5 into A7 and rearranging slightly:

$$\alpha_n = \frac{k_g}{k_g + k_t^{PF} + k_t^{OF} - \frac{w k_t^{OF}}{\left(\frac{\phi_{VG}}{RT k_{ra}^{OF}} + \frac{\phi_{VL}}{V_{mL} H_n^{OF} k_{ra}^{OF}} + w\right)}} \quad \text{...A8}$$

Derivation of olefin / paraffin ratio

From the reaction scheme provided, the observed olefin / paraffin ratio can be expressed as Equation A9. Substituting Equation A5 yields Equation A10, after which further rearrangement and simplification is performed.

$$(O/P)_n^{obs} = \frac{k_t^{OF}[C_n*] - k_{ra}^{OF} f_n^{OF}}{k_t^{PF}[C_n*]} = \frac{k_t^{OF}}{k_t^{PF}} - \frac{k_{ra}^{OF}}{k_t^{PF}} \frac{y_n^{OF} P}{[C_n*]} \quad \text{...A9}$$

$$(O/P)_n^{obs} = \frac{k_t^{OF}}{k_t^{PF}} - \frac{k_{ra}^{OF}}{k_t^{PF}} \frac{wk_t^{OF}}{\left(\frac{\phi_{VG}}{RT} + \frac{\phi_{VL}}{V_{mL} H_n^{OF}} + wk_{ra}^{OF} \right)} \quad \text{...A10}$$

$$(O/P)_n^{obs} = \frac{k_t^{OF}}{k_t^{PF}} - \frac{k_t^{OF}}{k_t^{PF}} \frac{wk_{ra}^{OF}}{\left(\frac{\phi_{VG}}{RT} + \frac{\phi_{VL}}{V_{mL} H_n^{OF}} + wk_{ra}^{OF} \right)} \quad \text{...A11}$$

$$(O/P)_n^{obs} = \frac{k_t^{OF}}{k_t^{PF}} \left[1 - \frac{w}{\left(\frac{\phi_{VG}}{RTk_{ra}^{OF}} + \frac{\phi_{VL}}{V_{mL} H_n^{OF} k_{ra}^{OF}} + w \right)} \right] \quad \text{...A12}$$

Nomenclature

$[C_n*]$	Surface concentration of growing intermediate
D_n	Diffusivity of olefins with n carbon numbers
f_n^{OF}	Fugacity of olefin with n carbon atoms
H_n^{OF}	Henry coefficient of olefin with n carbon atoms
k_g	Rate constant for chain growth of an FT intermediate in mol / unit mass of catalyst / unit time

k_t^{PF}	Rate constant for termination of an FT intermediate to a paraffin in mol / unit mass of catalyst / unit time
k_t^{OF}	Rate constant for termination of an FT intermediate to an olefin in mol / unit mass of catalyst / unit time
k_{ra}^{OF}	Rate constant for secondary olefin readsorption in mol / unit mass of catalyst / unit time
M_n	Total mol fraction of products with n carbon numbers
n	Carbon number
$(O/P)_n^{obs}$	Observed paraffin / olefin ratio
P	Reactor pressure
R	Universal gas constant
T	Temperature
V_{mL}	Molar volume of liquid phase
w	Catalyst mass
W_1, W_2	Weight fractions
x_n^{OF}	Mol fraction of olefin with n carbon atoms in the liquid phase
y_n^{OF}	Mol fraction of olefin with n carbon atoms in the gas phase
ϕ_{VG}	Volumetric flow rate of gas out of reactor
ϕ_{VL}	Volumetric flow rate of liquid out of reactor

References

1. Dry, M.E. in Anderson, J.R.; Boudart, M., Eds. *Catalysis Science and Technology Vol. 1*; Springer: Berlin, 1981, Chapter 4.
2. Van der Laan, G.P.; Beenackers, A.A.C.M. Kinetics and Selectivity of the Fischer-Tropsch Synthesis: A Literature Review. *Catal. Rev. – Sci. Eng.* 1999, 41 (3&4) 255.
3. Claeys, M., Van Steen, E., in Steynberg, A.P., Dry, M.E., Eds., *Stud. Surf. Sci. Catal.* Vol. 152, Elsevier, Amsterdam, 2004, Chapter 8.

4. Ji, Y., Xiang, H., Yang, J., Xu, Y., Li, Y., Zhong, B. Effect of Reaction Conditions on the Product Distribution During Fischer-Tropsch Synthesis over an Industrial Fe-Mn Catalyst. *Appl. Catal. A* 2001, 214, 77.
5. Kuipers, E.W., Scheper, C., Wilson, J.H., Vinkenburg, I.H., Oosterbeek, H. Non-ASF Product Distributions due to Secondary Reactions during Fischer-Tropsch Synthesis. *J. Catal.* 1996, 158, 288.
6. Huff, G.A., Satterfield, C.N. Evidence for Two Chain Growth Probabilities on Iron Catalysts in the Fischer-Tropsch Synthesis. *J. Catal.* 1984, 85, 370.
7. Egiebor, N.O., Cooper, W.C. The Polyfunctionality of Iron Catalysts during Carbon Monoxide Hydrogenation I. Occurrence of Dual Chain Propagation Sites. *Appl. Catal.* 1985, 14, 323.
8. Egiebor, N.O., Cooper, W.C., Wojciechowski, W. Carbon Number Distribution of Fischer-Tropsch CO-hydrogenation Products from Precipitated Iron Catalysts. *Can. J. Chem. Eng.* 1985, 63, 826.
9. Hanlon, R.T, Satterfield, C.N. Reactions of Selected 1-Olefins and Ethanol Added during the Fischer-Tropsch Synthesis. *Energy & Fuels* 1988, 2, 196.
10. Koenig, L., Gaube, J. Fischer-Tropcsh Synthesis – Recent Studies and Developments. *Chem.-Ing. Tech.* 1983, 55 (1), 14.
11. Stenger, H.G. Distributed Chain Growth Probabilities for the Fischer-Tropsch Synthesis. *J. Catal.*, 1985, 92 (2), 426.
12. Inoue, M., Miyake, T., Inui, T. Simple Criteria to Differentiate a Two-site Model from a Distributed-site Model for Fischer-Tropsch Synthesis. *J. Catal.* 1987, 105, 266.
13. Dictor, R.A., Bell, A.T. Fischer-Tropsch Synthesis over Reduced and Unreduced Iron Oxide Catalysts. *J. Catal.* 1986, 97, 121.
14. Donnelly, T.J., Satterfield, C.N. Product Distributions of the Fischer-Tropsch Synthesis on Precipitated Iron Catalysts. *Appl. Catal.* 1989, 52, 93.
15. Schulz, H., Claeys, M. Reaction of α-Olefins of Different Chain Length Added during Fischer-Tropsch Synthesis on a Cobalt Catalyst in a Slurry Reactor. *Appl. Catal.* 1999, 186, 71.

16. Patzlaff, J., Liu, Y., Graffmann, C., Gaube, J. Studies on Product Distributions of Iron and Cobalt Catalysed Fischer-Tropsch Synthesis. *Appl. Catal.* 1999, 186, 109.
17. Van der Laan, G.P. Kinetics, Selectivity and Scale Up of the Fischer-Tropsch Synthesis. Ph.D. Thesis, Rijksuniversiteit Groningen, 1999.
18. Puskas, I., Hurlburt, R.S. Comments about the Cause of Deviations from the Anderson-Schulz-Flory Distribution of the Fischer-Tropsch Reaction Products. *Catalysis Today* 2003, 84, 99.
19. Shi, B, Davis, B. Fischer-Tropsch Synthesis: Accounting for Chain Length Related Phenomena. *Appl. Catal. A* 2004, 277, 61.
20. Van der Laan, G.P.; Beenackers, A.A.C.M. Hydrocarbon Selectivity Model for the Gas-Solid Fischer-Tropsch Synthesis on Precipitated Iron Catalysts. *Ind. Eng. Chem. Res.* 1999, 38, 1277.
21. Donnelly, T.J.; Yates, I.C.; Satterfield, C.N. Analysis and Prediction of Product Distributions of the Fischer-Tropsch Synthesis. *Energy & Fuels* 1988, 2, 734.
22. Patzlaff, J.,; Liu, Y.; Graffmann, C.; Gaube, J. Interpretation and Kinetic Modelling of Product Distributions of Cobalt Catalysed Fischer-Tropsch Synthesis. *Catal. Today* 2002, 71, 381.
23. Tau, L.; Dabbagh, H.; Bao, S.; Davis, B.H. Fischer-Tropsch Synthesis. Evidence for Two Chain Growth Mechanisms. *Catal. Lett.* 1990, 7, 127.
24. Donnelly, T.J.; Satterfield, C.N. Fischer-Tropsch slurry phase process variations to understand wax formation (Quarterly report for period April 1, 1988 to June 30, 1988), *Report number DOE/PC80015-11* 1988.
25. Schulz, H.; Rao, B.R.; Elstner, M. ^{14}C-Studien zum Reaktionsmechanismus der Fischer-Tropsch Synthese. *Erdöl und Kohle – Erdgas – Petrochemie* 1970, 23 (10), 651.
26. Tau, L.; Dabbagh, H.; Davis, B.H. Fischer-Tropsch Synthesis: ^{14}C Tracer Study of Alkene Incorporation. *Energy & Fuels* 1990, 4, 94.

27. Iglesia, E.; Reyes, S.C.; Madon, R.J.; Soled, S. Selectivity Control and Catalyst Design in the Fischer-Tropsch Synthesis: Sites, Pellets and Reactors in Eley, D.D., Pines, H. Weisz, P.B., Eds., Advances in Catalysis, vol. 39, Academic Press: New York 1993, 221-302.
28. Zimmerman, W.; Bukur, D.; Ledakowicz, S. Kinetic Model of Fischer-Tropsch Synthesis Selectivity in the Slurry Phase. *Chem. Eng. Sci.* 1992, 47, 2707.
29. Kuipers, E.W.; Vinkenburg, I.H.; Oosterbeek, H. Chain Length Dependence of α-Olefin Readsorption in Fischer-Tropsch Synthesis. *J. Catal.* 1995, 152, 137.
30. Tau, L.; Dabbagh, H.; Davis, B.H. Fischer-Tropsch Synthesis: Comparison of ^{14}C Distributions when Labelled Alcohol is Added to the Synthesis Gas. *Energy & Fuels* 1991, 5, 174.
31. Hilmen, A.; Lindvåg, O.A.; Bergene, E.; Schanke, D.; Eri, S.; Holmen, A. Selectivity and Activity Changes upon Water Addition During Fischer-Tropsch Synthesis. *Stud. Surf. Sci. Cat.* 2001, 136, 295.
32. Erkey, C.; Rodden, J.B.; Akgerman, A. Diffusivities of synthesis gas and n-alkanes in Fischer-Tropsch wax. *Energy & Fuels* 1990, 4, 275.
33. Shi, B.; Davis, B.H. Fischer-Tropsch Synthesis: The Paraffin to Olefin Ratio as a Function of Carbon Number. *Catal. Today* 2005, 106, 129.
34. Schulz, H., Claeys, M. Kinetic Modelling of Fischer-Tropsch Product Distributions. *Appl. Catal. A* 1999, 186, 91.
35. Eckert, C.A. Molecular Thermodynamics of Chemical Reactions. *Ind. Eng. Chem.* 1967, 59(9), 20.
36. Breman, B.B. Personal Communications, 2006.
37. Botes, F.G. Proposal of a New Product Characterisation Model for the Iron-Based Low-Temperature Fischer-Tropsch Synthesis. *Energy & Fuels* 2007, 21, 1379.
38. Schulz, H. Comparing Fischer-Tropsch Synthesis on Iron- and Cobalt Catalysts. *Prepr. Symp. – Am. Chem. Soc., Div. Petr. Chem.* 2005, 50(2), 155.

39. Dwyer, D.J.; Somorjai, G.A. The Role of Readsorption in Determining the Product Distribution during CO Hydrogenation over Fe Single Crystals. *J. Catal.* 1979, 56, 249.
40. Boelee, J.H.; Cüsters, J.M.G.; Van der Wiele, K. Influence of Reaction Conditions on the Effect of Co-feeding Ethene in the Fischer-Tropsch Synthesis on a Fused-Iron Catalyst in the Liquid Phase. *Appl. Cat*. 1989, 53, 1.
41. Wang, Y.; Ma, W.; Lu, Y.; Yang, J.; Xu, Y.; Xiang, H.; Li, Y.; Zhao, Y.; Zhang, B. Kinetics Modelling of Fischer-Tropsch synthesis over an industrial Fe-Cu-K catalyst. *Fuel* 2003, 82, 195.

Chapter 4

Development and Testing of a New Macro Kinetic Expression for the Fe-LTFT Reaction

Publications from this chapter

Botes, F.G.; Breman, B.B. Development and Testing of a New Macro Kinetic Expression for the Iron-Based Low-Temperature Fischer-Tropsch Reaction. *Ind. Eng. Chem. Res.* 2006, 45, 7415.

Botes, F.G.; Breman, B.B. Development of a New Kinetic Expression for the Iron-Based Fischer-Tropsch Reaction. *AIChE Annual Meeting* 2006, November 12-17, San Francisco, CA.

Abstract

Based on the common belief that water inhibits the intrinsic FT reaction rate in the iron-FT synthesis, water is included in almost all iron-FT kinetic expressions. A new rate expression was now proposed where vacant sites, CO and water were all included in the denominator. This model was evaluated with data from various historic experimental studies. In all cases it was found that the effect of water was not statistically significant and should therefore be omitted. The new model describes the historic data more accurately than some other popular rate equations. To validate these conclusions, new experimental data were measured in a well-mixed slurry reactor in the absence of mass transfer limitations. The experimental methodology employed ensured that the iron-FT catalyst did not suffer measurable deactivation. It was confirmed that there is no basis for including water in the denominator of the new rate equation and that it is more accurate than the rival models considered.

1. Introduction

From the review by Van der Laan and Beenackers[1] it is clear that there is little consensus in the literature on the form of the rate expression for the iron-catalysed Fischer-Tropsch (FT) reaction. However, there seems to be a general belief that water (and possibly also CO_2) negatively influences the intrinsic FT reaction rate. As a result, the various rate equations that have been proposed essentially all assume rate inhibition by water or CO_2 (also see Table 1 of Chapter 2). Often these alleged inhibition effects have been specified (not tested) during the derivation of the rate equations by failing to account for the possibility of vacant sites on the catalyst surface[2,3,4]. In such cases, it can thus be argued that the denominator terms of the rate expressions have been prematurely simplified based on assumption rather than by testing the model against experimental data. In this chapter, a new macro kinetic expression is proposed for the FT reaction in the iron-based Low-Temperature Fischer-Tropsch (Fe-LTFT) synthesis. It is reported how this expression was developed from existing kinetic data and validated with a new experimental study.

2. Developing a rate equation for the iron-FT reaction

In this study, it is assumed that FT and water-gas-shift (WGS) are two distinct reactions that can be described with separate kinetic models, as has generally been the approach in macro kinetic studies on the iron-FT synthesis[1].

2.1 The reaction order of hydrogen

The reaction term (numerator) of a Langmuir-Hinshelwood-Hougen-Watson (LHHW) type rate equation represents the rate determining step of the set of elementary reactions that constitute the overall reaction scheme. Since the rate determining step of the FT reaction is normally assumed to be the hydrogenation of a carbon-containing species, the numerator is expected to include the partial pressures of hydrogen and CO. Most of the popular iron-FT rate equations assume first order dependency of the

reaction term on the partial pressure of CO, but there is disagreement about the reaction order of hydrogen. Two of the well-known kinetic expressions, namely the Anderson-Dry expression[4] and the Ledakowicz-Nettelhoff expression[3] (Equations 1 and 2, respectively) assume a reaction order of one for hydrogen. On the other hand, Huff and Satterfield[2] incorporated hydrogen in the inhibition term of Equation 1 to formulate the Satterfield-Huff rate expression (Equation 3), which implies that the reaction order of hydrogen becomes increasingly larger than one, eventually approaching a value of two, as the syngas conversion increases.

$$r_{FT} = A\frac{P_{H_2}P_{CO}}{P_{CO} + bP_{H_20}} \qquad \ldots 1$$

$$r_{FT} = A\frac{P_{H_2}P_{CO}}{P_{CO} + cP_{CO_2}} \qquad \ldots 2$$

$$r_{FT} = A\frac{P_{H_2}P_{CO}}{P_{CO} + b\left(P_{H_20} / P_{H_2}\right)} \qquad \ldots 3$$

Van Berge[5] considered the above three equations as the main rival kinetic models for the iron-FT reaction and realised that they can all be regarded as members of the same family represented by the following generalised expression:

$$r_{FT} = A\frac{P_{CO}P_{H_2}{}^{\alpha}}{P_{CO}P_{H_2}{}^{\beta} + bP_{H_20} + cP_{CO_2}} \qquad \text{where } \beta = \textit{maximum } \{\alpha\text{-}1, 0\} \qquad \ldots 4$$

An experimental investigation was then performed on a precipitated iron catalyst in a well-mixed laboratory slurry reactor (CSTR) to establish whether one of the three

original equations could be regarded as the most appropriate form of the generalised expression, or whether another form of Equation 4 was more suitable for describing the iron-FT reaction rate. To this end, a statistical design procedure was applied to suggest experimental conditions where the predicted reaction rates of the rival models (Equations 1 to 4) differed most. This approach eliminated all three of the original special cases as appropriate kinetic models and therefore showed that another form of the generalised expression was required. After further systematic parameter optimisation, it was concluded that Equation 4 could be simplified to the following form with a high degree of confidence:

$$r_{FT} = A\frac{P_{H_2}{}^{0.5}P_{CO}}{P_{CO} + bP_{H_2}0} \qquad \ldots 5$$

Evidently the principal difference between Equation 5 and the other special cases is the reaction order of hydrogen. It therefore appears that, in order to distinguish the general expression from the three original special cases, the statistical design procedure deliberately selected conditions which indicated that the reaction order of hydrogen is much lower than the values suggested by Equations 1 to 3. Moreover, it was shown quite clearly that the kinetic data could not be described very well with a rate equation that assumed a reaction order of one or higher for hydrogen. Due to the thorough experimental and statistical procedures followed by Van Berge[5], the reaction term (numerator) of his proposed rate expression (Equation 5) will be retained for the purpose of developing a new kinetic model.

2.2 The inhibition term

There is general consensus in the literature that CO must first adsorb onto the catalyst surface before it can be hydrogenated[1]. If the reaction order of hydrogen is 0.5, it implies that hydrogen is first dissociated before taking part in the FT reaction. Since

hydrogen dissociation under FT synthesis conditions can presumably only occur on the catalyst surface, this means that hydrogen also reacts from the adsorbed state, and not directly from the gas phase as assumed by Dry[4] for the derivation of Equation 1. Furthermore, from chemisorption studies[6] (albeit at 20°C), it seems fair to assume that hydrogen and carbon monoxide compete for adsorption onto the same types of sites. Under these assumptions, the FT reaction proceeds over two adjacent catalytic sites, which implies that the inhibition term (denominator) of the rate equation must be squared.

There seems to be convincing evidence in the literature that CO_2 does not have a notable influence on the iron-FT reaction rate[7,8]; consequently, CO_2 was not included in the new kinetic model. There further seems to be a belief that the catalyst surface is essentially completely covered with adsorbed CO and water[1,4]. However, the critical literature review of Chapter 2 showed that there is no convincing evidence for the notion that water competes with CO for adsorption onto the iron-FT catalyst. For example, the water co-feeding studies of Satterfield et al.[9] were performed without adjusting the reactor pressure, with the result that the additional water diluted the reaction medium. The co-fed water also increased the WGS reaction rate. The net result was a significant lowering in the CO partial pressure upon water co-feeding, so that the observed lowering in the FT reaction rate cannot unambiguously be ascribed to the additional water. In view of the foregoing, it was decided to include a constant term (representing vacant sites on the catalyst surface) in addition to CO and H_2O in the denominator of the new rate equation. If data analysis then revealed one of the terms in the denominator to be statistically insignificant, it could always be discarded at a later stage.

2.3 The final form of the new iron-FT rate equation

Combining the reaction and inhibition terms suggested above yields the following LHHW-type kinetic expression for the iron-FT reaction:

$$r_{FT} = A\frac{P_{H_2}{}^{0.5}P_{CO}}{\left(1+k_{CO}P_{CO}+k_{H_2O}P_{H_20}\right)^2} \qquad \ldots 6$$

This rate equation is in fact not new, as Van der Laan[10] has already shown that it is consistent with an FT mechanism where hydrogen first dissociates on the surface of the catalyst and then reacts with adsorbed CO. Davis[11,12,13] has reviewed the results from mechanistic studies and concluded that, in light of current data, the FT reaction over iron-based catalysts most likely proceeds via an oxygen containing intermediate, i.e. that hydrogen reacts with undissociated CO.

Van Steen and Schulz[14] argued that the LHHW approach of a single rate determining step (usually assumed to be the formation of the monomer), with all other elementary reactions close to equilibrium, is not valid for the FT synthesis. The objection centred on the fact that, if all other elementary reactions were in equilibrium, the thermodynamically predicted product spectrum of essentially only methane would be obtained. It is well known that the actual methane selectivity of the FT synthesis is much lower than that expected from thermodynamics. Therefore, the LHHW method was discarded in favour of another approach that is based on the irreversibility of the FT reaction, which yielded the following kinetic equation[14]:

$$r_{FT} = A\frac{P_{H_2}^{3/2}P_{CO}/P_{H_2O}}{(1+kP_{H_2}P_{CO}/P_{H_2O})^2} \qquad \ldots 7$$

However, it can be argued that this objection is not quite valid. The derivation of a LHHW-type kinetic expression for the FT reaction merely requires the assumption that the monomer is quickly removed by a subsequent reaction step after its formation. Whether this step is controlled by thermodynamics (which may predominantly result in the formation of methane) or by kinetics (which may favour hydrocarbon chain growth) is of no consequence to the overall rate of CO hydrogenation, as long as the

monomer is removed fast enough not to influence the overall reaction rate. In fact, by implication Van Steen and Schulz[14] made a similar assumption in the derivation of their own rate equation, since they only included vacant sites and surface carbon in their site balance equation. The surface concentrations of the other intermediate species (CH_x or C_yH_x) can only be negligible if polymerisation and subsequent desorption to final products are sufficiently fast reactions relative to the formation of surface carbon. If not, there would be a build-up of C_1 and higher intermediates on the catalyst surface, which would have to be included in the denominator of the kinetic expression. Nevertheless, as shown in Appendix A, the new iron-FT rate expression can be derived by following an approach analogous to that suggested by Van Steen and Schulz [14].

3. Evaluation of the new rate equation with existing kinetic data

In the historic studies that will subsequently be considered, kinetic models were fitted to the data by minimising the sum of the squares of the differences and the R^2–value was reported as a measure of the goodness of fit. Therefore, this convention will also be followed here for the reinterpretation of the existing data. For studies where the standard deviation of each measurement is available, "chi-square" (χ^2) fitting can also be performed as suggested by Press et al.[15]. In the latter method, the weight (importance) assigned to each observation is related to the accuracy of that specific measurement.

3.1 The kinetic study by Van Berge

Van Berge[5] performed a kinetic study on a precipitated iron catalyst in a well-mixed slurry reactor at a temperature of 250°C. As explained previously, a statistical design procedure was applied which showed that Equation 5 was the preferred form of a family of rate expressions that can in general be represented by Equation 4. The kinetic data are summarised in Appendix B and covered the ranges as presented in

Table 1. These data were now used to compare the new iron-FT rate expression (Equation 6) to some other popular kinetic equations. The model parameters were optimised to minimise the sum of the squares of the differences and the results are presented in Table 2. Two of the equations had negative regression coefficients, indicating that they describe the data substantially worse than the assumption of a constant reaction rate. This is probably a result of the experimental design procedure that was applied, which deliberately aimed at eliminating non-applicable kinetic models. The Van Steen and Anderson-Dry equations also fit the data quite poorly. Of the old rate equations, the one by Van Berge describes the data by far the best, which is in line with his conclusions[5]. The new expression, with quite a high regression coefficient, is a notable improvement on the Van Berge equation. Even though the coefficients of CO and water in the denominator term of the new equation assumed similar optimised values, this falsely creates the impression that water has an important influence on the reaction rate. In the last row of Table 2, it is shown that the omission of water from the inhibition term has a small influence on the R^2-value. It can therefore be argued that the coefficient of water in the new equation is not significantly different from zero, so that there is no basis for including water in the kinetic model. Since the standard deviations of the reaction rates reported by Van Berge[5] were available, the value of χ^2 could be calculated for every model fit and is reported in the last column of Table 2. These values confirm that the new kinetic model is better able to describe the FT reaction rate than the other equations considered here. Furthermore, by omitting water from the inhibition term of the new kinetic expression, the χ^2-value of the model fit actually decreased (i.e. the weighted error was lower), even though the sum of the squares of the differences ("unweighted" error) increased slightly. This means that the inclusion of water in the new expression merely improved the prediction of the "inaccurate" rate measurements, but that the measurements with a high degree of accuracy were in fact described worse. This suggests that the water term merely served to describe the erroneous variations in the

data, and corroborates the previous conclusion that there is no basis for including water in the inhibition term of the new equation. A parity plot of the new equation (without any water term in the denominator) is presented in Figure 1. Despite the fact that the model does not account for an influence of water, the agreement with the data is quite acceptable considering the wide range of process conditions covered (refer to Table 1).

The kinetic models were also fitted to the data by minimising the χ^2-value. Only selected results are presented in Table 3, because the other equations again fitted the data poorly. These results confirm all the previous findings. For the new rate equation, the optimised adsorption coefficient of water assumed a value of zero (under the physical constraint that this parameter cannot be negative), suggesting that FT site occupation by water is negligible. Furthermore, the new kinetic model is able to describe the data better than the best of the existing rate expressions without increasing the number of model parameters, as is evident from the lower χ^2-value. It therefore seems as if the following form of the new equation is an appropriate macro kinetic expression for the iron-FT reaction:

$$r_{FT} = A\frac{P_{H_2}{}^{0.5}P_{CO}}{\left(1+k_{CO}P_{CO}\right)^2} \qquad \ldots 8$$

Table 1: Range of experimental conditions covered by kinetic data measured by Van Berge[5] at 250°C in a well mixed slurry reactor with a Ruhrchemie-type precipitated iron catalyst. All values pertaining to conditions inside the CSTR.

Parameter	Range
P_{H_2}	1.4 – 15.3 bar
P_{CO}	0.9 – 7.2 bar
P_{H_2O}	0.3 – 2.0 bar
P_{CO_2}	1.1 – 5.5 bar
H_2/CO ratio	1.1 – 11.6

Tables 2 (top, model fitting by minimising the "sum of the squares of the differences") and 3 (bottom, model fitting by minimising χ^2): Comparison of iron-FT rate equations with data measured by Van Berge[5] at 250°C in a well mixed slurry reactor with a Ruhrchemie-type precipitated iron catalyst.

Kinetic equation	Parameter values	R^2	χ^2
Satterfield-Huff (Equation 3)	b = 9.2 [bar]	- 0.95	15005
Ledakowicz-Nettelhoff (Equation 2)	c = 0.4	- 0.62	9361
Van Steen (Equation 7)	k = 0.02 [bar $^{-1}$]	0.27	5690
Anderson-Dry (Equation 1)	b = 3.9	0.41	5138
Van Berge (Equation 5)	b = 1.6	0.76	4451
New model (Equation 6)	k_{CO} = 0.10 [bar $^{-1}$] k_{H2O} = 0.10 [bar $^{-1}$]	0.85	3818
New model* (Equation 6)	k_{CO} = 0.09 [bar $^{-1}$] k_{H2O} = 0*	0.82	3280

* Coefficient of water in the denominator specified as zero

Kinetic equation	Parameter values	χ^2
Van Berge (Equation 5)	b = 0.98	2918
New model (Equation 6)	k_{CO} = 0.11 [bar $^{-1}$] k_{H2O} = 0 [bar $^{-1}$]	2599

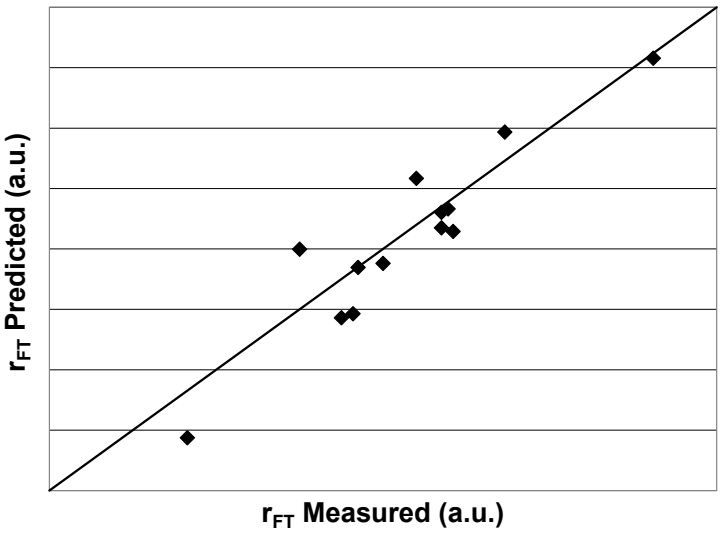

Figure 1: Parity plot of new FT rate expression (Equation 8) with no water term in the denominator for data measured by Van Berge[5] (experimental conditions as per Tables 1 to 3).

3.2 The Ledakowicz-Nettelhoff study

Ledakowicz et al.[3] reported an FT kinetic study on a potassium-promoted precipitated iron catalyst, performed in a stirred autoclave slurry-phase reactor. The catalyst had such a high WGS activity that the water concentration inside the reactor was negligible. It was expected that the measured FT reaction rate would be directly proportional to the hydrogen partial pressure, since both the Anderson-Dry and Satterfield-Huff rate expressions (Equations 1 and 3, respectively) approach simple first order kinetics in hydrogen at low water partial pressures. If the rate could be described by simple first order kinetics in hydrogen, then the ratio of the FT reaction rate to the hydrogen partial pressure should yield a constant value at each of the reaction temperatures investigated. However, from Figure 2, it is clear that this was not the case, especially at higher reaction temperatures. Because of this deviation from first order kinetics in hydrogen at negligible water partial pressure, rate inhibition due to competitive adsorption between CO and CO_2 was assumed. This yielded the Ledakowicz-Nettelhoff kinetic expression for the iron- FT reaction (Equation 2).

The data presented by Ledakowicz et al.[3] were now also used to validate the new FT rate equation. As the water partial pressure was negligible for all the points, it was not sensible to consider kinetic models that assume an influence of water on the reaction rate. Consequently, only the Ledakowicz-Nettelhoff expression and the new model in the form of Equation 8 were considered. Only three to four data points were measured at each of the four reaction temperatures. The reaction rate constants of the two involved equations were optimised for each temperature, but due to the limited amount of data, the respective adsorption coefficients were assumed to be constant (independent of temperature). The results of the re-analysis, presented in Table 4, indicate that both models described the data near perfectly. The excellent fit of these equations is probably on account of the small amount of data with a limited variation in the process conditions and is therefore in itself not much proof of the validity of either. However, this data set is of major significance, since the water concentration

Table 4: Comparison of iron-FT rate equations with data measured by Ledakowicz et al.[3] at 220°C to 260°C in a stirred slurry-phase reactor with a potassium-promoted precipitated iron catalyst.

Kinetic equation	Parameter values	R^2
Ledakowicz-Nettelhoff (Equation 2)	$c = 0.24$	0.99
New model (Equation 8)	$k_{CO} = 0.12$ [bar $^{-1}$]	0.99

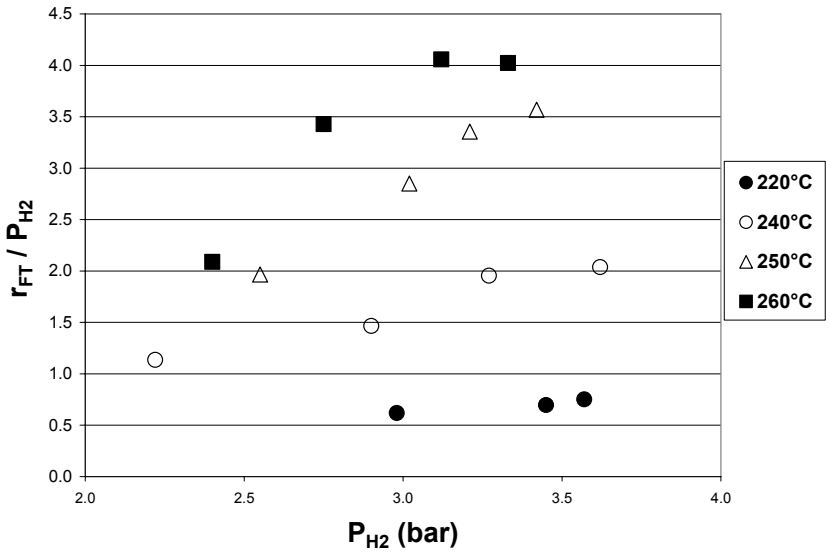

Figure 2: Testing the kinetic data of Ledakowicz et al.[3] (measured at 220°C to 260°C in a stirred slurry-phase reactor with a potassium-promoted precipitated iron catalyst) for first order kinetics in hydrogen.

inside the reactor was negligible. Figure 2 indicates that the reaction rate cannot be described by a first order rate equation in hydrogen, as suggested by Equations 1 and 3. The fact that an inhibiting effect on the kinetics was observed even in the absence of water suggests that the premise of rate inhibition by water is not correct. Based on CO_2 co-feeding studies[7,8], it was also concluded previously (see also Chapter 2) that CO_2 could not be responsible for this retarding effect, eliminating the Ledakowicz-Nettelhoff expression as well. Instead, it appears more and more that the presence of

vacant sites on the catalyst surface has a significant influence on the iron-FT reaction rate. Moreover, the value obtained for the CO coefficient is very similar to that obtained previously (compare the k_{CO} value of Table 4 with those reported in Tables 2 and 3 for the same equation).

3.3 The Zimmerman study

Zimmerman and Bukur[16] performed an FT kinetic study in a stirred-tank slurry reactor. For their "in-house"-prepared precipitated iron catalyst, seven data points were obtained at a reaction temperature of 250°C. It was reported that the Anderson-Dry expression (Equation 1) could describe this data better than the Satterfield-Huff expression (Equation 3). In the current study, these data were therefore used to compare the predictive capability of the new kinetic model (Equation 8) with that of the Anderson-Dry equation and the results are presented in Table 5. Both equations described the reaction rate well. Nevertheless, the new expression was somewhat better and the value obtained for the CO coefficient is reasonably well in line with the values reported earlier in Tables 2 and 3. The parity plot of the new rate equation (Figure 3) also indicates a very good fit of the data. It should also be noted that the inclusion of a water term in the denominator of the new rate expression merely improved the data fit marginally (as indicated in the last row of Table 5) so that once again there is not much basis for including water in this kinetic model.

Table 5: Comparison of iron-FT rate equations with data measured by Zimmerman and Bukur[16] at 250°C with an "in-house" prepared precipitated iron catalyst (promoted with potassium).

Kinetic equation	Parameter values	R^2
Anderson-Dry (Equation 1)	$b = 5.0$	0.90
New model (Equation 21)	$k_{CO} = 0.08$ [bar $^{-1}$]	0.96
New model (Equation 6)	$k_{CO} = 0.07$ [bar $^{-1}$] $k_{H2O} = 0.05$ [bar $^{-1}$]	0.97

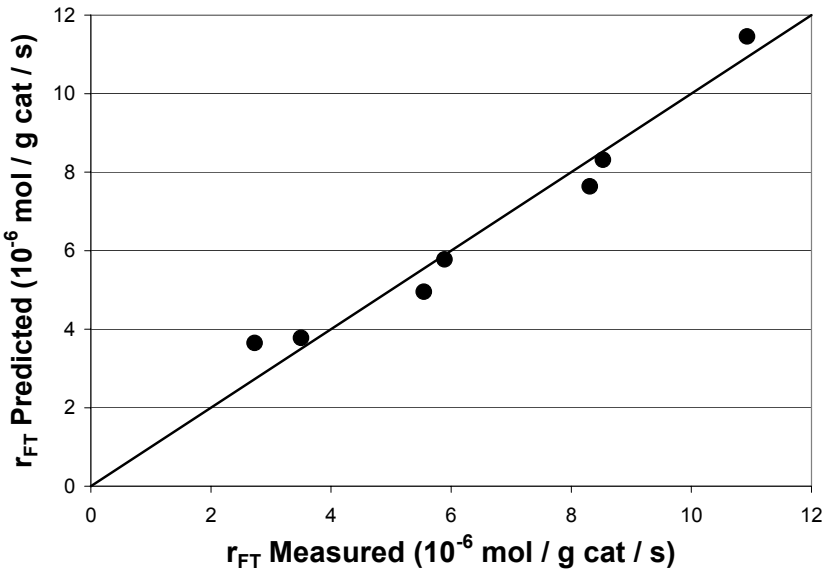

Figure 3: Parity plot of new FT rate expression (Equation 8) for kinetic data measured by Zimmerman and Bukur[16] at 250°C with an "in-house" prepared precipitated iron catalyst (promoted with potassium).

3.4 The kinetic study by Huff

Huff and Satterfield[2] performed a kinetic study on a potassium-promoted fused magnetite catalyst in a well-mixed slurry reactor. The experiments were performed at three different temperatures (232°C, 248°C and 263°C). It was shown graphically that the linearised form of the Satterfield-Huff expression (Equation 3) correlated reasonably well with the kinetic data and it was concluded that this model was an adequate description of the iron-FT reaction rate. The new iron-FT rate expression (Equation 6) was now compared to the Satterfield-Huff equation by means of non-linear regression of data reported by Huff[17] (Table 6). For all three reaction temperatures, the coefficient of water in the new equation assumed a value of zero under the physical constraint that this parameter cannot be negative. Furthermore, the regression coefficients of the new kinetic expression were comparable to or higher than those of the Satterfield-Huff equation. It should be noted that the coefficient of CO in the new model increases with temperature, which is opposite to what one would

expect from an adsorption coefficient. However, considering the derivation presented in Appendix A, this model parameter is not necessarily a real adsorption coefficient, since it may consist of the actual adsorption coefficient, as well as the rate constants of certain elementary reaction steps. If, for example, the value of rate constant k_3 increases significantly with temperature relative to the values of k_4, k_5 and k_6, the observed k_{CO} in the rate equation will increase. Therefore, depending on the relative activation energies of the involved elementary reaction steps, the value of the observed CO coefficient can either increase or decrease with temperature. A further notable observation is that the coefficient obtained for CO is much higher than that of the other studies considered here (see Tables 2 to 5). The only obvious difference between the Satterfield-Huff study and the other studies is that the former utilised a fused iron catalyst, whereas the others made use of precipitated (mostly Ruhrchemie-type) iron catalysts.

Table 6: Comparison of iron-FT rate equations with data from Run 9 reported by Huff[17]. Measurements performed in a mechanically stirred slurry reactor with a fused iron catalyst.

Reaction temperature	Satterfield-Huff (Equation 3)	New model (Equation 6)
232°C	b = 21.4 [bar] R^2 = 0.85	k_{CO} = 0.33 [bar $^{-1}$] k_{H2O} = 0 [bar $^{-1}$] R^2 = 0.83
248°C	b = 9.0 [bar] R^2 = 0.71	k_{CO} = 0.51 [bar $^{-1}$] k_{H2O} = 0 [bar $^{-1}$] R^2 = 0.82
263°C	b = 5.5 [bar] R^2 = 0.65	k_{CO} = 0.58 [bar $^{-1}$] k_{H2O} = 0 [bar $^{-1}$] R^2 = 0.81

3.5 The study by Van Steen

Van Steen and Schulz[14] proposed an FT rate equation that was intended to be valid for both iron- and cobalt-based FT catalysts (Equation 7 of this chapter). Using data

obtained with various iron-FT catalysts, Equation 7 was compared with the Satterfield-Huff model (Equation 3). To this end, the two equations were linearised to assume the following forms:

Van Steen (linearised): $$\left[\frac{P_{H_2}^{3/2} P_{CO}}{P_{H_2O}\ r_{FT}}\right]^{1/2} = \frac{1}{A^{1/2}} + \frac{k}{A^{1/2}} \frac{P_{H_2} P_{CO}}{P_{H_2O}} \qquad ...9$$

Satterfield-Huff (linearised): $$\frac{P_{H_2}}{r_{FT}} = \frac{1}{A} + \frac{b}{A} \frac{P_{H_2O}}{P_{H_2} P_{CO}} \qquad ...10$$

The regression coefficients (R^2-values) of the linearised Van Steen equation were reported to be between 0.94 and 0.97 for the various catalysts, while that of the linearised Satterfield-Huff model were much lower at around 0.1 to 0.5. Van Steen and Schulz [14] therefore concluded that the Satterfield-Huff equation described the kinetic data quite poorly, while the Van Steen equation could predict the FT reaction rate very accurately. It was, however, later acknowledged that Equation 7 cannot describe the FT reaction rate under all synthesis conditions, since a zero reaction rate is predicted in the absence of water[18]. An alteration in the scheme of elementary reaction steps was proposed to explain why the FT reaction could still proceed in the presence of pure syngas, but such schemes of possible reaction pathways can become so complex and numerous that one can probably provide an explanation for any deviation observed from the measured reaction rate. The zero reaction rate predicted when no water is present will probably remain a point of concern for the Van Steen kinetic model.

The iron-FT data used in the foregoing historic study were obtained[19] and now re-analysed as part of the current investigation. Firstly, the Satterfield-Huff model (Equation 3) was linearised in an alternative way to more closely resemble the linearised form of the Van Steen model:

Satterfield-Huff (alternative): $$\frac{P_{H_2}^2 P_{CO}}{P_{H_2O}\, r_{FT}} = \frac{b}{A} + \frac{1}{A}\frac{P_{H_2} P_{CO}}{P_{H_2O}} \qquad ...11$$

Tables 7 (top, linear regression) and 8 (bottom, non-linear regression): Regression coefficients (R^2-values) obtained from regression of the iron-FT data reported by Van Steen[19]. Data measured in a stirred slurry reactor with an iron catalyst at 225°C and an iron-manganese catalyst at 275°C.

Catalyst	Van Steen – linearised (Equation 9)	Satterfield-Huff – linearised (Equation 10)	Satterfield-Huff – alternative linearisation (Equation 11)
Fe	0.94	0.10	0.89
Fe/Mn	0.97	0.50	0.99

Catalyst	Van Steen (Equation 7)	Satterfield-Huff (Equation 3)
Fe	0.26	-0.30
Fe/Mn	-0.63	-0.39

The three linearised models (Equations 9 to 11) were then fitted to the iron-FT kinetic data and the regression coefficients obtained are presented in Table 7. As reported by Van Steen and Schulz [14], Equation 9 has very high R^2-values, while Equation 10 correlates very poorly with the data. However, contrary to expectation, the R^2-values obtained for Equation 11 are quite high and comparable to those of the linearised Van Steen expression. It is insightful to note that by merely changing the method of linearisation, the Satterfield-Huff model could be converted from a linear equation with almost no correlation with the data to a linear equation that describes the data as accurately as the linearised Van Steen model. This vividly illustrates the mathematical artefacts that can be created by linearisation of rate expressions. In view of this, the Van Steen and Satterfield-Huff equations were fitted to the same two sets of data by means of non-linear regression and the R^2-values are reported in Table 8. The regression coefficients assumed either negative or very small positive values, indicating that neither equation can describe the reaction rate well. As graphical

confirmation of the foregoing, the correlation between the Van Steen model and the data obtained with the pure iron catalyst is presented in linear and non-linear forms (Figures 4 and 5, respectively). Despite the apparent correlation between the data and the linearised model (Figure 4), the parity plot of the non-linear model (Figure 5) verifies that there is actually little agreement between the model and the data. This was indeed also the case when the other kinetic models mentioned in this chapter were considered.

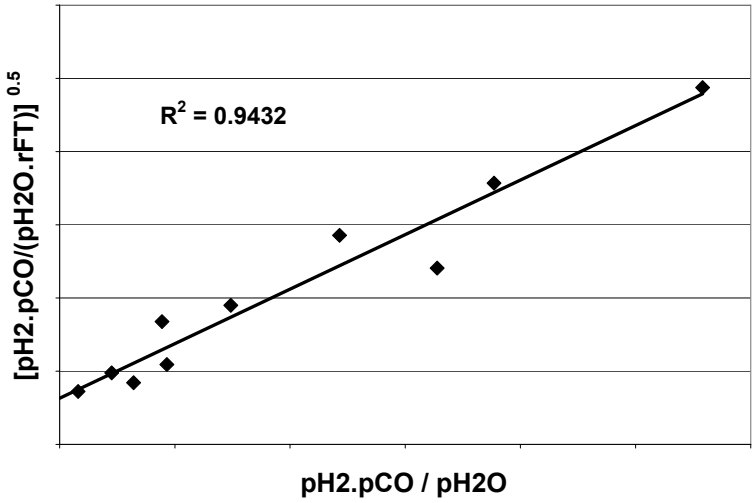

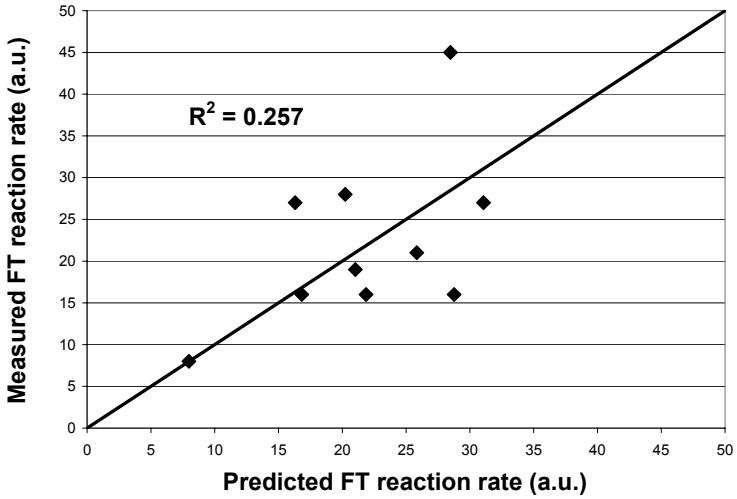

Figure 4 (top): Correlation between the linearised Van Steen kinetic model and the kinetic data for the pure iron catalyst. Figure 5 (bottom): Parity plot of non-linearised Van Steen kinetic model for data obtained with the pure iron catalyst. Data measured by Van Steen[19] at 225°C in a stirred slurry reactor.

3.6 Iron catalyst optimised for the production of olefins

An experimental study has been performed at Sasol on a precipitated iron-based catalyst optimised for olefins production. In addition to the normal promoters of the Ruhrchemie-type catalysts, this catalyst contained metals like zink and manganese. The study was performed in a laboratory slurry reactor and most of the measurements were made at 240°C. The data are summarised in Appendix B. Note that there is a fair amount of repetition in the data, as the original aim of the experimental study was wider than merely to investigate the shape of the kinetic model. Various rate expressions were fitted to this set of data and the results are presented in Table 9. The R^2-values for all the equations are reasonably high. Possibly the variation in the data was not extensive enough to allow for clear discrimination between the various kinetic models considered. Nevertheless, the results are well in line with those found previously. During model optimisation, the water coefficient in the new kinetic equation assumed a value of zero, while the CO coefficient was similar to the values obtained previously (around 0.1). Furthermore, the new kinetic model is better than all the other rate equations. It is also interesting to note that, for Equations 1, 2, 3 and 5, the coefficients of water and carbon dioxide are either zero or negligibly low, indicating that these models in their intended forms actually fail to describe the data measured with the catalyst optimised for olefins production.

4. Validation of the new kinetic model

The foregoing reinterpretation of existing data showed that the new kinetic expression is more generally applicable than any of the other equations considered here, since it could describe the data of various different historic studies. The proposed model is somewhat controversial, as it does not account for any effect of water on the reaction rate. Therefore, an experimental study was performed to discriminate unambiguously between the new kinetic equation and those rate expressions that incorporate water in the inhibition term. Since the study of Van Berge[5] was very effective to eliminate a

number of other rate expressions, Equations 5 and 8 are regarded as the main rival models; consequently, the current experimental design procedure will specifically aim to discriminate between these two expressions.

Table 9: Testing various iron-FT rate equations with the data obtained with a catalyst optimised for olefins production. Measurements performed at 240°C in a well-mixed slurry reactor.

Kinetic equation	Parameter values	R^2
Van Berge (Equation 5)	$b = 0$	0.75
Van Steen (Equation 7)	$k = 0.02$ [bar $^{-1}$]	0.77
Satterfield-Huff (Equation 3)	$b = 0$ [bar]	0.81
Ledakowicz-Nettelhoff (Equation 2)	$c = 0$	0.81
Anderson-Dry (Equation 1)	$b = 0.2$	0.82
New model (Equation 6)	$k_{CO} = 0.12$ [bar $^{-1}$] $k_{H2O} = 0$ [bar $^{-1}$]	0.85

4.1 Experimental design

In principle, the operating points of the kinetic study can be selected by means of a statistical design procedure which ensures that a wide range of random process conditions are covered. This will typically require a substantial number of measurements and still does not guarantee that the data obtained will allow for clear model discrimination. It is also trivial to prescribe specific conditions inside the reactor where the rival rate expressions predict different reaction rates, but it can be quite difficult in practice to bring about a specific set of reagent partial pressures at the outlet of a CSTR type of reactor. It was therefore decided to rather develop a methodology of varying the system inputs which would ensure that operating conditions are covered where the rival kinetic models differ significantly.

Since the aim of the study is to perform kinetic measurements under conditions where Equations 5 and 8 predict significantly different reaction rates, a range of conditions must be identified where the ratio of the two equations varies substantially. Since the reaction terms of the two expressions are the same, this essentially means that the experimental approach must ensure a large variation in the ratio of their inhibition terms (defined here as R_{inh}):

$$R_{inh} = \frac{P_{CO} + k_{H_20} P_{H_20}}{\left(1 + k_{CO} P_{CO}\right)^2} \qquad ...12$$

It thus follows that only the partial pressures of CO and H_2O are important. For the purpose of the current comparison, the hydrogen partial pressure is irrelevant, since the two expressions have exactly the same dependency on hydrogen. The values of the water and CO coefficients in the denominators of Equations 5 and 8, respectively, varied slightly according to the method of data analysis. Selecting the values obtained via "least squares" fitting (Table 2), the ratio of the inhibition terms is expressed in Equation 13. A three-dimensional plot of R_{inh} as a function of P_{CO} and P_{H2O} is presented in Figure 6.

$$R_{inh} = \frac{P_{CO} + 1.6 P_{H_20}}{\left(1 + 0.09 P_{CO}\right)^2} \qquad ...13$$

FT kinetic studies are often performed at constant total pressure and with a feed gas consisting only of hydrogen and carbon monoxide. Different conditions inside the reactor are then obtained by varying the space velocity (i.e. conversion) and the H_2/CO ratio of the feed. Since a mol of water is produced for every mol of CO consumed by the FT reaction, there is always a risk that FT kinetic data may contain an inverse relationship between the partial pressures of CO and H_2O (as illustrated in Figure 7). Considering Figure 6, it is clear that this type of interrelationship runs more or less

along a contour (band of constant values) of R_{inh}. Even if the newly-proposed expression (Equation 8) proves to be a more appropriate kinetic model than the traditional equations, it is not surprising that the Anderson-Dry type inhibition term was historically believed to be the correct denominator of the rate equation. Even for the kinetic study of Van Berge[5] where the reagent partial pressures were varied independently, the value of R_{inh} did not change extensively enough to make a final conclusion regarding the form of the inhibition term. For 10 of the 13 data points, the value of R_{inh} fell in the narrow band of 2.5 to 3.2.

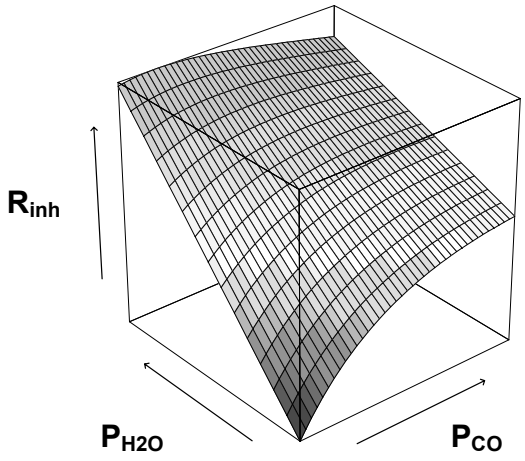

Figure 6: The ratio of the inhibition terms of the two rival kinetic models (Equations 5 and 8) as a function of the CO and water partial pressures.

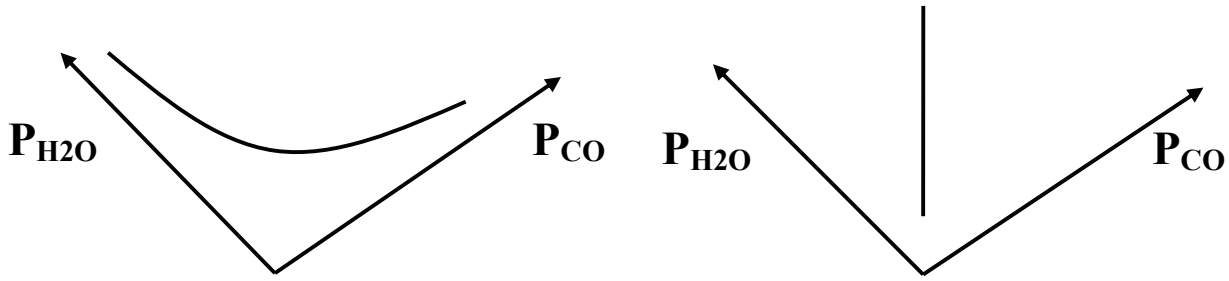

Figure 7 (left): Inverse relationship between P_{CO} and P_{H2O} that is often encountered in FT kinetic data. Figure 8 (right): Relationship required between P_{CO} and P_{H2O} to discriminate between the two candidate FT kinetic models.

For the new experimental program, it is thus clear that the partial pressures of CO and H_2O must be varied in a fairly constant ratio (as illustrated in Figure 8). This can be achieved by keeping the feed composition and conversion more or less constant, while varying the reactor pressure. By superimposing Figure 8 on Figure 6, it is clear that this approach will ensure a substantial variation in R_{inh}, and thereby generate data where the two rival kinetic models predict significantly different reaction rates. Very low reactor pressures are especially important, since the slope of the curved plane that represents R_{inh} is at its steepest when both P_{H2O} and P_{CO} are low.

4.2 Experimental and data analysis

4.2.1 Experimental set-up, gas analysis and data processing

A schematic showing the layout of the reactor rig is provided in Figure 9. The FT synthesis was performed in a mechanically-stirred slurry reactor with an internal volume of 600 ml. The reactor has a cylindrical shape with the impeller shaft running down the centre. The shaft is fitted with two impellers, namely one at the bottom of the reactor, and one about halfway up the reactor height. The reactor is also equipped with three vertical baffle plates which help to induce turbulent mixing inside the agitated reactor. Gas is supplied via a dip-tube that is situated next to the inner wall of the reactor. This tube extends down to just above the bottom impeller, where the gas is released into the slurry. The exit line at the top of the reactor is equipped with a sintered metal filter so that the catalyst particles are retained inside the reactor. The position of the exit line determines the liquid level inside the reactor, as the excess liquid, together with the gaseous effluent, passes through this line to the hot knock-out pot (maintained at 200°C). The waxy liquid that accumulates inside the hot pot is usually drained once a day. The gas flows to the cold knock-out pot (maintained at 25°C) where water and oil are condensed. From the cold pot, the gas passes through a back-pressure regulator (responsible for maintaining the pressure of the system) into the vent line. The tail gas sample point is situated between the cold knock-out pot and

the back-pressure regulator. The total feed and the tail gas are analysed with an online gas chromatograph (Gow-Mac Series 600) equipped with a thermal conductivity detector (TCD).

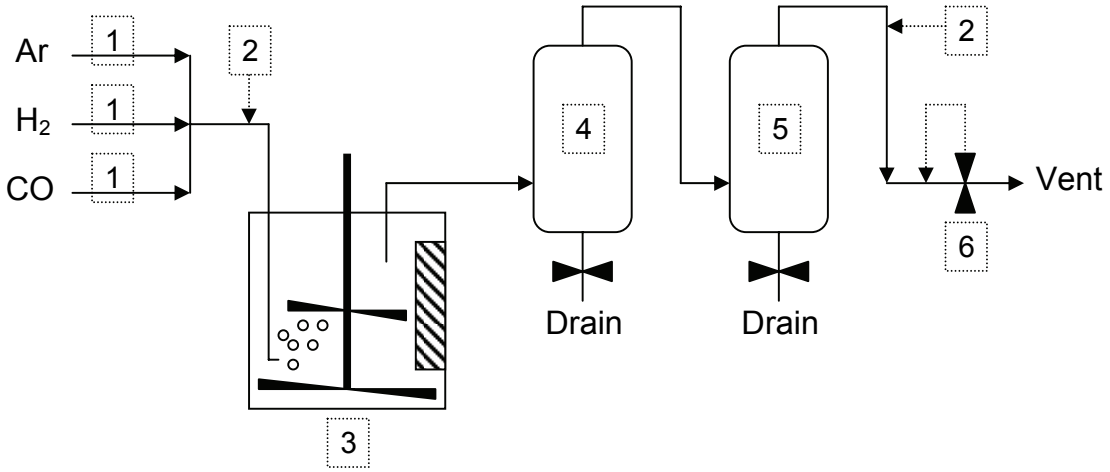

1. Gas supply lines
2. Gas sample points
3. Slurry reactor with gas supply, impeller system and baffles shown
4. Hot knock-out pot
5. Cold knock-out pot
6. Back-pressure regulator

Figure 9: Schematic diagram of reactor rig layout used for the kinetic validation experiments.

The catalyst used in this study was a Ruhrchemie-type spray-dried, precipitated iron catalyst as described in detail elsewhere[20]. Calcined catalyst (20 g) was loaded together with 350 g of FT wax into the reactor. The following gases, with minimum purities indicated, were fed from cylinders: hydrogen (99.999%), CO (99.9%) and Ar (99.999%). The feed gas composition and the temperature were kept constant during activation and synthesis. The feed consisted of the following gases with the approximate volume percentages given in brackets: hydrogen (50 %), carbon monoxide (32 %) and argon (18 %). The feed flow rates of the three gases were

controlled with Brooks mass flow controllers. Catalyst activation was performed for 16 hours at 240°C and 20 bar (gauge) with syngas of the same feed composition as used during synthesis, but at a very high space velocity (similar to the procedure followed elsewehere[21]). After activation, the total feed flow rate was lowered to a predetermined value, while the temperature and pressure were kept at 240°C and 20 bar (gauge), respectively. This represented the baseline operating condition, which was maintained until it was certain that the catalyst achieved stable performance before the kinetic measurements commenced. The stabilised syngas conversion at the reference conditions was about 45%.

Argon served as an internal standard for the purpose of data processing. Being an inert, it passes through the reactor unconverted, which means that the argon in- and outlet flow rates are known from the calibration curve of the Brooks mass flow controller. Combining this flow rate with the GC-TCD analyses, the in- and outlet flow rates of the other permanent gases (hydrogen, CO and CO_2) could be determined. Since water was not measured, its production rate was calculated from an oxygen balance under the assumption that the contribution from oxygenates in the product spectrum was negligible. The Fischer-Tropsch reaction rate was defined as the amount of CO converted to hydrocarbons per unit time per unit amount of catalyst, i.e. independent of the water-gas-shift rate. It was calculated as the total rate of CO consumption minus the rate of CO_2 production.

In FT kinetic measurements, significant errors are often unavoidable, but at the very least cognisance should be taken of these. E.g., if the error in the CO and CO_2 flow rates were assumed to be a mere one percent for the current set of experimental data, the accumulated error in the calculated FT reaction rate could be up to 6%. Furthermore, even though the catalyst is known to have a fairly low oxygenate selectivity under the reference conditions of the kinetic experiments, the omission of the oxygenate contribution from the oxygen balance could have resulted in an overestimation of between 4% and 7% in the water production rate, depending on the

CO_2 selectivity of the involved data point. Clearly errors in the primary data that appear insignificant can be accumulated and amplified via the data processing procedure to assume notably large values in the final results. The experimental design of FT kinetic experiments is therefore of the utmost importance to ensure that conditions are covered where rival kinetic models differ so extensively that model discrimination can be clear and unambiguous, despite the involved experimental errors.

4.2.2 Elimination of mass transfer restrictions

By means of calculation, it was estimated that the effectiveness factor of the catalyst particles was above 98% for all kinetic measurements (see Appendix C). The fine spray-dried catalyst particles used in this study therefore ensured that the kinetic measurements were not notably influenced by intra-particle mass transfer limitations. A run was also performed where the stirrer speed of the mechanical agitator was varied to confirm that inter-particle (gas-liquid and liquid-solid) mass transfer limitations were eliminated. This run was performed at 5, 20 and 40 bar (gauge) to cover the whole pressure range of the kinetic experiments, since both the mass transfer rate and the intrinsic FT reaction kinetics are dependent on pressure. High space velocities were also employed during this run so that the resulting FT reaction rate was between 30 % and 100% higher than during the actual kinetic measurements at the corresponding pressure. In other words, mass transfer restrictions were eliminated at higher chemical reaction rates than those encountered during the actual kinetic experiments. The effect of the stirrer speed on the FT reaction rate is presented in Figure 10. The data in this graph were normalised to the highest reaction rate of the run. Clearly there was no effect of the stirrer speed on the reaction rate beyond 450 rpm. Therefore, the stirrer speed of 450 rpm used during the actual kinetic measurements was sufficient to eliminate inter-particle mass transfer limitations.

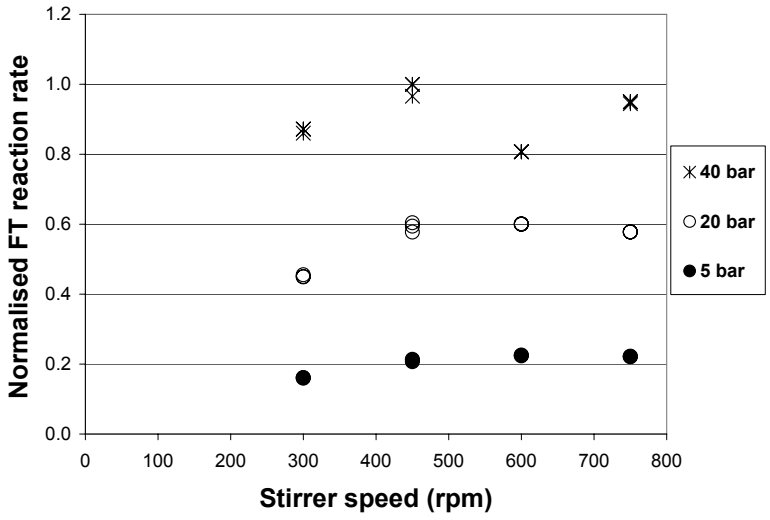

Figure 10: Effect of stirrer speed on FT reaction rate at various operating pressures. Run performed at high space velocities (high FT reaction rates) to demonstrate that mechanical stirring was sufficiently fast during the kinetic validation run to eliminate gas-liquid and liquid-solid mass transfer limitations. FT reaction rate normalised to the highest rate measured during the run.

4.2.3 Kinetic measurements

In our experience at Sasol, the iron-based catalyst in the LTFT synthesis can be notoriously unstable if operated over the wide range of process conditions normally required for a kinetic study. In order to ensure a stable intrinsic activity of the catalyst, the following methodology was employed. The reactor was essentially maintained at reference conditions and changes to other operating points were only made for short intervals. Calculations showed that, at the involved feed flow rates, it would not take more than about an hour for five replacements of the combined gas inventory of the reactor and the knock-out pots. Therefore, a change in operating conditions was made in the morning and three samples were taken between 2 and 6 hours after such a change had been effected. Subsequently, the system was returned to the reference conditions, which were maintained until the next morning when another kinetic measurement was made. The aim of this procedure was therefore to allow sufficient

time for the reactor to attain steady state with regard to the permanent gases, but insufficient time for the catalyst to respond notably to the new conditions. The reference measurements taken regularly throughout the run, as well as the three samples taken at the non-baseline conditions over a period of 4 hours, could confirm that the FT activity of the catalyst was indeed stable. It should be noted that two separate, duplicate runs were performed in this manner to ensure confidence in the outcome of the study. Since the results of the two runs were essentially the same, only one run will be discussed.

It can of course be argued that, for practical application of rate equations, it is only important to describe the overall steady state kinetics of the system. A rate equation that incorporates both the intrinsic reaction kinetics and the manner in which the catalyst responds to its environment should therefore be sufficient. However, since such a rate expression would attempt to combine two fundamentally unrelated aspects as one phenomenon, it would be highly empirical. It is believed that much better understanding and predictive accuracy can be achieved by rather studying and describing these two aspects separately. Therefore, this study is only concerned with the intrinsic kinetics of the FT reaction.

4.2.4 Data analysis

Since the operating pressure varied from 5 to 40 bar during the experimental runs and the iron-FT reaction rate is more or less proportional to the syngas partial pressure, the measured reaction rates covered a very broad range. If the kinetic models were fitted to the data by minimising the absolute error, it would have assigned a higher importance to the rates measured at high pressure. This would have defeated the aim of the experimental design procedure, which indicated that rate measurements at very low pressures are especially important for discriminating between the two rival models. In order to rather assign equal weights to the rate measurements across the whole range of reactor pressures, it was thought more appropriate to minimise a

relative error. Consequently, whenever rate expressions were fitted to the new kinetic data, the relative variance was minimised (as defined by Van der Laan[10]).

4.3 Results and discussion of the kinetic measurements

Apart from the reference operating pressure of 20 bar (gauge), kinetic measurements were also performed at reactor pressures of 5, 10, 30 and 40 bar (gauge). As mentioned previously, three samples were taken at each of the non-reference conditions between 2 and 6 hours after a change from the reference condition was made. The run history (operating pressure as a function of synthesis time) is presented in Figure 11, while the measured FT reaction rates (normalised to that of the first measurement at reference conditions) are presented in Figure 12. Apart from some limited scatter in the data, the reference FT reaction rate was fairly constant over the period of synthesis, indicating a stable FT activity during the intrinsic kinetic measurements. Furthermore, at each of the non-reference pressures, the three measurements taken were fairly similar to one another, indicating that the time allowed for the reactor to reach steady state was sufficient and that the catalyst did not respond significantly to the six-hour long change in conditions. It is further clear that the changes in the FT reaction rate due to varying operating pressures were substantially larger than the scatter in the data, so that the random experimental errors are not expected to have a significant influence on the interpretation of the results.

The kinetic data from this run are presented in Appendix B. For data analysis purposes, only three representative reference (baseline) points were selected: one at the beginning, one in the middle, and one at the end of the run. This ensured that the reference conditions did not have more weight than any of the other conditions. The two rival FT rate expressions were fitted to the kinetic data and the results are presented in Table 10. When the adsorption coefficients were assigned their original values (k_{H2O} = 1.6 in the case of Equation 5 and k_{CO} = 0.09 in the case of Equation 8), it was found that the Van Berge equation had a very high relative variance, whereas

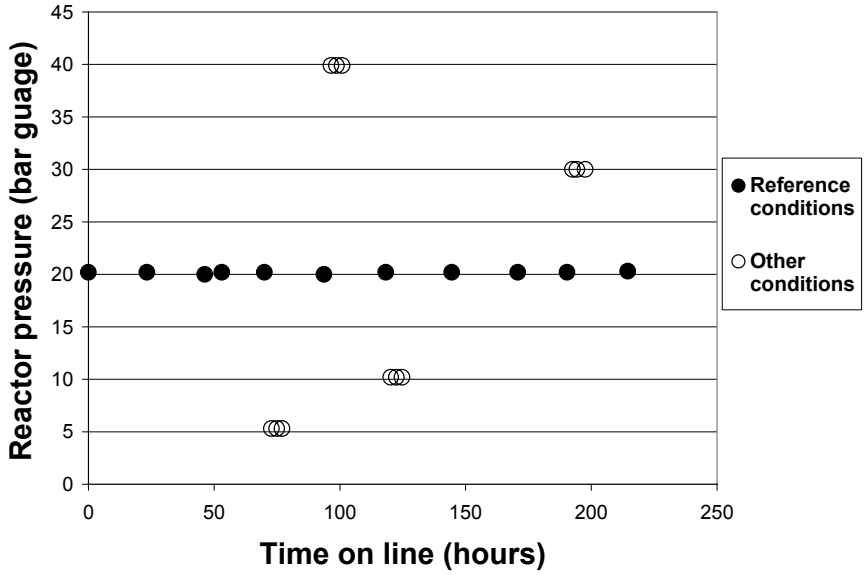

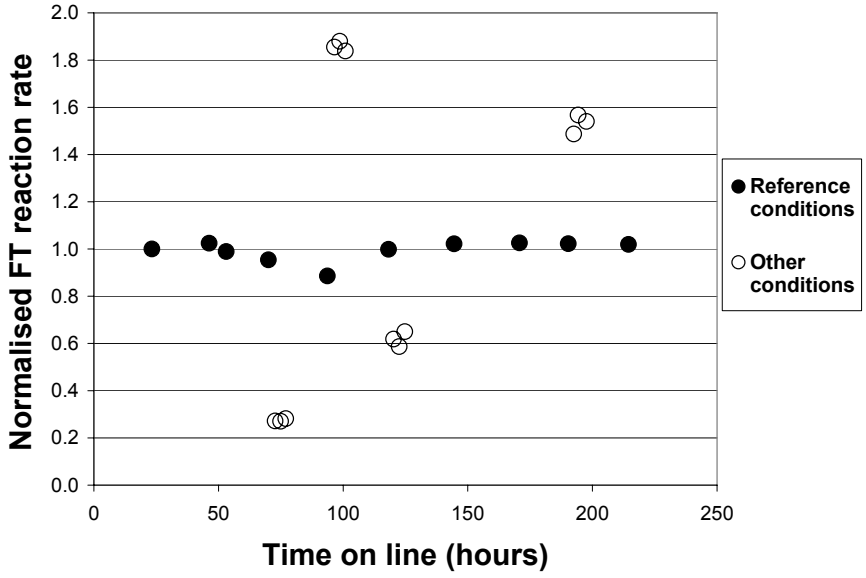

Figures 11 (top, reactor pressure versus time on line) and 12 (bottom, normalised FT reaction rate versus time on line) for the kinetic validation run performed with a precipitated (Ruhrchemie-type) iron catalyst at 240°C in a well-mixed slurry reactor. FT reaction rate normalised with respect to the first measurement taken at reference conditions.

Table 10: Testing the two rival iron-FT kinetic models, as well as some previously discarded models, with data from the new kinetic validation run. Experimental details as per Figures 11 and 12.

Kinetic equation	Optimised parameter values	S_{rel} (%)
Van Berge (Equation 5)	k_{H2O} = 1.6*	51.6
New model (Equation 8)	k_{CO} = 0.09* [bar $^{-1}$]	8.1
Van Berge (Equation 5)	k_{H2O} = 0 (k_{H2O} = - 1.3 unconstrained)	41.2
New model (Equation 8)	k_{CO} = 0.09 [bar $^{-1}$]	8.1
Van Steen (Equation 7)	k = 0.01 [bar $^{-1}$]	22.8
Anderson-Dry (Equation 1)	k_{H2O} = 0	11.2
Satterfield-Huff (Equation 3)	k_{H2O} = 0 [bar]	11.2
Ledakowicz-Nettelhoff (Equation 2)	k_{CO2} = 0	11.2

* Specified values

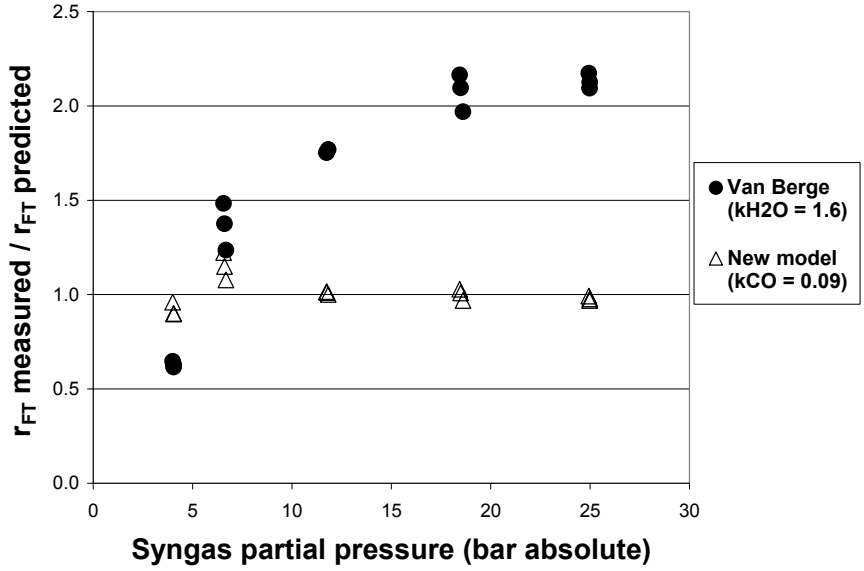

Figure 13: Accuracy of the two rival models as a function of syngas partial pressure for data from the kinetic validation run. Original adsorption parameter values were applied. Experimental details as per Figures 11 and 12.

the new kinetic model had a fairly low variance. This suggests that the Van Berge model is incapable of describing the data, but that the new model is very much in line with the measured data. The two models were also compared graphically by plotting the ratio of the measured to the predicted FT reaction rate as a function of the syngas partial pressure inside the reactor (Figure 13). Clearly the Van Berge equation has a very serious systematic deviation with variation in syngas pressure which is especially evident at low pressures. The slight deviations in the new kinetic expression appear to be random scatter and the model is generally very accurate.

The adsorption coefficients of Equations 5 and 8 were also re-optimised with the new data set to establish whether either of these expressions could benefit from improved parameter values. The results of this re-optimisation are also presented in Table 10. When the water coefficient in the Van Berge expression was unconstrained during the optimisation procedure, it assumed a significantly large negative value (-1.3). This physically impossible situation indicates that this rate equation does not correctly account for the effect of water on the FT reaction rate. In fact, it suggests that the inhibition term of Equation 5 (and especially the notion of FT rate inhibition by water) is principally flawed. By applying the physical constraint that an adsorption coefficient must be non-negative, the water coefficient assumed an optimised value of 0. Even though the omission of water from the denominator improved the fit of the Van Berge expression somewhat (as indicated by the slight decrease in S_{rel}), it reduced the model to a simple half-order equation in hydrogen. To the contrary, the re-optimised CO coefficient in the new FT rate expression was almost exactly the same as the original estimate taken from Table 2, which installs further confidence in the new model. As a further test of whether water should be included in this model, a water term was added to the denominator of the new rate equation. Although not shown here, the coefficient of water assumed a value of zero. This confirms that water should not be included in the denominator of the new FT kinetic equation. It is also an indirect indication that

water does not compete with the reactants (CO and hydrogen) for adsorption onto the FT catalytic sites.

Table 11: Effect of the water coefficient value in the Anderson-Dry equation on the ability of the model to fit data from the new kinetic validation run. Experimental details as per Figures 11 and 12.

Specified value of k_{H2O}	S_{rel} (%) after re-optimisation of the activity parameter
0	11.2
0.5	15.3
1.0	18.6
1.5	21.1

The other FT rate expressions considered in this study (Equations 1, 2, 3 and 7) were also fitted to the data of the kinetic validation run to verify that they have been rightfully discarded in the past. The results are included in Table 10. The Van Steen equation (Equation 7), which did not describe any of the historic data sets adequately, here also has a rather high relative variance. For Equations 1, 2 and 3, the fairly low values of S_{rel} suggest reasonable descriptions of the FT reaction rate, but this observation is misleading. In each case the coefficient of the inhibiting agent (water or carbon dioxide) assumed the lowest value that is physically meaningful, namely zero. This means that all three these expressions were reduced to a simple first order expression in hydrogen. As the Anderson-Dry expression previously appeared to be the best of these three equations, it was selected for a case study where the influence of the water coefficient on the relative variance of the model fit was investigated. The value of the water coefficient was increased stepwise, and at each of these values the activity parameter was re-optimised. The resulting values of the relative variance are reported in Table 11. As the assumed inhibiting influence of water on the reaction rate becomes significant, the model fit clearly becomes quite poor. This is despite the fact that the water coefficient values in Table 11 are still well below the range of about 4 to

5 that have typically been obtained when this kinetic model was used to describe historic kinetic data measured with similar catalysts. In view of the above, it is concluded that Equations 1,2,3 and 7 were indeed rightfully discarded in the past.

5. Findings and Conclusions

5.1 Experimental and data analysis methodology

- It was shown that linearisation of rate equations for the purpose of kinetic analysis may introduce mathematical artefacts that can make the correlation between the model and the data appear much better than it actually is. It is thus recommended that kinetic expressions rather be fitted to data by means of non-linear regression.
- The aim of the experimental study was to validate the new FT kinetic model under conditions where the catalyst activity was constant. Since iron-based LTFT catalysts are notorious for responding to changes in operating conditions, a specific methodology was followed. The catalyst was kept at reference conditions for most of the run. Changes to other conditions were only made for fairly short periods that allowed enough time for the reactor to reach steady state with respect to the permanent gases, but insufficient time for the catalyst to respond to these changes. In doing so, a wide range of water partial pressures could be covered without affecting the activity of the catalyst. It is believed that this approach is essential in iron-FT studies to separate chemical reaction kinetics from catalyst instability effects.
- An experimental design procedure was applied with the explicit aim of discriminating between two rival kinetic models. This procedure prescribed how system inputs should be varied, rather than stipulating specific reagent partial pressures inside the well-mixed reactor. The procedure was extremely effective - despite the fairly small number of kinetic measurements, the data could discriminate clearly between the two involved rate expressions.

- By varying the reactor operating pressure over a very wide range (5 to 40 bar) while keeping the conversion more or less constant, the water partial pressure inside the reactor could be varied from 0.4 to 3.5 bar without causing a measurable decrease in the intrinsic FT activity of the catalyst. These results can therefore be regarded as important information in the debate of whether or not water has an inhibition effect on the intrinsic FT reaction rate.

5.2 Iron-FT kinetic models

- From the historic kinetic studies considered in this paper, it appears as if a given set of kinetic data could usually be described well by the rate expression that was specifically developed from that set of data. However, these traditional iron-FT rate equations seem to lack general applicability, since none were found to describe various data sets satisfactorily.
- A new macro kinetic equation was proposed that included vacant sites, CO and water in the denominator (inhibition term). The denominator was also squared, as it seems difficult to rationalise a single site mechanism as implied by some of the existing rate expressions. When the new equation was fitted to historic kinetic data, as well as the data from a new experimental study, the effect of water was always found to be statistically insignificant. At the very least, this means that the hydrocarbon formation rate in the typical temperature range of the iron-based LTFT synthesis (around 240°C) can be described well without accounting for the influence of water. More generally speaking, it casts some doubt over the belief that water inhibits the iron-FT reaction rate at these temperatures.
- With the omission of water, the new rate equation had no more parameters than any of the other kinetic expressions it was compared to. Yet it was found that this new model could describe each set of historic data at least as well as (and often better than) the specific equation that was originally reported to be the most applicable. The new experimental study discriminated even more clearly between

the new model and the rival expressions considered here. Though not shown here, it should be noted that other equations with different reaction orders for hydrogen and CO and different inhibition terms were also tested. However, no other rate equation could be found that described the data from all the historic studies, and the data from the new kinetic data, as accurately as the proposed model.

- The new data were measured under conditions where some parameters were kept roughly constant, because this experimental study was designed with the explicit aim to discriminate between two specific rate equations. It should, however, be kept in mind that the combined variation in the historic data sets was quite extensive. E.g., in the study by Van Berge[5], the H_2/CO ratio varied from 1 to above 10, whereas the H_2/CO ratio varied from about 0.6 to 2.7 for the data reported by Zimmerman and Bukur[16] This indeed covers an extensive range as far as FT is concerned, yet the new model fitted the data from both these studies very well.
- The optimised value obtained for the CO coefficient of the new model was almost always close to 0.1 bar $^{-1}$, even though a variety of kinetic studies by different researchers were considered. This consistency in the value of the model parameter installs further confidence in the new kinetic expression.

Appendix A: Example of derivation of the new FT rate expression

The following serves merely to illustrate that the new rate equation can be derived by assuming irreversibility of the hydrogenation steps in the FT reaction, and not to suggest the precise mechanism whereby the reaction proceeds or the specific monomer involved in the polymerisation steps. Consider, for example, the following scheme of elementary reactions where it is assumed that all hydrogenation steps (Steps 3 to 6) are irreversible:

1. $CO + s \rightleftarrows COs$
2. $H_2 + 2s \rightleftarrows 2Hs$
3. $COs + Hs \rightarrow HCOs + s$
4. $HCOs + Hs \rightarrow Cs + H_2Os$
5. $Cs + Hs \rightarrow CHs + s$
6. $CHs + Hs \rightarrow CH_2s + s$
7. $H_2O + s \rightleftarrows H_2Os$

If Reactions 1, 2 and 7 are at equilibrium, the surface concentrations of CO, hydrogen, and water can be expressed as follows:

$$[COs] = K_1 P_{CO}[s] \quad \text{…A1}$$

$$[Hs] = K_2^{0.5} P_{H_2}^{0.5}[s] \quad \text{…A2}$$

$$[H_2Os] = K_7 P_{H_2O}[s] = k_{H_2O} P_{H_2O}[s] \quad \text{…A3}$$

In this example, the overall FT rate is taken as the formation rate of the CH_2-monomer (Step 6):

$$r_{FT} = k_6[CHs][Hs] \quad \text{…A4}$$

Under the steady-state approximation, the intermediate species (*HCOs*, *Cs*, *CHs*) cannot accumulate on the catalyst surface, so that their formation rates must equal their consumption rates, thus:

$$k_3[COs][Hs] = k_4[COHs][Hs] = k_5[Cs][Hs] = k_6[CHs][Hs] \qquad \ldots A5$$

By eliminating the surface concentration of hydrogen and rearranging:

$$[COs] = \frac{k_4}{k_3}[COHs] = \frac{k_5}{k_3}[Cs] = \frac{k_6}{k_3}[CHs] \qquad \ldots A6$$

This means that the surface concentrations of these intermediates are all directly proportional to [*COs*], which in turn is proportional to the partial pressure of CO in the gas phase (provided that the adsorption of CO is fast enough to be at equilibrium). By combining Equations A1, A2, A4 and A6, the FT reaction rate becomes:

$$r_{FT} = k'[COs][Hs] = kP_{CO}P_{H_2}^{0.5}[s]^2 \qquad \ldots A7$$

Due to the proportionality between the CO partial pressure and the surface concentrations of various C_1 intermediate species, the site balance equation can account for these intermediates without complicating the overall rate equation. Water is also included in the site balance equation. The site balance therefore becomes[22]:

$$[s_o] = [s] + [COs] + [COHs] + [Cs] + [CHs] + [H_2Os] = [s]\left(1 + k_{CO}P_{CO} + k_{H_2O}P_{H_2O}\right) \ldots A8$$

$$\frac{[s]}{[s_o]} = \frac{1}{1 + k_{CO}P_{CO} + k_{H_2O}P_{H_2O}} \qquad \ldots A9$$

Substituting the site balance equation into the FT rate equation yields the new LTFT kinetic expression (Equation 6 of the paper). It is thus evident that the third elementary reaction step in the scheme provided above is not necessarily a slow, rate determining step (as was assumed during the LHHW derivation), but can also be viewed as the first step in a series of consecutive irreversible hydrogenation reactions. It should be noted that k_{CO} (the observed coefficient of CO) in the new kinetic model does not necessarily only account for adsorbed molecular CO. From Equation A6, it follows that k_{CO} is a function of the actual CO adsorption coefficient (k_{CO}^{A}) and some reaction rate constants:

$$k_{CO} = k_{CO}^{A}\left(1+\frac{k_3}{k_4}+\frac{k_3}{k_5}+\frac{k_3}{k_6}\right) \qquad \ldots\text{A10}$$

From the derivation provided above, it is clearly impossible to distinguish between the surface coverage of molecularly adsorbed CO and that of the other C_1 intermediate species by merely describing the macro kinetics of the FT reaction with the new rate equation.

Appendix B: Historic and newly measured iron-FT kinetic data

Table B1: Kinetic data measured by Van Berge[1] at 250°C in a well mixed slurry reactor with a Ruhrchemie-type precipitated iron catalyst. The highest FT reaction rate was assigned a value of 100 (arbitrary units) and all other reaction rates were normalised with respect to this value.

Reagent partial pressures (bar)				FT reaction rate (normalised)	σ of FT reaction rate
H_2	CO	CO_2	H_2O		
6.4	2.25	1.4	1.31	55.2	1.38
4.58	3.7	2.41	1.0	66.9	0.83
12.1	2.25	1.57	2.02	60.8	2.62
4.6	1.99	1.09	0.91	50.3	1.38
5.41	3.7	1.77	1.2	66.0	0.55
5.75	2.68	2.12	0.99	41.4	0.28
5.72	3.43	2.06	0.89	64.9	0.69
7.64	7.21	3.6	0.96	100.0	2.07
12.0	1.04	5.5	1.26	48.3	0.41
1.36	0.93	4.83	0.33	22.8	3.04
15.3	2.32	2.23	1.23	75.4	0.55
4.76	2.75	2.25	0.43	51.1	0.83
10.3	1.97	5.46	0.99	64.9	1.38

Table B2: Data measured at 240°C in a well-mixed slurry reactor with a catalyst optimised for olefin production. Highest FT reaction rate assigned a value of 100 and all other reaction rates were normalised with respect to this value.

Reagent partial pressures (bar)				FT reaction rate
H_2	CO	H_2O	CO_2	(normalised)
19.74	5.34	2.74	3.68	99.55
19.39	4.66	3.16	3.65	100.00
20.12	5.31	2.21	3.54	83.64
19.38	5.31	2.43	3.93	91.21
18.53	5.35	2.36	4.01	84.39
10.73	4.14	1.33	2.25	55.15
11.99	3.77	0.96	2.13	55.61
19.26	4.99	1.51	4.29	97.27
19.64	5.61	1.92	3.65	89.09
20.12	5.76	1.50	3.56	85.15
20.15	5.42	1.92	3.90	93.03
19.16	5.01	2.12	4.34	85.15
19.62	5.55	2.09	3.87	98.94
20.46	5.95	2.85	3.35	84.85
19.63	5.95	2.46	2.93	83.33
22.85	4.96	2.78	2.81	93.94
22.23	5.29	2.81	2.74	89.39
27.26	5.45	3.12	2.63	92.42
19.71	6.29	2.44	2.46	80.30
18.83	9.64	2.69	2.50	86.36
19.11	9.36	2.64	2.52	86.36
18.98	12.17	2.77	2.49	78.79
20.21	6.11	2.29	2.53	81.82
19.80	6.25	2.30	2.56	81.82
10.67	3.02	0.82	1.36	50.00
10.49	3.00	0.86	1.42	51.52
10.99	3.59	1.35	3.89	50.00
10.75	3.40	1.06	2.03	48.48
10.63	3.30	1.05	2.11	48.48
10.45	3.15	1.00	1.36	46.97
10.38	3.16	1.01	1.36	45.45

Table B3: Data measured during the kinetic validation run. Measurements performed with a precipitated (Ruhrchemie-type) iron catalyst at 240°C in a well-mixed slurry reactor. The first measured FT reaction rate was assigned a value of 1.00 (arbitrary units) and all other reaction rates were normalised with respect to this value.

Time-on-line (h)	Reagent partial pressures (bar)				FT reaction rate (normalised)
	H_2	CO	CO_2	H_2O	
23	7.86	4.09	1.30	2.07	1.00
46	7.80	4.03	1.25	2.13	1.02
53	7.96	4.08	1.27	2.04	0.99
70	7.96	4.11	1.28	1.95	0.95
73	2.61	1.44	0.40	0.39	0.27
75	2.63	1.42	0.42	0.37	0.27
77	2.62	1.38	0.46	0.37	0.28
94	8.02	4.15	1.37	1.64	0.89
97	16.33	8.65	2.11	4.18	1.86
99	16.28	8.66	2.09	4.26	1.88
101	16.32	8.66	2.13	4.12	1.84
118	7.84	3.93	1.40	2.03	1.00
120	4.40	2.21	0.78	1.08	0.62
123	4.46	2.22	0.80	0.98	0.59
125	4.40	2.16	0.81	1.13	0.65
145	7.84	3.91	1.43	2.06	1.02
171	7.95	4.12	1.30	2.07	1.03
190	7.81	3.87	1.45	2.06	1.02
193	12.23	6.37	1.87	3.08	1.49
194	12.12	6.32	1.85	3.32	1.57
198	12.14	6.35	1.87	3.24	1.54
215	7.93	3.81	1.49	2.03	1.02

Appendix C: Calculation method to estimate the influence of intra-particle diffusion during the iron-FT slurry phase kinetic validation run

For the purpose of estimating the influence of intra-particle diffusion, the new iron-FT rate equation is expressed on the basis of the catalyst particle volume (and not on the usual basis of the catalyst mass):

$$r_{FT} = A_V \frac{P_{H_2}{}^{0.5} P_{CO}}{\left(1 + k_{CO} P_{CO}\right)^2} \qquad \ldots C1$$

with:

A_V = volume-based activity coefficient in (mol . bar $^{-1.5}$) / (m^3_{cat} . s)

k_{CO} = CO adsorption constant in bar $^{-1}$

P_{CO} = CO partial pressure in bar

P_{H2} = H_2 partial pressure in bar

Note that, since all experiments were performed at constant temperature, the Arrhenius term is incorporated into the activity coefficient. In the absence of gas-liquid mass transfer limitations, the liquid phase concentrations of H_2 and CO can be calculated from the following gas-liquid solubility relationships:

$$P_{CO} = c_{CO,L} H_{CO} V_{m,L} \qquad \ldots C2$$

$$P_{H2} = c_{H2,L} H_{H2} V_{m,L} \qquad \ldots C3$$

with:

$c_{CO,L}$ = liquid phase concentration of CO in mol / m^3

$c_{H2,L}$ = liquid phase concentration of H_2 in mol / m^3

H_{CO} = Henry coefficient for CO in bar

H_{H2} = Henry coefficient for H_2 in bar

$V_{m,L}$ = molar liquid volume of liquid phase in m^3 / mol

From the above relationships, Equation C1 can be rewritten in terms of liquid phase concentrations:

$$r_{FT} = A'' \frac{C_{CO,L}\, C_{H2,L}^{0.5}}{\left(1 + k''_{CO} C_{CO,L}\right)^2} \qquad \ldots C4$$

with:

A'' = $A_V\, H_{CO}\, H_{H2}^{0.5}\, V_{m,L}^{1.5}$

k''_{CO} = $k_{CO}\, H_{CO}\, V_{m,L}$

For cases where intra-particle diffusion limitations are significant, the kinetic expression based on the liquid phase concentrations is multiplied with an effectiveness factor (η_{FT}) to account for this influence on the overall reaction rate. Equation C4 must then be written as follows to obtain the observed FT reaction rate (r_{FT}^{O}):

$$r_{FT}^{O} = \eta_{FT}\ A'' \frac{C_{CO,L}\, C_{H2,L}^{0.5}}{\left(1 + k''_{CO} C_{CO,L}\right)^2} \qquad \ldots C5$$

The value of η_{FT} can be calculated for arbitrary kinetics by numerically solving the single particle differential equations[23]. It is, however, possible to approximate η_{FT} analytically with reasonable accuracy. To this end, Equation C4 needs to be simplified to pseudo-first order kinetics in one of the reactants[24]. Selecting CO as the key reactant and applying this simplifying approach yields:

$$r_{FT} = k_{PS,FT}\ C_{CO,L} \qquad \ldots C6$$

with $k_{PS,FT} = A^{"} \dfrac{C_{H2,l}^{0.5}}{(1 + k_{CO}^{"} C_{CO,L})^2}$

The above means that the pseudo constant $k_{PS,FT}$ is a function of composition. However, since the operating conditions in the current experimental study were not varied randomly, but were obtained by means of a procedure designed specifically to discriminate between two rival models, there are certain fixed relationships between the reagent partial pressures. It was thus found that the pseudo first order kinetics (Equation 6) could describe the FT reaction rate with a deviation less than ±10% for this set of data. Consequently, the approximation with first order kinetics is considered to be acceptable for the current purposes.

The observed FT reaction rate (Equation C5) can therefore also be simplified to first order kinetics:

$$r_{FT}^{O} = \eta_{FT}\ k_{PS,FT}\ C_{CO,L} \qquad \ldots C7$$

The effectiveness factor η_{FT} for the simplified pseudo-first order kinetics of Equation 7 is now given by the following analytical equations[23]:

$$M_T = \frac{r_{P,eq}}{3} \sqrt{\frac{k_{PS,FT}}{\dfrac{\varepsilon_P}{\tau} D_{CO,L}}} \qquad \ldots C8$$

$$\eta_{FT} = \frac{\tanh(M_T)}{M_T} \qquad \ldots C9$$

M_T = Thiele modulus (-)

$r_{P,eq}$ = equivalent sphere particle (m)

ε_P = particle porosity (-)

τ = tortuosity factor (-)

$k_{PS,FT}$ = pseudo first order reaction rate constant (1/s)

$D_{CO,L}$ = liquid phase diffusion coefficient of CO (m^2/s)

Using values for the parameters in Equation C8 from Table C1, the Thiele modulus (M_T) was calculated to vary from 0.39 to 0.45 for the kinetic experiments of this study. By applying Equation C9, the effectiveness factor was estimated to be above 0.98 for all experimental points. This means that intra-particle diffusion limitations were indeed insignificant for this kinetic study.

Table C1: Parameter values used to estimate Thiele modulus and effectiveness factor.

Property	**Value**	**Source**
ε_P / τ	0.34	Ref. 2: τ = 2 ε_P = 0.68 *
$D_{CO,L}$	$1.53 * 10^{-8}$ m^2/s	Ref. 3 #
H_{CO}	350 bar	Ref. 4 #
H_{H2}	430 bar	Ref. 4 #
$V_{m,L}$	$6.2 * 10^{-4}$ m^3/mol	Ref. 4 #
$r_{P,eq}$ $\sqrt{(k_{PS,FT})}$	$2.8 * 10^{-5} – 3.2 * 10^{-5}$ m / $s^{0.5}$	**

* experimental value for catalyst used

** determined from catalyst activity and d_{90} particle size, using Equations 1 to 4 and Equation 6

LTFT liquid phase represented as n-$C_{30}H_{62}$

References

1. Van der Laan, G.P.; Beenackers, A.A.C.M. Kinetics and Selectivity of the Fischer-Tropsch Synthesis: A Literature Review. *Catal. Rev. – Sci. Eng*. 1999, 41 (3&4) 255.
2. Huff, G.A.; Satterfield, C. N. Intrinsic Kinetics of the Fischer-Tropsch Synthesis on a Reduced Fused-magnetite Catalyst. *Ind. Eng. Chem. Process Des. Dev.* 1984, 23, 696.
3. Ledakowicz, S.; Nettelhoff, H.; KokuunR.; Deckwer, W.D. Kinetics of the Fischer-Tropsch Synthesis in the Slurry Phase on a Potassium-Promoted Iron Catalyst. *Ind. Eng. Chem. Process Des. Dev.* 1985, 24, 1043.
4. Dry, M.E. Practical and Theoretical Aspects of the Catalytic Fischer-Tropsch Process. *Appl. Catal. A* 1996, 138, 319.
5. Van Berge, P.J. Fischer-Tropsch studies in the slurry phase favouring wax production. Ph.D. Dissertation, Potchefstroomse Universiteit vir Christelike Hoër Onderwys, 1994.
6. Dry, M.E.; Shingles, T.; Boshoff, L.J.; Oosthuizen, G.J. Heats of Chemisorption on Promoted Iron Surfaces and the Role of Alkali in Fischer-Tropsch Synthesis. *J. Catal.* 1969, 15, 190.
7. Yates, I.C.; Satterfield, C.N. Effect of Carbon Dioxide on the Kinetics of the Fischer-Tropsch Synthesis on Iron Catalysts. *Ind. Eng. Chem. Res.* 1989, 28, 9.
8. Riedel, T.; Unruh, D.; Schaub, G. Fischer-Tropsch Synthesis in a Three Phase Slurry Reactor – Behaviour of CO_2. *DGMK Tagungsbericht* 2000, 2000-3, 231.
9. Satterfield, C.N.; Hanlon, R.T.; Tung, S.E.; Zou, Z.; Papaefthymiou, G.C. Effect of Water on the Iron-catalysed Fischer-Tropsch Synthesis. *Ind. Eng. Chem. Prod. Res. Dev.* 1986, 25, 407.
10. Van der Laan, G.P. Kinetics, Selectivity and Scale Up of the Fischer-Tropsch Synthesis. Ph.D. Thesis, Rijksuniversiteit Groningen, 1999.

11. Davis, B.H. Fischer-Tropsch Synthesis: current mechanism and futuristic needs. *Prepr. Symp. – Am. Chem. Soc., Div. Fuel Chem.* 2000, 45(1), 129.
12. Davis, B.H. Fischer-Tropsch Synthesis: current mechanism and futuristic needs. *Fuel Processing Technology.* 2001, 71, 157.
13. Davis, B.H. Fischer-Tropsch Synthesis Mechanism – Was Storch Correct ? *Prepr. Symp. – Am. Chem. Soc., Div. Fuel Chem.* 2002, 47(1), 237.
14. Van Steen, E.; Schulz, H. Polymerisation Kinetics of the Fischer-Tropsch CO Hydrogenation using Iron and Cobalt Based Catalysts. *Appl. Catal. A* 1999, 186, 309.
15. Press, W.H.; Flannery, B.P.; Teukolsky, S.A.; Vetterling, W.T. *Numerical recipes in Pascal*. Cambridge University Press: New York, 1989.
16. Zimmerman, W.H.; Bukur, D.B. Reaction Kinetics Over Iron Catalysts Used for the Fischer-Tropsch Synthesis. *Can. J. Chem. Eng.* 1990, 68, 292.
17. Huff, G.A. Fischer-Tropsch Synthesis in a Slurry Reactor. D.Sc. Dissertation, Massachusetts Institute of Technology, 1982.
18. Claeys, M.; Van Steen, E. in Steynberg, A.P.; Dry, M.E. (Eds.), Fischer-Tropsch Technology. *Stud. Surf. Sci. Catal.* Vol. 125, Elsevier: Amsterdam, 2004, Chapter 8.
19. Van Steen, E. Elementarschritte der Fischer-Tropsch CO-Hydrierung mit Eisen- und Kobaltkatalysatoren, Ph.D. Thesis, University of Karlsruhe, 1993.
20. Dry, M.E. in Steynberg, A.P.; Dry, M.E. (Eds.), Fischer-Tropsch Technology. *Stud. Surf. Sci. Catal.* Vol. 152, Elsevier: Amsterdam, 2004, Chapter 7.
21. Janse van Vuuren, M.J.; Govender, G.N.S.; Kotze, R.; Masters, G.J.; Pete, T.P. The Correlation between Double Bond Isomerisation, Water-Gas-Shift and Acid Production during Fischer-Tropsch Synthesis. *ACS Div. Petroleum Chem. Preprints* 2005, 50(2), 200.
22. Chorkendorff, I., Niemantsverdriet, J.W. *Concepts of Modern Catalysis and Kinetics*. WILEY-VCH: Weinheim, 2003.

23. G. F. Froment and K. M. Bisschoff, *Chemical Reactor Analysis and Design, 2nd edition, 1990, Wiley series in chemical engineering*, John Wiley and Sons, New York, U.S.A.
24. Erkey, C.; Rodden, J. B.; Akgerman, A. A Correlation for Predicting Diffusion Coefficients in Alkanes. *Can. J. Chem. Eng.* 1990, 68(4), 661.

Chapter 5

Water-Gas-Shift Kinetics in the Fe-LTFT Synthesis

Publications from this chapter

Botes, F.G. Water-Gas-Shift Kinetics in the Iron-Based Low-Temperature Fischer-Tropsch Synthesis. *Appl. Catal. A*. 2007, 328, 237.

Botes, F.G. Water-Gas-Shift (WGS) Kinetics in the Iron-Based Low-Temperature Fischer-Tropsch (Fe-LTFT) Synthesis. *Mexican Congress on Chemical Reaction Engineering* 2008, June 15-19, Ixtapa-Zihuatanejo, Mexico.

Abstract

The kinetic modelling of the water-gas-shift (WGS) reaction in the iron-based Low-Temperature Fischer-Tropsch synthesis was investigated. It was found that first order kinetics in CO provides a reasonable description of the CO_2 formation rate, but (due to systematic errors in this model) it should essentially be regarded as an empirical relationship. WGS rate expressions based on the formate mechanism were found to provide an improved description of the WGS kinetic data. By considering rate data measured over a wide range of reactor pressures, it was possible to discriminate between the various formate based rate equations considered during this study.

1. Introduction

In the cobalt-based Fischer-Tropsch synthesis, the oxygen from CO dissociation is almost completely discarded as water. However, in the iron-based Low-Temperature Fischer-Tropsch (Fe-LTFT) synthesis, both water and carbon dioxide are normally produced in substantial amounts, indicating two important routes for oxygen removal. As pointed out in literature[1], the relative rates of these two routes influence the H_2/CO ratio inside the reactor. Accurate modelling of the CO_2 formation kinetics is therefore essential for accurately predicting the syngas conversion; yet this aspect of the Fe-LTFT synthesis has received surprisingly little attention.

If carbon dioxide is a primary product of the FT synthesis, it means it is formed by one of the elementary steps that constitute the overall reaction scheme of hydrocarbon formation. Depending on how such a reaction scheme is laid out and where the rate determining steps occur, it may or may not be possible to describe the hydrocarbon formation reaction and the CO_2 formation reaction with separate kinetic models. If carbon dioxide is formed by a subsequent (separate) water-gas-shift (WGS) reaction occurring on the same catalytic site as the FT reaction, the two reactions will only influence each other via the gas phase concentrations of reactants and can thus be described with separate kinetic expressions. However, the inhibition terms of the two rate equations will then have to be exactly the same, because the coverage of the catalytic sites will be the same for the two reactions. Lastly, CO_2 can possibly also be formed by a subsequent WGS reaction occurring on a different type of site than FT, in which case the kinetic equations used to describe each of the reactions will be totally unrelated to each other.

In literature, it has generally been assumed that carbon dioxide is essentially formed by a subsequent (independent) WGS reaction[1-4]. This seems to be supported by Krishnamoorthy et al.[5], who studied CO_2 formation in the Fe-LTFT synthesis by varying the syngas space velocity. They concluded that the low CO_2 selectivities observed at low CO conversions (especially at a reaction temperature of 235°C) is

consistent with a high primary selectivity for oxygen removal as water. Furthermore, attempts to describe the kinetics of the FT and WGS reactions with expressions that share a common inhibition term have not been successful[1,6], which may suggest that the two reactions occur on separate catalytic sites. In the studies on the Fe-LTFT synthesis at Sasol, it has also not been possible to describe the FT and WGS kinetics with rate equations sharing the same denominator. This has led to the conclusion that the bulk of the carbon dioxide is formed by a subsequent reaction occurring on a different catalytic site than FT.

2. Kinetic models for the WGS reaction

Broadly speaking, two mechanisms have been proposed for the WGS reaction over metal oxide catalysts in a non-FT environment[7]. The regenerative mechanism comprises oxidation-reduction cycles. It is assumed that the catalyst surface is oxidised by water, producing H_2 as by-product. In a subsequent reaction, CO then reduces (regenerates) the surface with the formation of CO_2. In the associative mechanism, it is assumed that adsorbed species interact to form an adsorbed intermediate (possibly a formate), which then decomposes to H_2 and CO_2.

For the WGS in the Fe-LTFT synthesis, it was originally reported that the CO_2 formation rate can be adequately described by first order kinetics in CO provided the WGS reaction was still far from thermodynamic equilibrium[8]:

$$r_{WGS} = AP_{CO} \qquad \ldots 1$$

The above equation was presented as an empirical relationship, as no mechanistic implications were considered. However, it is clearly consistent with both the regenerative mechanism and the associative mechanism. The most obvious weakness of Equation 1 is the fact that it does not account for the reversibility of the WGS reaction; hence the provision that it is only applicable when the reaction is still far

from equilibrium. Nevertheless, since other researchers have also reported a good correlation between Equation 1 and their own data[1,9], there appears to be some consistency in the empirical observation that the WGS reaction rate is directly proportional to the CO partial pressure. Equation 1 can be expanded to account for the reversibility of the WGS reaction by assuming that the driving force for the WGS reaction is the difference between the actual CO partial pressure and its corresponding equilibrium value[9]:

$$r_{WGS} = A\left(P_{CO} - P_{CO}^{\ equilibrium}\right) = A\left(P_{CO} - \frac{P_{H_2}P_{CO2}}{K_{WGS}P_{H_2O}}\right) \qquad ...2$$

Zimmerman and Bukur[1] attempted to apply the functional form of the denominators in their FT rate equations to their WGS kinetic models as well. Two WGS rate equations were consequently formulated:

$$r_{WGS} = A\,\frac{P_{CO}P_{H_2O} - \frac{1}{K_{WGS}}P_{H_2}P_{CO2}}{P_{CO} + k_{H_2O}P_{H_2O} + k_{CO_2}P_{CO_2}} \qquad ...3$$

$$r_{WGS} = A\,\frac{P_{CO}P_{H_2O} - \frac{1}{K_{WGS}}P_{H_2}P_{CO2}}{P_{CO}P_{H_2} + k_{H_2O}P_{H_2O}} \qquad ...4$$

However, their attempts were not very meaningful, because the optimised values of the adsorption parameters in the above WGS expressions differed substantially from those obtained for the corresponding FT kinetic models. The rationalisation for using the same denominator in the FT and WGS kinetic models would be that the two reactions possibly occur on the same catalytic sites. However, then both the functional

form of the denominator and the optimised parameter values should be the same. In agreement with the foregoing, Lox and Froment[6] reported that all the kinetic models with first order denominators they derived for the WGS reaction failed completely to describe the measured reaction rates.

It appears as if the most successful descriptions of the WGS kinetics in the iron-FT synthesis have come from rate equations derived on the basis of a formate mechanism[6,10,11,12]. Wang et al.[11] and Yang et al.[12] favoured a rate equation where the rate determining step was the decomposition of the formate species. However, each of these two research groups only considered one scheme of elementary reaction steps, even though different rate determining steps were tested. On the other hand, Lox and Froment[6] and Van der Laan and Beenackers[10] covered a wider selection of reaction schemes and favoured models where the rate determining step was the formation of the formate intermediate.

In this study, the initial screening of various WGS kinetic models during a preliminary round of data analysis revealed that rate equations based on the associative formate mechanism yielded the best description of the data. Therefore, in line with the findings of Lox and Froment[6] and Van der Laan and Beenackers[10], kinetic models were derived on the basis that the rate determining step was the formation of the formate intermediate. These reaction schemes were called Models A, B and C and are provided in Appendix A. Comprehensive rate equations, accounting for site occupation by various intermediates (e.g. CO or CO containing species, water, hydroxyl, formate species, dissociated hydrogen), were derived. Evaluation of the rate expressions with experimental data showed that some of the adsorption constants assumed negative values and could therefore be eliminated from the denominator. Consequently, the models could be simplified to the following forms:

Model A:
$$r_{WGS} = A\,\frac{P_{CO}P_{H_2O} - \frac{1}{K_{WGS}}P_{H_2}P_{CO2}}{\left(1 + k_{CO}P_{CO} + k_{H_2O}P_{H_2O}\right)^2} \qquad \ldots 5$$

Model B:
$$r_{WGS} = A \frac{P_{CO}P_{H_2O} - \frac{1}{K_{WGS}} P_{H_2}P_{CO2}}{\left(1 + k_{H_2O}P_{H_2O} + k_{OH}\frac{P_{H_2O}}{P_{H_2}^{0.5}}\right)^2} \quad \ldots 6$$

Model C:
$$r_{WGS} = A \frac{\frac{P_{CO}P_{H_2O}}{P_{H_2}^{0.5}} - \frac{1}{K_{WGS}} P_{H_2}^{0.5}P_{CO2}}{\left(1 + k_{CO}P_{CO} + k_{OH}\frac{P_{H_2O}}{P_{H_2}^{0.5}}\right)^2} \quad \ldots 7$$

3. Evaluation of the kinetic expressions

Van Berge[13] performed a kinetic study on a precipitated Fe-LTFT catalyst in a well-mixed slurry reactor (CSTR) at a temperature of 250°C. The main aim of the study was to discriminate between various FT rate expressions. To this end, a statistical design procedure was applied to suggest experimental conditions where the predicted reaction rates of the rival FT models differed most. Nevertheless, even though the primary objective of that study was to investigate FT kinetics, the statistical procedure did ensure an extensive variation in the reagent partial pressures (as is evident from Table 1). Therefore, the data set from this study was considered to be appropriate for evaluating WGS rate expressions as well.

The rival WGS models (Equations 1,2,5,6 and 7) were fitted to the data presented by Van Berge[13]. Since the standard deviation (σ) of each rate measurement was reported, the value of "chi-square" (χ^2) could be minimised (as opposed to the sum of the squares of the differences) as suggested by Press et al.[14]:

$$\chi^2 = \sum_{i=1}^{n}\left[\left(\frac{r_i^{measured} - r_i^{predicted}}{\sigma_i}\right)^2\right] \quad \ldots 8$$

Table 1: Range of experimental conditions covered by data measured by Van Berge[13] at 250°C in a well mixed slurry reactor with a Ruhrchemie-type precipitated iron catalyst. All values pertaining to conditions inside the CSTR.

Parameter	Range
P_{H_2}	1.4 – 15.3 bar
P_{CO}	0.9 – 7.2 bar
P_{H_2O}	0.3 – 2.0 bar
P_{CO_2}	1.1 – 5.5 bar
H_2/CO ratio	1.1 – 11.6

In this approach, the difference between the measured and predicted rates is divided by the standard deviation of the involved rate measurement. Data points with a high accuracy have low standard deviations and therefore count more heavily towards the sum of errors than inaccurate data. In other words, the weight (importance) assigned to each observation is related to the accuracy of that specific measurement. Whereas the value of chi-square was used for model optimisation and discrimination, the mean absolute relative residual (MARR) is reported as a measure of the goodness of fit:

$$MARR = 100\sum_{1}^{n}\left|\frac{r_i^{measured} - r_i^{predicted}}{r_i^{measured}}\right|\frac{1}{n} \qquad ...9$$

The results of the model fitting are presented in Table 2. First order kinetics in CO (Equation 1) fits the data reasonably well. Surprisingly though, the addition of a reversibility term (Equation 2) results in a significantly poorer description of the WGS kinetics, as is evident from the much higher χ^2 –value, as well as the higher MARR value. Of the three rate expressions based on the formate mechanism, Model A does not seem like much of an improvement over first order kinetics in CO. Models B and C, however, have much lower χ^2 –values and are therefore regarded as substantial improvements over first order kinetics. Model B has a fairly high MARR value (high

unweighted error sum), despite the small weighted sum of errors. This means that there are some rate measurements with low accuracy that are not predicted well by Model B, but the accurate measurements are generally predicted quite well. Therefore, Model B is still regarded as an appropriate rate expression.

Table 2: Comparison of WGS rate equations with data measured by Van Berge[13] at 250°C in a well mixed slurry reactor with a Ruhrchemie-type precipitated iron catalyst. Model fitting by minimising χ^2.

Rate equation	Adsorption coefficients	χ^2	MARR (%)
First order in CO (Equation 1)		2634	17.6
First order in CO with reversibility (Equation 2)		4044	19.2
Model A (Equation 3)	k_{CO} = 0.5 bar^{-1} k_{H2O} = 3.4 bar^{-1}	2640	16.1
Model B (Equation 4)	k_{H2O} = 1.1 bar^{-1} k_{OH} = 6.3	1389	16.0
Model C (Equation 5)	k_{CO} = 0.7 bar^{-1} k_{OH} = 21.9	1003	9.1

In order to check for systematic deviations, the agreement between each of the rival rate equations and the measured reaction rates is presented as a function of the approach to WGS equilibrium. The approach to equilibrium was defined as:

$$\textit{Approach to equilibrium} = \frac{P_{H_2} P_{CO2}}{P_{CO} P_{H_2O}} \Big/ K_{WGS} \qquad ...10$$

Figure 1 shows that the errors in prediction of Equations 1 and 2 form clear trends with the approach to equilibrium, suggesting a systematic deviation in the first order models which may be indicative of a fundamental incorrectness in these expressions.

To the contrary, the deviations in the models based on the formate mechanism appear to be random scatter rather than consistent errors (see Figure 2). There is one data point that is particularly badly predicted by Model B, which may be the reason for its high MARR value despite the small weighted sum of errors (χ^2 –value).

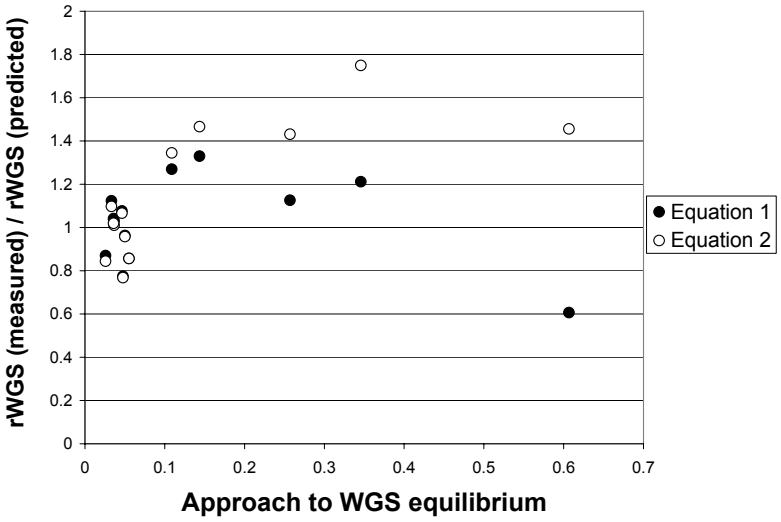

Figure 1: Predictability of first order rate equations in CO as the WGS reaction approaches equilibrium. Experimental details as per Tables 1 and 2.

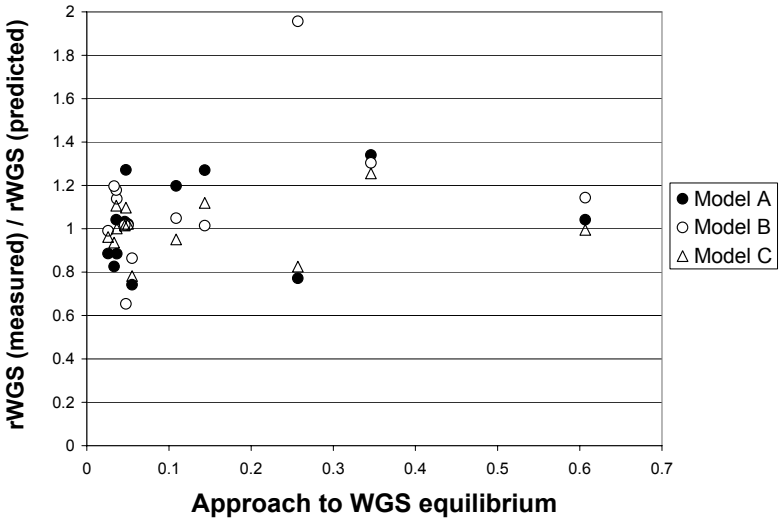

Figure 2: Predictability of formate based rate equations as the WGS reaction approaches equilibrium. Experimental details as per Tables 1 and 2.

In agreement with the findings of other researchers[1,8,9], first order kinetics in CO seems to be an adequate description of the WGS kinetics in the Fe-LTFT synthesis. However, it appears as if this relationship must be regarded as purely empirical, since the addition of a term to account for the reversibility of the reaction actually made the description of the reaction rate substantially worse. Furthermore, the rate expressions based on first order CO kinetics (both with and without a reversibility term) had clear systematic deviations as the WGS reaction approached thermodynamic equilibrium. To the contrary, the new rate expressions considered here had no systematic deviations as the reaction approached equilibrium and some of these expressions fitted the WGS kinetic data significantly better than first order kinetics. Therefore, the rate expressions derived from the formate mechanism of the WGS reaction are regarded as a notable improvement over first order kinetics in CO.

It should further be noted that the adsorption coefficients of CO or CO containing intermediates are either zero (in the case of Model B) or small (in the case of Models A and C) compared to the adsorption coefficients of water or hydroxyl groups. This is in agreement with the findings of other studies on the WGS reaction in the Fe-LTFT synthesis. For example, Van der Laan and Beenackers[10] also described the CO_2 formation rate with formate-based kinetic models, but only accounted for site coverage by molecular CO and water. From the values reported for their model parameters, it is clear that the water coefficient in the denominator was substantially larger than the CO coefficient (by a factor of up to 12, depending on the specific kinetic expression involved). Lox and Froment[6] also proposed WGS rate expressions based on the formate mechanism. Their best fit kinetic model only accounted for the coverage of the catalytic sites by hydroxyl groups, similar to Model B of the current study.

The foregoing seems to suggest that, if most of the carbon dioxide is indeed produced via a formate mechanism, the WGS catalytic sites are mainly covered with adsorbed water and hydroxyl species. Little or no adsorbed CO or CO derived species are apparently present on the WGS catalytic sites. This is distinctly different from the

findings regarding the FT kinetics in the Fe-LTFT synthesis[15] (also see Chapter 4 of this thesis). One of the main conclusions of the study on FT kinetics was that water has a negligible influence on the FT reaction rate and that the only species abundant on the FT catalytic sites are adsorbed CO and possibly C_1 intermediates.

4. The effect of pressure on the predictive capability of WGS rate expressions

In a recent study, kinetic data were measured over a wide range of reactor pressures in order to discriminate between rival FT kinetic models for the Fe-LTFT synthesis[15] (see also Chapter 4 of this thesis). In an attempt to discriminate between the WGS rate equations based on the formate mechanism (more specifically Models B and C), the effect of pressure on the predictive capabilities of the WGS models was now investigated.

4.1 Experimental

Since a detailed experimental description is provided in Chapter 4 and elsewhere[15], only the most important aspects will be covered here. The experiments were performed with Sasol's commercial spray-dried, precipitated iron catalyst. The commercial catalyst has been manufactured more or less according to the Ruhrchemie preparation procedure for iron-FT catalysts, which has been described by Dry[4] and typically yields a catalyst containing 25 g SiO_2, 5 g Cu and 5 g K_2O per 100 g Fe. Catalysts prepared via the Ruhrchemie procedure will typically have a total pore volume of between 0.35 and 0.75 cm^3/g and a BET surface area in the range of 275 to 405 m^2/g. [4]

The experiments were performed in a well-mixed slurry reactor free from internal or external mass transfer limitations (see Chapter 4). The catalyst was activated for 16 hours at 240°C and 20 bar (gauge) with syngas having an H_2/CO ratio of 1.55 and containing argon as internal standard. The kinetic experiments were performed with

the same syngas feed composition used for activation (constant composition throughout the run). During the course of the run, the reactor pressure was varied over a range from 5 to 40 bar (gauge). It is well known that, for a constant feed gas composition, the conversion achieved in the iron-FT synthesis stays more or less constant if the gas feed rate (space velocity) is varied proportionally to the total pressure[4]. Therefore, by varying the space velocity concomitantly with the operating pressure, the syngas conversion could be maintained at a level of approximately 45%, irrespective of the reactor pressure.

4.2. Kinetic measurements

In our experience at Sasol, the intrinsic behaviour of the iron-based catalyst in the LTFT synthesis can be affected by the wide variation in process conditions typically required for a kinetic study. In order to ensure a stable intrinsic activity of the catalyst, the following methodology was employed. The reactor was essentially maintained at reference conditions (20 bar operating pressure) and changes to other operating points were only made for short intervals. Calculations showed that, at the involved feed flow rates, it would not take more than about an hour for five replacements of the combined gas inventory of the reactor and the knock-out pots. Therefore, a change in operating conditions was made in the morning and three samples were taken between 2 and 6 hours after such a change had been effected. Subsequently, the system was returned to the reference conditions, which were maintained until the next morning when another kinetic measurement was made. The aim of this procedure was therefore to allow sufficient time for the reactor to attain steady state with regard to the permanent gases, but insufficient time for the catalyst to respond notably to the new conditions. The reference measurements taken regularly throughout the run, as well as the three samples taken at the non-baseline conditions over a period of 4 hours, could confirm that the catalyst performance was indeed stable.

4.3 Results and discussion

Apart from the reference operating pressure of 20 bar (gauge), kinetic measurements were also performed at reactor pressures of 5, 10, 30 and 40 bar (gauge). The run history (operating pressure as a function of synthesis time) is presented in Figure 3, while the measured WGS reaction rates (normalised to that of the first measurement during the run) are presented in Figure 4. The WGS reaction rate measured under reference conditions was quite constant over the duration of the run, apart from some scatter and possibly a slight increase towards the end of the run. This indicates a stable catalyst activity during the kinetic measurements. Furthermore, at each of the non-reference pressures, the three measurements taken were fairly similar to one another, suggesting that the catalyst did not respond significantly to the six-hour long change in conditions. It is further clear that the changes in the WGS reaction rate due to varying operating pressures were substantially larger than the scatter in the data, so that the random experimental errors are not expected to have a significant influence on the interpretation of the results.

The three rate expressions with adsorption coefficients as obtained previously (values reported in Table 2) were fitted to the new kinetic data and the results are presented in Table 3. Models A and C appear to deviate substantially from the new kinetic data, judging by the high values for the relative variance and the MARR. To the contrary, Model B seems to fit the data quite well. The models were also evaluated graphically by plotting the ratio of the measured to the predicted WGS reaction rate as a function of the syngas partial pressure inside the reactor (Figure 5). Models A and C clearly have very serious systematic deviations with variation in pressure. At very low syngas pressures, the reaction rate is overestimated, while it is increasingly under predicted as the syngas pressure increases. Model B may contain a slight systematic deviation, but this trend is much less evident. Moreover, Model B predicts the reaction rate accurately to within about 20% of the measured values over the whole broad range of

pressures. This seems quite acceptable, seeing that the adsorption parameters were not re-optimised for the newly-measured data set.

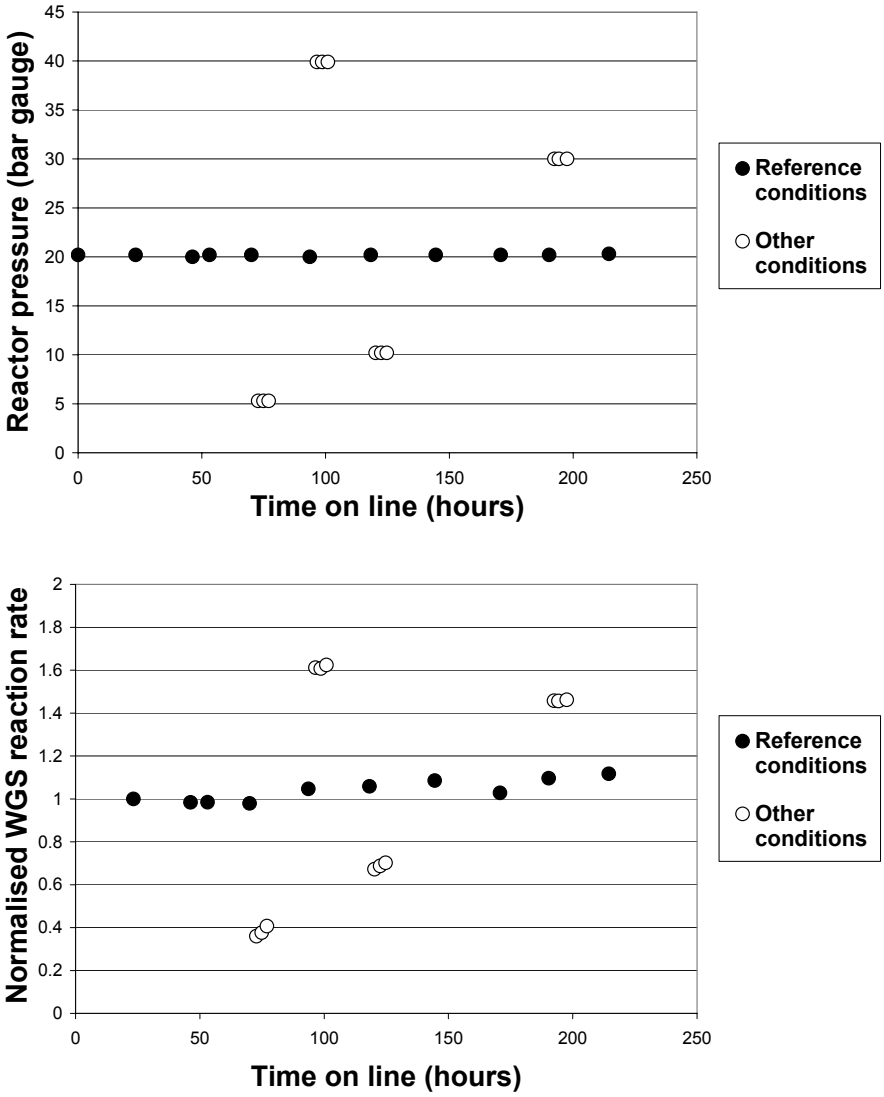

Figures 3 (top, reactor pressure versus time on line) and 4 (bottom, normalised WGS reaction rate versus time on line) for the kinetic validation run performed with a precipitated (Ruhrchemie-type) iron catalyst at 240°C in a well-mixed slurry reactor. WGS reaction rate normalised with respect to the first measurement taken at reference conditions.

Table 3: Discrimination between the three WGS kinetic models based on the formate mechanism by using the new kinetic data. Values for adsorption coefficients were taken from Table 2. Experimental details as per Figures 3 and 4.

Rate equation	S_{rel} (%)	MARR (%)
Model A (Equation 3)	33.2	27.5
Model B (Equation 4)	13.3	11.1
Model C (Equation 5)	39.3	34.2

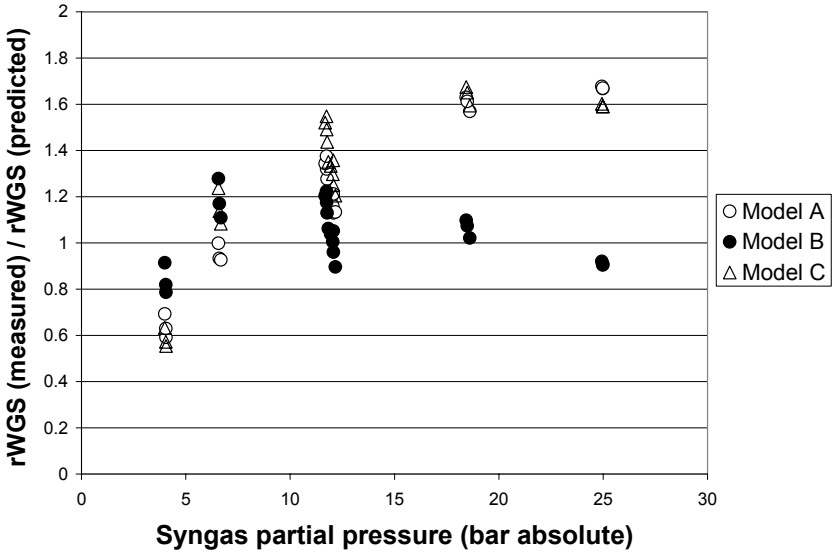

Figure 5: Predictive capability of the formate based rate expressions as a function of syngas partial pressure for the new kinetic data. Experimental details as per Figures 3 and 4.

Due to strong interrelationships between the reactant partial pressures in the new kinetic data set (the syngas conversion was kept more or less constant), it is not sensible to re-optimise the adsorption coefficients of the kinetic expressions. It can be argued though that the adsorption coefficient values obtained previously are strictly speaking not applicable to the new data set, as the two studies were performed at

different temperatures (250°C versus 240°C) and the catalysts may have differed slightly as well. However, it should be noted that reasonable changes in the adsorption parameters of Models A and C could not remove the serious systematic errors in these equations. The adsorption coefficients had to be adapted extensively (up to an order of magnitude) before Models A and C could correctly account for the effect of syngas pressure on the WGS reaction rate. Since such dramatic changes are not considered realistic, it appears justifiable to discard these two rate expressions.

5. Conclusions

First order kinetics in CO provides a reasonable description of the CO_2 formation rate in the Fe-LTFT synthesis. However, this appears to be a purely empirical relationship, since the predictive capability of the model diminishes significantly when a term is included to account for the reversibility of the WGS reaction. In addition, the model has a clear systematic error with the approach to thermodynamic equilibrium of the WGS reaction.

WGS rate equations were derived by assuming a formate mechanism. These kinetic models described an existing data set significantly better than first order kinetics in CO and also did not have notable systematic errors with the approach to equilibrium. However, evaluating the formate models with new kinetic measurements suggested that only one of the rate expressions correctly accounts for the effect of pressure on the WGS reaction rate. Therefore, the most appropriate WGS rate expression that can currently be proposed from this study is (all reactant partial pressures in bar absolute):

$$r_{WGS} = A \frac{P_{CO}P_{H_2O} - \frac{1}{K_{WGS}} P_{H_2}P_{CO2}}{\left(1+1.1P_{H_2O}+6.3\frac{P_{H_2O}}{P_{H_2}^{0.5}}\right)^2} \qquad ...11$$

In the above equation, the terms in the denominator accounts for the effects of vacant sites, site occupation by adsorbed molecular water, and site occupation by hydroxyl groups, respectively.

In line with reports by other researchers[1,6], attempts at Sasol to describe the FT and WGS kinetics in the Fe-LTFT synthesis with rate equations sharing a common denominator have not been successful. This is consistent with the notion that the bulk of the carbon dioxide is formed by a separate WGS reaction occurring on a different catalytic site than FT. If the WGS reaction indeed proceeds via a formate mechanism, it appears as if the WGS sites are mainly covered with water and / or hydroxyl species. To the contrary, the FT sites appear to be mainly covered by CO and possibly C_1 intermediates according to a recently published FT kinetic model for the Fe-LTFT synthesis[15] (see also Chapter 4).

It is well known that, under synthesis conditions, iron-FT catalysts consist of a variety of different iron phases. Metallic iron, if present before the introduction of synthesis gas, normally disappears fairly rapidly in the presence of synthesis gas, leaving the working catalyst as a mixture of various iron carbides and iron oxide (mainly magnetite)[4]. The nature of the active sites on iron-FT catalysts has been the subject of much debate in the literature, as briefly summarised by Van der Laan and Beenackers[10]. Several authors have proposed that magnetite is active for the WGS reaction, whereas the FT reaction proceeds over one or more of the carbidic phases. Macro kinetic investigations, such as the subject of this paper, can unfortunately not shed much light on the actual nature of the active site. Nevertheless, if the macro kinetic models proposed recently for the FT and WGS reactions are broadly correct, it does appear as if the sites responsible for hydrocarbon formation have a high propensity for adsorbing CO, while those responsible for CO_2 formation have a higher affinity for water and hydroxyl groups.

Appendix A: Reaction schemes for the WGS reaction based on the formate mechanism

Model A

1. $CO + s \rightleftarrows COs$
2. $H2O + s \rightleftarrows H_2Os$
3. $H_2 + 2s \rightleftarrows 2Hs$
4. $COs + H_2Os \rightleftarrows COOHs + Hs$ …rate determining step
5. $COOHs \rightleftarrows CO_2 + Hs$

Model B

1. $H_2 + 2s \rightleftarrows 2Hs$
2. $H_2O + s \rightleftarrows H_2Os$
3. $H2Os + s \rightleftarrows HOs + Hs$
4. $CO + s \rightleftarrows COs$
5. $COs + Hs \rightleftarrows CHOs + s$
6. $CHOs + HOs \rightleftarrows COOHs + Hs$ …rate determining step
7. $COOHs \rightleftarrows CO_2 + Hs$

Model C

1. $CO + s \rightleftarrows COs$
2. $H_2 + 2s \rightleftarrows 2Hs$
3. $H2O + 2s \rightleftarrows HOs + Hs$
4. $COs + HOs \rightleftarrows COOHs + s$ …rate determining step
5. $COOHs \rightleftarrows CO_2 + Hs$

Nomenclature

A	Kinetic rate constant (activity parameter).
k_i	Adsorption coefficient of component or reaction intermediate *i*.
K_{WGS}	Equilibrium constant for WGS reaction.
n	Number of data points in a set of kinetic data.
r_{FT}	FT reaction rate (moles CO converted to hydrocarbons / unit time / unit catalyst amount).
r_{WGS}	WGS reaction rate (moles CO_2 formed / unit time / unit catalyst amount).
$r^{measured}$	Measured reaction rate.
$r^{predicted}$	Predicted reaction rate.
P_i	Partial pressure of component *i* in gas phase (bar).
σ	Standard deviation

References

1. Zimmerman, W.H.; Bukur, D.B. Reaction Kinetics Over Iron Catalysts Used for the Fischer-Tropsch Synthesis. *Can. J. Chem. Eng.* 1990, 68, 292.
2. Lox, E.S.; Froment, G.F. Kinetics of the Fischer-Tropsch Reaction on a Precipitated Promoted Iron Catalyst. 1. Experimental Procedure and Results. *Ind. Eng. Chem. Res.* 1993, 32, 61.
3. Van der Laan, G.P.; Beenackers, A.A.C.M. Kinetics and Selectivity of the Fischer-Tropsch Synthesis: A Literature Review. *Catal. Rev. – Sci. Eng.* 1999, 41 (3&4) 255.
4. Dry, M.E. in Steynberg, A.P., Dry, M.E., Eds., *Stud. Surf. Sci. Catal. Vol. 152*, Elsevier, Amsterdam, 2004, Chapter 7.
5. Krishnamoorthy, S.; Li, A.; Iglesia, E. Pathways for CO_2 Formation and Conversion During Fischer-Tropsch Synthesis on Iron-based Catalysts. *Catal. Lett.* 2002, 80 (1-2), 77.

6. Lox, E.S.; Froment, G.F. Kinetics of the Fischer-Tropsch Reaction on a Precipitated Promoted Iron Catalyst. 2. Kinetic Modelling. *Ind. Eng. Chem. Res.* 1993, 32, 71.
7. Rethwisch, D.G.; Dumesic, J.A. Adsorptive and Catalytic Properties of Supported Metal Oxides. III. Water-Gas-Shift over Supported Iron and Zinc Oxides. *J. Catal.* 1986, 101,35.
8. Dry, M.E. Advances in Fischer-Tropsch Chemistry. *Ind. Eng. Chem. Prod. Res. Dev.* 1976, 15, 282.
9. Riedel, T.; Unruh, D.; Schaub, G. Fischer-Tropsch Synthesis in a Three Phase Slurry Reactor – Behaviour of CO_2. *DGMK Tagungsbericht* 2000, 2000-3, 231.
10. Van der Laan, G.P.; Beenackers, A.A.C.M. Intrinsic Kinetics of the Gas-Solid Fischer-Tropsch and Water Gas Shift Reactions over a Precipitated Iron Catalyst. *Appl. Catal. A* 2000, 193, 39.
11. Wang, Y.; Ma, W.; Lu, Y.; Yang, J.; Xu, Y.; Xiang, H.; Li, Y.; Zhao, Y.; Zhang, B. Kinetics Modelling of Fischer-Tropsch synthesis over an industrial Fe-Cu-K catalyst. *Fuel* 2003, 82, 195.
12. Yang, J.; Liu, Y.; Chang, J.; Wang, Y.; Bai, L.; Xu, L.; Xiang, H.; Li, Y.; Zhong, B. Detailed Kinetics of Fischer-Tropsch Synthesis on an Industrial Fe-Mn Catalyst. *Ind. Eng. Chem. Res.* 2003, 42, 5066.
13. Van Berge, P.J. Fischer-Tropsch studies in the slurry phase favouring wax production. Ph.D. Dissertation, Potchefstroomse Universiteit vir Christelike Hoër Onderwys, 1994.
14. Press, W.H.; Flannery, B.P.; Teukolsky, S.A.; Vetterling, W.T. *Numerical recipes in Pascal*. Cambridge University Press: New York, 1989.
15. Botes, F.G.; Breman, B.B. Development and Testing of a New Macro Kinetic Expression for the Iron-Based Low-Temperature Fischer-Tropsch Reaction. *Ind. Eng. Chem. Res.* 2006, 45, 7415.

Chapter 6

Proposal of a New Product Characterisation Model for the Fe-LTFT Synthesis

Publications from this chapter

Botes, F.G. Proposal of a New Product Characterisation Model for the Iron-Based Low-Temperature Fischer-Tropsch Synthesis. *Energy & Fuels* 2007, 21, 1379.

Botes, F.G. Proposal of a New Product Characterisation Model for the Iron-Based Low-Temperature Fischer-Tropsch Synthesis. *Mexican Congress on Chemical Reaction Engineering* 2008, June 15-19, Ixtapa-Zihuatanejo, Mexico.

Abstract

A new product characterisation model has been proposed for the Fe-LTFT synthesis. The chain length dependent desorption model is based on the premise that the increase in chain growth probability and decrease in olefin / paraffin ratio with carbon number in the iron-FT synthesis is essentially a characteristic of the primary product spectrum. The model could successfully describe the olefin and paraffin distributions in the C_{3+} range. The ethylene / ethane ratio is overestimated by the model because of the high reactivity of ethylene for secondary hydrogenation. However, the total C_2 formation rate was predicted almost perfectly, while the methane formation rate was described adequately, by using parameter values that were obtained from the C_3 to C_{10} product fraction. This is a true extrapolation, as the C_1 and C_2 data were not used for the estimation of the parameter values. This may be the first product characterisation model that can successfully be extrapolated to the C_1 and C_2 components without introducing additional (unique) parameter values for these products.

1. Introduction

Since the Fischer-Tropsch (FT) product spectrum contains a vast number of components, it is impractical to relate the selectivity of each individual component with the process conditions. The only realistic approach to describing selectivities is to characterise the product spectrum with a product distribution model containing a limited number of model parameters. If these model parameters can be successfully correlated with process conditions, the FT product slate can be reconstructed during model simulations. Since the FT reaction is believed to be a polymerisation-type synthesis where hydrocarbon chain growth occurs by the addition of one carbon atom at a time, the chain growth probability factor (α) is an example of one such parameter that can be used to characterise the product spectrum. If the value of α is independent of carbon chain length, then the well-known ideal Schulz-Flory distribution would be obtained. It is, however, generally accepted that there are certain omnipresent deviations in the actual FT product spectrum from the ideal Schulz-Flory distribution[1,2]. These include a higher methane and a lower C_2 selectivity than predicted by the equation. In addition, there seems to be an increase in the chain growth probability factor and concomitant decrease in the olefin / paraffin ratio with hydrocarbon chain length. The product characterisation models that have been proposed to describe these deviations can broadly be organised into two classes, namely double-α models and olefin reincorporation models.

Double-α models are based on the premise that the observed FT product spectrum is a combination of two ideal product distributions with different growth probabilities. The existence of the two growth probabilities have been ascribed to the presence of two types of sites on the catalyst surface[3] or two types of mechanisms occurring simultaneously in the FT synthesis[4,5,6]. Even though qualitative explanations have been offered for the concomitant decrease in olefin / paraffin ratio with carbon number[4,7], we are not aware of a double-α model that can quantitatively describe both the variations in α-value and olifinicity with hydrocarbon chain length. Furthermore,

double-α models are usually only applied to the C_{3+} part of the product spectrum, as they cannot explain the deviations in C_1 and C_2 components[5,8]. As discussed in Chapter 3, a double-α model normally provides a good empirical fit of the carbon number distribution in the C_{3+} range, but there appears to be a high degree of covariance between the independent parameters of the model.

Secondary reactions of olefins have also been postulated to be the reason for the variations in α-value and olefin / paraffin ratio with carbon number. It is envisaged that desorbed olefins can readsorb onto the catalyst surface and undergo an array of secondary reactions, including growth and hydrogenation[9]. The selectivities of the C_1 and C_2 components can usually be described with this type of model, but unique parameter values must normally be assumed in the case of these components (see, for example, the model by Van der Laan[10]). The chain length dependent effects can only be ascribed to olefin reincorporation if the propensity for secondary reaction increases with increasing carbon number, which is indeed claimed to be the case[9,11]. The reasons proposed for the dependency of secondary reactions on carbon number have sparked some debate in the literature and include the following: slower diffusion of longer molecules through catalyst pores[12]; higher concentrations of heavier olefins in the liquid phase due to an increase in solubility with chain length[13,14]; stronger physisorption of longer molecules on the catalyst surface[10,14,15]; variations in reactor residence times due to different solubilities in the liquid phase[13,16]. Various models based on one or more of these mechanisms have been developed to describe measured FT product spectra.

Iglesia and co-workers[12] (and references therein) proposed an elaborate model that not only accounts for the diffusion-enhanced readsorption of olefins, but also for the influence of mass transfer limitations of reactants (most notably CO) on the product selectivities. The model was mainly validated with ruthenium- and cobalt-based FT catalysts and could describe various trends in the data, e.g. the effects of bed residence time (space velocity) and catalyst particle diameter. A structural parameter (χ) was

also defined which depends on the physical properties (particle size, pore diameter, etc.) and site density of the catalyst pellets. The model predicts that, with increasing values of χ, the C_{5+} selectivity will first increase due to enhanced readsorption of olefins and then decrease due to CO transport limitations (that will lead to an increase in the H_2/CO ratio at the catalytic sites). This trend was corroborated by their experimental data measured in fixed bed reactors. However, as discussed in Chapter 3, the increase in C_{5+} selectivity with increasing values of χ could not be reproduced experimentally by other researchers.

Schulz et al.[17] reported that it was highly unlikely that olefin mass transfer effects could have influenced the secondary olefin reactions in their own gradientless slurry reactor. They developed an olefin reincorporation model based mainly on chain length dependent solubilities of products in the liquid medium. This is despite arguments presented by Iglesia et al.[12] that deviations from the Schulz-Flory distribution cannot be due to the higher solubility of larger olefins, since thermodynamic equilibrium between the gas and liquid phase requires that the chemical potential for each component be the same in the two phases. As discussed in Chapter 3, the differences in solubilities of olefins with different chain lengths suggest a decreasing propensity of secondary olefin reactions with carbon number rather than the experimentally observed increase. Schulz et al.[17] compared their model to product distributions measured with both cobalt- and iron-based catalysts, but a very limited number of experimental product spectra were considered. Even though the correct trends were predicted, the model was merely moderately successful in describing the two product spectra obtained with iron catalysts. Van der Laan[10] developed a model where the rate of olefin readsorption depends on the chain length because of both increasing physisorption strength on the catalyst surface and increasing solubility of long chain molecules in the liquid medium. It was shown that the model could be fitted to a large number of product spectra measured with an iron-FT catalyst at 250°C under various process conditions.

Much of the debate around olefin reincorporation models has centred on the various reasons that have been proposed for the increased likelihood of secondary reactions with olefin chain length[1]. This seemed to have distracted from another important issue, namely the apparent disparity in behaviour between co-fed olefins and olefins formed in situ in the FT synthesis. Schulz et al.[9] stated that, under their conditions, hydrogenation was the fastest of all reactions of added olefins, while Shi et al.[18] concluded that the hydrogenation rate of co-fed olefins exceeds the rate of chain initiation by at least a factor of 4. Schulz et al.[9] accounted for the high hydrogenation probability of added olefins by proposing two modes of olefin readsorption. If the readsorbed olefin is attached to the catalyst surface at the penultimate carbon atom, limited growth (to form branched products) or isomerisation can occur, but the main reaction would be hydrogenation. Attachment at the ultimate carbon atom was assumed to yield a species indistinguishable from those formed in situ by the FT reaction, which can grow, desorb as an olefin, or be hydrogenated to a paraffin. However, Patzlaff et al.[6] pointed out that Schulz et al.[9,17] did not explicitly present the selectivity of 1-alkene incorporation calculated with their olefin reincorporation model and (in particular) did not compare it to the results of co-feeding studies. Patzlaff et al.[6] claimed that the assumed selectivity of olefin reincorporation has to become unrealistically high before secondary reactions can start to explain the observed deviations in the Schulz-Flory distribution. A similar anomaly was already encountered by Kuipers et al.[15] a few years earlier. These authors found that the measured reinsertion rate of co-fed 1-olefins were much lower than expected on the basis of the changes in the net chain growth probability in the typical FT product spectrum. Furthermore, the deviations in the ideal Schulz-Flory distributions were not affected by the gas flow rate to the reactor vessel. Arguably the strongest argument against olefin reincorporation models is the fact that significant insertion of C_{3+} olefins apparently does not occur over iron-based FT catalysts under commercially relevant synthesis conditions[11,19]. This is despite the fact that the bend in the Schulz-Flory

distribution is especially prominent over alkali-promoted iron catalysts[3,20]. As shown in Chapter 3, there seems to be a huge discrepancy between the model-predicted ratio of growth to hydrogenation for in situ formed olefins and the experimentally observed growth to hydrogenation ratio of co-fed olefins in the iron-FT synthesis.

In a comparison between iron- and cobalt-FT catalysts, Schulz[21] mentions that secondary reactions significantly influence the product distribution obtained over cobalt catalysts, but that secondary olefin reactions are almost absent in the case of alkali-promoted iron catalysts. Therefore, it is difficult to rationalise the application of olefin reinsertion models for the iron-based FT synthesis. Even though double-α models provide good empirical fits for the carbon number distribution of hydrocarbons in the C_{3+} range, these models have quite restricted application, as they can neither describe the C_1 and C_2 selectivities, nor the olefin / paraffin ratio as a function of chain length. Consequently, a new product characterisation model for the iron-based Low-Temperature Fischer Tropsch (Fe-LTFT) synthesis will be proposed here.

2. Proposal of a new product characterisation model

2.1 The extent of secondary reactions

Co-feeding studies have shown that ethylene and heavier olefins are readily hydrogenated or converted to heavier hydrocarbons over cobalt-based FT catalysts[9,19]. However, there seems to be substantial evidence in the literature that, apart from ethylene, light olefins do not undergo extensive secondary reactions over potassium-promoted iron catalysts under commercially relevant FT operating conditions. Hanlon et al.[22] found that co-fed 1-butene and 1-hexene only underwent secondary reactions to a notable extent when the CO partial pressure was very low. When the olefin / CO ratio was more realistic in terms of industrially relevant conditions, these secondary reactions essentially ceased, presumably due to competitive adsorption between the olefins and CO. Boelee [23] also reported that the secondary hydrogenation of olefins is highly dependent on the olefin / CO ratio inside the reactor. Tau et al.[11] co-fed

radioactively-labelled pentene to the iron-FT synthesis in a slurry reactor and found that almost none of the co-fed pentene partook in secondary reactions of any kind (including hydrogenation, isomerisation or reincorporation). Other researchers have also concluded that insignificant amounts of olefins are hydrogenated in the FT synthesis[7,24]. Donnelly et al.[25] oddly enough concluded that paraffins are mainly formed from olefins via a secondary hydrogenation reaction. This conclusion is in disagreement with their own finding that the space velocity (varied almost threefold) did not have any effect on the butene / butane ratio, suggesting that secondary hydrogenation does not significantly influence the olefin / paraffin ratio of the C_4 products. The above findings are in line with our experience at Sasol. We have also found that light olefins are not significantly incorporated or hydrogenated in the Fe-LTFT synthesis. The only exception is ethylene, which clearly has a high reactivity for secondary hydrogenation.

2.2 Model description and assumptions

Due to perceived differences in behaviour between co-fed olefins and olefins formed in situ in the FT synthesis, Kuipers et al.[15] concluded that, for an olefin to be reinserted, it does not necessarily have to desorb and leave its site of formation. It was proposed that, after the breaking of the chemical bond, the physisorption of the molecule on the catalyst surface keeps the molecule in the vicinity of the growth site and increases its chances of readsorption onto this site. Vapour phase olefins were assumed to have a relatively larger probability of adsorption onto special hydrogenation sites; hence the high hydrogenation rates of these components. This explanation for the difference in behaviour between in situ formed and co-fed olefins obviously begs the question why the chemical bond of the growing intermediate needs to break in the first place. The logical extension of the model by Kuipers et al.[15] is of course that the intermediate stays physically and chemically attached to the surface, i.e. that the deviations from the ideal product distribution is a primary characteristic of

the FT product spectrum. It is along these lines that a new product characterisation model for the Fe-LTFT synthesis will now be proposed.

In its first and current form, the new model has the following general characteristics:

- The model only concerns primary reactions, defined as reactions that take place before the growing intermediate has left the catalyst surface. It would not attempt in any way to account for secondary reactions (i.e. those reactions that occur after a desorbed component is readsorbed onto the catalyst surface). In light of the foregoing discussions, this seems to be a reasonable simplification at least in the case of the light end of the product spectrum (excluding ethylene) obtained over an alkali-promoted iron catalyst.
- Since the model will be independent of the gas phase concentration of olefins formed by the FT reaction, the gas- and liquid space velocities do not have to be taken into account via a macroscopic reactor model. The new selectivity model can thus be formulated in explicit form (in contrast to olefin reincorporation models).
- The model only considers two generic product classes, namely olefins and paraffins. No distinction will be made between internal and terminal olefins, or between linear and branched products. Oxygenates will also be omitted for the time being.
- The formation of olefins and paraffins is assumed to be governed by three generic reactions, namely chain growth (whereby one carbon atom is added to the growing intermediate), chain desorption (resulting in the formation of an olefin as end product) and chain hydrogenation (resulting in the formation of a paraffin as end product).

The cornerstone assumption of the model is that the rates of chain growth and hydrogenation are independent of chain length, but that the rate of desorption is a function of carbon number. This assumption can be rationalised from the perspective that growth and hydrogenation only occurs at the active endpoint of the intermediate.

It thus seems justified to assume that the length of the chain connected to the active endpoint would not influence either of these reactions. However, the chain connected to the active endpoint may well be expected to have an interaction with the catalyst surface, for example via physisorption. Therefore, the longer the chain, the greater the interaction with the catalyst surface, and the more difficult it would be for the chain to desorb. The results of the kinetic study on the iron-FT synthesis suggested a fairly low coverage of the catalytic surface by adsorbed reactants and intermediates (see Chapter 4), so presumably there is sufficient space available on the surface for adsorption of long chain intermediates. Since longer chains are hypothesised to desorb at a lower rate, their residence time on the catalyst surface would be longer, so that the probability that they will grow or be hydrogenated becomes larger. This can explain both observations that the probability of chain growth as well as the degree of saturation increases with increasing carbon number, thereby mechanistically relating these two observed characteristics of the product spectrum. This new approach has been termed the chain length dependent desorption model.

2.3 Mathematical formulation of the new model

As pointed out by Van der Laan and Beenackers[26], data reported in literature show that the enthalpy of adsorption of hydrocarbons on solid surfaces increases linearly with carbon number. By analogy, it can thus be expected that there would be a linear relationship between the energy required for desorption (E_d) and the number of carbon atoms in an FT intermediate (n):

$$E_d = k'n \qquad \ldots 1$$

If this quantity is also taken as the activation energy of the desorption step (in other words, the energy barrier that must be overcome for desorption to occur), then it can be incorporated as an Arrhenius term into the equation for the rate of desorption (r_d).

Therefore, the rate of desorption of a species with *n* carbon atoms can be expressed as Equation 2. At constant temperature, the Arrhenius term can be simplified by lumping some of the quantities together as one constant to obtain Equation 3.

$$r_d = k_d[C_n^*]\ e^{-\frac{k'n}{RT}} \qquad ...2$$

$$r_d = k_d[C_n^*]\ e^{-kn} \qquad ...3$$

Since the rates of growth (r_g) and hydrogenation (r_h) are assumed to be independent of carbon number, these can be expressed as follows:

$$r_g = k_g[C_n^*] \qquad ...4$$

$$r_h = k_h[C_n^*] \qquad ...5$$

Note that the rate expressions for the three generic reactions (Equations 3 to 5) all assume first order dependency on the surface concentration of the growing intermediate ($[C_n^*]$), since only one such molecule is involved in each of these reaction steps. Furthermore, the rate constants (k_d, k_g and k_h) are actually pseudo constants, since they probably account for the contributions of other species partaking in the reactions and may therefore incorporate the surface concentrations of species like hydrogen, the C_1 monomer, and even vacant sites. Since hydrogenation and desorption are both termination steps in the scheme of the model, the chain growth probability as a function of carbon number (α_n) can be calculated as follows:

$$\alpha_n = \frac{r_g}{r_g + r_h + r_d} \qquad ...6$$

By substitution of Equations 3 to 5 and simplifying, the above equation becomes:

$$\alpha_n = \frac{k_g}{k_g + k_h + k_d e^{-kn}} \qquad ...7$$

Because hydrogenation and desorption represents termination towards a paraffin and an olefin, respectively, the olefin / paraffin ratio $(O/P)_n$ can also be expressed as a function of carbon number:

$$(O/P)_n = \frac{r_d}{r_h} = \frac{k_d}{k_h} e^{-kn} \qquad ...8$$

Since it is the competition between the three generic reactions (rather than their absolute rates) that governs the product distribution, the number of model parameters can be reduced by expressing the rate constants relative to that of the chain growth reaction. Thus, the following model parameters are defined:

$$T_P = \frac{k_h}{k_g} \qquad ...9$$

$$T_O = \frac{k_d}{k_g} \qquad ...10$$

According to the above definitions, T_P can be viewed as the competition between hydrogenation (termination to paraffin) and chain growth, whereas T_O can be viewed as the competition between desorption (termination to olefin) and growth. From Equations 9 and 10 it follows that:

$$\frac{T_O}{T_P} = \frac{k_d}{k_h} \qquad ...11$$

Substituting Equations 9 to 11 into Equations 7 and 8 yields the following expressions for the chain growth probability and the olefin / paraffin ratio:

$$\alpha_n = \frac{1}{1 + T_P + T_O e^{-kn}} \qquad ...12$$

$$(O/P)_n = \frac{T_O}{T_P} e^{-kn} \qquad ...13$$

In the above model, k is only determined by the catalyst properties, but is independent of the process conditions at constant temperature. The parameters T_P and T_O are independent of the carbon number, but will be functions of the process conditions (temperature and reactant partial pressures). Clearly the only physical constraints on these parameters are that all three must assume positive values. Considering Equations 12 and 13 above, as well as the parameter constraints, it is evident that the olefin / paraffin ratio will decrease exponentially with carbon number, while the value of α will increase gradually until the following limiting value is approached:

$$\alpha_{\lim} = \frac{1}{1 + T_P} \qquad ...14$$

Both these characteristics of the model are qualitatively in line with experimental observations regarding the FT product spectrum[10].

It is important to consider the carbon number range in which the newly-developed model is valid. Due to the well-known deviations in the C_1 and C_2 selectivities from

the statistical-type distributions derived from the polymerisation character of the FT reaction, the model is for the time being only applicable to C_3 and higher hydrocarbons. Furthermore, the effect of secondary reactions (most notably hydrogenation) may also become significant for heavier components. Even though Equation 12 may still hold in the heavier end of the product spectrum (especially for the case of iron-FT where olefin reincorporation is believed to be negligible), it is anticipated that Equation 13 may significantly overestimate the olefinicity of the product spectrum in this region. If the heavier end is of interest, either the secondary hydrogenation reactions must be described with an additional model, or only the overall carbon number distribution must be considered in this range.

2.4 Application of the model

The distribution of FT products can be reported on a molar basis (M_n) or on a carbon atom basis (S_n). From the ideal Schulz-Flory distribution, it follows that:

$$M_{n+1} = \alpha M_n \qquad \text{or} \qquad \frac{S_{n+1}}{n+1} = \alpha \frac{S_n}{n} \qquad \ldots 15$$

It should be noted that the current study is concerned with the development of a product characterisation model that establishes relationships between different products, but it cannot directly predict absolute product selectivities. Therefore, the definitions of M_n and S_n are not restricted to absolute selectivities, but can also be the relative amounts of products on a molar basis and carbon atom basis, respectively. It is further evident that Equation 15 is only valid for the case where α is constant over the whole carbon number distribution. The relationship between the formation rates of products with consecutive carbon numbers is somewhat more complicated for the case where α varies with carbon number. This relationship can be obtained from Figure 1.

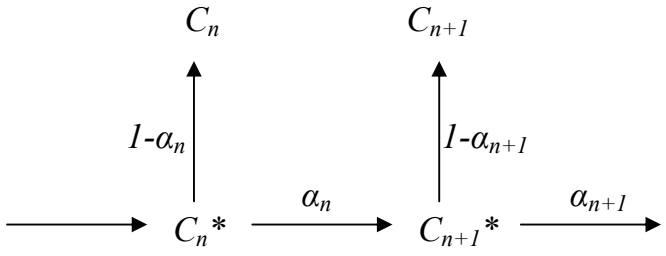

Figure 1: Scheme used to derive the relationship between selectivities of consecutive carbon numbers

If the growth probability of a surface species with *n* carbon atoms is α_n, then the probability that this species will terminate to an end product is $(1-\alpha_n)$. Thus:

$$M_n = (1-\alpha_n)[C_n*] \quad ...16$$

$$[C_{n+1}*] = \alpha_n[C_n*] \quad ...17$$

$$M_{n+1} = (1-\alpha_{n+1})[C_{n+1}*] \quad ...18$$

Combining the above three equations yields the relationship between the formation rates, on a molar basis, of end products with sequential carbon numbers (Equation 19). This relationship can also be expressed on a carbon atom basis (Equation 20).

$$M_{n+1} = \alpha_n \frac{(1-\alpha_{n+1})}{1-\alpha_n} M_n \quad ...19$$

$$\frac{S_{n+1}}{n+1} = \alpha_n \frac{(1-\alpha_{n+1})}{1-\alpha_n} \frac{S_n}{n} \quad ...20$$

It is again emphasised that the new model currently only predicts the chain growth probability and the olefin / paraffin ratio as a function of carbon number. In other words, it cannot predict absolute selectivities, but merely the variations in selectivity

with carbon number. Therefore, the model can be applied by specifying the absolute selectivity or even the relative amount produced (in any units) of a certain carbon number. This will be termed the reference component. Depending on whether this is specified on a molar basis (M_n) or a carbon atom basis (S_n), either Equation 19 or 20 is used in conjunction with the expression for α as a function of carbon number (Equation 12), to calculate the selectivity (or amount produced) of the next carbon number (M_{n+1} or S_{n+1}). By repeating this process sequentially, the carbon number distribution of a desired range can be predicted relative to the reference component. Afterwards, the olefin / paraffin ratio as a function of carbon number (Equation 13) is used to calculate the amounts of olefins and paraffins, respectively, in every carbon number fraction.

3. Testing the model against experimental data

3.1 Fitting the model to the C_{3+} fraction

Van der Laan[10] reported an experimental study on a Ruhrchemie precipitated iron catalyst (promoted with potassium, silica and copper). Run A was performed in a gas-solid spinning basket reactor, while Run C was performed in a slurry reactor. Both reactors could be regarded as continuously stirred tank reactors (CSTR's). Selectivity data were reported up to C_{10}. The new model was fitted to these data by minimising the relative variance (S_{rel}), defined as follows[10]:

$$S_{rel} = 100\sqrt{\frac{1}{n-m}\sum_{i=1}^{n}\left(\frac{r_i^{observed} - r_i^{predicted}}{r_i^{observed}}\right)^2} \qquad ...21$$

The data of Run A consisted of 24 product spectra measured under different feed conditions. Since only one catalyst was used for the measurements and the temperature was kept constant at 250°C, the model parameter k must be constant for

all 24 conditions and can therefore be regarded as a "global" parameter for this whole set of data. On the other hand, the values of T_P and T_O are dependent on the reagent partial pressures and therefore vary from one condition to another; consequently, these can be regarded as "local" parameters. Since there were 24 different values of T_P and T_O each, as well as the one global parameter, the selectivity data were described with a total of 49 parameters. The mol fractions of products in the gas phase effluent from the reactor were only reported up to C_{10}. This means there were 8 olefin and 8 paraffin mol fractions to be predicted for each of the 24 product slates (i.e. a total number of 384 selectivities). As explained previously, the model can only predict the formation rates of olefins and paraffins relative to that of a reference component. In this case, the mol fraction of the total C_3's in the gas phase (as reported by Van der Laan[10]) was taken as the reference component of the product distribution. By applying Equations 12 and 19, the mol fractions of the C_4 to C_{10} products in the gas phase effluent can be predicted. Subsequently, Equation 13 is used to divide each carbon number into paraffins and olefins. The mol fractions of paraffins and olefins in the gas phase effluent obtained by this procedure can then be compared to the reported (measured) values. The values of the model parameters were optimised to minimise the relative variance between the reported paraffin and olefin mol fractions and the model predictions.

Table 1: Results of fitting the new model on the C_3 to C_{10} selectivity data reported by Van der Laan[10] for a potassium-promoted precipitated iron catalyst. The data were measured in well mixed reactors. Run A: performed in a gas-solid spinning basket reactor. Run C: performed in a slurry reactor.

	k	T_P (range)	T_O (range)	S_{rel} (%)	Predictability of Total C_2's *
Run A	0.19	0.02 – 0.33	0.36 – 0.86	13.7	1.55 – 2.17
Run C	0.20	0.03 – 0.32	0.41 – 0.91	13.2	1.54 – 2.03

* Predictability of the C_2 fraction is defined as the predicted / measured value of the total C_2's (ethylene and ethane together)

The results of the fit are presented in Table 1. The value of k is an indication of the adsorption strength per carbon number of a growing intermediate on the catalyst surface. The values of T_P are generally quite low, with that of T_O substantially higher. Considering the definitions of these two parameters (Equations 9 and 10), the reported values are indicative of a heavy, olefinic product spectrum, typical of what one would expect for an alkali-promoted iron catalyst at this operating temperature. The lowest value obtained for T_P admittedly looks somewhat suspicious, as it corresponds to a limiting value for α of 0.98. However, this specific product slate was measured at a reactor H_2/CO ratio of 0.18, which is an extreme condition for the Fe-LTFT synthesis. For the full data set, the limiting values of α generally varied between 0.75 and 0.95, which is quite possible considering the wide range of reagent partial pressures covered. Considering the fairly low value of the relative variance, it is clear that the model fits the data quite well. In Table 1, the ratio of the predicted to the measured amount of total C_2's is also reported. Since this value is always higher than unity, it means that the new model systematically over predicts the total C_2 fraction, in other words the growth probability for the C_2 intermediate is systematically underestimated. This is in line with the well-known deviation of the C_2's from the rest of the product distribution.

In the same way, the new model was also fitted to the 15 product distributions of Run C. The results, included in Table 1, are very similar to those obtained previously. Not only was the relative variance quite low, but the value of k was essentially the same as for Run A. It is again very clear that the new model systematically overestimates the formation rate of the total C_2 fraction.

3.2 Predicting the total C_2 fraction

It has been mentioned previously that the double-α model circumvents the anomaly of the total C_2 fraction by only considering the C_{3+} part of the product spectrum, while the olefin reincorporation models have introduced an additional model parameter in

order to predict the C_2 fraction. In line with other product characterisation models, the new selectivity model overestimates the C_2 formation rate if the same parameter values are used as for the rest of the product spectrum. However, if a rational explanation can be supplied of why and how these parameters should be adapted in the case of C_2, it would lend strong support to the new model. Dry[27] proposed a plausible reason for the observed negative deviation in the total C_2 selectivity. Generally, the one end of a growing intermediate species of the FT reaction is a saturated, inactive chain. It can therefore be assumed that the intermediate of a higher hydrocarbon only has one active growth position. To the contrary, a C_2 surface species only has two carbon atoms. Consequently, it was hypothesised that this intermediate has two active growth positions, giving this species a higher probability of chain growth than the heavier species; hence the lower-than-expected C_2 selectivity.

The above hypothesis by Dry[27] can easily be incorporated into the new product characterisation model. The model assumes that the intrinsic rates of growth and hydrogenation are independent of chain length, whereas the rate of desorption is dependent on carbon number according to Equation 3. These assumptions can also be applied to the C_2 fraction, provided it is taken into account that the involved intermediate has a growth rate twice as large as that of the C_{3+} species due to the two active growth positions. Therefore, considering the parameter definitions expressed by Equations 9 and 10, it is clear that the values of both T_P and T_O must be halved in the case of the C_2 fraction to account for this higher growth rate. Even though this does not affect the olefin / paraffin ratio (Equation 13), the expression for the α-value (Equation 12) then becomes:

$$\alpha_2 = \frac{1}{1 + 0.5T_P + 0.5T_O e^{-2k}} \qquad ...22$$

By using the parameter values obtained previously from the C_3 to C_{10} fraction, the total C_2 products could be predicted with the above equation. The predicted values are

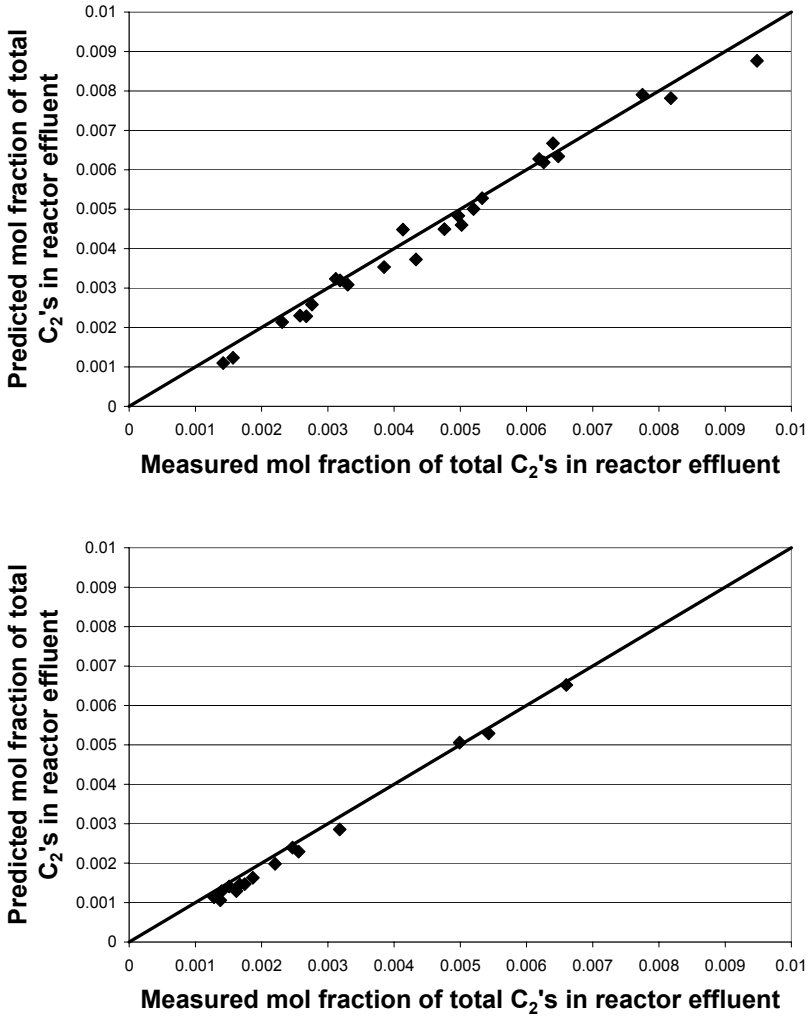

Figures 2 (top) and 3 (bottom): Parity plots of total C_2's for Runs A (gas-solid spinning basket reactor) and C (slurry reactor), respectively, predicted by extrapolation of the chain length dependent desorption model. Data measured by Van der Laan[10]. Experimental details as per Table 1.

presented as a function of the measured values in Figures 2 and 3 for the cases of Runs A and C, respectively. The model accuracy is indeed excellent and it is concluded that the new model can be extended by means of logical reasoning to cover the C_2 fraction as well. It should be noted that this is a true extrapolation, since parameters values were estimated with data from a different product range (excluding the C_2's) and then applied to the C_2 fraction. However, it seems as if there may be a slight systematic

deviation between the model and measured data, since most of the predictions fall just below the parity line. No explanation can be offered at this stage.

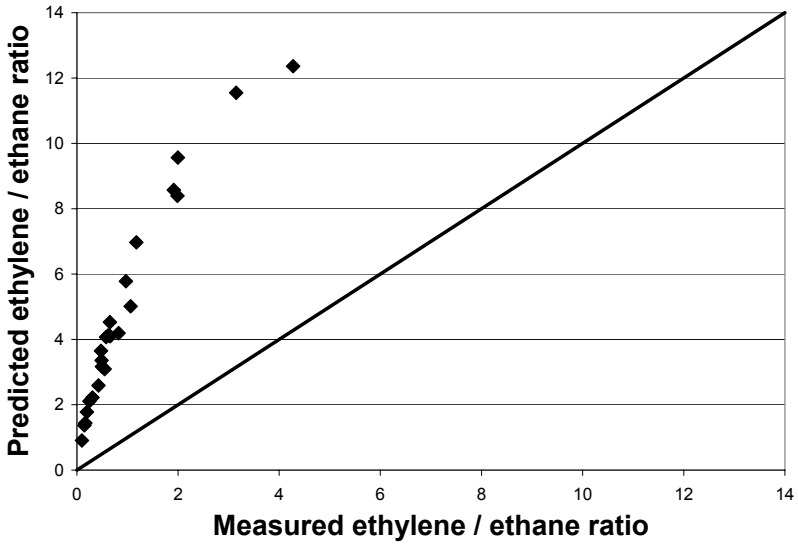

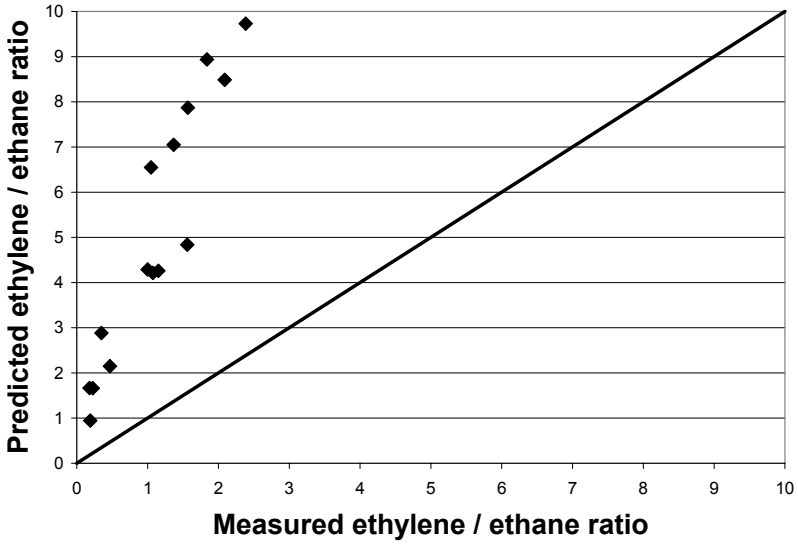

Figures 4 (top) and 5 (bottom): Parity plots for Runs A (gas-solid spinning basket reactor) and C (slurry reactor), respectively, of the ethylene / ethane ratio as predicted by the chain length dependent desorption model. Data measured by Van der Laan[10]. Experimental details as per Table 1.

The predicted ethylene / ethane ratio is presented as a function of the measured values in Figures 4 and 5 for the cases of Runs A and C, respectively. For every data point, the predicted olefinicity is clearly much higher than the measured value. Recalling that the model only considers primary reactions, this deviation could be due to the high propensity of ethylene for secondary hydrogenation over the iron catalyst. Substantial secondary hydrogenation of ethylene has indeed been found during various co-feeding studies[19,22], and the extent of it is expected to be dependent on (amongst others) the ethylene / CO ratio inside the reactor[23]. Should it be desired to predict the selectivities of ethane and ethylene separately, an additional model accounting for secondary reactions would therefore have to be developed.

3.3 Predicting the methane production

In order to predict the methane production from the rest of the product distribution, the growth probability of the C_1 intermediate must be estimated. Equation 12 makes provision for a termination step to olefins via desorption, but there is no olefinic product compound that only contains one carbon atom. The logical step would be to set the value of T_O equal to zero, in line with the notion that the C_1 surface species can only terminate via hydrogenation to methane. Then the growth probability of the C_1 intermediate would be equal to the limiting (maximum) value of α reached at very high carbon numbers (Equation 14). To the contrary, from the higher-than-expected methane selectivities generally observed, it is known that the growth probability of the C_1 surface species is actually much lower than that of the other intermediates. It thus appears as if the chain length dependent desorption model would not be able to predict the methane selectivity if termination via hydrogenation only is assumed.

Nevertheless, Equation 12 will be applied to the C_1 intermediate as if this species can terminate via both hydrogenation and desorption without considering the mechanistic implications for the time being. In other words, the growth probability of the C_1 surface species becomes:

$$\alpha_1 = \frac{1}{1 + T_P + T_O e^{-k}} \qquad ...23$$

By taking the values of the model parameters (T_P, T_O and k) estimated for the C_3 to C_{10} part of the product spectrum, Equation 23 can therefore be used to predict the methane formation rate relative to the reference compound (in this case the mol fraction of total C_3's in the reactor effluent). The methane parity plots are presented in Figures 6 and 7 for Runs A and C, respectively. For Run A, there are two points that deviate notably from the parity line (as circled on Figure 6), whereas the remaining points generally lie much closer to the line. For Run C, the methane prediction is quite good, as is evident from the parity plot of Figure 7. It therefore seems as if the chain length dependent desorption model can indeed be extrapolated to methane as well without introducing any additional model parameters. However, the mechanistic requirement is the C_1 intermediate can also terminate via a type of desorption step in addition to the expected termination via hydrogenation, the nature of which is not currently known. Again there may be a slight systematic deviation in the model, especially evident in Figure 7 where most of the model predictions lie above the parity line. No plausible reason can be proposed at present for the possible systematic deviation.

3.4 The complete model

Finally, the complete model was fitted to the C_1 to C_{10} data reported by Van der Laan[10]. All the data from Runs A and C were combined, yielding a total of 39 product spectra to model. Each product spectrum contained 10 paraffins and 9 olefins, i.e. 19 data points per product distribution. The total mol fraction of C_3's in the gas phase effluent was again taken as the reference component, which sacrificed one degree of freedom. Furthermore, the ethylene / ethane ratio was also specified as the measured value, since the chain length dependent desorption model cannot account for the substantial extent of secondary hydrogenation of ethylene. This sacrificed one more

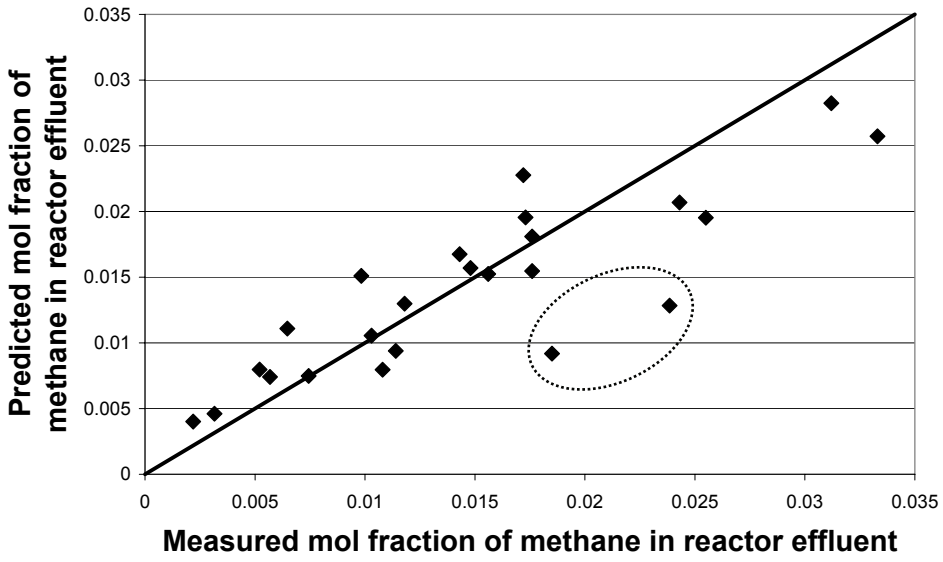

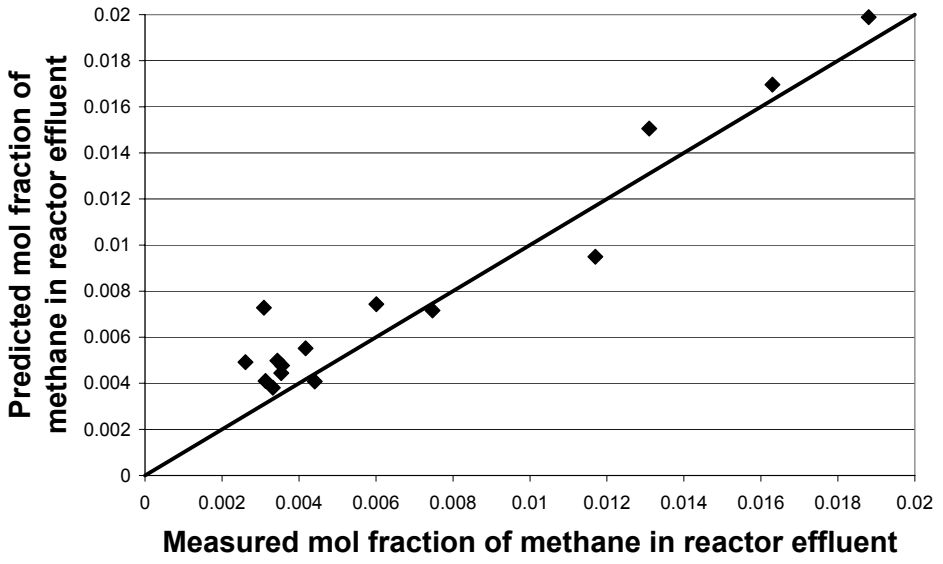

Figures 6 (top) and 7 (bottom): Methane parity plots for Runs A (gas-solid spinning basket reactor) and C (slurry reactor), respectively, predicted by the chain length dependent desorption model. Data measured by Van der Laan[10]. Experimental details as per Table 1.

Table 2: Results of fitting the new model to the C_1 to C_{10} selectivity data reported by Van der Laan[10] for a potassium-promoted precipitated iron catalyst. Measurements performed in well mixed reactors. Data from Run A (performed in a gas-solid spinning basket reactor) and Run C (performed in a slurry reactor) were grouped together as one set.

	k	T_P (range)	T_O (range)	S_{rel} (%)
Runs A and C	0.19	0.02 – 0.33	0.35 – 0.86	15.0

degree of freedom per product spectrum. The results of the model fitting are presented in Table 2. The relative variance of the model fit is quite low, considering that the C_1 and C_2 formation rates are predicted without introducing any additional model parameters.

As visual confirmation of the new model's ability to characterise the Fe-LTFT product distribution, three product spectra were selected. These correspond to the spectra that yielded the lowest error ("best fit"), the median error ("median fit") and the largest error ("worst fit") and are presented in Figures 8 to 10, respectively. Methane is omitted from these plots, as it increases the scale of the graphs to such an extent that that the fit of the higher hydrocarbons are obscured (detailed information about the methane prediction is presented in the parity plots of Figures 6 and 7). For both the "best fit" and the "median fit" cases, the model description of the olefins and paraffins is near perfect. Even for the "worst fit" case where the deviations are somewhat more notable, the fit seems quite acceptable.

4. Comparison between model predictions and qualitative experimental observations

In the past, some researchers have lent mechanistic interpretations to certain observed characteristics of the FT product spectrum. Egiebor et al.[20] considered the Schulz-

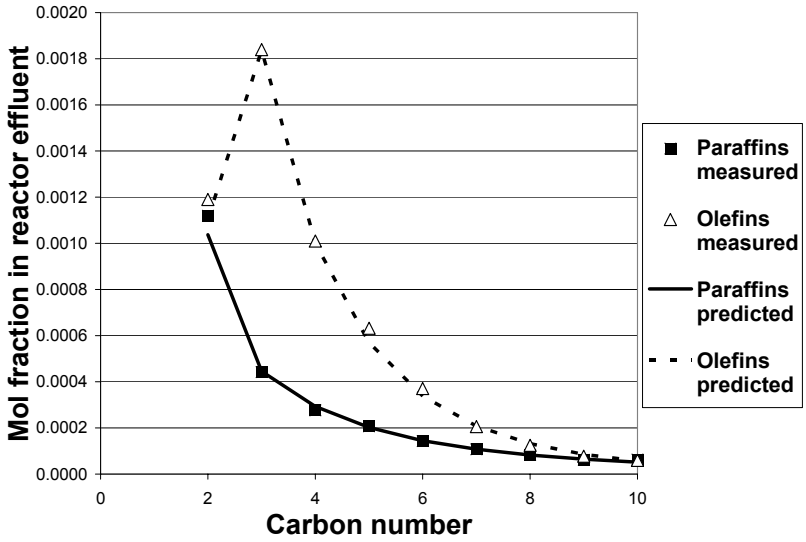

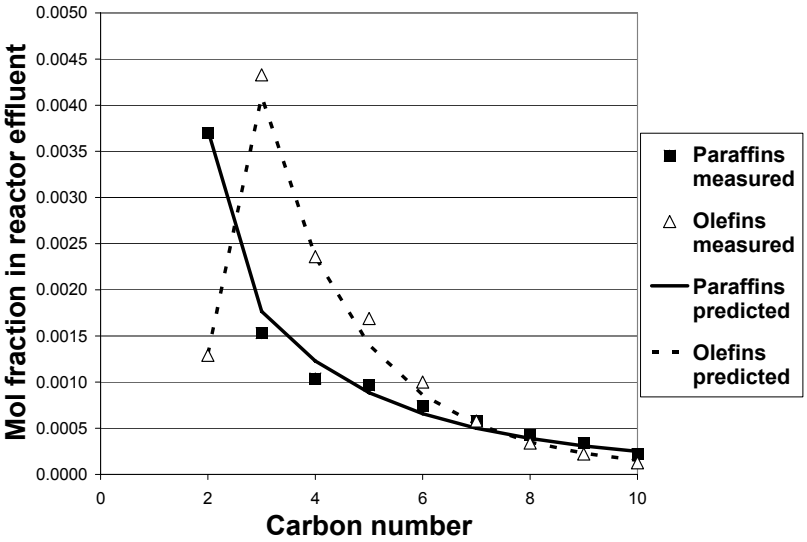

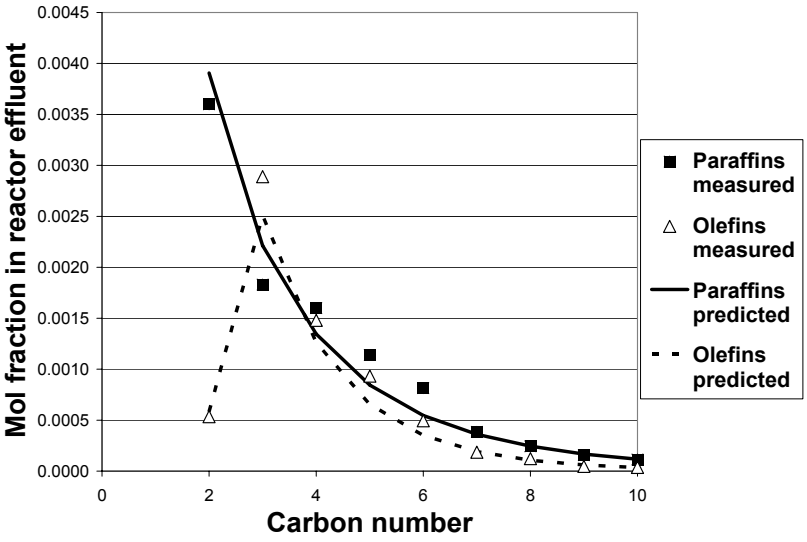

Figures 8 (top, "best fit"), 9 (middle, "median fit") and 10 (bottom, worst fit): Ability of the chain length dependent desorption model to describe product spectra from Runs A and C reported by Van der Laan[10]. Experimental details as per Table 1.

Flory plots of olefins and paraffins separately and found that the olefin distribution could be characterised by a straight line. To the contrary, the paraffins started off with the same slope as the olefins, but this slope increased significantly with increasing carbon number. It was therefore concluded that the break in the total product spectrum is solely due to a break in the paraffin distribution and some mechanistic explanations for this finding were proposed. Donnelly et al.[25] challenged this conclusion, since they presented data where a bend in the olefin distribution was visible. However, considering their graphs, the break in the paraffin distribution was substantially more pronounced than in the case of the olefins. More recently Van der Laan[10] also reported as a general characteristic of the FT product spectrum that the bend in the Schulz-Flory distribution is only observed for the paraffins and not for the olefinic products.

In order to investigate whether the new model is qualitatively in line with the above experimental observations, different sets of parameter values were selected for the chain length dependent desorption model. These sets of parameter values covered a broad range. For each set of values, the product distribution was predicted with the new model and the olefin and paraffin selectivities plotted separately on a Schulz-Flory graph. For all cases, the shapes of the Schulz-Flory curves were essentially the same; consequently, only one is presented in Figure 11 as a typical example. Clearly the olefin distribution has a slight deviation from linearity, but (as indicated on the graph) the change in the slope is so small that the curve could easily be mistaken for a straight line. This would be especially true for actual experimental data containing measurement errors. The slope of the paraffin curve is similar to that of the olefin curve in the lower carbon number range. However, the break in the paraffin curve (occurring around C_{10}) is so pronounced that it is justified to claim that the bend in the overall carbon number distribution is essentially caused by the shape of the paraffin distribution. It therefore seems as if the predictions of the new selectivity model are also qualitatively in line with the observations reported in the literature.

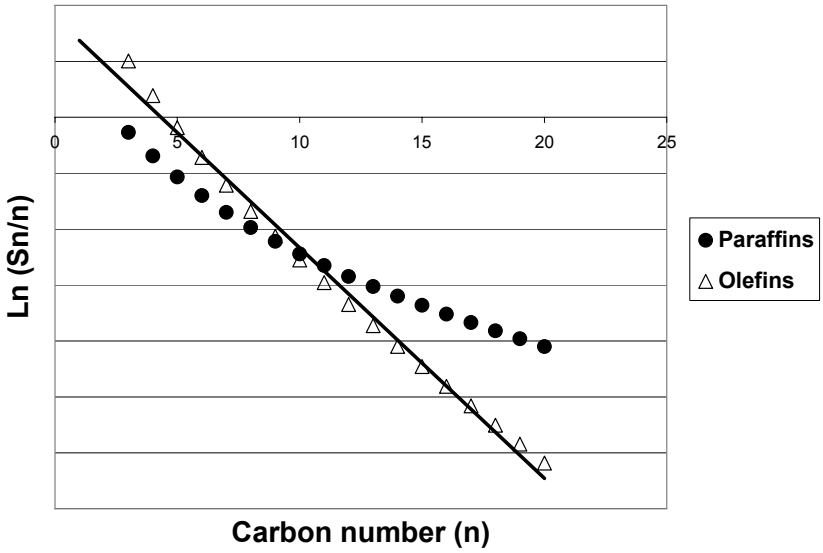

Figure 11: A Schulz-Flory plot of paraffins and olefins separately of a typical product distribution predicted with the chain length dependent desorption model. The olefin distribution is essentially linear as indicated, while there is a prominent bend in the paraffin distribution.

5. Sensitivity of the model accuracy to variations in the parameter values

A short study was performed to investigate the sensitivity of the model accuracy to variations in the parameter values. To this end, the optimised value of the global parameter (k) was decreased and increased, respectively, followed by re-optimisation of the local parameters for all the data from Runs A and C reported by Van der Laan[10]. The results are presented in Table 3 and the relative variance is once again taken as a measure of the model accuracy. Even though the value of k was varied by about 20% to both sides, the relative variance did not increase by more than one percentage point. It therefore seems as if the model accuracy is not highly dependent on the value of k. The implication is that the global parameter of the new product characterisation model cannot be determined with a high degree of confidence from measured selectivity data.

Table 3: The sensitivity of the model fit to variations in the value of the global parameter *k*. Model fitted to the C_1 to C_{10} selectivity data reported by Van der Laan[10]. Data from Run A (gas-solid spinning basket reactor) and Run C (slurry reactor) were grouped together as one set.

	Optimised Model	Decreased value of *k*	Increased value of *k*
k	0.19	0.15*	0.23*
S_{rel} (%)	15.0	16.0	15.9

* Specified values

Tables 4 (top) and 5 (bottom): The sensitivity of the model fit to variations in the values of the local parameters T_P and T_O, respectively. Model fitted to the "best fit" product spectrum of Run A (Van der Laan[10]) as an example.

	Optimised Model	Decreased value of T_P	Increased value of T_P
k	0.19	0.19*	0.19*
T_P	0.12	0.10*	0.14*
T_O	0.86	0.84	0.88
S_{rel} (%)	7.4	12.0	11.6
α (limit)	0.89	0.91	0.88

* Specified values

	Optimised Model	Decreased value of T_O	Increased value of T_O
k	0.19	0.19*	0.19*
T_P	0.12	0.11	0.12
T_O	0.86	0.77*	0.95*
S_{rel} (%)	7.4	15.3	13.6
α (limit)	0.89	0.90	0.89

* Specified values

Subsequently, it was investigated how much the goodness of fit was influenced by changes in the local parameters (T_P and T_O) for a given value of the global parameter. For this purpose, the "best fit" product spectrum of Run A was used and the value of *k* was kept constant at the previously optimised value. One of the local parameters was

then varied, followed by re-optimisation of the other local parameter. From the results presented in Table 4, it is evident that a variation in the value of T_P by about 20% to either side (corresponding to a range of 0.88 to 0.91 in the asymptotic value of α) caused a notable increase in the relative variance. However, the optimised value of T_O was not much affected. The results of Table 5 indicate that the model accuracy is even more sensitive to changes in the value of T_O, since a 10% increase or decrease in the value of this parameter had an even larger impact on the relative variance. Again, the value of the other local parameter was not influenced too much.

From the above, it appears as if the value of the global parameter cannot be determined very accurately from selectivity data. However, once the value of k is fixed, it seems as if the two local parameters (T_P and T_O) can be estimated with a high degree of confidence. Furthermore, these two local parameters appear to be truly independent of one another, since there does not seem to be a strong cross-correlation between them. For a given catalyst, k is a global constant independent of reagent concentrations; consequently, it does not have to be predicted for commercial application, but is merely measured and applied. Therefore, the accuracy with which it can be estimated is arguably not of critical importance. However, the local parameter values, which are dependent on the reagent partial pressures and must therefore be expressed as functions of the operating conditions, can apparently be determined quite accurately. Therefore, purely from a mathematical perspective, it is expected that the correlations between model parameters and process conditions will be much more meaningful for the new model than for the case of the double-α model.

The chain length dependent desorption model characterises a given FT product spectrum with three parameters, which is strictly speaking the same as in the case of the double-α model. Nevertheless, considering the discussion in Chapter 3, it is clear that the parameter values estimated for the new model are statistically much more meaningful. The reason for this is probably two-fold. Firstly, the three parameters are totally unique to each product spectrum in the case of the double-α model, whereas

one of the parameters is constant for all product distributions in the case of the new model. Secondly, the double-α model is fitted only to the total carbon number distribution and, moreover, the C_2 and C_1 selectivities are omitted. To the contrary, the new model differentiates between olefins and paraffins, while the C_1 and C_2 products are included in the model fit. The double-α model therefore uses more parameters to describe fewer system outputs, which means that the system is probably over-specified. This causes the extensive co-variance between the model parameters that was discussed in Chapter 3.

6. Findings and conclusions

From results presented in literature, as well as from our own experience, we believe that light olefins do not undergo secondary reactions to a large extent under commercially relevant conditions in the Fe-LTFT synthesis. The only exception is ethylene, which has a high reactivity for secondary hydrogenation. A new product characterisation model was proposed for the Fe-LTFT synthesis, based on the premise that the increase in α-value and decrease in olefin / paraffin ratio with carbon number are both characteristics of the primary product spectrum. The chain length dependent desorption model could successfully describe the olefin and paraffin distributions in the C_3 to C_{10} range. Furthermore, the model could also be extended to the C_1 and C_2 product fractions via logical reasoning. The total C_2 formation rate was described almost perfectly, while the methane formation rate was described adequately, by using parameter values that were obtained from the C_3 to C_{10} product fraction. This is a true extrapolation, as the C_1 and C_2 data were not used for the estimation of the parameter values. This is presumably the first product characterisation model that can be extrapolated to the C_1 and C_2 components without introducing additional (unique) parameter values for these products.

It should be noted that the chain length dependent desorption model is not a complete selectivity model, as it merely establishes relationships between the compounds in the

FT product distribution. One of the model parameters (k) is only dependent on the catalyst properties and on the temperature (via an Arrhenius relationship), while the other two model parameters (T_P and T_O) are dependent on process conditions. Sensible relationships between these two parameters and the reagent partial pressures must still be developed before a usable selectivity model can be obtained. This can be done by making certain mechanistic assumptions regarding the three generic reactions (growth, hydrogenation and desorption) and testing the resulting expressions against experimental data.

From the findings of this study, one can speculate in a broad sense on the mechanisms that determine the product distribution of the Fe-LTFT synthesis. Two chain termination steps have been considered here. Hydrogenation, which is independent of carbon number, saturates the chain with the result that the intermediate species can only leave the catalyst surface as a paraffin. Desorption to an unsaturated end product was assumed to occur via a reconstruction that is not readily reversible, which could be why significant olefin reinsertion over iron catalysts has not been demonstrated. In the new model, the rate of desorption is controlled by the physical interaction between the growing intermediate and the catalyst surface. The strength of this interaction is directly proportional to the number of carbon atoms in the intermediate, i.e. there is apparently no distinction between the active growth position and the other carbon atoms in the species. Since the model could be successfully extrapolated to methane as well, it appears as if the termination of the C_1 intermediate (which can be viewed as merely an active growth position) is governed by the same two steps as the longer chain intermediates. In other words, it seems as if the physical interaction between the C_1 species and the catalyst surface has to be maintained to enable this intermediate to grow. It appears that, once this physical interaction is terminated, the C_1 surface species also transforms irreversibly, so that it cannot partake any further in chain propagation. Since it cannot exist as a freestanding unsaturated entity, it stays near the surface until it is fully hydrogenated, but its final fate will be to terminate as methane.

Possibly for this reason, the contribution of the physical interaction between the C_1 intermediate and the catalyst surface has to be accounted for in order to successfully predict the methane formation rate with the chain length dependent desorption model, even though there is no C_1 olefinic product. The foregoing is of course speculative. Microscopic experimental evidence that can either support or refute this view of the mechanism that governs olefin and paraffin formation in the Fe-LTFT synthesis will be welcomed.

References

1. Van der Laan, G.P.; Beenackers, A.A.C.M. Kinetics and Selectivity of the Fischer-Tropsch Synthesis: A Literature Review. *Catal. Rev. – Sci. Eng.* 1999, 41 (3&4) 255.
2 Claeys, M.; Van Steen, E. in A.P. Steynberg, M.E. Dry (Eds.), *Stud. Surf. Sci. Catal.* Vol. 152, Elsevier, Amsterdam, 2004, Chapter 8, pp. 628-633.
3. Koenig, L., Gaube, J. Fischer-Tropcsh Synthesis – Recent Studies and Developments. *Chem.-Ing. Tech.* 1983, 55 (1), 14.
4. Tau, L.; Dabbagh, H.; Bao, S.; Davis, B.H. Fischer-Tropsch Synthesis. Evidence for Two Chain Growth Mechanisms. *Catal. Lett.* 1990, 7, 127.
5. Patzlaff, J., Liu, Y., Graffmann, C., Gaube, J. Studies on Product Distributions of Iron and Cobalt Catalysed Fischer-Tropsch Synthesis. *Appl. Catal.* 1999, 186, 109.
6. Patzlaff, J.,; Liu, Y.; Graffmann, C.; Gaube, J. Interpretation and Kinetic Modelling of Product Distributions of Cobalt Catalysed Fischer-Tropsch Synthesis. *Catal. Today* 2002, 71, 381.
7. Egiebor, N.O., Cooper, W.C., Wojciechowski, W. Carbon Number Distribution of Fischer-Tropsch CO-hydrogenation Products from Precipitated Iron Catalysts. *Can. J. Chem. Eng.* 1985, 63, 826.

8. Donnelly, T.J.; Yates, I.C.; Satterfield, C.N. Analysis and Prediction of Product Distributions of the Fischer-Tropsch Synthesis. *Energy & Fuels* 1988, 2, 734.
9. Schulz, H., Claeys, M. Reaction of α-Olefins of Different Chain Length Added during Fischer-Tropsch Synthesis on a Cobalt Catalyst in a Slurry Reactor. *Appl. Catal.* 1999, 186, 71.
10. Van der Laan, G.P. Kinetics, Selectivity and Scale Up of the Fischer-Tropsch Synthesis. Ph.D. Thesis, Rijksuniversiteit Groningen, 1999.
11. Tau, L.; Dabbagh, H.; Davis, B.H. Fischer-Tropsch Synthesis: ^{14}C Tracer Study of Alkene Incorporation. *Energy & Fuels* 1990, 4, 94.
12. Iglesia, E.; Reyes, S.C.; Madon, R.J.; Soled, S. Selectivity Control and Catalyst Design in the Fischer-Tropsch Synthesis: Sites, Pellets and Reactors in Eley, D.D., Pines, H. Weisz, P.B., Eds., Advances in Catalysis, vol. 39, Academic Press: New York 1993, 221-302.
13. Zimmerman, W.; Bukur, D.; Ledakowicz, S. Kinetic Model of Fischer-Tropsch Synthesis Selectivity in the Slurry Phase. *Chem. Eng. Sci.* 1992, 47, 2707.
14. Kuipers, E.W.; Vinkenburg, I.H.; Oosterbeek, H. Chain Length Dependence of α-Olefin Readsorption in Fischer-Tropsch Synthesis. *J. Catal.* 1995, 152, 137.
15. Kuipers, E.W., Scheper, C., Wilson, J.H., Vinkenburg, I.H., Oosterbeek, H. Non-ASF Product Distributions due to Secondary Reactions during Fischer-Tropsch Synthesis. *J. Catal.* 1996, 158, 288.
16. Tau, L.; Dabbagh, H.; Davis, B.H. Fischer-Tropsch Synthesis: Comparison of ^{14}C Distributions when Labelled Alcohol is Added to the Synthesis Gas. *Energy & Fuels* 1991, 5, 174.
17. Schulz, H., Claeys, M. Kinetic Modelling of Fischer-Tropsch Product Distributions. *Appl. Catal. A* 1999, 186, 91.
18. Shi, B, Davis, B. Fischer-Tropsch Synthesis: Accounting for Chain Length Related Phenomena. *Appl. Catal. A* 2004, 277, 61.

19. Schulz, H.; Rao, B.R.; Elstner, M. ^{14}C-Studien zum Reaktionsmechanismus der Fischer-Tropsch Synthese. *Erdöl und Kohle – Erdgas – Petrochemie* 1970, 23 (10), 651.
20. Egiebor, N.O., Cooper, W.C. The Polyfunctionality of Iron Catalysts during Carbon Monoxide Hydrogenation I. Occurrence of Dual Chain Propagation Sites. *Appl. Catal.* 1985, 14, 323.
21. Schulz, H. Comparing Fischer-Tropsch Synthesis on Iron- and Cobalt Catalysts. *Prepr. Symp. – Am. Chem. Soc., Div. Petr. Chem.* 2005, 50(2), 155.
22. Hanlon, R.T, Satterfield, C.N. Reactions of Selected 1-Olefins and Ethanol Added during the Fischer-Tropsch Synthesis. *Energy & Fuels* 1988, 2, 196.
23 Boelee, J.H. The Fisher-Tropsch synthesis in slurry phase reactors, Ph.D. Dissertation, Technische Universiteit Eindhoven, 1988.
24. Huff, G.A., Satterfield, C.N. Evidence for Two Chain Growth Probabilities on Iron Catalysts in the Fischer-Tropsch Synthesis. *J. Catal.* 1984, 85, 370.
25. Donnelly, T.J., Satterfield, C.N. Product Distributions of the Fischer-Tropsch Synthesis on Precipitated Iron Catalysts. *Appl. Catal.* 1989, 52, 93.
26. Van der Laan, G.P.; Beenackers, A.A.C.M. Hydrocarbon Selectivity Model for the Gas-Solid Fischer-Tropsch Synthesis on Precipitated Iron Catalysts. *Ind. Eng. Chem. Res.* 1999, 38, 1277.
27. Dry, M.E. Practical and Theoretical Aspects of the Catalytic Fischer-Tropsch Process. *Appl. Catal. A* 1996, 138, 319.

Chapter 7

Secondary Reactions of Light Olefins as Studied in a Laboratory-Scale Recycle Slurry Reactor

Publications from this chapter

Botes, F.G.; Govender, N.S. Secondary Reactions of Ethylene as Studied in a Laboratory-Scale Recycle Slurry Reactor. *Energy & Fuels* 2007, 21, 3095.

Abstract

Data from a recycle laboratory slurry reactor were considered to investigate the secondary reactions of ethylene in Sasol's commercial iron-based Low-Temperature Fischer-Tropsch synthesis. In particular, the behaviour of ethylene was compared to that of propylene. No evidence could be found for significant reincorporation of either of these two olefins. Propylene was hydrogenated to a very small extent, whereas ethylene was substantially hydrogenated. The estimated primary olefin / paraffin ratio for the C_2 fraction was higher than for the C_3 fraction, in line with the prediction of a recently proposed chain length dependent desorption model.

1. Introduction

The FT reaction is believed to be a polymerisation-type synthesis where hydrocarbon chain growth occurs by the addition of one carbon atom at a time. As a consequence, the product spectrum can normally be characterised with the well-known Schulz-Flory distribution[1]. It is, however, generally accepted that there are certain omnipresent deviations in the actual FT product spectrum from the ideal distribution[2,3]. These include a higher methane and a lower C_2 selectivity than predicted by the Schulz-Flory equation. In addition, there seems to be an increase in the chain growth probability factor and concomitant decrease in the olefin / paraffin ratio with hydrocarbon chain length. It has been proposed that the occurrence of secondary reactions might be the reason for all these deviations but the higher-than-expected methane selectivity[2,4]. Even though secondary reactions of olefins are generally facile over cobalt-based FT catalysts, it was pointed out recently that, apart from ethylene, light olefins seem to have a very low propensity for secondary reactions over potassium promoted iron-FT catalysts under commercially relevant conditions[5]. This viewpoint seems to be shared in literature by others as well[6,7]. We therefore find it questionable to ascribe all the chain length dependent deviations to secondary reactions for the case of iron-FT catalysts. Consequently, a chain length dependent desorption model has been proposed for characterising the product slate of the iron-based Low-Temperature Fischer-Tropsch (Fe-LTFT) synthesis[5] (see also Chapter 6). This model only accounts for primary reactions, and not for any reaction occurring after a desorbed product is readsorbed onto the catalyst surface. The variations in α-value and olefin / paraffin ratio with carbon number are described in terms of three generic reactions, namely chain growth (adding one carbon atom to a growing intermediate), hydrogenation (forming a paraffin as end product) and desorption (forming an olefin as end product). The scheme thus mechanistically links the variations in α-value and olefin / paraffin ratio with each other. The model was found to describe the olefin and paraffin selectivities in the C_3 to C_{10} range very well. It was even successfully extrapolated to

the total C_2 fraction by incorporating a proposal by Dry[8] that the reason for the low ethylene plus ethane selectivity may be that the C_2 intermediate has two active growth positions as opposed to the one active position of the longer chain species, resulting in a higher probability of chain propagation. In other words, the lower-than-expected total C_2 selectivity could be modelled by only considering primary reactions. However, the chain length dependent desorption model substantially overestimated the ethylene / ethane ratio. This seemed to suggest that the deviation was due to the secondary hydrogenation of ethylene, which is of course not included in the model. The purpose of the current study is to consider the secondary reactions of ethylene over iron-FT catalysts with the aim of establishing whether secondary hydrogenation is a plausible explanation for the overestimation of the ethylene / ethane ratio.

2. Background literature on secondary olefin reactions over iron-FT catalysts

It has been shown by various researchers that olefins, in particular ethylene, can undergo an array of secondary reactions in the cobalt-based FT synthesis, including conversion to heavier products and hydrogenation to the corresponding paraffin[9-11]. It has, however, been mentioned that iron-based FT catalysts have a much lower propensity for secondary olefin reactions than cobalt-based catalysts[2,6,7]. Additionally, according to Boelee[12], potassium promotion generally has a strong negative influence on the rate of secondary olefin reactions over iron-FT catalysts. Since commercial iron-FT catalysts will presumably always be promoted with alkali[13], it is not only important to distinguish between cobalt- and iron-based FT catalysts when secondary olefin reactions are considered, but also to take note of the promoter levels in the iron catalyst. It further appears as if the extent of secondary reactions is highly dependent on the olefin / CO ratio inside the reactor[12,14]. In order to ensure relevance to commercial operation, the olefin / CO ratio under which the secondary reactions are studied should therefore not be excessive. From the review by Van der Laan and

Beenackers[2], it seems as if there are not that many ethylene co-feeding studies that meet these two requirements for industrial relevance. Sometimes excessive amounts of ethylene have been added to the iron-FT synthesis in an attempt to clearly follow the conversion pathways. Tau et al.[15] pointed out that, due to the complexity of the FT product slate, it is quite difficult to identify the products of secondary olefin conversion when unlabelled olefins have been co-fed and the olefins are converted to an array of products. These authors have also remarked that even isotope tracer studies have frequently been conducted at conditions far from commercial relevance.

Many researchers have ascribed the variations in chain growth probability and olefin / paraffin ratio with hydrocarbon chain length observed in the iron-based FT synthesis to olefin reincorporation and hydrogenation, respectively. Bukur and co-workers[16,17] attributed the bell shaped curve of the olefin / paraffin ratio as a function of carbon number to secondary hydrogenation, but the deviations in the carbon number distribution from the Schulz-Flory curve was explained in terms of two types of sites on the catalyst surface yielding two different α-values. More recently, a model based on the premise of two types of sites was proposed, but provision was made for olefin reinsertion and hydrogenation on one of these two types of sites[18]. Van der Laan and Beenackers[19] proposed a product distribution model for the iron-FT synthesis, based on the secondary incorporation and hydrogenation of olefins, which was able to describe their data quite well. However, their model was not fitted to data where olefins were co-fed to the FT synthesis. Schulz and Claeys[11] co-fed olefins to a cobalt-based FT catalyst and reported that hydrogenation was generally the fastest of all secondary olefin reactions, even though reinsertion was also found. A model based on secondary reactions of olefins was then developed for both the cobalt- and the iron-based FT synthesis, even though the co-feeding studies were only performed for the cobalt-based FT process. Ji et al.[20] also explained the deviations in the product spectra measured with an Fe-Mn catalyst in terms of olefin readsorption, but olefin co-feeding was not performed.

Dwyer and Somorjai[21] studied the FT reaction over unpromoted iron single crystal surfaces. It was found that between 80% and 90% of ethylene added to the system was converted. Of the converted amount, about 90% was merely hydrogenated to ethane, while the balance was converted to heavier compounds. The addition of propylene yielded similar results, but it was reported that propylene was even less likely to reincorporated than ethylene. Schulz et al.[9] co-fed radioactively labelled ethylene to the iron-FT synthesis in a fixed bed reactor and found that a significant portion of the additional ethylene was converted. The bulk of the labelled ethylene (about 90% of the converted amount) was merely hydrogenated to ethane, with the balance reporting as heavier products. Boelee[12] co-fed unlabelled ethylene to a fused iron catalyst in a well-mixed slurry reactor operated at 250°C. During periods of co-feeding, the partial pressure ratio of ethylene to CO was between about 0.1 and 0.3, which is above what one would expect for commercial operation. The extent of ethylene conversion varied extensively (from 3 to 60 % of the added olefin) and the rate of hydrogenation was anything from 2.5 to 35 times higher than the rate of reincorporation. Hanlon et al.[14] studied the co-feeding of ethylene to a fused iron catalyst in a slurry reactor at conditions of low CO conversion (ca. 30%) and high CO conversion (ca 90%) at a temperature of 248°C. It was reported that, at low conversion, essentially all the ethylene that was converted was merely hydrogenated to ethane. At conditions of high CO conversion, between 70 and 80 % of the ethylene that was consumed was converted to ethane. It was assumed that the balance was incorporated into heavier products. However, it should be noted that the ethylene / CO ratio inside the reactor was very high for the case of the high CO conversion. In one extreme case, the ethylene partial pressure was almost the same as that of CO. Tau et al.[15] co-fed ^{14}C labelled ethylene to the iron-FT synthesis operated in a laboratory slurry reactor at a temperature of 260°C. In line with other researchers, they found that the bulk of the converted ethylene was hydrogenated to ethane. They also reported that a significant amount of labelled ethylene was transformed into 1-propanol. Since the ^{14}C activity in

the product butanol was far too low to be consistent with a Schulz-Flory distribution of the alcohols, they ascribed this transformation to a carbonylation reaction rather than traditional Fischer-Tropsch. Some of the added ethylene did, however, appear to act as a chain initiator and – propagator.

In this study, the results of a recycle laboratory slurry reactor are considered to investigate the secondary reactions of ethylene in Sasol's commercial Fe-LTFT process. Recycling increases the partial pressures of light olefins inside the well-mixed slurry reactor; consequently, it should be possible to determine which secondary reactions occur to an extent sufficient enough to notably alter the product distribution. In particular, the behaviour of ethylene will be compared to that of propylene.

3. Experimental

Since a detailed experimental description is provided elsewhere[22], only the most important aspects will be covered here. The experiments were performed with a commercial Ruhrchemie-type spray-dried, precipitated iron catalyst in a well-mixed laboratory slurry reactor operated at 240°C and 20 bar. The flow rates of the feed gases to the reactor (H_2 and CO, as well as Ar as an internal standard) were controlled with Brooks mass flow controllers. The reactor effluent passed through a hot knock-out pot (200°C) and a cold knock-out pot (15-20°C) to condense most of the water and organic products of the FT synthesis. After the cold knock-out, the tail gas was split into a purge stream and a recycle stream. The recycle stream was compressed with an air-driven Haskel gas booster. The recycle line went through a buffer tank to avoid pressure fluctuations. The recycle stream contained unconverted reactants and uncondensed products, with ethylene and propylene being the two components of interest for this study. The partial pressures of reactants and light olefins inside the reactor were calculated from the GC-TCD and GC-FID analyses of the reactor effluent. The recycle ratio is defined as the ratio of the recycle flow rate to the fresh feed flow rate on a volumetric basis.

A number of runs were performed, each at a different fresh feed H_2/CO ratio. However, during the course of a specific run, the fresh feed H_2/CO ratio was kept constant, while the recycle ratio was varied. During periods of recycle, the fresh feed flow rate was lowered by the appropriate amount to maintain a constant total feed flow rate to the reactor, irrespective of the recycle ratio. Consequently, recycling caused an increase in the overall conversion achieved.

4. The effect of recycle on the C_2 and C_3 product selectivities

The overall usage ratio of the Fe-LTFT synthesis is defined as the rate of H_2 conversion divided by the rate of CO conversion. The influence of the fresh feed H_2/CO ratio relative to the overall usage ratio on the H_2/CO ratio inside the reactor has been discussed in detail elsewhere[22]. Suffice to mention here that, when the fresh feed H_2/CO ratio is higher than the overall usage ratio of the FT synthesis, the H_2/CO ratio of the reactor effluent will be higher than the fresh feed ratio. The higher the recycle ratio, the higher the conversion and the more the exit ratio will increase above the feed ratio. The converse is true for a situation where the fresh feed H_2/CO ratio is lower than the overall usage ratio. If the fresh feed ratio is precisely at the usage ratio, there is no change in the reactor H_2/CO ratio with recycle or conversion. At the prevailing conditions of this study, the overall usage ratio of the Fe-LTFT synthesis was in the region of 1.3 to 1.4. The results of three runs will be considered here, namely those with fresh feed H_2/CO ratios of 1.08 (below the usage ratio), 2.01 (above the usage ratio) and 1.32 (approximately at the usage ratio). The influence of recycle on the outlet H_2/CO ratio for various fresh feed H_2/CO ratios, as discussed above, are illustrated by the results of Table 1. Furthermore, the data in Tables 2 and 3 indicate that the ratio of light olefins to CO inside the reactor has indeed increased due to the higher overall conversion achieved under recycle conditions. The influence of recycle on the C_2 and C_3 product selectivities is presented in Figures 1 to 6.

Table 1: Influence of recycle on the H_2/CO ratio inside the well-mixed slurry reactor for various inlet H_2/CO ratios.

Fresh feed H_2/CO ratio	Reactor H_2/CO ratio		
	No recycle	Low recycle ratio*	High recycle ratio**
1.08	1.0	0.9	
1.32	1.3		1.3
2.01	2.3	3.8	5.3

* *Low recycle ratio ≅ 0.8*

** *High recycle ratio ≅ 1.7*

Tables 2 (top) and 3 (bottom): Influence of recycle on the ethylene / CO and propylene / CO molar ratios, respectively, inside the well-mixed slurry reactor for various inlet H_2/CO ratios.

Fresh feed H_2/CO ratio	Reactor ethylene / CO molar ratio		
	No recycle	Low recycle ratio*	High recycle ratio**
1.08	0.002	0.003	
1.32	0.003		0.011
2.01	0.006	0.012	0.018

Fresh feed H_2/CO ratio	Reactor propylene / CO molar ratio		
	No recycle	Low recycle ratio*	High recycle ratio**
1.08	0.002	0.004	
1.32	0.004		0.019
2.01	0.008	0.022	0.059

* *Low recycle ratio ≅ 0.8*

** *High recycle ratio ≅ 1.7*

For the run where the feed H_2/CO ratio was 1.08, higher recycle ratios resulted in higher overall conversions and consequently in a lowering of the reactor H_2/CO ratio[22]. This is probably the reason why the propylene / propane ratio seemed to increase slightly with recycling (Figure 1). Despite the less hydrogenating conditions at increased recycle ratios, there was a substantial decrease in the ethylene / ethane

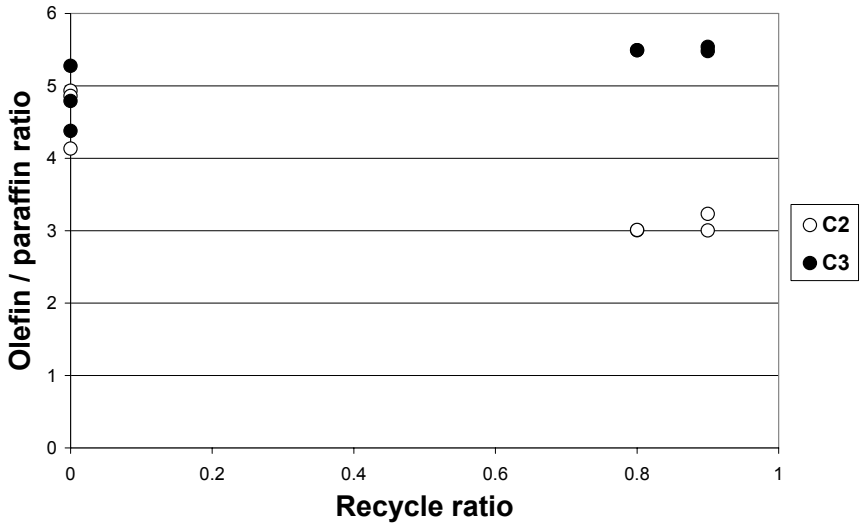

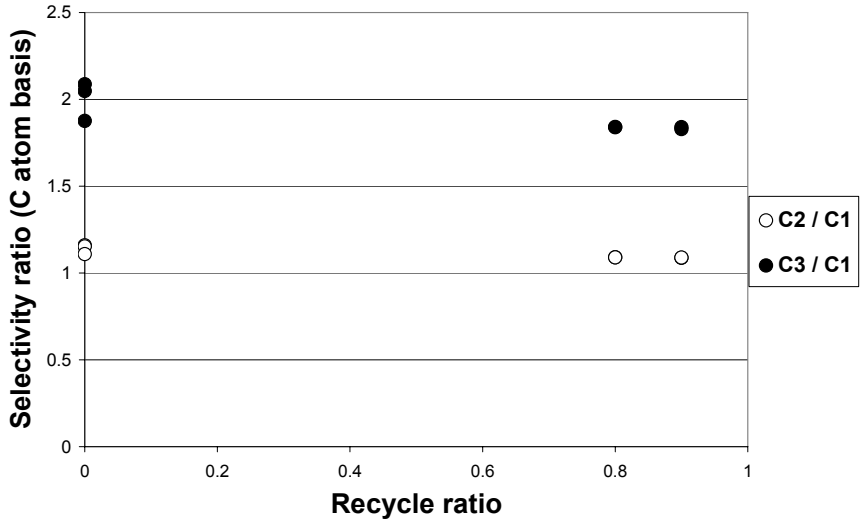

Figures 1 (top, C_2 and C_3 olefin / paraffin ratios) and 2 (bottom, C_2/C_1 and C_3/C_1 selectivity ratios): The effect of recycle for a fresh feed H_2/CO ratio of 1.08 (i.e. below the usage ratio).

ratio. The only plausible explanation seems to be that ethylene is prone to substantial secondary hydrogenation, while propylene hydrogenation occurs to a significantly lesser extent or is possibly negligible. The total C_2 and C_3 selectivities are presented relative to the methane selectivity in order to reduce data scatter brought on by mass balance inaccuracies (Figure 2). Recycling increases the ethylene and propylene

partial pressures inside the reactor and should therefore increase the rate of secondary reactions. If olefin reinsertion were significant enough to notably alter the FT product distribution, then one would have expected higher reinsertion rates under recycle conditions and consequently a decrease in the C_2/C_1 and C_3/C_1 selectivity ratios. However, from Figure 2 it is evident that at most there appears to be a very slight lowering in the C_2/C_1 and C_3/C_1 ratios, which may be due to a catalyst aging effect. The recycle was only started in the latter part of the run and it is known that the product spectrum shifts somewhat to the lighter side as the catalyst ages. A shift to the lighter end will increase the methane selectivity more than that of the other light components and is therefore expected to lead to a lowering of the C_2/C_1 and C_3/C_1 ratios. Clearly there is no notable evidence of enhanced reincorporation of either ethylene or propylene at the higher concentrations of these olefins inside the reactor under recycle conditions.

As expected, the reactor H_2/CO ratio increased with increasing recycle when the fresh feed H_2/CO ratio was 2.01 (see Table 1). Up to a recycle ratio of 0.9 there was no effect on the propylene / propane ratio (Figure 3). This means that neither the primary propylene / propane ratio was notably affected by the increase in reactor H_2/CO ratio, nor was there significant secondary conversion of propylene at its higher partial pressure inside the reactor. At a recycle ratio of 1.8, there was a drop in the propylene / propane ratio. It is not clear whether this was mainly due to a shift in the primary olefin / paraffin ratio or to secondary hydrogenation. However, it should be noted that this can be regarded as quite extreme conditions in terms of commercial Fe-LTFT operation, since the reactor H_2/CO ratio rose to well above 5 at this high recycle ratio. The lowering of the C_2 olefin / paraffin ratio was very pronounced, even at a recycle ratio of 0.8 where the C_3 olefin / paraffin ratio was not affected. Again this is very strong support for the notion that ethylene readily undergoes secondary hydrogenation. The drop in the C_2/C_1 and C_3/C_1 ratios (Figure 4) was caused by the strong increase in methane selectivity due to the steep rise in reactor H_2/CO ratio with recycle.

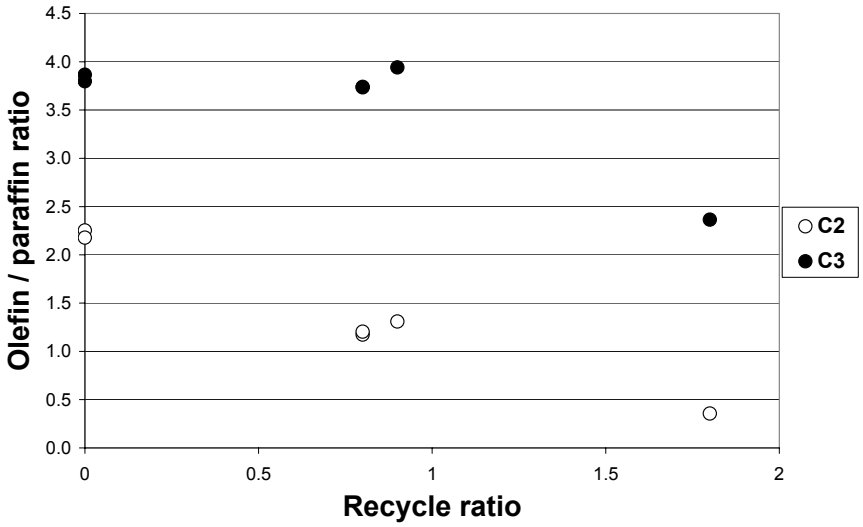

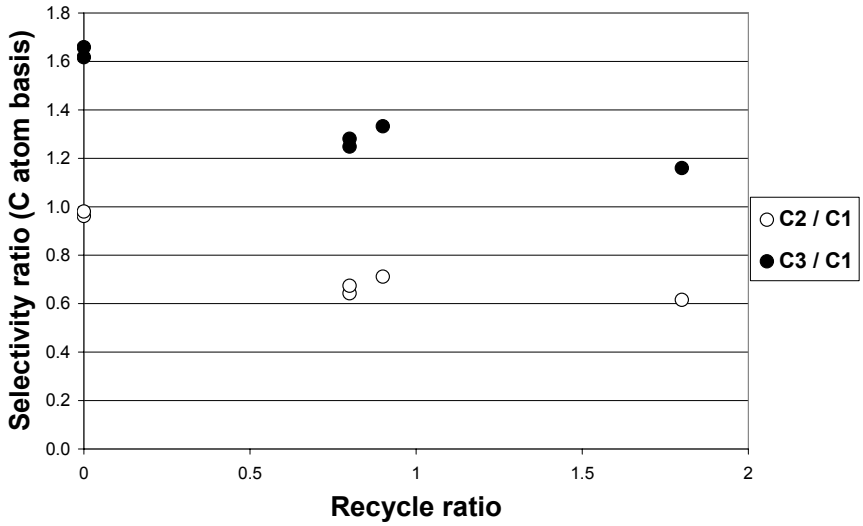

Figures 3 (top, C_2 and C_3 olefin / paraffin ratios) and 4 (bottom, C_2/C_1 and C_3/C_1 selectivity ratios): The effect of recycle for a fresh feed H_2/CO ratio of 2.01 (i.e. above the usage ratio).

A fresh feed H_2/CO ratio of 1.32 was virtually at the usage ratio, because the reactor H_2/CO ratio changed very little upon recycling (see Table 1). Even at the very high recycle ratios (close to 2) explored during this run, the effect on the C_3 olefin / paraffin ratio was quite small, but clearly ethylene was hydrogenated extensively (Figure 5). Despite the high recycle ratios, the C_2/C_1 and C_3/C_1 ratios were essentially unaffected

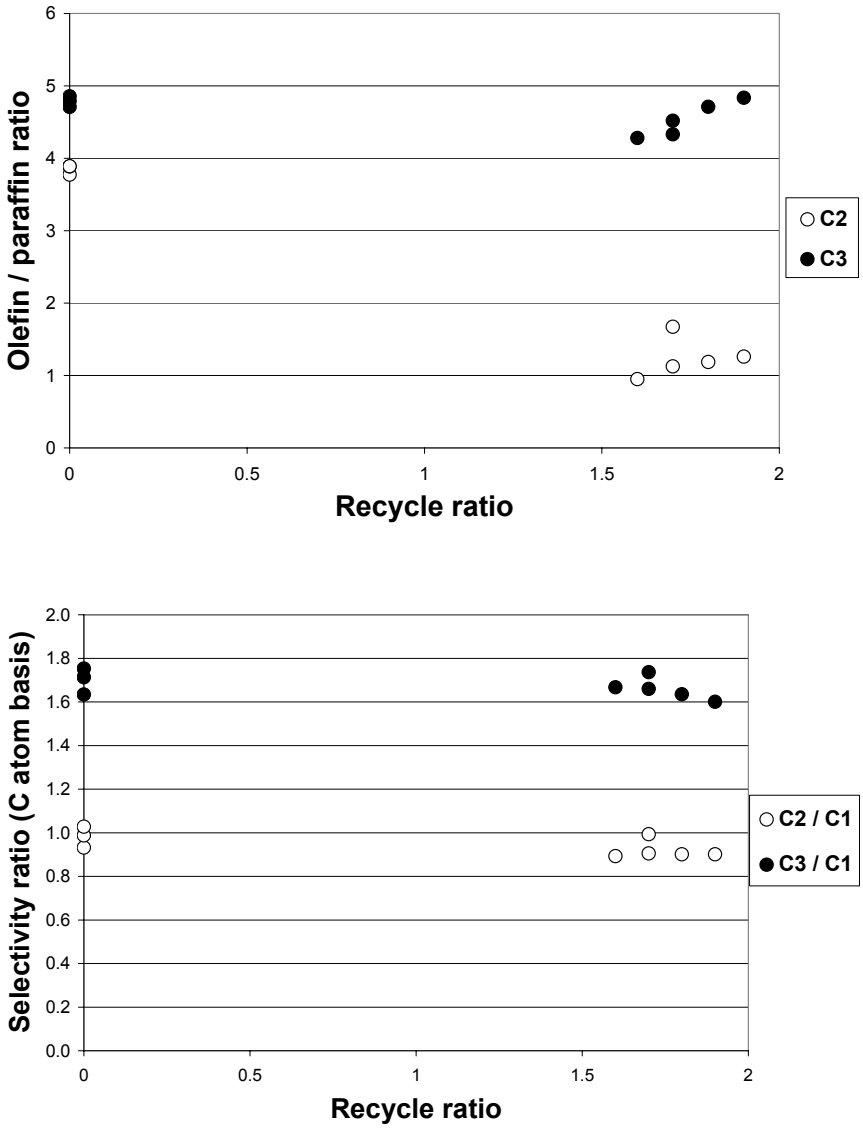

Figures 5 (top, C_2 and C_3 olefin / paraffin ratios) and 6 (bottom, C_2/C_1 and C_3/C_1 selectivity ratios): The effect of recycle for a fresh feed H_2/CO ratio of 1.32 (i.e. approximately at the usage ratio).

(Figure 6). Even if one considers the absolute C_2 and C_3 selectivities, there were no indications that they were notably lower under recycle conditions. It therefore appears as if the reinsertion of C_2 and C_3 olefins did not occur to a significant extent.

The ethylene / CO and propylene / CO ratios were substantially higher at the high recycle ratios than under once-though operating conditions (see Table 2 and 3). One

would thus have expected to see some effect on the product spectrum if secondary reactions could in fact alter the overall product distribution significantly. The only secondary reaction clearly observed was the hydrogenation of ethylene. Only at a reactor H_2/CO ratio well above 5 was there possible evidence of secondary propylene hydrogenation, and even then it was not clear to what extent the observations could be ascribed to a shift in the primary propylene / propane ratio. No evidence could be found for substantial reincorporation of either of these two olefins. These findings are largely in agreement with the olefin co-feeding studies discussed previously, where the bulk of the added ethylene was always hydrogenated to ethane. This supports the premise of the chain length dependent desorption model as far as the Fe-LTFT synthesis is concerned, namely that the only secondary reaction of note for light olefins under realistic commercial conditions is the hydrogenation of ethylene.

5. The primary C_2 and C_3 olefin / paraffin ratios

In the chain length dependent desorption model, the primary olefin / paraffin ratio is a function of carbon number according to the following relationship where T_O, T_P, and k are constant for a given product spectrum and n refers to carbon number[5] (see also Chapter 6):

$$(O/P)_n = \frac{T_O}{T_P} e^{-kn} \qquad \ldots 1$$

The above implies that the primary ethylene / ethane ratio is always higher than the primary propylene / propane ratio. From Figures 1,3 and 5, it is however seen that the measured C_2 olefin / paraffin ratio is generally lower than that of the C_3 fraction. In Figure 7, the measured olefin / paraffin ratios are presented as a function of the reactor H_2/CO ratio for once through operating conditions. Since the foregoing analysis suggested negligible secondary hydrogenation of propylene under these conditions, it

is assumed that the measured propylene / propane ratio is in fact approximately its primary ratio. The primary C_3 olefin / paraffin ratio then increases with decreasing H_2/CO ratio, as would be expected. The ethylene / ethane ratio also increases with decreasing H_2/CO ratio, but the increase is much steeper than for the case of the C_3 fraction. In fact, at an H_2/CO ratio of 1 the measured C_2 and C_3 olefin / paraffin ratios are about the same. The only feasible explanation for these observations appears to be that the secondary hydrogenation of ethylene causes the observed ethylene / ethane ratio to be lower than the propylene / propane ratio. At a high reactor H_2/CO ratio, the conditions of high H_2 and low CO partial pressures are favourable for secondary hydrogenation, so that the C_2 olefinicity is well below that of the C_3 fraction. As the CO partial pressure increases and the H_2 partial pressures decreases with decreasing H_2/CO ratio, secondary hydrogenation slows down and the measured ethylene / ethane ratio starts to approach the primary ethylene / ethane ratio. Via extrapolation of the data in Figure 7, the primary C_2 olefin / paraffin ratio indeed seems to be higher than the primary C_3 olefin / paraffin ratio, consistent with Equation 1 of the chain length dependent desorption model.

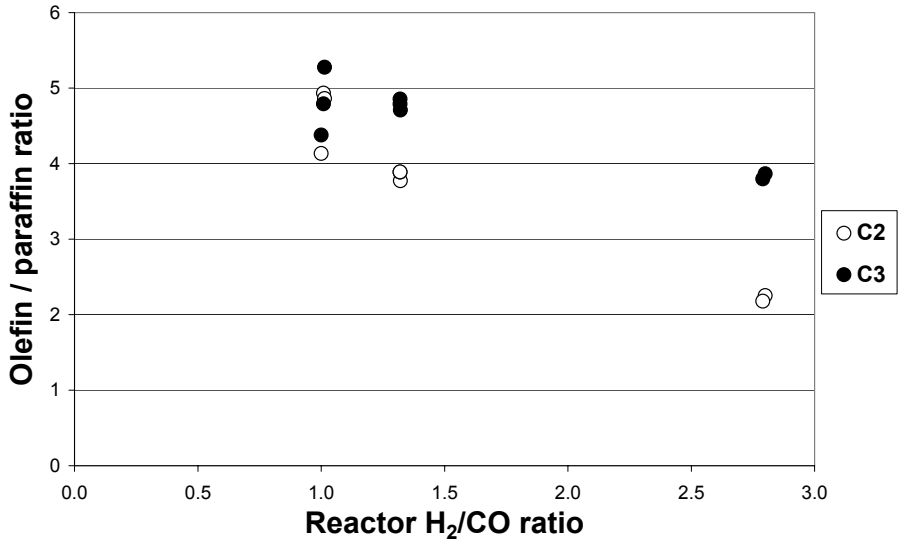

Figure 7: The effect of the reactor H_2/CO ratio on the measured C_2 and C_3 olefin / paraffin ratios for once-through operating conditions (i.e. no recycle applied).

6. Estimating reaction rate constants for secondary hydrogenation

Under recycle conditions, there was an increase in the partial pressures of light olefins inside the reactor, which should enhance the extent of secondary conversion of these olefins. Additionally, the partial pressures of H_2 and CO were also affected, but to a much lesser extent than that of the C_2 and C_3 olefins. The variation in olefin partial pressures brought about by recycling affords the opportunity to estimate rate constants for secondary olefin hydrogenation. For this purpose, a simple model was developed according to the following assumptions:

- The only secondary reaction of note is hydrogenation, consistent with the foregoing findings.
- The recycling of tail gas does not only affect the partial pressures of olefins inside the reactor, but also that of the reactants (most importantly H_2 and CO). Therefore, in addition to influencing the rate of secondary hydrogenation, recycling can in general also be expected to change the primary olefin / paraffin ratio. With the data available, it is not possible to distinguish variations in the primary olefin / paraffin ratios from the effect of secondary hydrogenation. Consequently, it was decided to take the methane selectivity as an indicator of primary selectivities. In other words, it was assumed that if the methane selectivity was not significantly affected by recycle, the primary C_2 and C_3 olefin / paraffin ratios were also unaffected. Any observed changes in the measured olefin / paraffin ratios could then be ascribed to secondary hydrogenation. Two experimental runs were performed close to the overall usage ratio of about 1.35 and their methane selectivities are presented as a function of the recycle ratio in Figure 8. For Run R008, the methane selectivity was clearly quite constant and the data can be used with reasonable confidence. For Run R012, only a small amount of somewhat scattered data was available. Nevertheless, it was decided to include Run R012 in this analysis so that there was at least an additional run available with which to compare the results of Run R008.

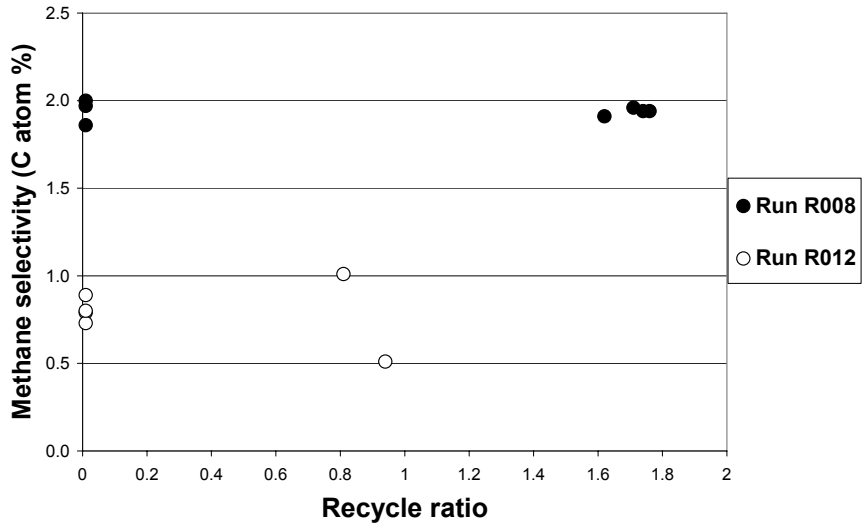

Figure 8: The effect of recycle on the methane selectivity measured during two runs performed close to the usage ratio.

- A rate expression for secondary olefin hydrogenation had to be assumed, since there are obviously not sufficient data available for the development and rigorous validation of a kinetic model. It was assumed that the hydrogenation rate is half order in hydrogen (consistent with the findings of Stacchiola et al.[23] that the addition of the first hydrogen atom to adsorbed ethylene is the rate limiting step in the hydrogenation reaction) and first order with respect to the olefin. It was further assumed that the hydrogenation occurs on the normal FT catalytic sites, which means that it must have the same denominator as the FT rate expression. The latter was obtained from a recently proposed FT kinetic equation for the Fe-LTFT synthesis[24] (see also Chapter 4). Combining the foregoing yielded the following kinetic equation for secondary olefin hydrogenation:

$$r_{sh} = k_{sh} m_{cat} \frac{P_{H2}^{0.5} \; P_{olefin}}{\left(1 + 0.09 P_{CO}\right)^2} \qquad ...2$$

where

r_{sh} is the rate of secondary olefin hydrogenation

k_{sh} is the reaction rate constant for secondary hydrogenation per mass of catalyst

m_{cat} is the mass of catalyst

- It was assumed that all C_2 and C_3 hydrocarbons left the system with the cold tail gas, i.e. insignificant amounts of these components were dissolved in the condensed phases. The following mass balance was set up for the involved light olefin (shown here for the case of C_2, but exactly the same for C_3):

$$f_2\left(\dot{n}_{ethylene} + \dot{n}_{ethane}\right) - r_{sh}^{ethylene} = \dot{n}_{ethylene} \qquad ...3$$

where

$\dot{n}$ is the molar flow rate of a component in the cold tail gas

f_2 is the molar fraction of ethylene in the primarily formed C_2 hydrocarbons

$r_{sh}^{ethylene}$ is calculated at the prevalent partial pressures inside the CSTR reactor

As a side comment, it can be noted for interest's sake that the following equation for the ethylene / ethane ratio can be derived for a once-through reactor system by applying Equations 2 and 3 together with the new Fe-LTFT rate expression[25]:

$$\frac{S_{ethylene}}{S_{ethane}} = \frac{S_{C2's,total} f_2 - k'' \dfrac{P_{ethylene}}{P_{CO}}}{S_{C2's,total}\left(1 - f_2\right) + k'' \dfrac{P_{ethylene}}{P_{CO}}} \qquad ...4$$

where

S refers to the molar selectivity

k'' is the ratio of the reaction rate constant for secondary hydrogenation of ethylene to that of the FT reaction

Equation 4 is well aligned with the conclusion of Boelee[12] that the partial pressure ratio of ethylene to CO determines the extent of secondary ethylene hydrogenation in the Fe-LTFT synthesis.

The secondary hydrogenation model (Equation 3) has two unknown parameters that must be obtained from the experimental data, namely f (determined by the primary olefin / paraffin ratio) and k_{sh} (the reaction rate constant for secondary hydrogenation). Each of the two runs under consideration essentially had only two different operating conditions, namely once-though operation and one specific recycle ratio. Therefore, even though the model was fitted to a few data points from each run, the number of different conditions was actually equal to the number of parameters to be determined, leaving no degree of freedom. This means that the model could not be tested (validated) with the available data, but did allow for the estimation of the two parameters under the assumptions listed above.

The results of the model fitting are presented in Table 4, as well as in Figures 9 and 10. Clearly the reactivity of propylene for secondary hydrogenation is very low. For Run R012, the recycle ratio of about 0.9 was not sufficient to effect a measurable lowering in the propylene / propane ratio (Figure 10); consequently, the value obtained for the rate constant of the hydrogenation reaction was zero (Table 4). For Run R008, a higher recycle ratio was applied, which caused a slight but measurable lowering in the propylene / propane ratio (Figure 9). Nevertheless, the reaction rate constant estimated for propylene hydrogenation was almost two orders of magnitude smaller than for ethylene. The consequence of the enormous difference in reactivity between ethylene and propylene is that the observed propylene / propane ratio can for practical purposes be assumed to be equal to the primary ratio, whereas the observed ethylene / ethane ratio will be substantially lower than the primary ratio (Figures 9 and 10). A

further very significant result of the study is that the estimated primary ethylene / ethane ratio is somewhat higher than the primary propylene / propane ratio, precisely what is predicted by Equation 1 (the expression for the olefin / paraffin ratio as a function of carbon number in the chain length dependent desorption model discussed in Chapter 6).

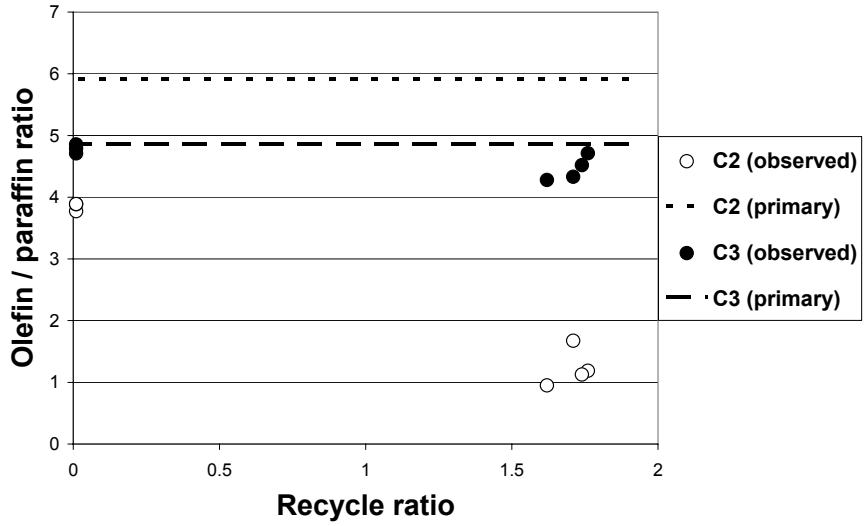

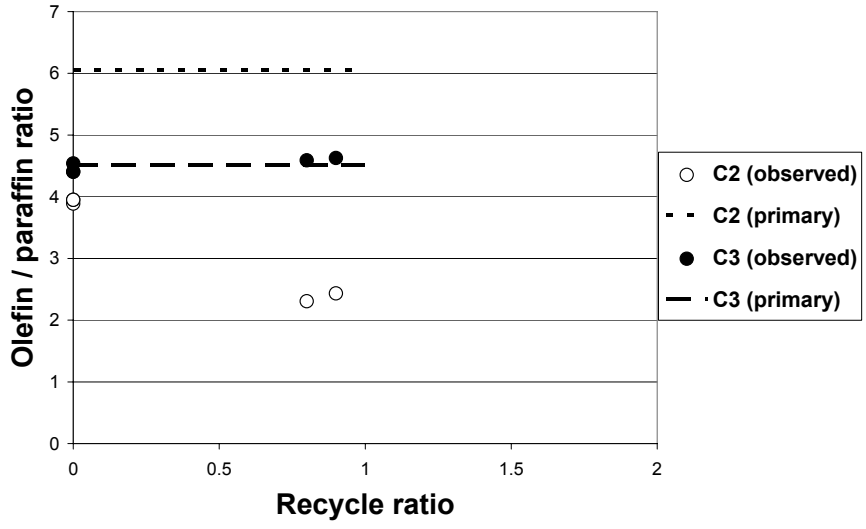

Figures 9 (top, Run R008) and 10 (bottom, Run R012): The model-estimated primary C_2 and C_3 olefin / paraffin ratios, as well as the corresponding actual olefin / paraffin ratios, for two runs performed close to the usage ratio.

By using the estimated primary ethylene / ethane ratios from Table 4 together with the observed ethylene / ethane ratios, it could be calculated what percentage of the primarily formed ethylene was hydrogenated under different recycle ratios. These results are presented in Table 5. If the estimated primary olefin / paraffin ratios are correct, it means that merely about 7% of the primarily formed ethylene needs to be hydrogenated to explain the observed ethylene / ethane ratio under once-through conditions for Runs R008 and R012. This seems realistic, considering the significant extent of ethylene hydrogenation that occurred under recycle conditions.

Table 4: Estimated parameter values of the secondary hydrogenation model as determined with data measured in a recycle laboratory slurry reactor with an Fe-LTFT catalyst at 240°C.

		Run R008	Run R012
C_2	k_{sh} (1 x 10^{-5} $mol.h^{-1}.bar^{-1.5}.g\ cat^{-1}$)	63.3	47.1
	f	0.855	0.858
	Primary olefin / paraffin ratio	5.9	6.1
C_3	k_{sh} (1 x 10^{-5} $mol.h^{-1}.bar^{-1.5}.g\ cat^{-1}$)	1.7	0
	f	0.829	0.819
	Primary olefin / paraffin ratio	4.9	4.5

Table 5: Estimated percentage of primarily formed ethylene hydrogenated under various recycle conditions for a feed H_2/CO ratio close to the usage ratio.

Recycle ratio	Percentage of primary ethylene hydrogenated
0	7.2 * // 7.1 **
0.85	18.1 **
1.7	35.5 *

* *Data from Run R008*

** *Data from Run R012*

7. Conclusions

Data measured in a laboratory recycle slurry reactor were analysed to better understand the secondary reactions of ethylene and propylene in the Fe-LTFT synthesis. No evidence could be found for significant reincorporation of either of these two olefins. Furthermore, recycling barely affected the propylene / propane ratio. To the contrary, the ethylene / ethane ratio always decreased significantly with increasing recycle, irrespective of the effect of recycle on the reactor H_2/CO ratio. It was shown for once-through operating conditions that, at high reactor H_2/CO ratios that will favour secondary hydrogenation, the ethylene / ethane ratio was substantially lower than the propylene / propane ratio. At a low reactor H_2/CO ratio (conditions less favourable for secondary hydrogenation), the C_2 olefin / paraffin ratio was comparable to that of the C_3 fraction. Lastly a kinetic model was assumed in order to estimate rate constants for secondary hydrogenation of the two involved olefins, as well as the primary olefin / paraffin ratios. The rate constant for propylene was very small, whereas that for ethylene was quite large. The estimated primary olefin / paraffin ratio for the C_2 fraction was higher than for the C_3 fraction, in line with the prediction of a recently proposed product characterisation model (see Chapter 6).

It is therefore concluded that, in Sasol's Fe-LTFT synthesis operated under commercially relevant conditions, propylene does not undergo a significant degree of secondary conversion, whereas ethylene is extensively hydrogenated to ethane. These findings are well in line with the experience gained from Sasol's Fe-LTFT pilot plants. It also seems to be consistent with the published results of ethylene co-feeding studies for similar alkali-promoted iron catalysts operated under industrially relevant conditions.

References

1. Dry, M.E. in Steynberg, A.P., Dry, M.E., Eds., *Stud. Surf. Sci. Catal.* Vol. 152, Elsevier, Amsterdam, 2004, Chapter 3, pp. 211-223.
2. Van der Laan, G.P.; Beenackers, A.A.C.M. Kinetics and Selectivity of the Fischer-Tropsch Synthesis: A Literature Review. *Catal. Rev. – Sci. Eng.* 1999, 41 (3&4) 255.
3. Claeys, M., Van Steen, E., in Steynberg, A.P., Dry, M.E., Eds., *Stud. Surf. Sci. Catal.* Vol. 152, Elsevier, Amsterdam, 2004, Chapter 8.
4. Schulz, H., Claeys, M. Kinetic Modelling of Fischer-Tropsch Product Distributions. *Appl. Catal. A* 1999, 186, 91.
5. Botes, F.G. Proposal of a New Product Characterisation Model for the Iron-Based Low-Temperature Fischer-Tropsch Synthesis. *Energy & Fuels* 2007, 21, 1379.
6. Patzlaff, J., Liu, Y., Graffmann, C., Gaube, J. Studies on Product Distributions of Iron and Cobalt Catalysed Fischer-Tropsch Synthesis. *Appl. Catal.* 1999, 186, 109.
7. Schulz, H. Comparing Fischer-Tropsch Synthesis on Iron- and Cobalt Catalysts. *Prepr. Symp. – Am. Chem. Soc., Div. Petr. Chem.* 2005, 50(2), 155.
8. Dry, M.E. Practical and Theoretical Aspects of the Catalytic Fischer-Tropsch Process. *Appl. Catal. A* 1996, 138, 319.
9. Schulz, H.; Rao, B.R.; Elstner, M. ^{14}C-Studien zum Reaktionsmechanismus der Fischer-Tropsch Synthese. *Erdöl und Kohle – Erdgas – Petrochemie* 1970, 23 (10), 651.
10. Iglesia, E.; Reyes, S.C.; Madon, R.J.; Soled, S. Selectivity Control and Catalyst Design in the Fischer-Tropsch Synthesis: Sites, Pellets and Reactors in Eley, D.D., Pines, H. Weisz, P.B., Eds., Advances in Catalysis, vol. 39, Academic Press: New York 1993, 221-302.

11. Schulz, H., Claeys, M. Reaction of α-Olefins of Different Chain Length Added during Fischer-Tropsch Synthesis on a Cobalt Catalyst in a Slurry Reactor. *Appl. Catal. A* 1999, 186, 71.
12. Boelee, J.H. The Fisher-Tropsch synthesis in slurry phase reactors, Ph.D. Dissertation, Technische Universiteit Eindhoven, 1988.
13. Schulz, H. Short History and Present Trends of Fischer-Tropsch Synthesis. *Appl. Catal. A* 1999, 186, 3.
14. Hanlon, R.T, Satterfield, C.N. Reactions of Selected 1-Olefins and Ethanol Added during the Fischer-Tropsch Synthesis. *Energy & Fuels* 1988, 2, 196.
15. Tau, L.; Dabbagh, H.; Davis, B.H. Fischer-Tropsch Synthesis: ^{14}C Tracer Study of Alkene Incorporation. *Energy & Fuels* 1990, 4, 94.
16. Bukur, D.B.; Mukesh, D.; Patel, S.A. Promoter effects on precipitated iron catalysts for Fischer-Tropsch synthesis. *Ind. Eng. Chem. Res.* 1990, 29, 194.
17. Bukur, D.B.; Patel, S.A.; Lang, X. Fixed Bed and Slurry Reactor Studies of Fischer-Tropsch Synthesis on Precipitated Iron Catalyst. *Appl. Catal. A* 1990, 61, 329.
18. Nowicki, L.; Ledakowicz, S.; Bukur, D.B. Hydrocarbon selectivity model for the slurry phase Fischer-Tropsch synthesis on precipitated iron catalysts. *Chem. Eng. Sci.* 2001, 56, 1175.
19. Van der Laan, G.P.; Beenackers, A.A.C.M. Hydrocarbon Selectivity Model for the Gas-Solid Fischer-Tropsch Synthesis on Precipitated Iron Catalysts. *Ind. Eng. Chem. Res.* 1999, 38, 1277.
20. Ji, Y.Y.; Xiang, H.W.; Yang; J.L.; Xu, Y.Y.; Li, Y.W.; Zhong, B. Effect of Reaction Conditions on the Product Distribution During Fischer-Tropsch Synthesis over an Industrial Fe-Mn Catalyst. *Appl. Catal. A* 2001, 214 (1), 77.
21. Dwyer, D.J.; Somorjai, G.A. The Role of Readsorption in Determining the Product Distribution during CO Hydrogenation over Fe Single Crystals. *J. Catal.* 1979, 56, 249.

22. Govender, N.S.; Janse van Vuuren, M.; Claeys, M.; Van Steen, E. Importance of the Usage Ratio in Iron-Based Fischer-Tropsch Synthesis with Recycle. *Ind. Eng. Chem. Res.* 2006, 45 (25), 8629.
23. Stacchiola, D.; Azad, S.; Burkholder, L.; Tysoe, W.T. An Investigation of the Reaction Pathway for Ethylene Hydrogenation on Pd(111). *J. Phys. Chem. B* 2001, 105 (45), 11233.
24. Botes, F.G.; Breman, B.B. Development and Testing of a New Macro Kinetic Expression for the Iron-Based Low-Temperature Fischer-Tropsch Reaction. *Ind. Eng. Chem. Res.* 2006, 45, 7415.
25. Breman, B.B. Personal Communications, 2006.

Chapter 8

Conclusions and Outlook

1. Commercial Fischer-Tropsch processes

Sasol currently has three different types of commercial FT processes. The iron-based Low-Temperature Fischer-Tropsch (Fe-LTFT) synthesis is typically operated at 240°C and the product spectrum extends well into the wax range. The temperature of the cobalt-based Low-Temperature Fischer-Tropsch (Co-LTFT) synthesis is generally slightly lower, but the product spectrum has a similar carbon number distribution. The iron-based High-Temperature Fischer-Tropsch (Fe-HTFT) synthesis can be operated at temperatures up to about 350°C and produces a lighter product spectrum that is essentially completely in the gas phase under synthesis conditions.

There are some clear similarities between these three processes. For all three, it is generally believed that the slow step in the conversion of syngas to hydrocarbons is the formation of the monomer (building block), implying that the rate of hydrocarbon formation is independent of the hydrocarbon product distribution. This allows for a separation of the kinetic and selectivity models, i.e. the syngas conversion rate can be described with an explicit *kinetic model* accounting for the influence of reactants (and possibly water and carbon dioxide) only, while the hydrocarbon product spectrum can be described with a separate *selectivity model*.

There are also distinct differences between the three FT technologies. The Co-LTFT process produces so little CO_2 that it is arguably not of critical importance to accurately model the CO_2 formation rate. It has been reported that the water-gas-shift (WGS) reaction in the Fe-HTFT synthesis can generally be assumed to be at equilibrium, also implying that the development of an accurate WGS kinetic model is not crucial. However, in the Fe-LTFT synthesis, a substantial portion of the CO is converted to CO_2, while the WGS reaction is normally still far from equilibrium. A comprehensive description of the Fe-LTFT process therefore requires an FT

kinetic model, a WGS kinetic model, as well as a hydrocarbon selectivity model. These three modelling aspects of the Fe-LTFT synthesis have been the subject of this dissertation.

The models proposed in this study for the Fe-LTFT process cannot be applied directly to the other FT processes, due to possible mechanistic differences. For example, there is evidence that CO dissociation over cobalt-based catalysts occurs without any interaction with hydrogen, while over iron catalysts the reaction may proceed via an oxygen-containing intermediate. A further difference is that secondary reactions of olefins are much more facile over cobalt than over iron. Additionally it should be remembered that the ca. 100°C higher operating temperature of the Fe-HTFT synthesis could make kinetic routes possible that are insignificant in the lower temperature processes. Nevertheless, the approach followed here and the types of models proposed may give guidance to the modelling efforts in the other processes as well.

2. Kinetic models for the Fe-LTFT synthesis

2.1 FT kinetics

A review of the literature revealed that the firm belief that water inhibits the FT reaction rate over iron catalysts is not based on conclusive evidence. It was shown that the lowering in the overall syngas conversion observed when water was co-fed to the process can also be explained by the role of the WGS, which altered the gas phase partial pressures of CO and hydrogen. It was also found that the effect of water was self-specified in the traditional FT rate equations, and not tested.

The denominator of the Langmuir-Hinshelwood type rate equation formulated in this study initially accounted for the effects of CO, water and vacant sites. By testing this expression against various existing sets of data, it was shown in all cases that there was no statistical basis for including water in the inhibition term. Consequently, the model could be simplified to the following form:

$$r_{FT} = A\frac{P_{H_2}{}^{0.5} P_{CO}}{\left(1 + k_{CO} P_{CO}\right)^2} \qquad ...1$$

A new experimental study was also designed which enabled a conclusive discrimination between the proposed new model and the traditional models based on the premise of water inhibition. A further consistency was that the CO adsorption coefficient in almost all cases assumed a value of around 0.1. This implies a fairly low coverage of the iron catalyst surface with adsorbed CO and C_1 intermediates. It also means that the CO reaction order is positive up to fairly high CO partial pressures (around 11 bar), consistent with the original models that only allowed for positive CO reaction orders.

2.2 WGS kinetics

The model for the CO_2 formation rate was based on the premise that the bulk of the CO_2 is formed by a separate WGS reaction. An analysis of existing data showed that first order kinetics in CO (as proposed by some in the literature) is a reasonable description of the WGS rate, but contains systematic deviations indicating its empirical nature. An initial screening of a wide variety of rate equations revealed that models based on a formate mechanism yielded the best results, as also reported in literature by others. Newly-measured kinetic data were used to discriminate between the rival formate-based expressions. The following model was found to describe the WGS kinetics the best:

$$r_{WGS} = A\ \frac{P_{CO} P_{H_2O} - \frac{1}{K_{WGS}} P_{H_2} P_{CO2}}{\left(1 + k_{H_2O} P_{H_2O} + k_{OH}\frac{P_{H_2O}}{P_{H_2}^{0.5}}\right)^2} \qquad ...2$$

2.3 Mechanistic and practical implications

The new FT kinetic model has some notable mechanistic implications. The CO reaction order of unity in the numerator of the equation is consistent with a reaction pathway where undissociated CO interacts with surface hydrogen. If this is correct, it suggests that the activation energy of the CO dissociation step is lowered by the interaction with hydrogen, making this the main route for the formation of the monomer. There is indeed mechanistic evidence for the existence of an oxygen-containing intermediate in the iron-FT reaction sequence, although this does not appear to be the case for the cobalt-FT synthesis. The much higher selectivity towards oxygenated compounds in the iron-FT synthesis compared to the cobalt-based reaction may be a consequence of the difference in main reaction pathways.

The fact that water does not appear in the denominator of the rate equation implies that the FT active sites do not have a large affinity for this component. The FT sites rather seem to be predominantly covered with adsorbed CO and / or C_1 intermediates. To the contrary, according to the kinetic model for CO_2 formation, the WGS active sites are mostly covered with adsorbed water and hydroxide species. Based on this observation alone, it may well be expected that there are at least two separate catalytically active phases with significantly different properties in the working Fe-LTFT catalyst. These findings therefore seem to be aligned with the age-old belief that the FT reaction mainly occurs over one or more iron carbide phase(s) and the WGS reaction over magnetite.

The absence of water from the new FT kinetic model (in contrast to the traditional rate equations) has some practical consequences as well. Previously it was believed that the lowering in the FT reaction rate with increasing conversion is mainly due to a build-up of water inside the reactor which inhibits the kinetics, but it is now clear that the real reason is the decrease in the CO and hydrogen partial pressures. For a commercial plant design, lower reactant partial pressures can of course be counteracted by increasing operating pressure. It is not surprising then that the new rate expression could be distinguished from the old equations by merely varying the reactor pressure over a wide range. The new model is therefore better suited to

quantify the benefits of higher operating pressures and higher per pass conversions from a reaction kinetic point of view. It would, however, be critically important to also consider the influence of these process changes on the catalyst stability, since water is known to cause sintering and reoxidation of the iron catalyst.

2.4 Future scope

Apart from irreversible deactivation, it appears as if the Fe-LTFT catalyst can undergo reversible variations in activity caused by changes in process conditions. Although not shown in the thesis, this observed response to changes in conditions occurred over the time scale of two to three days. The kinetic data reported in this study were measured by maintaining a certain predefined baseline operating condition and only making changes to other conditions for short periods of time. Typically two to six hours away from reference conditions proved sufficient to achieve steady state from a hydrodynamic perspective, but appeared to be insufficient to effect significant changes in the catalyst performance. It is believed that this approach should be adopted for future kinetic studies as well to distinguish between the influence of chemical reaction kinetics and the effect of changes in the catalyst behaviour.

After a reliable chemical reaction kinetic model has been obtained, the influence of process conditions on the intrinsic activity of the catalyst can be studied. To this end, experimental conditions should be maintained for longer periods of time (a few days). The kinetic model can be used to back-calculate the intrinsic catalyst activity from the measured data at a variety of different conditions, thereby helping to study and describe the response of the catalyst to its environment. It will probably not be trivial to develop a model for the response in catalyst behaviour, as it is not immediately clear whether any existing theory will be useful in this regard. Possibly the changes in activity are related to the competition of catalyst oxidation by water (the strongest oxidising agent) and catalyst reduction or carbidisation by CO (the strongest reducing agent).

3. Selectivity modelling of the Fe-LTFT synthesis

3.1 Existing product characterisation models

Two types of FT product characterisation models are known in literature to describe the observed deviations from the ideal Schulz-Flory type product distribution.

Double-α models are based on the premise that two types of sites or two types of mechanisms, each with a unique and constant growth probability, separately contribute to the observed product spectrum. These models generally fit the measured carbon number distribution in the FT synthesis very well. However, it was shown in this thesis that the three parameters of the model, as normally obtained from experimentally measured data, have a high degree of covariance. It appears as if too many parameters are used to describe the product distribution, i.e. that the system is over-specified. If these models are to be pursued further, it is important to find a method of estimating the values of the independent parameters with a higher degree of confidence. The model should also be expanded to account for the decrease in olefin / paraffin ratio with carbon number.

Olefin reinsertion models ascribe the increase in α-value and decrease in olefin / paraffin ratio to secondary reactions of olefins. However, alkali-promoted iron-FT catalysts generally produce a product spectrum with a very pronounced upward bend, despite their low propensity for secondary olefin reactions. Consequently, olefin reinsertion models do not seem applicable to the Fe-LTFT synthesis. It has been shown that the model predicted behaviour of in situ formed olefins in the iron-FT synthesis and the measured behaviour of olefins co-fed to the reactor differ vastly. The same kind of discrepancy may also exist in the case of the cobalt-FT synthesis, albeit to a lesser extent. It therefore seems imperative for researchers that propose olefin reinsertion models to compare the rate constants for secondary olefin reactions (as obtained via fitting the model to in situ formed products) to the corresponding rate constants measured for co-fed olefins. Alternatively, it should be shown that an olefin reinsertion model can accurately predict the product distribution when olefins are added to the reactor in increasing amounts. This type

of validation is very important, since a commercial FT process often has recycle streams that carry light olefins back to the reactor. If a reincorporation model overestimates the reinsertion propensity of light olefins (as suspected here), the model could overestimate the liquid product selectivities of the commercial design.

3.2 New product characterisation model

In this study, a new product characterisation model was proposed according to which hydrocarbon formation is governed by three generic reactions: chain growth by one carbon atom at a time; chain desorption, resulting in the formation of an olefin; chain hydrogenation, resulting in the formation of a paraffin. The cornerstone assumption is that the rates of chain growth and hydrogenation are independent of chain length, but that the rate of desorption is a function of carbon number due to the physisorption of the chain on the catalyst surface. The longer the chain, the greater the physisorption and the slower the rate of desorption relative to growth and hydrogenation; consequently, there is an increase in growth probability and saturation with chain length. The parameter values were obtained by fitting the model to the C_3 to C_{10} fraction of the product spectrum. Based on mechanistic reasoning, the model equations were adapted for the case of the C_2 intermediate, which allowed for extrapolation of the model to the C_1 and C_2 fractions as well. This is a true extrapolation, as the C_1 and C_2 data were not used for the estimation of the parameter values. This may be the first product characterisation model that can successfully be extrapolated to the C_1 and C_2 components without introducing additional (unique) parameter values for these products. It also shows that the Fe-LTFT product spectrum can largely be described by only considering primary reactions.

It was found that the newly-proposed chain length dependent desorption model overestimates the ethylene / ethane ratio. Moreover, a higher olefin / paraffin ratio is predicted for the C_2 fraction than for the C_3 fraction. Consistent with the results of ethylene co-feeding studies reported in literature, this was ascribed to the secondary hydrogenation of ethylene. Data measured in a laboratory slurry reactor

operated under recycle were used as further support for some of the assumptions and implications of the product characterisation model. These results indicated negligible reinsertion rates of both ethylene and propylene, high rates of secondary ethylene hydrogenation and very low (almost negligible) rates of secondary propylene hydrogenation. After estimating rate constants for secondary hydrogenation, it was shown that the primary ethylene / ethane ratio may well be expected to be higher than the primary propylene / propane ratio, consistent with the chain length dependent desorption model.

3.3 Mechanistic and practical implications of the new model

The assumption that the rate constants for growth and hydrogenation are independent of carbon number is not strictly necessary for the chain length dependent desorption model to be valid. What the model actually implies is that the variation in hydrogenation relative to growth is much less significant than the variation in desorption relative to growth. The analogy between hydrogenation and growth (both entail the addition of a small surface species to a growing intermediate) contrasted with the dissimilarity between desorption and growth (the former requires the intermediate to leave the surface) lends plausibility to this premise of the model. In more general terms it can therefore be concluded that the increase in α-value and decrease in olefin / paraffin ratio are in essence caused by a lower propensity of growing chains to terminate towards olefins as the chain length becomes longer.

The deviations in the C_1 and C_2 products from the ideal Schulz-Flory distribution have led to much speculation in the literature. The results of the current study suggest that the methane selectivity in the iron-FT synthesis is in fact not anomalous, since the model could be extrapolated to methane without any changes in the parameter values. The only discontinuity found in the statistical distribution was for the case of the C_2's due to the higher growth rate of the involved intermediate (possibly on account of two active growth positions). The foregoing implies that the behaviour of the C_1 intermediate is in essence not any different

from that of the longer chain intermediates, nor that some additional methane is formed on special catalytic sites unable to promote carbon-carbon coupling. Practically this means that the hope of selectively suppressing methane formation in the iron-FT synthesis (e.g. by poisoning specifically the methanation sites) may not be feasible. Similarly, since the low C_2 selectivity is not principally due to ethylene reincorporation, the recycling of light olefins to a commercial iron-FT reactor will not cause a measurable improvement in the product spectrum either. The most realistic option is to select process conditions where chain growth is favoured over chain termination so that the whole product distribution is shifted towards the heavier end.

3.4 Future scope

A basic assumption of the new product characterisation model is that the formation rate of olefins is determined by the energy required to desorb the involved intermediate from the catalyst surface, and that there is a linear relationship between the heat of desorption and the number of carbon atoms in the intermediate. The so-called "global" parameter of the chain length dependent desorption model (k in Chapter 6) is representative of the heat of desorption per carbon atom. As applied in this study, the global parameter was estimated by fitting the model to measured selectivity data. However, it would be more desirable to obtain the parameter value from a direct experimental measurement. It is thus proposed to measure the heats of adsorption / desorption of linear hydrocarbons (with different chain lengths) on the actual FT catalyst. These results could validate the assumed linear relationship between desorption heat and chain length. Furthermore, it could also be used to estimate a desorption energy per carbon atom, from which the value of the global parameter can be obtained. If successful, this independent determination of one of the model parameters would install more confidence in the chain length dependent desorption model.

The new product characterisation model also has two "local" parameters, namely T_P and T_O. The former represents the competition between hydrogenation

(termination to a paraffin) and growth, while the latter represents the competition between desorption (termination to an olefin) and growth. As explained previously in Chapter 6, these parameters are combinations of reaction rate constants, as well as surface concentrations of species like the C_1 monomer, hydrogen, vacant sites, etc. In order to obtain a usable selectivity model, the two local parameters should be related to the reactant gas phase partial pressures. Empirical correlations can of course be established to predict the parameter values, but it would be more desirable to propose a correlation that can be rationalised mechanistically. For example, using the notation of Chapter 6, it can be postulated that the rates of the three generic reactions can be represented as follows:

Growth: $$r_g = k'_g [C_n*][C_1*] \quad ...3$$

Hydrogenation: $$r_h = k'_h [C_n*][H*] \quad ...4$$

Desorption: $$r_d = k'_d [C_n*]\ e^{-kn} \quad ...5$$

From the definitions of the local parameters, it then follows that:

$$T_P = \frac{k_h[H*]}{k_g[C_1*]} \quad ...6$$

$$T_O = \frac{k_d}{k_g[C_1*]} \quad ...7$$

The important thing to note is that both parameters contain the surface concentration of the C_1 monomer. Even if other (sensible) forms of Equations 3 to 5 are assumed, it is difficult to see how T_P and T_O will not be dependent on the C_1 monomer concentration. This poses the biggest challenge in relating the model parameters to the process conditions. The assumption that the formation of the

monomer is the rate determining step in the overall FT synthesis means that the surface concentration of the monomer is not directly related to the gas phase reactant partial pressures. Presumably the monomer concentration has to be obtained from a mass balance equating its formation rate by the FT reaction to its consumption rate via various growth or desorption steps, which will probably yield a complicated implicit model. More work will be required to obtain usable expressions for these two parameters.

Acknowledgements

I have great respect and appreciation for the three key people who have been instrumental in my career at Sasol.

Rafael Espinoza first got me involved in the field of FT Catalysis. His Latin flair and exuberant character made it more fun than work. If the world is a stage and we are all merely actors, then he has the cunning ability to play the whole cast, being especially proficient at taking the lead role or acting the classical fool. The latter, when played well, is easily mistaken for silliness, but the fool of course has a profound understanding of the plot and only a few can grasp his innuendos.

Philip Gibson has been my line manager for a large part of my career. He has unselfishly supported me over many years, showing a genuine consideration for my interests in addition to that of the company. I sincerely appreciate the trust he has shown in me and the opportunities that he has helped to create for me.

Berthold Breman has challenged me in so many respects that I had no option but to lift my game to another level. I even succumbed to his persistent urging to submit some of my work as a Ph.D., so I guess he can be regarded as the father of this thesis. He is not at all good at playing the fool – his opinion on any matter is always crystal clear and offered freely.

I would like to end with a quote from the great Jackson Browne, and leave it to the reader to decide its relevance here.

And there's a shadow on the faces, of the men who send the guns
To the wars that are fought in places, where their business interest runs

I want to know who the men in the shadows are
I want to hear somebody asking them why
They can be counted on to tell us who our enemies are
But they're never the ones to fight or to die.

Lives in the Balance, 1986

List of Publications

Publications

1. Botes, F.G. The Effects of Water and CO_2 on the Reaction Kinetics in the Iron-Based Low-Temperature Fischer-Tropsch Synthesis: a Literature Review. *Catal. Rev. Sci. Eng.* 2008, accepted for publication.
2. Botes, F.G.; Govender, N.S. Secondary reactions of ethylene as studied in a laboratory-scale recycle slurry reactor. *Energy & Fuels* 2007, 21, 3095.
3. Botes, F.G. Water-Gas-Shift Kinetics in the Iron-Based Low-Temperature Fischer-Tropsch Synthesis. *Appl. Catal. A.* 2007, 328, 237.
4. Botes, F.G. Proposal of a New Product Characterisation Model for the Iron-Based Low-Temperature Fischer-Tropsch Synthesis. *Energy & Fuels* 2007, 21, 1379.
5. Botes, F.G.; Breman, B.B. Development and Testing of a New Macro Kinetic Expression for the Iron-Based Low-Temperature Fischer-Tropsch Reaction. *Ind. Eng. Chem. Res.* 2006, 45, 7415.
6. Botes, F.G. The Effect of a Higher Operating Temperature on the Fischer-Tropsch / HZSM-5 Bifunctional Process. *Appl. Catal. A.* 2005, 284, 21.
7. Botes, F.G.; Böhringer, W. The Addition of HZSM-5 to the Fischer-Tropsch Process for Improved Gasoline Production. *Appl. Catal. A.* 2004, 267, 217.
8. Kleingeld, A.W.; Lorenzen, L.; Botes, F.G. The Development and Modelling of High-Intensity Impinging Stream Jet Reactors for Effective Mass Transfer in Heterogeneous Systems. *Chem. Eng. Sci.* 1999, 54, 4991.
9. Botes, F.G.; Lorenzen, L.; Van Deventer, J.S.J. The Development of High Intensity Gas-Liquid Jet Reactors. *Chem. Eng. Comm.* 1998, 170, 217.

Oral Presentations at International Conferences

1. Botes, F.G.; Breman, B.B. Development of a New Kinetic Expression for the Iron-Based Fischer-Tropsch Reaction. *AIChE Annual Meeting* 2006, November 12-17, San Francisco, CA.
2. Botes, F.G. Proposal of a New Product Characterisation Model for the Iron-Based Low-Temperature Fischer-Tropsch Synthesis. *Mexican Congress on Chemical Reaction Engineering* 2008, June 15-19, Ixtapa-Zihuatanejo, Mexico.
3. Botes, F.G. Water-Gas-Shift (WGS) Kinetics in the Iron-Based Low-Temperature Fischer-Tropsch (Fe-LTFT) Synthesis. *Mexican Congress on Chemical Reaction Engineering* 2008, June 15-19, Ixtapa-Zihuatanejo, Mexico.

About the Author

Gideon Botes was born in Stellenbosch, South Africa, on 1 October 1971. He matriculated in 1989 from De Kuilen High School in Kuilsrivier, achieving the fifth highest aggregate in the Cape Provincial Education Department's matriculation examination. In the same year, he also received a silver medal in the South African National Mathematics Olympiad for high school pupils. In 1993, he completed his Bachelors degree in Chemical Engineering (cum laude) at the University of Stellenbosch. Amongst other academic recognitions, he was one of fifteen students to receive academic colours from the University of Stellenbosch in 1994. He obtained his Masters in Chemical Engineering from the University of Stellenbosch in 1996 (cum laude) with a thesis entitled "The Development and Modelling of Jet Reactors", which also earned him a medal from the South African Association for the Advancement of Science. In 2002, he obtained a Taught Masters in Catalysis from the University of Cape Town. Gideon has been employed by Sasol Technology since 1996 where he has mainly been involved in the modelling of commercial coal gasifiers, Fischer-Tropsch catalysis research and the kinetic and selectivity modelling of Sasol's various FT processes.